Metabolic Engineering of *Saccharomyces cerevisiae* for Tocochromanol Production

Dissertation
zur Erlangung des Doktorgrades
der Naturwissenschaften

vorgelegt beim Fachbereich Biowissenschaften
der Johann Wolfgang Goethe-Universität
in Frankfurt am Main

von
Julia Michaela Bauer
aus Wiesbaden

Frankfurt am Main, 2023

(D 30)

Vom Fachbereich Biowissenschaften der

Johann Wolfgang Goethe-Universität als Dissertation angenommen.

Dekan: Prof. Dr. Sven Klimpel

1. Gutachter: Prof. Dr. Eckhard Boles
2. Gutachterin: Prof. Dr. Claudia Büchel

Datum der Disputation:

Table of Contents

Summary 1

1 Introduction 5

1.1 The Importance of Metabolic Engineering in the Field of Synthetic Biology 5

1.1.1 The Host *S. cerevisiae* is a Powerful Workhorse for Metabolic Engineering 6

1.2 Tocochromanols 8

1.2.1 Antioxidative Properties of Tocochromanols 9

1.2.2 Natural Tocochromanol Biosynthesis 11

1.3 Metabolic Engineering of *S. cerevisiae* 13

1.3.1 Homogentisic Acid Biosynthesis 14

1.3.2 Isopentenyl Diphosphate Biosynthesis 17

1.3.3 Recombinant Tocochromanol Biosynthesis 19

1.4 Aim of this Study 21

2 Materials and Methods 22

2.1 Microbiological Methods 22

2.1.1 Media 22

2.1.2 Cultivation and Storage of *S. cerevisiae* 23

2.1.2.1 Shake Flask Fermentations of *S. cerevisiae* 24

2.1.2.2 *In-situ* Extraction during Fermentations 24

2.1.2.3 Online Biomass Monitoring by Cell Growth Quantifier (CGQ) 25

2.1.2.4 Shake Flask Fermentation and Fluorescence Intensity Measurement 25

2.1.2.5 Fed-Batch Fermentation 25

2.1.2.6 Cultivation for Fluorescence Microscopy 26

2.1.3 *S. cerevisiae* Strain Construction 26

2.1.3.1 Preparation of Competent *S. cerevisiae* Cells and Transformation 27

2.1.3.2 Screening of the Transformants 28

2.1.3.3 CRISPR/Cas9 28

2.1.3.4 Evolutionary Engineering 29

2.1.4 Plasmids 29
2.1.5 Cultivation and Storage of *E. coli* 38
2.1.6 DNA Isolation 39
2.1.6.1 Isolation of DNA from *S. cerevisiae* 39
2.1.6.2 Isolation of DNA from *E. coli* 39
2.2 Molecular Biological Methods 40
2.2.1 Synthetic DNA 40
2.2.2 Polymerase Chain Reaction 40
2.2.2.1 Q5 DNA Polymerase PCR Reactions 41
2.2.2.2 Phusion DNA Polymerase PCR Reactions 41
2.2.2.3 DreamTaq Polymerase PCR Reactions 42
2.2.3 Agarose Gel Electrophoresis and DNA Extraction from Agarose Gels 42
2.2.4 Cloning Procedures 42
2.2.4.1 Golden Gate Assembly 43
2.2.4.2 Gibson Isothermal Assembly 44
2.2.5 DNA Sequencing 45
2.3 Analysis 45
2.3.1 Sample Preparation 45
2.3.1.1 Sample Preparation for HGA Measurement 46
2.3.1.2 Methanol Extraction 46
2.3.1.3 Homogenisation for GGOH and Tocochromanol Analysis 46
2.3.1.4 *In-situ* Extraction for GGOH and Tocochromanol Analysis 47
2.3.2 HPLC Analysis 47
2.3.2.1 Analysis of HGA by HPLC 47
2.3.2.2 Analysis of Tocochromanols and GGOH by HPLC 47
2.3.2.3 Qualitative Analysis of β-Carotene 48
2.3.3 Gas Chromatography 48
2.4 Chemicals, Kits and Devices 49

2.5 Software 52
3 Results 53
3.1 Artificial Promoter Engineering 53
3.2 Metabolic Engineering of the Isopentenyl Diphosphate Biosynthesis 54
3.2.1 Eliminating *HMG1* Downregulation and Identification of *BTS1* Limitation 55
3.2.2 Downregulation of the Competing Ergosterol Pathway 58
3.2.3 Genome-based *BTS1* Overexpression 59
3.2.4 Increase of GGPP Synthesis by *ERG20* Overexpression 60
3.2.5 Plasmid-based Characterisation of Heterologous GGPP Synthases 62
3.3 Proof of Concept by δ-Tocotrienol Biosynthesis 65
3.3.1 Increasing δ-Tocotrienol Titers by *XdcrtE* Expression and the Truncation of the Chloroplast Targeting Signal of *AtVTE1* 69
3.3.2 Comparison of Genome-based *BTS1* and *XdcrtE* Overexpression 70
3.3.3 Limitations of Endogenous Gene Overexpression 73
3.3.4 Heterologous Tocotrienol Pathway Affecting Precursor Titers 75
3.4 Beta Carotene Synthesis Illustrating a Sufficient GGPP Supply 77
3.4.1 Proof of Concept for β-Carotene Synthesis Using a Plasmid-Based Approach 77
3.4.2 Construction of a Stable β-Carotene Producer Strain 78
3.5 Metabolic Engineering of the Tocochromanol Biosynthesis Pathway 80
3.5.1 Identification of a Second Functional HPT 80
3.5.2 *DPP1*Δ and Integration of a Second *HPT-trVTE1* Expression Cassette 82
3.5.3 Evaluation of Fermentative Conditions 86
3.6 Synthesis of Further Tocochromanol Forms in *S. cerevisiae* 88
3.7 Laboratory Tocotrienol Producer Strains 90
3.8 Evolutionary Engineering by Ozone Treatment 91
4 Discussion 97
4.1 Tried and Trusted Engineering Strategies Improving Production Titers 97
4.1.1 Sufficient Precursor Supply 98

4.1.2 Restriction and Elimination of Competing Pathways 100
4.1.3 Transcriptional Regulation in Metabolic Engineering 103
4.2 Challenges of Recombinant Protein Expression 105
4.2.1 The Heterologous Prenyltransferase HPT is Limiting Production Titers 106
4.2.2 Protein Localisation and Truncation of the Chloroplast Transit Peptide 107
4.3 Evaluation of the Evolutionary Engineering 110
4.4 Establishment of a Fermentation Process and Potential of a Microbial Platform Organism for Tocotrienol Biosynthesis 112
5 Deutsche Zusammenfassung 115
6 References 120
7 Appendix 136
7.1 Abbreviations 136
7.2 Synthetic Oligomers 138
7.3 Codon Optimized Sequences of Heterologous Genes 144

Summary

For thousands of years, *S. cerevisiae* has been employed by humans in brewing and baking. Nowadays, this budding yeast is more than that: it is a well investigated model organism and an established workhorse in biotechnology. *S. cerevisiae* serves as a production host for various applications such as i) bioethanol production ii) the biosynthesis of hormones including insulin or iii) cannabinoid biosynthesis. Hereby, the robustness of *S. cerevisiae* and its high tolerances regarding pH and salt concentrations qualifies it for a wide range of industrial applications. Moreover, products of *S. cerevisiae* are generally recognised as safe (GRAS), enabling diverse biotechnological applications. Various mechanisms for genetic engineering of *S. cerevisiae* are applicable and the engineering process itself is straightforward since methods are established and widely known. Due to the wide range of industrial applications of *S. cerevisiae*, this organism is an ideal candidate for applied research and implementation of the recombinant biosynthesis of tocochromanols in this study.

Tocochromanols encompass tocotrienols and tocopherols, which are lipid-soluble compounds that are commonly associated with vitamin E activity. Hereby, α-tocopherol is the most prevalent form, as it is an essential nutrient in the diet of humans and animals. Naturally, tocochromanols are almost exclusively synthesised by photoautotrophic organisms such as plants or cyanobacteria. They consist of an aromatic head group and a polyprenyl side chain which is saturated in tocopherols and 3-fold unsaturated in tocotrienols. The methylation status of the chromanol ring distinguishes α-, β-, γ- and δ-tocochromanol. All forms of tocochromanols represent a group of powerful antioxidants, scavenging reactive oxygen species (ROS) and preventing the propagation of lipid oxidation in lipophilic environments. Recently, attention has been drawn to tocotrienols, due to their benefits in neuroprotection as well as cholesterol-lowering and anti-cancer properties. Consequently, tocochromanols are valuable additives in the food, feed, cosmetic and pharmaceutical industries.

The metabolic engineering strategy of *S. cerevisiae* to enable tocochromanol biosynthesis was started in a preceding master thesis with the provision of the aromatic moiety, homogentisic acid (HGA), from the aromatic amino acid biosynthesis. Hereby, the upregulation and redirection of the native pathway was essential. Therefore, a strain with an engineered aromatic amino acid pathway for improved 4-hydroxyphenylpyruvate (HPP) production (MRY33) was utilised from Reifenrath and Boles (2018). Furthermore, a heterologous hydroxyphenylpyruvate dioxygenase (HPPD) was required to convert HPP into HGA. Thus, several heterologous HPPDs were expressed and characterised regarding their HGA production

within the previous study. The best variant originated from *Yarrowia lipolytica, YlHPPD,* and was integrated into the genome of MRY33. The resulting strain JBY2, produced 435 mg/L HGA in a shake flask fermentation.

This work was started with the genetically highly modified strain JBY2, whose genome already contained a large number of genes artificially expressed behind strong promoters. For further strain development, it was advantageous to maintain a high degree of sequence variability in order to prevent genomic instabilities due to sequence homologies. Thus, 17 artificial promoters (*AP1-AP17*) were characterised regarding their strength of expression by the yellow fluorescent protein (YFP). These sequences were also part of a patent that was filed during this work (WO2023094429A1).

The key point of this study was the development of a metabolic engineering strategy for the strain JBY2. First, the sufficient supply of the second precursor, the polyprenyl side chain, was investigated. Natively, *S. cerevisiae* produces the precursor, geranylgeranyl diphosphate (GGPP), from the isopentenyl diphosphate pathway. However, without further engineering, GGPP was barely detectable in JBY2 (< 0.1 mg/L). Thus, engineering of the isopentenyl diphosphate biosynthesis was necessary. The limiting enzyme of the mevalonate pathway was the 3-hydroxy-3-methylglutaryl coenzyme A reductase (HMGCR), which is encoded by *HMG1*. Therefore, a truncation for feedback-resistance and its overexpression by a promoter exchange was performed. Furthermore, the promoter of the gene for the squalene synthase (*pERG9)* was exchanged by the ergosterol sensitive promoter *pERG1* to limit the metabolic flux of the mevalonate pathway into the ergosterol pathway. The native GGPP synthase (*BTS1)* was another limitation that was observed throughout this study. To overcome this bottleneck, plasmid-based and integrative overexpression of the native *BTS1* and a codon optimised *BTS1* were investigated. Other strategies to improve GGPP production were the deletion of the gene for the diacylglycerol pyrophosphate phosphatase (*DPP1*) to prevent excessive dephosphorylation of GGPP to geranylgeraniol (GGOH), and the overexpression of the farnesyl pyrophosphate synthetase, encoded by *ERG20*. However, the best improvements of the GGPP biosynthesis, inferred through GGOH measurements, were achieved from the screening of several heterologous GGPP synthases in *S. cerevisiae*. The best performing strain was JBY61 (JBY2, *hmg1Δ::pTDH3-HMG1$^{tr[1573–3165]}$, pERG9Δ::pERG1, ChrIV-49293-49345Δ::pTDH3-XdcrtE-tSSA1_LEU2)*, bearing the heterologous GGPP synthase crtE of *Xanthophyllomyces dendrorhous* and produced 64.23 mg/L GGOH. Consequently, this engineering strategy improved the GGOH production by a factor of 642 compared to the parent strain JBY2.

With respect to the successful production of the two precursors HGA und GGPP, the foundation was laid to establish the third pathway, the biosynthesis of tocochromanols. Therefore, the enzymes of the corresponding pathway from plants and cyanobacteria needed to be heterologously expressed in yeast. First, the condensation of HGA and GGPP is performed by a homogentisate phytyltransferase (HPT), generating 2-methyl-6-geranylgeranyl-1,4-benzoquinol (MGGBQ). Subsequently, a cyclisation step by a tocopherol cyclase (TC) converts MGGBQ into the first tocochromanol metabolite, δ-tocotrienol. This was achieved in *S. cerevisiae* by the integration of the heterologous *SynHPT* of *Synechocystis* sp. PCC 6803 and a truncated variant of the TC, $AtVTE1^{tr[142-1467]}$, from *Arabidopsis thaliana,* generating the strain JBY20.

However, δ-tocotrienol production titers were significantly lower compared to the produced precursor titers, implying a limitation of the enzymes of the tocochromanol pathway. To verify this hypothesis, a β-carotene producer strain was constructed. The genomic modifications of the preceding pathways were identical in the δ-tocotrienol producer strain JBY20 and the β-carotene producer JBY63. However, JBY63 expressed the genes *crtI* and *crtYB* of *X. dendrorhous* for the biosynthesis of β-carotene, instead of the tocochromanol pathway genes, *SynHPT* and $AtVTE1^{tr[142-1467]}$. The strong β-carotene production was visible by the orange staining of the cells immediately after transformation. Of higher importance, the GGOH titers in JBY63 dropped 60 % compared to JBY20. Consequently, higher amounts of the precursor GGPP were utilised for the β-carotene synthesis than for the δ-tocotrienol biosynthesis. These results implied a better performance of the enzymes of the β-carotene pathway and verified the predicted limitation of the tocochromanol pathway enzymes. Conclusively, the HGA and GGPP precursor supply in JBY20 was sufficient.

Thereupon, the metabolic engineering strategy was focused on the tocochromanol pathway of JBY20. The limitation of the HPT and VTE1 was underlined since an integration of a second *SynHPT-*$AtVTE1^{tr[142-1467]}$ expression cassette improved the δ-tocotrienol titers. Thereby, the second expression cassette was integrated into the *DPP1* locus, generating the strain JBY67. This improved δ-tocotrienol titers to 2.79 mg/L, which corresponds to an improvement by a factor of 6.83 compared to the parent strain JBY20. Due to the engineering strategy, the ClonNAT antibiotic resistance cassette remained in the genome of JBY67. Successful deletion of the resistance cassette further enhanced the δ-tocotrienol titer by a factor of 1.47, reaching a titer of 4.09 mg/L in the new strain JBY70.

A second functionally active HPT of *Nostoc* sp. TCL240-02 was identified, enabling further sequence variation when additional HPT overexpression is desired. Besides the biosynthesis of δ-tocotrienol, the synthesis of the other tocotrienol forms in *S. cerevisiae* was achieved. The truncated variants of two heterologous methyltransferases (*AtMPBQMT*$^{tr-[153-864]}$ and *Atγ-TMT*$^{tr[121-1047]}$) from *A. thaliana* were integrated into the genome of *S. cerevisiae*, generating the strain JBY69. All tocotrienol forms were detected in this strain with δ-tocotrienol remaining the most abundant form, followed by γ-tocotrienol as the second most abundant form with half the titer of the δ-tocotrienol.

Due to the obvious limitation of the heterologous tocochromanol pathway enzymes, a concept for an evolutionary engineering approach was developed, which is based on the antioxidant properties of δ-tocotrienol. Therefore, the powerful oxidant ozone was utilised to obtain an evolutionary pressure for a higher antioxidant biosynthesis in *S. cerevisiae*. A procedure was developed of several successive ozone treatments of yeast cultures, in which cells might have a survival benefit if they produce higher concentrations of δ-tocotrienol. Several rounds of ozone treatment with different δ-tocotrienol producer strains were performed. Thereby, the method was continuously improved and the δ-tocotrienol titers increased in several evolutionary engineered strains. The δ-tocotrienol titers of the third generation of the strain JBY67 increased by 50 % compared to the parent strain JBY67. Consequently, the ozone treatment developed in this study is a promising tool for the evolutionary engineering of tocochromanols and possibly other antioxidants in *S. cerevisiae*.

1 Introduction

1.1 The Importance of Metabolic Engineering in the Field of Synthetic Biology

The origins of synthetic biology lie in the discovery of regulatory mechanisms of genetics and the development of molecular biological cloning methods, enabling recombinant gene expression (Cameron et al., 2014). Nowadays, the field encompasses a much wider perspective, such as the understanding of biological enigmas through the utilisation of unnatural, and therefore synthetic, compounds (Benner and Sismour, 2005). Synthetic biology involves the strategic redesign and rational engineering of organisms for the creation of new characteristics and thus creating new biosynthetic production routes (Voigt, 2020). Hereby, a purposeful application of the new capabilities and improvements of these organisms is essential.

With regard to the concept of metabolic engineering, two terms aspire to be discussed more precisely. First, metabolism, which refers to anabolic and catabolic processes of nutrients within a cell. New cell compounds are constructed from smaller subunits within anabolic pathways. Generally, these assimilatory pathways require energy and relate to reductive processes. Therefore, anabolic build-up mechanisms are in a balance with catabolic proceedings. The breakdown of metabolites, whereby energy is released, is defined as catabolism. These dissimilatory processes often remove electrons from substrates and require cofactors (Feldmann, 2012). Anabolic and catabolic processes build a complex network of pathways in a cell. Consequently, a deep understanding of metabolic processes is essential for biotechnology. Particularly, the application of this principal concept to utilise the metabolism of microorganisms to convert simple carbon sources into desired compounds.

Second, in this context, engineering encompasses the strategic design and reasonable creation of genetic modifications in accordance with molecular biotechnological knowledge. Hereby, the focus is on the targeted and comprehensive analysis of environmental conditions to ensure a thoughtful procedure (Cameron et al., 2014). Metabolic engineering as we understand it nowadays has its roots in the late 1970s. At the time being, *E. coli* was first employed for the production of recombinant proteins such as human insulin (Hong and Nielsen, 2012; Baeshen et al., 2014). Prior to this, insulin for diabetic patients was obtained from bovine or porcine pancreatic extracts. However, this approach had several disadvantages, including anti-insulin antibody formation and further the increasing demand from a growing number of people suffering from diabetes mellitus (Walsh, 2005). As a result, the biosynthesis of human insulin

from microbial cell factories is a successful demonstration of an application of metabolic engineering (Baeshen et al., 2014). With a deeper understating of complex metabolic networks, the development of genome editing methods and the rise of bioinformatics and modelling, the field of metabolic engineering has expanded (Nielsen and Keasling, 2016; Khalil, 2020). This has paved the way for a sustainable future, by the biosynthesis of desired compounds from microbial cell factories. Moreover, it creates opportunities to work on solutions for global food supply and enables unique answers to problems in modern medicine (Voigt, 2020).

1.1.1 The Host *S. cerevisiae* is a Powerful Workhorse for Metabolic Engineering

The budding yeast *S. cerevisiae*, a well investigated model organism and established workhorse in biotechnology, was employed as the production host for this study. For thousands of years, yeast has been unintentionally domesticated for the production of beer, wine and bakery products. The earliest discoveries of fermented grape beverages date back to around 7000 BC in China (McGovern et al., 2017). However, the first yeast strain was isolated in the 19th century by Emil Christian Hansen in the Carlsberg laboratories, laying the foundation for today's yeast research (Nielsen, 2019). In the last years, interest in the capabilities of *S. cerevisiae* has continued to grow. Recently, *S. cerevisiae* was announced as the microbe of the year 2022 by the Association for General and Applied Microbiology (Vereinigung für Allgemeine und Angewandte Mikrobiologie, 2022).

The yeast *S. cerevisiae* has proven to be a successful model organism for eukaryotic cells. Its genome was the first eukaryotic genome to be completely sequenced, enabling studies of the functions of human orthologs (Skrzypek et al., 2018). Furthermore, the research with *S. cerevisiae* has also provided fundamental knowledge of the physiology and cell division cycle. Thereby, it contributed to a comprehensive understanding of biological mechanisms, leading to essential insights of various diseases like cancer and physiological processes such as ageing (Ewald, 2018). As pathways are highly conserved between yeast and humans, studies in yeast have provided crucial answers for the development of anti-cancer drugs and vaccines (Ferreira et al., 2019). From a biotechnological perspective, yeast moved into the spotlight by ethanol production for biofuels (Weber et al., 2010). One trait of *S. cerevisiae* is the Crabtree effect. More specifically, glucose is rapidly converted to ethanol and CO_2 under both aerobic and anaerobic conditions. Generally, O_2 serves as the final electron acceptor, however, alcoholic fermentation is preferred under glucose-rich conditions by Crabtree-positive yeasts such as *S. cerevisiae* (De Deken, 1966; Dashko et al., 2014). Thereby high glucose concentrations lead

to various processes in glucose repression (Kayikci and Nielsen, 2015). Subsequent to glucose consumption, the metabolism changes (diauxic shift) and the accumulated ethanol serves as substrate of the alcohol dehydrogenase, producing acetaldehyde (Piskur et al., 2006). However, the influence of different carbon sources and rewiring the metabolism of *S. cerevisiae* for the biosynthesis of products beyond ethanol is well investigated (Gambacorta et al., 2020). The metabolic profile of *S. cerevisiae* can be manipulated and adapted to synthesise a desired product, due to the common knowledge of the different stages of yeast metabolism.

Excessive depletion of fossil fuels has necessitated research into alternative resources, including a range of biofuels and their precursors that can be produced by yeast (Liu et al., 2022). Nowadays, research focuses on the biosynthesis of second-generation bioethanol. Hereby, the engineering of *S. cerevisiae* for the metabolisation of xylose and arabinose contributed to a large extent on the research for the bioconversion of lignocellulose into biofuels (Farwick et al., 2014; Nielsen, 2019). Further successful examples of biotechnological applications are the production of cannabinoids, hormones including insulin and the non-glycosylated human growth hormone, and vaccines such as the hepatitis B virus surface antigen (Liu et al., 2012; Baeshen et al., 2014; Luo et al., 2019). The combination of these applications and the robustness of *S. cerevisiae* for the biosynthesis of various chemicals, qualified it as so called platform cell factory (Nielsen, 2015). In addition to its robustness during industrial processes, *S. cerevisiae* distinguishes itself due to its high tolerances regarding low pH, high salt concentration and stress during fermentative processes (Gibson et al., 2007; Gottardi et al., 2017; Nielsen, 2019). Another advantage is the GRAS status of products synthesised in *S. cerevisiae*, assigned by the Food and Drug Administration (FDA), and the inclusion of *S. cerevisiae* strains in the Qualified Presumption of Safety (QPS) list of the European Food Safety Authority (EFSA), enabling diverse biotechnological applications. Furthermore, various databases and numerous online tools for genetic engineering are available. The engineering process itself is straightforward since methods for genetic modifications are established and widely known in *S. cerevisiae* (Nandy and Srivastava, 2018). Another favourable feature of *S. cerevisiae* is that it favours DNA repair by homologous recombination over mechanisms such as non-homologous end joining (NHEJ) (Mathiasen and Lisby, 2014). Thereby, modifications using the CRISPR/Cas9 system are quickly feasible (Generoso et al., 2016). Taken together, *S. cerevisiae* is an ideal candidate for the fundamental investigation and implementation of the heterologous biosynthesis of tocochromanols within this study.

1.2 Tocochromanols

Tocochromanols include tocopherols and tocotrienols, which are lipid-soluble compounds commonly associated with vitamin E activity (Falk and Munné-Bosch, 2010). Vitamins are essential molecules since humans and animals are unable to synthesise sufficient amounts and therefore require nutritional supplementation (Bonrath and Netscher, 2005). Evans and Bishop (1922) discovered that the dietary absence of vitamin E (α-tocopherol) in the diet of rats resulted in sterility. In humans, it owns essential functions as a vitamin in reproduction, regulation of the cell cycle and embryonic development (Blaner et al., 2021). Naturally, tocochromanols are almost exclusively synthesised by photoautotrophic organisms and are most abundant in oilseeds (DellaPenna and Pogson, 2006). However, tocochromanol biosynthesis in the non-photosynthetic parasite *Plasmodium falciparum* has recently been proposed (Sussmann et al., 2011; Pellaud and Mène-Saffrané, 2017). The industry focuses on (all-*rac*)-α-tocopherol synthesis by catalytic reaction of trimethylhydroquinone and isophytol (Bonrath and Netscher, 2005).

Regarding phototrophic organisms, the term vitamin E is misleading concerning the function in plants and cyanobacteria (Falk and Munné-Bosch, 2010). Thus, the term tocochromanol will be used throughout this thesis, especially in relation to its function in plants. As the term already implies, tocochromanols consist of a chromanol ring and a polyprenyl chain, which is saturated in tocopherols and 3-fold unsaturated in tocotrienols (Figure 1). Depending on the methylation status of the chromanol ring, the forms α-, β-, γ-, δ-tocotrienol and α-, β-, γ-, δ-tocopherol are classified (Kamal-Eldin and Appelqvist, 1996; Valentin and Qi, 2005). Tocopherols are ubiquitously present in photoautotrophic organisms, with particularly high concentrations detectable in photosynthetically active environments, whereas tocotrienols predominantly occur in monocots, prevalently localised in seeds and fruits (Falk and Munné-Bosch, 2010). The group of tocochromanols also include tocomonoenols, tocodienols, rare tocochromanol-related compounds and plastochromanol-8 (PC-8) (Górnaś et al., 2022). Lately, attention has been drawn to their beneficial antioxidant properties, although further research awaits these compounds (Szymańska and Kruk, 2010). The latter of them, PC-8, consists of a 2-fold methylated chromanol ring homologous to γ-tocotrienol, while the unsaturated side chain consists of eight isoprene units. The antioxidant has been identified in various plant species, predominantly inside the chloroplasts (Kruk et al., 2014). However, PC-8 occurrence is rather rare compared to other tocochromanols (Falk and Munné-Bosch, 2010).

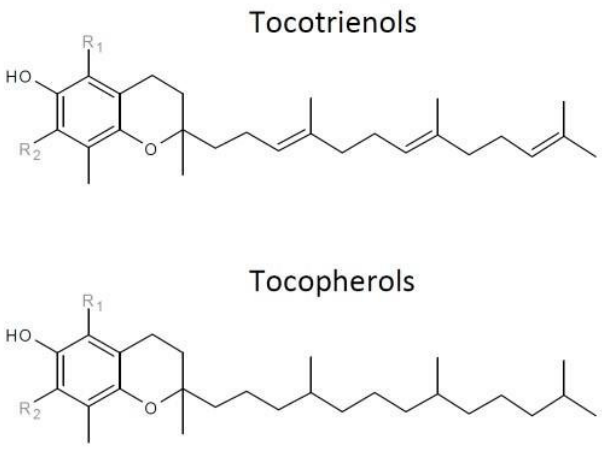

	R1	R2
α-	CH_3	CH_3
β-	CH_3	H
γ-	H	CH_3
δ-	H	H

Figure 1 Tocotrienols and tocopherols

Structure of tocotrienols and tocopherols. The different forms α-, β-, γ- and δ-tocochromanol are illustrated in the table on the right. The number and position of methyl-groups on the aromatic head group are indicated by residues R1 and R2.

1.2.1 Antioxidative Properties of Tocochromanols

Besides the vitamin E activity, tocochromanols are powerful antioxidants. They are able to scavenge ROS and predominantly prevent the propagation of lipid oxidation (Mesa and Munné-Bosch, 2023). Unsaturated fatty acids are a destinated target of free radicals, leading to a chain reaction of fatty acid autooxidation. Thereby, a fatty acid radical is generated, which forms a peroxyl radical in presence of oxygen. By the abstraction of hydrogen from another fatty acid, a hydroperoxide and another fatty acid radical are formed and lipid peroxidation propagates (Schneider, 2005). Antioxidants, such as tocochromanols, can break this propagation since they reduce peroxyl radicals considerably faster than unsaturated lipids (Buettner, 1992; Traber and Stevens, 2011). The mechanism is well studied for α-tocopherol, whereby the chromanol ring confers antioxidant properties by donating a hydrogen from its hydroxyl group (Kamal-Eldin and Appelqvist, 1996). This involves further reduction of the lipid peroxyl radicals into lipid hydroperoxides by α-tocopherol, generating an α-tocopheroxyl radical. Subsequently, ascorbic acid regenerates α-tocopherol by reduction of the α-tocopheroxyl radical (Blaner et al., 2021).

Naturally, tocochromanols protect the thylakoid membranes of photoautotrophic organisms from ROS and lipid oxidation. They are involved in specialised functions in the maintenance of the photosystems and their protection against singlet oxygen and superoxides under high light stress (Szymańska and Kruk, 2010). Humans and animals require dietary supplementation

with tocochromanols. Hereby, α-tocopherol is the most prevalent form of tocochromanols, due to its greater bioavailability (Hsu et al., 2019). Nevertheless, intestinal uptake of all tocochromanol forms is rather unspecific, for instance, the γ-tocopherol uptake is equate with α-tocopherol (Valentin and Qi, 2005). Furthermore, γ-tocopherol has been shown to exhibit even superior detoxifying properties (Cooney et al., 1993). In mammals, however, γ-tocopherol has only a low double-digit vitamin E activity compared to α-tocopherol due to mammalian storage and distribution processes (Traber and Sies, 1996; Valentin and Qi, 2005). In humans, all forms of tocochromanols and other lipophilic compounds form micelles that are absorbed by intestinal cells. More importantly, the preference for α-tocopherol is due to the α-tocopherol transfer protein (α-TTP). At 100 % affinity for α-tocopherol and α-TTP, the affinity for γ-tocopherol is only 9 % and for α-tocotrienol 12 % (Miyazawa et al., 2019). However, extensive neuroprotective, cholesterol-lowering and anti-cancer properties have been associated with tocotrienols (Khanna et al., 2005). More recently, research of the antioxidant capacity of other tocochromanol forms has increased. It has been shown, that δ-tocotrienol significantly reduces anti-proliferative properties in various cell types and stimulates the downregulation of gene expression of pro-inflammatory cytokines (Qureshi, 2022). Moreover, δ-tocotrienol is involved in the downregulation of the 3-hydroxy-3-methylglutaryl-coenzyme A (HMG-CoA) reductase and thereby reduces the secretion of β-amyloid and cholesterol biosynthesis (Wei et al., 2022). *In vitro* experiments have demonstrated even higher capabilities of tocotrienols to scavenge free radicals and the reduction of lipid peroxidation, compared to tocopherols (Cahoon et al., 2003). Thus, these properties make tocotrienols valuable candidates to complement the prevailing α-tocopherol antioxidant market. Another fact is that the chemical industry is producing antioxidants such as butylated hydroxytoluene and propyl gallate in large quantities for the food industry due to their antioxidant properties. Opposed to this, nowadays, the trend is towards the sustainable production of natural antioxidants (Oswell et al., 2018). Consequently, all natural tocochromanols are of great interest to the cosmetic, food, feed and pharmaceutical industries.

1.2.2 Natural Tocochromanol Biosynthesis

Tocochromanols are predominantly synthesised by photosynthetic organisms and their biosynthesis is conserved between plants and cyanobacteria (Cheng et al., 2003). Therefore, this section focuses on tocochromanol biosynthesis in these organisms (Figure 2). The condensation of the aromatic head group with the polyprenyl side chain is performed by enzymes of the prenyltransferases family. The aromatic moiety homogentisic acid (HGA) derives from hydroxyphenylpyruvate (HPP) and is converted by the HPPD in *A. thaliana* (Norris et al., 1998). Phytyl diphosphate (PDP) is the second substrate in tocopherol synthesis. It was originally proposed that PDP derives from the reduction of geranylgeranyl diphosphate (GGPP) by a geranylgeranyl reductase (GGR) (Keller et al., 1998). However, the identification and characterisation of two kinases in *A. thaliana* (VTE5 and VTE6) has revealed another pathway as the primary route of PDP biosynthesis (Valentin et al., 2006; vom Dorp et al., 2015). Naturally, phytol is the prenyl side chain of chlorophyll. It is released from chlorophyll by hydrolysis, making phytol one of the most prevalent isoprenoid compounds (Gutbrod et al., 2019). Subsequently, two sequential phosphorylation steps convert phytol to phytyl monophosphate (PMP) and PMP to PDP. The first tocochromanol intermediate is formed by the condensation of HGA and GGPP or HGA and PDP, generating 2-methyl-6-geranylgeranyl-1,4-benzoquinol (MGGBQ) or 2-methyl-6-phytyl-1,4-benzoquinol (MPBQ), respectively (Collakova and DellaPenna, 2001). This reaction is catalysed by the homogentisate geranylgeranyl transferase (HGGT) or the homogentisate phytyl transferase (HPT), which differ in their substrate specificity regarding the isopentenyl substrate (Chen et al., 2006). Generally, monocots such as barley, wheat and rice rather contain genes encoding for HGGTs. Opposed to this, dicots predominantly express HPTs. Conclusively, tocotrienol-rich environments such as seeds exhibit a high expression of HGGTs (Collakova and DellaPenna, 2001; Cahoon et al., 2003). Naturally, tocotrienols are absent in *A. thaliana* leaves, whereas the transgenic expression of a HGGT of barley enabled tocotrienol accumulation in *A. thaliana* (Cahoon et al., 2003). This illustrates the mutual applicability of the enzymes of the following tocochromanol pathway.

Further conversion of the tocochromanol intermediates involves cyclisation of the chromanol ring and methylation of the aromatic head group. These processes are shared by the tocotrienol and tocopherol biosynthetic pathways (Cahoon et al., 2003). Figure 2 illustrates these reactions using the natural tocopherol biosynthetic pathway in plants as an example. Starting from MPBQ, the MPBQ methyltransferase (MPBQMT) transfers a methyl group from

S-adenosylmethionine (SAM) to the aromatic head group, generating 2,3-dimethyl-5-phytyl-1,4-benzoquinone (DMPBQ). The TC directly forms a chromanol ring within the two precursors, MPBQ and DMPBQ, producing δ-tocopherol and γ-tocopherol, respectively (Porfirova et al., 2002). Parallel to this, a second methyltransferase is essential for further conversion to β- and α-tocopherol. The γ-tocopherol methyltransferase (γ-TMT) can utilise both precursors and transfers another methyl group. Hereby, β-tocopherol is generated from δ-tocopherol and γ-tocopherol is converted to the 3-fold methylated α-tocopherol. The biosynthesis of all forms of tocotrienol proceeds analogously, using the same enzymes and starting from MGGBQ and DMGGBQ (DellaPenna and Pogson, 2006).

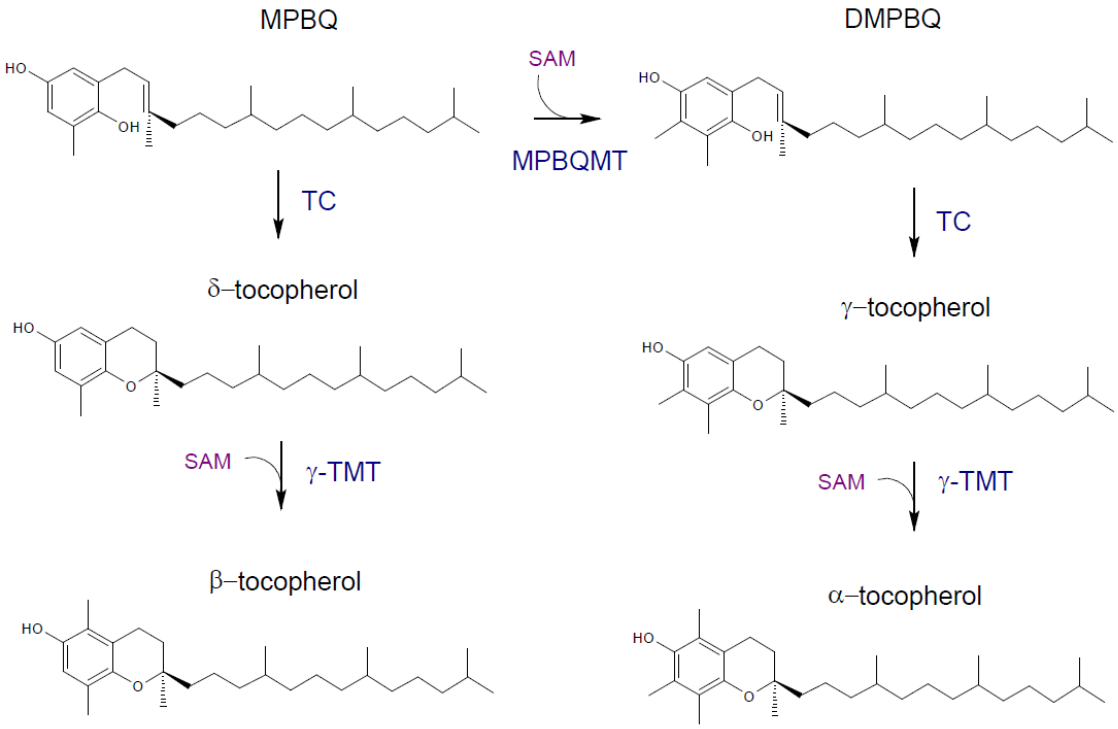

Figure 2 Tocopherol biosynthetic pathway

The biosynthesis of all 4 tocopherol forms in plants starts from MPBQ. No further methylation is required for δ-tocopherol biosynthesis and the TC directly forms the chromanol ring. Subsequent methylation by the γ-TMT leads to β-tocopherol formation. For the biosynthesis of γ- and α-tocopherol, MPBQ is first methylated by the MPBQMT, before the chromanol ring is formed by TC. Then, methylation by the γ-TMT leads to the conversion of γ-tocopherol to α-tocopherol. DMPBQ, 2,3-dimethyl-5-phytyl-1,4-benzoquinone; MPBQ, 2-methyl-6-phytyl-1,4-benzoquinol; MPBQMT, MPBQ methyltransferase; SAM, S-adenosylmethionine; TC, tocopherol cyclase; γ-TMT, γ-tocopherol methyltransferase.

1.3 Metabolic Engineering of *S. cerevisiae*

The basic concept of the metabolic engineering strategy for the *de novo* biosynthesis of tocochromanols in *S. cerevisiae* is illustrated in Figure 3. Glucose is the main, quickly accessible carbon source for the metabolism of *S. cerevisiae* and therefore a source of energy and a key building block for the construction of more complex metabolites (Newcomb et al., 2003; Kayikci and Nielsen, 2015). In this study, the precursors HGA and GGPP are required for the biosynthesis of δ-tocotrienol and other tocotrienol forms. Thereby, the native aromatic amino acid biosynthesis pathway and the isopentenyl diphosphate biosynthesis pathway will be employed to produce both precursors. Furthermore, the heterologous tocochromanol pathway will be introduced into *S. cerevisiae* for the biosynthesis of δ-tocotrienol (Figure 3).

Within this engineering strategy, glucose is utilised to supply the aromatic amino acid pathway with phosphoenolpyruvate (PEP) and erythrose-4-phosphate (E4P) for the biosynthesis of HGA. Thereby, glucose catabolism is utilised to supply PEP directly from glycolysis to the aromatic amino acid pathway (Fuller and Kim, 2021). On the other hand, E4P is generated by the pentose phosphate pathway (PPP), which consumes glucose in form of glucose-6-phosphate (G6P), providing E4P and the important reducing power nicotinamide adenine dinucleotide (NADPH) (Liu et al., 2019). Moreover, the glucose dissimilation feeds the acetyl coenzyme A (acetyl-CoA) pool, which is required by the isopentenyl diphosphate (IPP) biosynthetic pathway for further synthesis of GGPP. Acetyl-CoA is synthesised in different cellular compartments in *S. cerevisiae*. For cytosolic acetyl-CoA biosynthesis, the pyruvate dehydrogenase (PDH) bypass is utilised through the pyruvate decarboxylase converting glycolytic pyruvate into acetaldehyde (Pronk et al., 1996; Liu et al., 2017). Further formation into acetate is performed by the acetaldehyde dehydrogenase, Ald6p, using nicotinamide adenine dinucleotide phosphate ($NADP^+$) as cofactor. The final conversion to acetyl-CoA by the acetyl-CoA synthase requires adenosine triphosphate (ATP) (Schadeweg and Boles, 2016). However, it must be considered that competing pathways consume pyruvate and acetate, and ethanol biosynthesis often limits cytosolic acetyl-CoA biosynthesis (Krivoruchko et al., 2013).

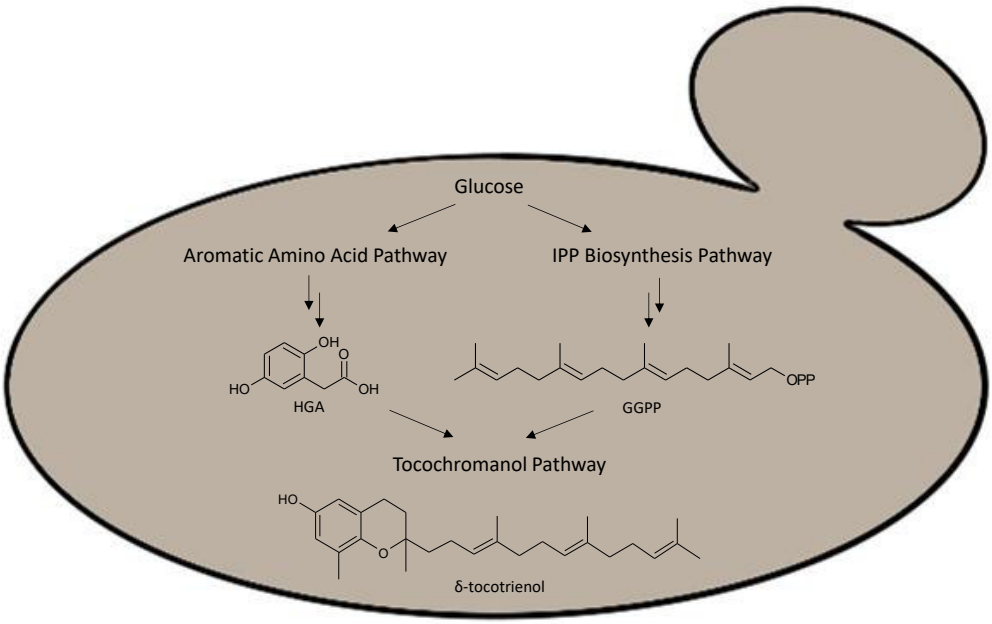

Figure 3 *De novo* tocochromanol biosynthesis in *S. cerevisiae*

Scheme of the yeast *S. cerevisiae* giving an overview of the metabolic strategy for the *de novo* biosynthesis of tocochromanols. Glucose is utilised as carbon source to feed the two precursor pathways, the aromatic amino acid pathway and the IPP pathway. Hereby, the aromatic head group HGA and the isopentenyl side chain GGPP are synthesised for the further production of tocochromanols by the heterologous tocochromanol pathway. The first unmethylated form, δ-tocotrienol, is illustrated here as a representative of the group of tocochromanols. IPP, isopentenyl diphosphate; HGA, homogentisic acid; GGPP, geranylgeranyl diphosphate.

1.3.1 Homogentisic Acid Biosynthesis

The aromatic head group of the tocochromanols derives from the metabolite HGA. In *S. cerevisiae*, aromatic compounds are synthesised via the aromatic amino acid biosynthesis pathway (Gottardi et al., 2017). Specifically, the native tyrosine biosynthesis pathway can be employed for HGA biosynthesis, utilising the intermediate HPP as a precursor (Bauer, 2019). Figure 4 illustrates the relevant metabolic pathways for the tocochromanol biosynthesis. The route for HGA biosynthesis is illustrated within the green box. For the sake of clarity, the colour code of Figure 4 will be retained within this thesis and HGA related results will be presented in green in the results section.

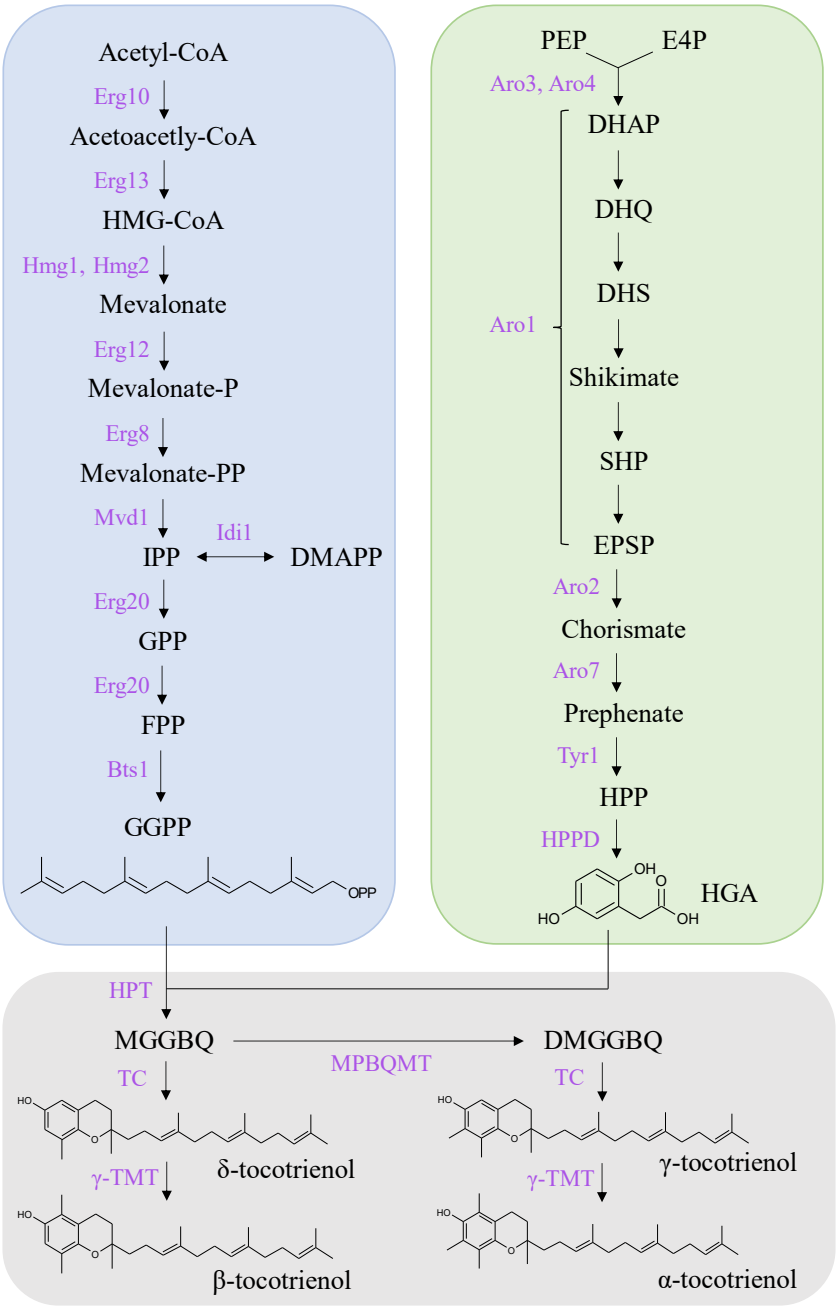

Figure 4 Metabolic pathways for tocochromanol biosynthesis

Overview of the relevant pathways for the tocotrienol biosynthesis in *S. cerevisiae*. The blue box inhabits the native mevalonate pathway and further isopentenyl diphosphate conversion into GGPP. The aromatic amino acid biosynthetic pathway combined with recombinant HPPD expression for HGA biosynthesis is shown in the green box. Further conversion of both precursors GGPP and HGA into all tocotrienol forms is illustrated by the heterologous tocotrienol pathway within the grey box. HMG-CoA, 3-hydroxy-3-methylglutaryl-CoA; mevalonate-P, mevalonate-5-phosohat; mevalonate-PP, mevalonate diphosphate; IPP, isopentenyl diphosphate; DMAPP, dimethylallyl diphosphate; GPP, geranyl diphosphate; FPP, farnesyl diphosphate; GGPP, geranylgeranyl diphosphate; PEP, phosphoenolpyruvate; E4P, erythrose-4-phosphate; DAHP 3-deoxy-D-arabino-heptulosonate-7-phosphate; DHQ, 3-dehydroquinate; DHS, 3-dehydroshikimate; SHP, shikimate-5-phosphate; EPSP, 5-enolpyruvylshikimate-3-phosphate; HPP, 4-hydroxyphenylpyruvate; HGA, homogentisic acid; MGGBQ, 2-methyl-6-geranylgeranyl-1,4-benzoquinol, DMGGBQ, 2,3-dimethyl-5-geranylgeranyl-1,4-benzoquinone.

The metabolic route initiates with the shikimic acid pathway utilising PEP and E4P for the synthesis of chorismate, which is the common precursor of the aromatic amino acids, tryptophan, phenylalanine and tyrosine (Paravicini et al., 1989; Gold et al., 2015). The 3-deoxy-D-arabino-heptulosonate-7-phosphate (DAHP) synthase catalyses the first enzymatic step of the shikimic acid pathway. By this step, PEP and E4P are condensed to DAHP (Liu et al., 2019). Thereby, E4P was shown to be the limiting substrate (Schnappauf et al., 1998a; Liu et al., 2019). There are two isoforms of the DAHP synthase which are encoded by *ARO3* and *ARO4* in *S. cerevisiae*. (Braus, 1991; Schnappauf et al., 1998a). The overall protein sequence of both isoforms is highly similar. However, each isoform is individually feedback-inhibited. Phenylalanine inhibits Aro3p, whereas Aro4p is feedback-regulated by tyrosine (Paravicini et al., 1989; Hartmann et al., 2003). Here, the introduction of the feedback-resistant variants $ARO3^{K222L}$ and $ARO4^{K229L}$ enhances the aromatic amino acid biosynthesis in yeast (Hartmann et al., 2003; Reifenrath and Boles, 2018). The following catalytic steps from DAHP to chorismate are carried out by the pentafunctional enzyme Aro1p. Chorismate defines the node for the tryptophan biosynthesis pathway and the phenylalanine-tyrosine branch on the other side (Braus, 1991; Schnappauf et al., 1998b). Here, the deletion of the anthranilate synthase, which is encoded by *TRP2* leads to tryptophan auxotrophy, directing the metabolic flux into the phenylalanine-tyrosine branch (Miozzari et al., 1978; Reifenrath and Boles, 2018). This pathway is initiated by the chorismate mutase Aro7p, catalysing the formation of chorismate to prephenate (Reifenrath et al., 2018). Prephenate is the last common precursor before the phenylalanine biosynthetic pathway branches out, while the dehydrogenase reaction from prephenate to HPP is carried out by Tyr1p within the tyrosine branch (Mannhaupt et al., 1989). This branch can be enriched by the deletion of the gene encoding the competing prephenate dehydratase (*PHA2*) (Reifenrath and Boles, 2018). Furthermore, additional deletions of downstream processes, such as the amino acid degradation in the Ehrlich pathway, further direct the flux into the desired branch (Hazelwood et al., 2008). Namely, deletion of the genes encoding the aromatic aminotransferase I (*ARO8*), the aromatic aminotransferase II (*ARO9*) and the phenylpyruvate decarboxylases (*ARO10* and *PDC5*), as it was shown by Reifenrath and Boles (2018).

Subsequently, the heterologous hydroxyphenylpyruvate dioxygenase (HPPD) can be introduced into the genome of *S. cerevisiae* to enable the reaction from HPP to HGA (Bauer, 2019). The widespread occurrence of this α-keto dependent oxygenase in several species comes along with different functions. In animals, the HPPD is directly involved in the tyrosine catabolic pathway, whereas plants utilise the HPPD for the synthesis of tocochromanol and

plastoquinone (Garcia et al., 1997; Moran, 2014). Natively, *S. cerevisiae* does not own a gene encoding for a HPPD, and thus recombinant protein expression of the HPPD is essential for its synthesis of tocochromanols. By virtue of that, one advantage of the host *S. cerevisiae* is the absence of potential HGA degradation pathways. The HPPD is a Fe(II)-dependent oxygenase, reducing molecular oxygen for the decarboxylation of HPP (Moran, 2005). The α-keto group of the HPP itself is utilised as electron donor for this reaction. Hereby, the HPP is decarboxylated and hydroxylated yielding HGA (Moran, 2014). Consequently, the aromatic amino acid pathway of *S. cerevisiae* is a valuable route to supply HGA to the heterologous tocochromanol pathway.

1.3.2 Isopentenyl Diphosphate Biosynthesis

GGPP is the precursor of the isopentyl chain in tocotrienols. In *S. cerevisiae* it is produced natively from the isoprenoid biosynthesis pathway. The blue box in Figure 4 illustrates the endogenous mevalonate pathway and further conversion by the isopentenyl diphosphate biosynthesis into GGPP. This compatible colour code has been adapted to present the GGPP related results in blue in the results section.

Acetyl-CoA is the building block of the preceding mevalonate pathway. First, the acetoacetyl-CoA thiolase, encoded by *ERG10*, transfers an acetyl group from one acetyl-CoA to another, producing acetoacetyl-CoA (Hiser et al., 1994; Zhou et al., 2018). Acetoacetyl-CoA is the substrate for the 3-hydroxy-3-methylglutaryl-CoA synthase (HMGS). The HMGS is encoded by *ERG13* and catalyses the formation of HMG-CoA, which is further reduced to mevalonate by the HMGCR. Two molecules of NADPH provide the reducing power for this reaction (Grabińska and Palamarczyk, 2002). Due to the whole-genome duplication (WGD) event in the ancestral lineage of *S. cerevisiae,* two isoforms, *HMG1* and *HMG2,* are responsible for this reaction (Hampton and Rine, 1994; Kellis et al., 2004). What is more important, the HMGCR has been identified as the rate-limiting enzyme in the mevalonate pathway. Consequently, HMGCR protein levels are highly regulated. Particularly, regulation of transcription, regulation at the translational level and protein degradation are the main mechanisms which control the HMGCR activity (Thorsness et al., 1989; Dimster-Denk et al., 1994; Hampton and Rine, 1994; Donald et al., 1997). While Hmg1p protein levels are quite stable, Hmg2p is rapidly degraded while it still remains in the ER (Hampton and Rine, 1994). Therefore, *HMG1* is the main target for biotechnological improvement of the mevalonate pathway. A truncated version of the *HMG1* is known to be feedback-resistant and is therefore widely used in biotechnology (Donald

et al., 1997). The following enzyme, the mevalonate kinase, is encoded by *ERG12* and further activates mevalonate by the consumption of ATP (Oulmouden and Karst, 1991). A further ATP is required for a second phosphorylation step by the phosphomevalonate kinase Erg8p. Hereby, mevalonate diphosphate (MPP) is synthesised (Tsay and Robinson, 1991). The final step of the IPP synthesis is catalysed by the mevalonate diphosphate decarboxylase (*MVD1*). During this step, ATP is converted to ADP, and CO_2 is released. Hereby, IPP is generated from MPP (Cordier et al., 1999). The essential isopentenyl diphosphate:dimethylallyl diphosphate isomerase is encoded by *IDI1* (Anderson et al., 1989). IPP and its isomer dimethylallyl diphosphate (DMAPP) are the key building blocks of all naturally occurring isoprenoids and are therefore valuable precursors for many molecules (Ma et al., 2023). Sequential condensation reactions of these lead to the formation of geranyl diphosphate (GPP), farnesyl diphosphate (FPP) and geranylgeranyl diphosphate (GGPP). Hereby, the farnesyl diphosphate synthase, encoded by *ERG20* and the geranylgeranyl diphosphate synthase (Bts1p) enable the biosynthesis of the ubiquitous intermediates of monoterpenes (C_{10}), sesquiterpenes (C_{15}) and diterpenes (C_{20}) (Chang et al., 2013; Callari et al., 2018). Given the low efficiency of the Bts1p compared to competing enzymes, the overexpression of improved or recombinant variants is often considered (Ohnuma et al., 1994; Toyomasu et al., 2007; Xie et al., 2014; Chen et al., 2016; Callari et al., 2018). IPP-derived molecules are highly demanded for the biosynthesis of numerous chemicals. Thus, metabolic engineering of the mevalonate pathway, and further downstream proceedings are established and well known in *S. cerevisiae*. Major modifications are the truncation and overexpression of the *HMG1*, downregulation or deletion of the ergosterol branch, and the overexpression of *ERG20* and *BTS1* (Dai et al., 2012). Consequently, these genes are essential targets to be considered, to ensure a sufficient supply of GGPP for the tocochromanol biosynthesis.

1.3.3 Recombinant Tocochromanol Biosynthesis

The enzymes of the tocochromanol pathway need to be heterologously expressed in *S. cerevisiae*. The required recombinant tocotrienol biosynthesis pathway is illustrated in Figure 4 in the grey box. First, the aromatic head group and the polyprenyl chain are condensed by an enzyme from the prenyltransferase family. Thereby, the HGA and the polyprenyl diphosphates can be utilised by various prenyltransferases (Schledz et al., 2001). The substrate specificity varies considerably between different prenyltransferases. For instance, the homogentisate geranylgeranyl transferase (HGGT) often prefers GGPP as a substrate. These enzymes are frequently expressed in tocotrienol-rich tissues such as seeds of monocots (Yang et al., 2011). The homogentisate phytyltransferase (HPT) of *Synechocystis* sp. PCC 6803 (SynHPT) is well studied. The enzyme performs both, the condensation of HGA and GGPP to MGGBQ and of HGA and PDP to MPBQ, whereby the latter is preferred if both substrates are available (Collakova and DellaPenna, 2001). Consequently, a purposeful selection of a suitable prenyltransferase is essential depending on the desired product. Shen et al. (2020) characterised the recombinant expression of twelve HPT/HGGTs from plants in *S. cerevisiae*. However, none of them was successful. Thus, the *SynHPT* is predominantly expressed for recombinant tocochromanol biosynthesis. The second enzyme to be heterologously expressed is a tocopherol cyclase, which forms the chromanol ring of MGGBQ or MPBQ (Falk and Munné-Bosch, 2010). The expression of the tocopherol cyclase *VTE1* of *A. thaliana* (*AtVTE1*) in *E. coli* resulted in tocopherol and tocotrienol cyclase activity (Porfirova et al., 2002). Consequently, heterologous expression of a selected HPT and TC theoretically enables the biosynthesis of δ-tocotrienol in a microbial HGA and GGPP producer strain. The other tocochromanol forms differ in the methylation status on their chromanol ring. Thus, two methyltransferases are essential for further conversion into α-, β- and γ-tocochromanol.

The heterologous biosynthesis of tocochromanols was first achieved in recombinant *E. coli* by Albermann et al. (2008). Here, the recombinant expression of the *SynHPT* and *AtVTE1* enabled the biosynthesis of 15 µg/g dry cell weight (DCW) of δ-tocotrienol. Both, MGGBQ and δ-tocotrienol accumulated in the cell pellets, indicating the localisation of its lipophilic chain within the membrane. As the accumulation of the precursor MGGBQ was 15 times higher, the *AtVTE1* was considered to be the rate-limiting enzyme. Alternatively, the TC of *Synechocystis* was expressed in *E. coli*, but did not lead to any δ-tocotrienol production (Albermann et al., 2008). In addition to this, further strain engineering by stable integration of the heterologous enzymes did not result in the desired titers. An additional overexpression of the GGPP synthase

crtE of *X. dendrorhous* (*XdcrtE*) did not increase GGPP titers, suggesting that the precursor supply in *E. coli* was insufficient (Ghanegaonkar et al., 2012).

But it was more than a decade later until the fermentative biosynthesis of δ-tocotrienol was achieved in *S. cerevisiae*. Sun et al. (2020) heterologously expressed the *SynHPT* and the *AtVTE1* in a yeast strain with an enhanced GGPP precursor supply, reaching titers of 4.1 mg/L δ-tocotrienol in a 2 L fed-batch fermentation. Hereby, the truncation and overexpression of the *HMG1* and the overexpression of the GGPP synthase of *Sulfolobus acidocaldarius* (*SaGGPPS*) were performed to increase the GGPP precursor supply. However, the HGA biosynthetic branch was not improved and only the recombinant *HPPD* of *Pseudomonas putida* was integrated into the rDNA integration site (Sun et al., 2020). Lately, the scientific community indicates increasing interest in the fermentation-based biosynthesis of tocochromanols. Shen et al. (2020) generated a strain with an optimised precursor supply and utilised the heterologous *AtVTE1* and HPPD of *A. thaliana* (*AtHPPD*), *SynHPT* and the *XdcrtE* for the biosynthesis of 7.6 mg/g DCW of tocotrienols. Hereby, the identification of two functional active methyltransferases in *S. cerevisiae* enabled the biosynthesis of the other tocotrienol forms α-, β- and γ-tocotrienol. Moreover, optimisation of the fermentation process through a two-stage fermentation triggered by a cold-shock in a 5 L bioreactor led to the biosynthesis of 320 mg/L of total tocotrienols (Shen et al., 2020). Further pathway optimisation was performed by an increased NADPH supply and transcriptional regulation by the deletion of *MOT3* and *ROX1*. Additionally, putative transporters for the secretory production by a biphasic fermentation were described, yielding 25.57 mg/g DCW of all tocotrienol forms (Jiao et al., 2022).

In *E. coli* and *S. cerevisiae* only GGPP, the precursor of tocotrienols, is produced. Thus, a geranylgeranyl reductase (GGR) is essential for the conversion of GGPP into PDP, the precursor of tocopherols. First, the recombinant expression of the GGR of *Synechocystis (*ChlP*)* was not successful in *E. coli* (Albermann et al., 2008). A phylogenetic analysis and subsequent in vitro screening of GGR activity of 31 selected putative GGRs was performed by Meadows et al. (2018). Besides plant and cyanobacterial enzymes, a bacterial GGR of *Streptomyces coelicolor* was identified. Furthermore, it has been observed that complete reduction of all double bonds is more likely in isoprenoid alcohols (GGOH and FOH) compared to isoprenoid pyrophosphates (GGPP and FPP) (Meadows et al., 2018). However, a functional GGR for the complete reduction of GGPP has not been demonstrated in *S. cerevisiae* yet.

1.4 Aim of this Study

Tocochromanols are natural products bearing vitamin E activity and powerful antioxidative capacities. Previously, industrial production processes and extraction from natural products predominantly focused on α-tocopherol. However lately, the scientific community sees great potential in the antioxidative properties and beneficial traits that tocotrienols have to offer. These include higher antioxidant capacities, anti-cancer properties and anti-inflammatory traits, making tocotrienols valuable candidates to complement the antioxidant market (Cahoon et al., 2003; Qureshi, 2022; Wei et al., 2022). Nowadays, a sustainable synthesis of these natural products is essential. As natural products are also subject to natural fluctuations, their biosynthesis within a microbial host would provide independency over climatic conditions and crop. At the time this study was started, tocochromanol biosynthesis was only investigated in *E. coli* (Albermann et al., 2008). However, during the last few years the interest of the heterologous tocochromanol biosynthesis increased, representing the topicality and importance of this subject (Shen et al., 2020; Sun et al., 2020; Jiao et al., 2022).

The aim of the study was to successfully establish a tocochromanol biosynthesis pathway in a laboratory yeast strain (CEN.PK2-1C). Thereby, the metabolism of *S. cerevisiae* was engineered to accomplish tocotrienol biosynthesis on a laboratory scale. Furthermore, the identification of limitations within the pathways were essential for the development of strategies to overcome these constraints. Therefore, efficient routes for the synthesis of the precursors needed to be implemented. The upregulation of the aromatic amino acid biosynthesis and the characterisation of a recombinant HPPD were already addressed in a foregoing master thesis (Bauer, 2019). Consequently, the attention was first drawn on the provision of the second precursor GGPP. Therefore, metabolic engineering of the native mevalonate pathway and further optimisation for an enhanced isopentenyl diphosphate biosynthesis were performed. Then, the heterologous tocotrienol pathway needed to be introduced into *S. cerevisiae*. Thereby, characterisation of various recombinant enzymes was necessary. Beside the upregulation of essential pathways, limiting and competing processes had to be identified and restricted. As tocochromanols are lipid soluble compounds, their extraction was another challenge. Hereby, different extraction methods and the *in-situ* extraction with an organic overlay were characterised. After the successful generation of a tocotrienol producer strain, an evolutionary engineering approach was started. Hereby, the antioxidative capacity of δ-tocotrienol was utilised for the development of an evolutionary engineering method using ozone as selection pressure.

2 Materials and Methods

2.1 Microbiological Methods

2.1.1 Media

The experiments of this study were conducted with the yeast *S. cerevisiae.* The bacterium *E. coli* was utilised for subcloning. The microorganisms were cultivated in appropriate media, whose compositions are displayed in Table 1.

Table 1 Media and components

Microorganism	Media	Components and Reference
E. coli	Lysogeny broth (LB) (Lennox)	• 10 g/L Tryptone • 5 g/L Yeast Extract • 5 g/L NaCl pH 7.5 was adjusted (NaOH)
	Stable Outgrowth Medium	NEB (New England Biolabs) 10-beta/Stable Outgrowth Medium
	S.O.C. (super optimal broth with catabolite repression) medium	NEB S.O.C. outgrowth medium
S. cerevisiae	Yeast extract peptone (YP)	• 20 g/L Peptone • 10 g/L Yeast Extract • 20 g/L appropriate carbon source
	Synthetic complete medium (SCM)	• 1.7 g/L Yeast Nitrogen Base without Amino Acids and Ammonium Sulphate • 5 g/L Ammonium Sulphate • 20x Amino Acid and Nucleobase solution (Bruder et al., 2016) except for L-phenylalanine (76 mg/L), L-tryptophane (76 mg/L) and L-tyrosine (76 mg/L) • 20 g/L appropriate carbon source pH 6.3 was adjusted (KOH)
	Synthetic complete (SC)	• 1.7 g/L Yeast Nitrogen Base without Amino Acids and Ammonium Sulphate • Yeast Synthetic Drop-out medium according to the manufacture's preparation instructions • 20 g/L appropriate carbon source pH 6.3 was adjusted (KOH)
	Feeding medium	• 500 g/L Glucose • 9 g/L KH_2PO_4 • 2.5 g/L $MgSO_4$ • 3.5 g/L K_2SO_4

		• 0.28 g/L Na_2SO_4 10 ml/L Trace Element Solution and 1 ml/L Vitamin Solution according to van Hoek et al. (2000)
	Synthetic low fluorescent medium	• 6.9 g/L Yeast Nitrogen Base without Amino Acids and Ammonium Sulphate, without Folic Acid and without Riboflavin • 20x Amino Acid and Nucleobase solution (Bruder et al., 2016) • 2 % (w/v) Glucose

Solid medium was prepared by adding 19 g/L agar-agar. Prior to use, the media and carbon source were autoclaved separately. The Synthetic low fluorescent medium, trace element and vitamin solutions were sterile filtered. Appropriate carbon sources and antibiotics were added to the medium after autoclaving. The antibiotic stock solutions (1000x) were prepared according to the manufacturer with the concentrations mentioned in Table 2. These stock solutions were stored at -20 °C.

Table 2 Antibiotic stock solutions

Antibiotic	Antibiotic resistance	Concentration stock solution [mg/ml]	Target
Geneticin - G418 (K)	*KanMX*	200	antifungal
Nourseothricin - ClonNAT (N)	*ClonNAT*	100	
Hygromycin (H)	*hphNT1*	200	
Ampicillin	*AmpR*	100	antibacterial
Carbenicillin	*AmpR*	100	
Chloramphenicol	*CamR*	25	
Kanamycin	*KanR*	50	

2.1.2 Cultivation and Storage of *S. cerevisiae*

General cultivation and growth of *S. cerevisiae* was performed in YP medium with 20 g/L of glucose (YPD) at 30 °C. According to the selection marker, either the corresponding antibiotics (Table 2) were added to the medium, or appropriate selective synthetic complete medium (SCM or SC medium) was used. Uracil (-URA), L-leucine (-LEU) and L-histidine (-HIS) were omitted from the medium and used as selective auxotrophic markers. SCM medium was prepared as described in Table 1 and the following drop out compounds were added as required: L-histidine (19.2 mg/L), L-leucine (57.6 mg/L) and uracil (19.2 mg/L). Due to the change of laboratories, the experiments in the later stage of this work were performed in SC medium with appropriate commercially available drop out medium (Table 1). If not mentioned otherwise, sterile glucose

(D) was used as carbon source and added to SCM and SC medium (SCM-D, SC-D) after autoclaving to a final concentration of 2 % (w/v). For galactose-induced gene expression with *pGAL1,* galactose was added to the medium after autoclaving to a final concentration of 2 % (w/v). Strains were streaked on solid YPD agar plates for storage up to 1 month at 4 °C. For long term storage, verified strains were cultivated in YPD medium to stationary phase and stored at -80 °C in 25 % (v/v) glycerol. Growth measurements of liquid cultivations were performed by measuring the optical density (OD). A spectrophotometer was obtained to measure the OD at λ=600 nm (OD_{600}).

2.1.2.1 Shake Flask Fermentations of *S. cerevisiae*

S. cerevisiae strains were cultivated in SCM-D, SC-D or YPD medium, the corresponding medium of each experiment is mentioned within the experiment in the result section. Single colonies were inoculated for the characterisation of strains, while a mixture of transformants was utilised for plasmid-based approaches. Typically, cultures were grown in biological duplicates or triplicates. Pre-cultures were grown for 16 – 20 h. Then, the cultures were washed with sterile double-distilled water (ddH_2O) and each culture was inoculated to an OD_{600} of 0.1 in 50 ml medium (300 ml sterilised flasks). If *pGAL1* was used for galactose induced gene expression, pre-cultures were grown in medium containing 2 % (w/v) glucose. After two washing steps, cultures were inoculated to an OD_{600} of 3 in appropriate medium containing 2 % (w/v) galactose. Shake flask cultivations were cultivated at 200 rpm and 30 °C for 144 h if not described otherwise. Usually, samples were taken at 0, 24, 48, 72, 96, 120 and 144 h under sterile conditions. Moreover, growth determination was performed by measurement of the OD_{600} in a spectrophotometer. 2 ml samples of the culture were taken for intra- and extracellular metabolite analysis (described in 2.3.1).

2.1.2.2 *In-situ* Extraction during Fermentations

Shake flask fermentations with an organic solvent for the *in-situ* extraction of metabolites were generally performed as described in 2.1.2.1. It was shown that dodecane does not impair the cultivation of *S. cerevisiae* (Asadollahi et al., 2008; Henritzi et al., 2018). Therefore, a 30 % (v/v) dodecane overlay was added to the medium (Hitschler and Boles, 2020). Usually, the cells were inoculated from their preculture to an OD_{600} of 0.1 in 40 ml fresh medium (SCM-D or SC-D) in 300 ml flasks. Then, the 30 % dodecane overlay (12 ml) was added to the flasks under

aseptic conditions. Samples of the dodecane phase were taken additionally to the culture samples at the end of the fermentation.

2.1.2.3 Online Biomass Monitoring by Cell Growth Quantifier (CGQ)

Detailed biomass formation of liquid cultures was monitored by the CGQ system from Scientific Bioprocessing, former Aquilabiolabs. The procedure, which is based on backscatter light measurements was performed according to the manufacturer's instructions. Data evaluation was performed with the software DOTS (Scientific Bioprocessing).

2.1.2.4 Shake Flask Fermentation and Fluorescence Intensity Measurement

Following transformations of CEN.PK2-1C with vectors bearing *YFP-Venus* under the control of artificial promoters and their corresponding controls, shake flask cultivations were performed in SCM-D$_{-URA}$ medium. Pre-cultures were grown for 24 h. Then, the cultures were inoculated to an OD_{600} of 0.8 in 25 ml medium (300 ml sterilised flasks) and cultivated for 24 h. The cultivations were performed as biological duplicates and subsequent fluorescence intensity measurement were performed with technical triplicates in 96-well plates. For this, 20 µl of each culture was diluted with 180 µl fresh SCM-D$_{-URA}$ medium in 1 well. The fluorescence intensity was analysed at 497 nm excitation / 540 nm emission and the OD_{600} values were measured in a plate reader. The relative fluorescence signal was normalised to the OD_{600}. Furthermore, all signals were normalised to the control, *pPGK1,* which was set to 1.

2.1.2.5 Fed-Batch Fermentation

A 250 ml bioreactor (*MiniBioreactor*, Applikon) was utilised for fed-batch fermentations, according to the manufacturer's instructions. Precultures, grown in shake flasks to exponential phase were used for inoculation (OD_{600} 1). The fermentation was started with 50 ml SC-D medium for a 24 h batch phase. Subsequently, the fed-batch was performed by adding 1.5 ml of the feeding medium (Table 1) with a feeding period of 1 h over 3 days. KOH was used for pH control, which was usually offset at pH 5.5. The setpoint for dissolved oxygen was set at 40 %. Samples were taken every 24 h under sterile conditions. Biomass formation was determined by measurement of the OD_{600} in a spectrophotometer and 2 ml samples of the culture were taken for metabolite analysis.

2.1.2.6 Cultivation for Fluorescence Microscopy

CEN.PK2-1C transformants, carrying vectors with GFP-tagged constructs, were cultivated in 50 ml synthetic low fluorescent medium in 300 ml flasks for 24 h. The genes of interest were fused to a linker and the envy-GFP at the C-terminus based on the plasmid FDG97. Subsequently, preparation of the cultures and fluorescence microscopy were performed according to Tamayo Rojas et al. (2021). Visualisation of the mitochondria was enabled by a MitoTracker™ according to the manufacturer's protocol.

2.1.3 *S. cerevisiae* Strain Construction

For the precise genetic engineering of *S. cerevisiae,* the native DNA repair machinery for homologous recombination was employed. Based on this mechanism, CRISPR/Cas9 approaches or stable integration by co-integration of marker genes were performed. A donor DNA was utilised as a template for homologous recombination. Furthermore, a randomized approach was conducted for evolutionary engineering by ozone treatment. Table 3 displays all *S. cerevisiae* strains which were employed during this study, while the strains generated during the evolutionary engineering are presented in the results section.

Table 3 *S. cerevisiae* strains used in this work

Strain	Parent Strain	Characteristics	Reference
CEN.PK113-7D		*MATa; MAL2-8c; SUC2*	Laboratory stock, Prof. Dr. Boles
CEN.PK2-1C		*MATa; MAL2-8c; SUC2; ura3-52; leu2-3,112; trp1-289; his3-Δ1;*	Laboratory stock, Prof. Dr. Boles
MRY33	CEN.PK2-1C	*TRP1, aro4Δ::pHXT7-ARO1-tCYC1, ura3Δ::pTPI1-ARO4^{fb-}-tARO4_pHXT7-ARO3^{fbr}-tCYC1, aro10Δ, aro8Δ, pdc5Δ, trp2Δ, aro9Δ, pha2Δ*	Reifenrath and Boles (2018)
JBY2	MRY33	*pyk2Δ::pPGK1-YlHPPD-tFBA1*	Bauer (2019)
JBY3	JBY2	*hmg1Δ::pTDH3-HMG1$^{tr[1573–3165]}$*	This study
JBY4	JBY3	*perg9Δ::pERG1*	This study
JBY5	JBY3	*leu2Δ::pPGK1-BTS1-tADH1_ClonNAT*	This study
JBY6	JBY4	*leu2Δ::pPGK1-BTS1-tADH1-pTEF_ClonNAT*	This study
JBY9	JBY6	*rox1Δ::pTEF2-ERG20-tENO2*	This study
JBY10	JBY4	*leu2Δ::pESK110-ERG20-tENO1-AP8-BTS1-tSSA1_ClonNAT*	This study
JBY11	JBY4	*leu2Δ::AP8-SynHPT-tPGK1-AP6-AtVTE1-tTDH_ClonNAT*	This study
JBY12	JBY11	*ChrIV-49293-49345Δ::AP7-BTS1-tADH1_LEU2*	This study

JBY13	JBY11	*ChrIV-49293-49345Δ::pRPL18B-PaGGPPS-tSSA1_LEU2*	This study
JBY14	JBY11	*ChrIV-49293-49345Δ::pRPL18B-SaGGPPS-tSSA1_LEU2*	This study
JBY15	JBY11	*ChrIV-49293-49345Δ::AP11-PaGGPPS-tSSA1-AP7-ERG20-tENO1_LEU2*	This study
JBY16	JBY6	*ChrIV-49293-49345Δ::AP7-BTS1-tADH1_LEU2*	This study
JBY17	JBY4	*leu2Δ::AP8-SynHPT-tPGK1-pPGK1-AtVTE1$^{tr[142-1467]}$-tTDH1_ClonNAT*	This study
JBY18	JBY17	*ChrIV-49293-49345Δ::AP7-BTS1-tADH1_LEU2*	This study
JBY20	JBY17	*ChrIV-49293-49345Δ::pTDH3-XdcrtE-tSSA1*	This study
JBY21	JBY4	*leu2Δ::pPGK1-AtVTE1$^{tr[142-1467]}$-tTDH1-AP8-NosHPT-tADH1-pTEF_ClonNAT*	This study
JBY22	JBY21	*ChrIV-49293-49345Δ::AP7-BTS1-tADH1_LEU2*	This study
JBY23	JBY17	*ChrIV-49293-49345Δ::pTEF1-ERG20-tENO1-pTDH3-BTS1-tSSA1_LEU2*	This study
JBY24	JBY17	*ChrIV-49293-49345Δ::pTEF1-ERG20-tENO1-pTDH3-XdcrtE-tSSA1_LEU2*	This study
JBY57	JBY20	*dpp1Δ*	This study
JBY58	JBY17	*ChrIV-49293-49345Δ::pTDH3-BTS1^{co}-tSSA1_LEU2*	This study
JBY59	JBY17	*ChrIV-49293-49345Δ::pTDH3-PaGGPPS-tSSA1_LEU2*	This study
JBY61	JBY4	*ChrIV-49293-49345Δ::pTDH3-XdcrtE-tSSA1_LEU2*	This study
JBY62	JBY4	*leu2Δ::pPGK1-XdcrtI-tTDH1-pTEF1-XdCrtYB-tENO2-ClonNAT*	This study
JBY63	JBY62	*ChrIV-49293-49345Δ::pTDH3-XdcrtE-tSSA1_LEU2*	This study
JBY66	JBY63	*dpp1Δ*	This study
JBY67	JBY20	*dpp1Δ::pPGK1-AtVTE1$^{tr[142-1467]}$-tTDH1-AP8-SynHPT-tADH1-pTEF*	This study
JBY68	JBY20	*ChrIV-53688-53756Δ::pPGK1-AtVTE1$^{tr[142-1467]}$-tTDH1-AP8-SynHPT-tADH1*	This study
JBY69	JBY67	*ClonNATΔ::pTEF1-AtMPBQMT$^{tr-[153-864]}$-tENO1_pHFF2-Atγ-TMT$^{tr[121-1047]}$-tENO2*	This study
JBY70	JBY67	*ClonNATΔ*	This study

2.1.3.1 Preparation of Competent *S. cerevisiae* Cells and Transformation

The protocol of Gietz and Schiestl (2007) was applied for the preparation of competent yeast cells and transformations of *S. cerevisiae* with expression plasmids, linearized integration vectors and CRISPR/Cas9 plasmids with the corresponding donor DNA. The protocol was utilised with the following modifications: yeast cultures were grown in 50 ml YPD medium and harvested during the exponential phase (OD_{600} 0.5 - 1). Furthermore, a storage mix of the transformation mix was prepared according to Table 4, stored at 4 °C, and used for up to

3 months. 306 µl of the storage mix were used for each transformation and mixed with 500-1500 ng DNA. Next, the mixture was filled up to 360 µl with sterile ddH_2O and added to the cells. If the procedure was applied for genetic engineering by CRISPR/Cas9, the yeast cells were regenerated for 5 h in 5 ml YPD medium at 30 °C, before plated on appropriate selective agar plates. The transformants were incubated at 30 °C for 3-5 days.

Table 4 Transformation mixture

Component	Stock concentration	Volume storage mix [µl]	Volume per transformation [µl]
PEG 4000	50 % (w/v)	5200	260
Lithium Acetate	1.0 M	720	36
Single stranded carrier DNA	2 mg/mL	200	10

2.1.3.2 Screening of the Transformants

A mixture of transformants following plasmid-based transformations was directly used for inoculation in shake flasks as described in section 2.1.2.1. Transformants with genome-based modifications as integrations and deletions were verified in a screening process. Therefore, single colonies were isolated twice by streaking on appropriate fresh agar plates. The genomic DNA of an individual colonies was isolated as described in 2.1.6.1 and verified by PCR and sequencing (2.2.2 and 2.2.5).

2.1.3.3 CRISPR/Cas9

To target specific genomic regions, a plasmid-based CRISPR/Cas9 system was utilised. The construction of the CRISPR/Cas9 plasmids was performed according to Generoso et al. (2016). All constructed CRISPR/Cas9 plasmids with their genomic target and corresponding guide DNA are displayed in Table 5. The specific CRISPR guide RNA was designed online with the *CRISPR gRNA design tool* (ATUM) and ordered as oligomers with overlapping regions for the backbone vector, pRCC-K or pRCC-N. Subsequently, CRISPR/Cas9 plasmids were built by PCR and Gibson assembly. When *S. cerevisiae* was transformed with a CRISPR/Cas9 plasmid, a corresponding donor DNA was used as a template for the DNA repair by homologous recombination. The donor DNA contained overlapping regions of 45 bp on each side, homologous to the integration site.

Table 5 CRISPR/Cas9 Plasmids

Name	Backbone	Target	Guide DNA sequence
JBV27	pRCC-K	*pERG9*	TATAAATGGAAAGTTAGGAC
JBV28	pRCC-N	*HMG1*	GGACGTCAAACGGGTCTGCT
JBV70	pRCC-K	Upstream of the *HO* locus: *ChrIV 49293-49345Δ* (wt) and *ChrIV 53688-53756Δ* (JBY20), respectively	AGTACAGTGCCCTGAGCGTA
JBV169	pRCC-K	*DPP1*	ACATCTGAATCGTCCATCAA
JBV188	pRCC-K	*ClonNAT*	TACTCTAAAGACGGTGTCGG

2.1.3.4 Evolutionary Engineering

An ozone treatment was performed as selection pressure for evolutionary engineering of *S. cerevisiae* for higher tocochromanol production. The strain to be engineered was cultivated to exponential phase in SC-D medium. Then, the cells were harvested (5 min, 3000 g, room temperature (RT)) and washed with sterile ddH_2O. The ozone treatment was performed in 96-well plates and the cells were inoculated to an OD_{600} of 1.5 in 100 µl sterile ddH_2O. The ozone generator (AQUARIZON 4.0) was used to generate an ozone gas flow. Dry air was pumped into the generator with a stable flow, controlled by a pressure valve. The 10-level potentiometer was set to level 10 and the air fumigated through the generator with a stable air flow of 2 L/min. This corresponds to a maximum ozone entry of 4 g/h, according to the manufacturer. With these conditions set, the variable factor was the time of ozone exposure. The gas flow was conducted through an ozone-stable tube and a sterile pipette tip into the well bearing the culture. The sterile pipette tip was exchanged after each sample to maintain an aseptic environment and prevent carryover. The ozone treatment was performed for different lengths of time, which were increased during the evolutionary engineering process. After the ozone treatment, the treated cells of each well were inoculated in 25 ml fresh SCD medium, each. These cells were cultivated until grown to exponential phase (usually 2-4 days). The cultures which survived the longest time of ozone exposure were kept and used for the next round of ozone treatment.

2.1.4 Plasmids

Table 6 displays the plasmids which were used during this study. Usually, the Golden Gate system (2.2.4.1) was used for the cloning of genes into storage, expression, or integration vectors as indicated. Gibson assembly (2.2.4.2) was utilised for the construction of the CRISPR/Cas9 plasmids and certain other plasmids. Appropriate enzymatic restriction digests

were performed to screen the assembled plasmids. Restriction enzymes were obtained from NEB and applied according to the protocols of the manufacturer. Furthermore, the verification of the correct DNA sequence was validated by sequencing (2.2.5).

Table 6 Plasmids

Name	Characteristics	Reference
FGD97	Localisation plasmid for gene expression with a GFP tag: *CEN6, ARS4, ColE1, URA3, pMET25-linker-GFPenvy-tCYC1, AmpR*	Laboratory Stock, Prof. Dr. Boles
LBGV22	Golden Gate backbone plasmid: *ConLS, GFP-dropout, ConRE, URA3, CEN6, ARS4, KanR, ColE1*	Laboratory Stock, Prof. Dr. Boles
LBGV23	Golden Gate backbone plasmid: *ConLS, GFP-dropout, ConRE, LEU2, CEN6, ARS4, KanR, ColE1*	Laboratory Stock, Prof. Dr. Boles
LBGV24	Golden Gate backbone plasmid: *ConLS, GFP-dropout, ConRE, HIS3, CEN6, ARS4, KanR, ColE1*	Laboratory Stock, Prof. Dr. Boles
MRV110	p426HXT7, *ARO7*	Laboratory Stock, Prof. Dr. Boles
MRV135	p426HXT7, $ARO7^{G141S}$	Laboratory Stock, Prof. Dr. Boles
p425MET25	*2µ, LEU2, AmpR, pMET25, tCYC1*	Mumberg et al. (1994)
p426HXT7	*2µ, URA3, AmpR, pHXT7, tCYC1*	Hamacher et al. (2002)
pGG2.4	Golden Gate storage plasmid of *pMET25*; assembled fragments: YTK001, *pMET25*	Laboratory Stock, Prof. Dr. Boles
pRCC-K	*2µ, KanMX, AmpR, pROX3, Cas9, tCYC1, pSNR52-gDNA*	Generoso et al. (2016)
pRCC-N	*2µ, ClonNAT, AmpR, pROX3, Cas9, tCYC1, pSNR52-gDNA*	Generoso et al. (2016)
SiHV005	Golden Gate backbone plasmid: *ConLS, GFP-dropout, ConRE, URA3, 2µ, KanR, ColE1*	Laboratory Stock, Prof. Dr. Boles
SiHV006	Golden Gate backbone plasmid: *ConLS, GFP-dropout, ConRE, LEU2, 2µ, KanR, ColE1*	Laboratory Stock, Prof. Dr. Boles
SiHV007	Golden Gate backbone plasmid: *ConLS, GFP-dropout, ConRE, HIS3, 2µ, KanR, ColE1*	Laboratory Stock, Prof. Dr. Boles
SiHV008	Golden Gate backbone plasmid: *ConLS, GFP-dropout, ConRE, KanMX, 2µ, KanR, ColE1*	Laboratory Stock, Prof. Dr. Boles
SiHV110	Golden Gate backbone plasmid for genomic integrations in the *LEU2* locus: *ConLS, GFP-dropout-ConRE, ClonNAT, LEU2 3′ homologous sequence, KanR, ColE1, LEU2 5′ homologous sequence*	Laboratory Stock, Prof. Dr. Boles
SiHV111	Golden Gate backbone plasmid for genomic integrations upstream of the *HO* locus (*ChrIV-49293-49345*): *ConLS, GFP-dropout-ConRE, LEU2, HO 3′ homologous sequence, KanR, ColE1, HO 5′ homologous sequence*	Laboratory Stock, Prof. Dr. Boles
SiHV190	Golden Gate backbone plasmid for CRISPR/Cas9: *pROX3, Cas9, tCYC1, AmpR, GFP-dropout, URA3, repair fragment insertion site 1*	Laboratory Stock, Prof. Dr. Boles

SiHV193	Golden Gate backbone plasmid for CRISPR/Cas9: *pROX3, Cas9, tCYC1, AmpR, GFP-dropout, URA3, repair fragment insertion site 1, 2*	Laboratory Stock, Prof. Dr. Boles
YTK001	Golden Gate entry vector: *GFP-drop out-cassette, CamR, ColE1*	Lee et al. (2015)
YTK002	Golden Gate part plasmid: *ConLS, CamR, ColE1*	Lee et al. (2015)
YTK003	Golden Gate part plasmid: *ConLS, CamR, ConL1*	Lee et al. (2015)
YTK009	Golden Gate part plasmid: *ConLS, CamR, pTDH3*	Lee et al. (2015)
YTK010	Golden Gate part plasmid: *ConLS, CamR, pCCW12*	Lee et al. (2015)
YTK011	Golden Gate part plasmid: *ConLS, CamR, pPGK1*	Lee et al. (2015)
YTK012	Golden Gate part plasmid: *ConLS, CamR, pHHF2*	Lee et al. (2015)
YTK013	Golden Gate part plasmid: *ConLS, CamR, pTEF1*	Lee et al. (2015)
YTK014	Golden Gate part plasmid: *ConLS, CamR, pTEF2*	Lee et al. (2015)
YTK015	Golden Gate part plasmid: *ConLS, CamR, pHHF1*	Lee et al. (2015)
YTK017	Golden Gate part plasmid: *ConLS, CamR, pRPL18B*	Lee et al. (2015)
YTK025	Golden Gate part plasmid: *ConLS, CamR, pRAD27*	Lee et al. (2015)
YTK030	Golden Gate part plasmid: *ConLS, CamR, pGAL1*	Lee et al. (2015)
YTK033	Golden Gate part plasmid: *ConLS, CamR, YFP-Venus*	Lee et al. (2015)
YTK034	Golden Gate part plasmid: *ConLS, CamR, mRuby2*	Lee et al. (2015)
YTK051	Golden Gate part plasmid: *ConLS, CamR, tENO1*	Lee et al. (2015)
YTK052	Golden Gate part plasmid: *ConLS, CamR, tSSA1*	Lee et al. (2015)
YTK053	Golden Gate part plasmid: *ConLS, CamR, tADH1*	Lee et al. (2015)
YTK054	Golden Gate part plasmid: *ConLS, CamR, tPGK1*	Lee et al. (2015)
YTK055	Golden Gate part plasmid: *ConLS, CamR, tENO2*	Lee et al. (2015)
YTK056	Golden Gate part plasmid: *ConLS, CamR, tTDH1*	Lee et al. (2015)
YTK067	Golden Gate part plasmid: *ConLS, CamR, ConR1*	Lee et al. (2015)
YTK068	Golden Gate part plasmid: *ConLS, CamR, ConR2*	Lee et al. (2015)
YTK095	Golden Gate cassette assembly plasmid: *ColE1, AmpR*	Lee et al. (2015)
JBV5	*YlHPPD* expression plasmid: *2μ, LEU2, AmpR, pMET25, YlHPPD, tCYC1*	Bauer (2019)
JBV11	Golden Gate storage plasmid of *SynHPT*; assembled fragments: YTK001, *SynHPT*	Bauer (2019)
JBV12	Golden Gate storage plasmid of *AtVTE1*; assembled fragments: YTK001, *AtVTE1*	Bauer (2019)
JBV15	Golden Gate cassette plasmid; assembled fragments: YTK095, JBV11, YTK009, YTK053	Bauer (2019)
JBV16	Golden Gate cassette plasmid; assembled fragments: YTK095, JBV12, YTK010, YTK051	Bauer (2019)
JBV18	Golden Gate plasmid for the expression of *SynHPT* and *AtVTE1* with *HIS3* as selection marker; assembled fragments: SiHV007, JBV015 and JBV016	Bauer (2019)
JBV24	Golden Gate cassette plasmid; assembled fragments: YTK095, JBV021, YTK010, YTK051	Bauer (2019)
JBV27	pRCC-K, CRISPR/Cas9 plasmid targeting the *ERG9* promoter	This study
JBV28	pRCC-N, CRISPR/Cas9 plasmid targeting the *HMG1*	This study
JBV29	Golden Gate storage plasmid of *BTS1*; assembled fragments: YTK001, *BTS1*	This study
JBV30	Golden Gate plasmid for the expression of *BTS1* with *URA3* as selection marker; assembled fragments: SiHV005, YTK011, JBV029 and YTK051	This study

JBV31	Golden Gate plasmid for the expression of *BTS1* with *LEU2* as selection marker; assembled fragments: SiHV006, YTK011, JBV029 and YTK051	This study
JBV32	Golden Gate storage plasmid of *PaGGPPS*; assembled fragments: YTK001, *PaGGPPS*	This study
JBV33	Golden Gate plasmid for the expression of *PaGGPPS* with *LEU2* as selection marker; assembled fragments: SiHV006, YTK011, JBV032, YTK052	This study
JBV35	Golden Gate storage plasmid of *pZEO1*; assembled fragments: YTK001 and *pZEO1*	This study
JBV36	Golden Gate storage plasmid of the artificial promoter 1 (*AP1*); assembled fragments: YTK001 and *AP1*	This study
JBV37	Golden Gate storage plasmid of the artificial promoter 2 (*AP2*); assembled fragments: YTK001 and *AP2*	This study
JBV38	Golden Gate storage plasmid of the artificial promoter 3 (*AP3*); assembled fragments: YTK001 and *AP3*	This study
JBV39	Golden Gate storage plasmid of the artificial promoter 4 (*AP4*); assembled fragments: YTK001 and *AP4*	This study
JBV40	Golden Gate storage plasmid of the artificial promoter 5 (*AP5*); assembled fragments: YTK001 and *AP5*	This study
JBV41	Golden Gate storage plasmid of the artificial promoter 6 (*AP6*); assembled fragments: YTK001 and *AP6*	This study
JBV42	Golden Gate storage plasmid of the artificial promoter 7 (*AP7*); assembled fragments: YTK001 and *AP7*	This study
JBV43	Golden Gate storage plasmid of the artificial promoter 8 (*AP8*); assembled fragments: YTK001 and *AP8*	This study
JBV44	Golden Gate storage plasmid of the artificial promoter 9 (*AP9*); assembled fragments: YTK001 and *AP9*	This study
JBV45	Golden Gate storage plasmid of the artificial promoter 10 (*AP10*); assembled fragments: YTK001 and *AP10*	This study
JBV46	Golden Gate storage plasmid of the artificial promoter 11 (*AP11*); assembled fragments: YTK001 and *AP11*	This study
JBV47	Golden Gate storage plasmid of the artificial promoter 12 (*AP12*); assembled fragments: YTK001 and *AP12*	This study
JBV48	Golden Gate plasmid for the expression of *YFP* under the control of *pZEO1* with *URA3* as selection marker; assembled fragments: SiHV005, YTK033, JBV035 and YTK051	This study
JBV49	Golden Gate plasmid for the expression of *YFP* under the control of *pPGK1* with *URA3* as selection marker; assembled fragments: SiHV005, YTK033, YTK011 and YTK051	This study
JBV50	Golden Gate plasmid for the expression of *YFP* under the control of *AP1* with *URA3* as selection marker; assembled fragments: SiHV005, YTK033, YTK051 and JBV036	This study
JBV51	Golden Gate plasmid for the expression of *YFP* under the control of *AP2* with *URA3* as selection marker; assembled fragments: SiHV005, YTK033, YTK051 and JBV037	This study
JBV52	Golden Gate plasmid for the expression of *YFP* under the control of *AP3* with *URA3* as selection marker; assembled fragments: SiHV005, YTK033, YTK051 and JBV038	This study
JBV53	Golden Gate plasmid for the expression of *YFP* under the control of *AP4* with *URA3* as selection marker; assembled fragments: SiHV005, YTK033, YTK051 and JBV039	This study
JBV54	Golden Gate plasmid for the expression of *YFP* under the control of *AP5* with *URA3* as selection marker; assembled fragments: SiHV005, YTK033, YTK051 and JBV040	This study

JBV55	Golden Gate plasmid for the expression of *YFP* under the control of *AP6* with *URA3* as selection marker; assembled fragments: SiHV005, YTK033, YTK051 and JBV041	This study
JBV56	Golden Gate plasmid for the expression of *YFP* under the control of *AP7* with *URA3* as selection marker; assembled fragments: SiHV005, YTK033, YTK051 and JBV042	This study
JBV57	Golden Gate plasmid for the expression of *YFP* under the control of *AP8* with *URA3* as selection marker; assembled fragments: SiHV005, YTK033, YTK051 and JBV043	This study
JBV58	Golden Gate plasmid for the expression of *YFP* under the control of *AP9* with *URA3* as selection marker; assembled fragments: SiHV005, YTK033, YTK051 and JBV044	This study
JBV59	Golden Gate plasmid for the expression of *YFP* under the control of *AP10* with *URA3* as selection marker; assembled fragments: SiHV005, YTK033, YTK051 and JBV045	This study
JBV60	Golden Gate plasmid for the expression of *YFP* under the control of *AP11* with *URA3* as selection marker; assembled fragments: SiHV005, YTK033, YTK051 and JBV046	This study
JBV61	Golden Gate plasmid for the expression of *YFP* under the control of *AP12* with *URA3* as selection marker; assembled fragments: SiHV005, YTK033, YTK051 and JBV047	This study
JBV63	Golden Gate plasmid for the expression of *PaGGPPS* with *URA3* as selection marker; assembled fragments: SiHV005, YTK011, JBV032 and YTK052	This study
JBV64	Golden Gate plasmid for the expression of *PaGGPPS* with *URA3* as selection marker; assembled fragments: SiHV005, YTK030, JBV032 and YTK052	This study
JBV65	Golden Gate integrational plasmid of *BTS1* and *LEU2*; assembled fragments: SiHV111, YTK011, JBV029 and YTK053	This study
JBV66	Golden Gate integrational plasmid of *BTS1* and *ClonNAT*; assembled fragments: SiHV110, YTK011, JBV029 and YTK054	This study
JBV68	Golden Gate plasmid for the expression of *YFP* under the control of *pMET25* with *URA3* as selection marker; assembled fragments: SiHV005, YTK033, YTK051 and pGG2.4	This study
JBV69	Golden Gate plasmid for the expression of *YFP* under the control of *pRAD27* with *URA3* as selection marker; assembled fragments: SiHV005, YTK025, YTK051 and JBV047	This study
JBV70	pRCC-K, CRISPR/Cas9 plasmid targeting a region upstream of the *HO* locus: *ChrIV 49293-49345Δ* (wt) and *ChrIV 53688-53756Δ* (JBY20), respectively	This study
JBV72	Golden Gate storage plasmid of the artificial promoter 13 (*AP13*); assembled fragments: YTK001 and *AP13*	This study
JBV73	Golden Gate storage plasmid of the artificial promoter 14 (*AP14*); assembled fragments: YTK001 and *AP14*	This study
JBV74	Golden Gate storage plasmid of the artificial promoter 15 (*AP15*); assembled fragments: YTK001 and *AP15*	This study
JBV75	Golden Gate storage plasmid of the artificial promoter 16 (*AP16*); assembled fragments: YTK001 and *AP16*	This study
JBV76	Golden Gate storage plasmid of the artificial promoter 17 (*AP17*); assembled fragments: YTK001 and *AP17*	This study

JBV77	Golden Gate storage plasmid of the *pHXT7*; assembled fragments: YTK001 and *pHXT7*	This study
JBV78	Golden Gate plasmid for the expression of *YFP* under the control of *AP13* with *URA3* as selection marker; assembled fragments: SiHV005, YTK033, YTK051 and JBV072	This study
JBV79	Golden Gate plasmid for the expression of *YFP* under the control of *AP14* with *URA3* as selection marker; assembled fragments: SiHV005, YTK033, YTK051 and JBV073	This study
JBV80	Golden Gate plasmid for the expression of *YFP* under the control of *AP15* with *URA3* as selection marker; assembled fragments: SiHV005, YTK033, YTK051 and JBV074	This study
JBV81	Golden Gate plasmid for the expression of *YFP* under the control of *AP16* with *URA3* as selection marker; assembled fragments: SiHV005, YTK033, YTK051 and JBV075	This study
JBV82	Golden Gate plasmid for the expression of *YFP* under the control of *AP17* with *URA3* as selection marker; assembled fragments: SiHV005, YTK033, YTK051 and JBV076	This study
JBV83	Golden Gate plasmid for the expression of *YFP* under the control of *AP18* with *URA3* as selection marker; assembled fragments: SiHV005, YTK033, YTK051 and JBV077	This study
JBV84	Golden Gate plasmid for the expression of *SynHPT* and *AtVTE1* with *URA3* as selection marker; assembled fragments: SiHV005, JBV015, JBV016	This study
JBV85	Golden Gate plasmid for the expression of *SynHPT* and *AtVTE1*$^{tr[229\text{-}1467]}$; with *URA3* as selection marker; assembled fragments: SiHV005, JBV015, JBV024	This study
JBV86	Golden Gate plasmid for the expression of *SynHPT* with *LEU2* as selection marker; assembled fragments: SiHV006, JBV011, YTK030, YTK052	This study
JBV87	Golden Gate plasmid for the expression of *SynHPT* with *URA3* as selection marker; assembled fragments: SiHV005, JBV011, YTK030, YTK052	This study
JBV88	Golden Gate plasmid for the expression of *AtVTE1* with *URA3* as selection marker; assembled fragments: SiHV005, JBV012, YTK030, YTK052	This study
JBV89	Golden Gate plasmid for the expression of *AtVTE1*$^{tr[229\text{-}1467]}$; with *URA3* as selection marker; assembled fragments: SiHV005, JBV021, YTK030, YTK052	This study
JBV90	Golden Gate storage plasmid of *ERG20*; assembled fragments: YTK001 and *ERG20*	This study
JBV91	Golden Gate plasmid for the expression of *ERG20* with *URA3* as selection marker; assembled fragments: SiHV005, JBV090, YTK014, YTK055	This study
JBV93	Golden Gate storage plasmid of *SaGGPPS*; assembled fragments: YTK001 and *SaGGPPS*	This study
JBV94	Golden Gate plasmid for the expression of *SaGGPPS* with *URA3* as selection marker; assembled fragments: SiHV005, JBV093, YTK011, YTK052	This study
JBV95	Golden Gate plasmid for the expression of *BTS1* with *URA3* as selection marker; assembled fragments: SiHV005, JBV029, *AP8*, YTK051	This study
JBV96	Golden Gate CRISPR/Cas9 plasmid targeting the *ROX1* locus, assembled parts: SiHV190, *ROX1* oligomer	This study
JBV97	Golden Gate CRISPR/Cas9 plasmid targeting the *YJL064W* locus, assembled parts: SiHV190, *YJL064W* oligomer	This study

JBV98	Golden Gate CRISPR/Cas9 double cutter plasmid targeting the *ROX1* and *YJL064W* locus, assembled parts: SiHV193, *YJL064W* and *ROX1* oligomer	This study
JBV100	Golden Gate cassette plasmid; assembled fragments: YTK095, JBV090, YTK014, YTK055, YTK003, YTK072	This study
JBV101	Golden Gate plasmid for the expression of *SaGGPPS* with *URA3* as selection marker; assembled fragments: SiHV005, JBV93, YTK030, YTK052	This study
JBV102	Golden Gate plasmid for the expression of *SynHPT* with *URA3* as selection marker; assembled fragments: SiHV005, *AP8*, JBV11, YTK054	This study
JBV103	Golden Gate plasmid for the expression of *AtVTE1* with *LEU2* as selection marker; assembled fragments: SiHV006, *AP6,* JBV12, YTK056	This study
JBV104	Golden Gate cassette plasmid; assembled fragments: YTK095, YTK002, JBV11, YTK054, YTK067, *AP8*	This study
JBV105	Golden Gate cassette plasmid; assembled fragments: YTK095, *AP6*, JBV12, YTK056, YTK003, YTK072	This study
JBV106	Golden Gate plasmid for the expression of *SynHPT* and *AtVTE1* with *URA3* as selection marker; assembled fragments: SiHV005, JBV104, JBV105	This study
JBV107	Golden Gate storage plasmid of *EgHPT*; assembled fragments: YTK001 and *EgHPT*	This study
JBV108	Golden Gate storage plasmid of *HvHGGT*; assembled fragments: YTK001 and *HvHGGT*	This study
JBV109	Golden Gate storage plasmid of *NosHGGT*; assembled fragments: YTK001 and *NosHGGT*	This study
JBV110	Golden Gate storage plasmid of *NosHPT*; assembled fragments: YTK001 and *NosHPT*	This study
JBV111	Golden Gate storage plasmid of *AnaTC*; assembled fragments: YTK001 and *AnaTC*	This study
JBV114	Golden Gate storage plasmid of *SynTC*; assembled fragments: YTK001 and *SynTC*	This study
JBV115	Golden Gate plasmid for the expression of *EgHPT* with *LEU2* as selection marker; assembled fragments: LBGV023, JBV107, *AP8*, YTK054	This study
JBV116	Golden Gate plasmid for the expression of *HvHGGT* with *LEU2* as selection marker; assembled fragments: LBGV023, JBV108, *AP8*, YTK054	This study
JBV117	Golden Gate plasmid for the expression of *NosHGGT* with *LEU2* as selection marker; assembled fragments: LBGV023, JBV109, *AP8*, YTK054	This study
JBV118	Golden Gate plasmid for the expression of *NosHPT* with *LEU2* as selection marker; assembled fragments: LBGV023, JBV110, *AP8*, YTK054	This study
JBV119	Golden Gate plasmid for the expression of *AnaTC* with *URA3* as selection marker; assembled fragments: LBGV023, JBV111, *AP6*, YTK056	This study
JBV120	Golden Gate plasmid for the expression of *HvTC* with *URA3* as selection marker; assembled fragments: LBGV023, *HvTC*, *AP6*, YTK056	This study
JBV121	Golden Gate plasmid for the expression of *OsTC* with URA3 as selection marker; assembled fragments: LBGV023, *OsTC*, *AP6*, YTK056	This study

JBV122	Golden Gate plasmid for the expression of *SynTC* with *URA3* as selection marker; assembled fragments: LBGV023, JBV114, *AP6*, YTK056	This study
JBV123	*HPPD* expression plasmid with a C-terminal *GFP* tag for the intracellular localisation, assembled fragments: FGD97, *YlHPPD*	This study
JBV124	*BTS1* expression plasmid with a C-terminal *GFP* tag for the intracellular localisation; assembled fragments: FGD97, *BTS1*	This study
JBV125	*SynHPT* expression plasmid with a C-terminal *GFP* tag for the intracellular localisation; assembled fragments: FGD97, *SynHPT*	This study
JBV126	*AtVTE1* expression plasmid with a C-terminal *GFP* tag for the intracellular localisation; assembled fragments: FGD97, *AtVTE1*	This study
JBV127	Golden Gate plasmid for the expression of *BTS1* with *KanMX* as selection marker; assembled fragments: SiHV008, *AP8*, JBV29, YTK053	This study
JBV128	Golden Gate cassette plasmid; assembled fragments: YTK095, YTK002, *AP7*, JBV90, YTK051, YTK067	This study
JBV129	Golden Gate cassette plasmid; assembled fragments: YTK095, YTK003, *AP8*, JBV29, YTK052, YTK072	This study
JBV130	Golden Gate integrational plasmid of *BTS1*, *ERG20* and *ClonNAT*; assembled fragments: SiHV110, JBV128, JBV129	This study
JBV131	Golden Gate integrational plasmid of *SynHPT*, *AtVTE1* and *ClonNAT*; assembled fragments: SiHV110, JBV104, JBV105	This study
JBV132	Golden Gate integrational plasmid of *SynHPT*, *AtVTE1* and *LEU2*; assembled fragments: SiHV111, JBV104, JBV105	This study
JBV133	Golden Gate integrational plasmid of *BTS1*, *ERG20* and *LEU2*; assembled fragments: SiHV111, JBV128, JBV129	This study
JBV134	Golden Gate integrational plasmid of *BTS1* and *LEU2*; assembled fragments: SiHV111, *AP7*, JBV29, YTK053	This study
JBV135	Golden Gate cassette plasmid; assembled fragments: YTK095, YTK003, *AP11*, JBV32, YTK052, YTK072	This study
JBV136	Golden Gate cassette plasmid; assembled fragments: YTK095, YTK003, *AP11*, JBV93, YTK052, YTK072	This study
JBV137	Golden Gate integrational plasmid of *PaGGPPS*, *ERG20* and *LEU2*; assembled fragments: SiHV111, JBV135, JBV128	This study
JBV138	Golden Gate integrational plasmid of *SaGGPPS*, *ERG20* and *LEU2*; assembled fragments: SiHV111, JBV136, JBV128	This study
JBV139	Golden Gate integrational plasmid of *PaGGPPS* and *LEU2*; assembled fragments: SiHV111, JBV32, YTK017, YTK052	This study
JBV140	Golden Gate integrational plasmid of *SaGGPPS* and *LEU2*; assembled fragments: SiHV111, JBV93, YTK017, YTK052	This study
JBV141	Golden Gate storage plasmid of $AtVTE1^{tr[142-1467]}$; assembled fragments: YTK001 and $AtVTE1^{tr[142-1467]}$	This study
JBV142	Golden Gate cassette plasmid; assembled fragments: YTK095, YTK003, YTK011, JBV141, YTK056, YTK072	This study
JBV143	Golden Gate plasmid for the expression of *SynHPT* and $AtVTE1^{tr[142-1467]}$ with *URA3* as selection marker; assembled fragments: SiHV005, JBV104, JBV142	This study
JBV144	Golden Gate integrational plasmid of *SynHPT*,	This study

	AtVTE1$^{tr[142-1467]}$ and *LEU2*; assembled fragments: SiHV111, JBV104, JBV142	
JBV145	Golden Gate storage plasmid of *XdcrtE*; assembled fragments: YTK001 and *XdcrtE*	This study
JBV146	Golden Gate plasmid for the expression of *XdcrtE* with *URA3* as selection marker; assembled fragments: SiHV005, YTK014, JBV145, YTK051	This study
JBV147	Golden Gate integrational plasmid of *XdcrtE* and *LEU2*; assembled fragments: SiHV111, YTK009, JBV145, YTK052	This study
JBV148	Golden Gate cassette plasmid; assembled fragments: YTK095, YTK003, YTK009, JBV145, YTK052, YTK072	This study
JBV149	Golden Gate integrational plasmid of *XdcrtE*, *ERG20* and *LEU2*; assembled fragments: SiHV111, YTK009, JBV128, JBV148	This study
JBV150	Golden Gate integrational plasmid of *SynHPT*, *AtVTE1*$^{tr[142-1467]}$ and *ClonNAT*; assembled fragments: SiHV110, JBV104, JBV142	This study
JBV151	Golden Gate plasmid for the expression of *AtVTE1*$^{tr[142-1467]}$ with *URA3* as selection marker; assembled fragments: LBGV022, JBV141, *AP6,* YTK056	This study
JBV152	Golden Gate plasmid for the expression *AtVTE1*$^{tr[142-1467]}$ with *URA3* as selection marker; assembled fragments: LBGV022, JBV141, *AP6*, YTK056	This study
JBV153	Golden Gate plasmid for the expression of *EgHPT* with *HIS3* as selection marker; assembled fragments: SiHV007, JBV107, *AP8*, YTK053	This study
JBV154	Golden Gate plasmid for the expression of *HvHGGT* with *HIS3* as selection marker; assembled fragments: SiHV007, JBV108, *AP8*, YTK053	This study
JBV155	Golden Gate plasmid for the expression of *NosHGGT* with *HIS3* as selection marker; assembled fragments: SiHV007, JBV109, *AP8*, YTK053	This study
JBV156	Golden Gate plasmid for the expression of *NosHPT* with *HIS3* as selection marker; assembled fragments: SiHV007, JBV110, *AP8*, YTK053	This study
JBV157	Golden Gate plasmid for the expression of *BTS1* with *HIS3* as selection marker; assembled fragments: SiHV007, JBV29, YTK009, YTK051	This study
JBV158	Golden Gate cassette plasmid; assembled fragments: YTK095, YTK002, *AP8*, JBV110, YTK051, YTK067	This study
JBV159	Golden Gate integrational plasmid of *NosHPT*, *AtVTE1*$^{tr[142-1467]}$ and *ClonNAT*; assembled fragments: SiHV110, JBV158, JBV142	This study
JBV160	Golden Gate storage plasmid of *AtGGR*; assembled fragments: YTK001 and *AtGGR*	This study
JBV161	Golden Gate storage plasmid of *SaGGR*; assembled fragments: YTK001 and *SaGGR*	This study
JBV162	Golden Gate storage plasmid of *ScGGR*; assembled fragments: YTK001 and *ScGGR*	This study
JBV163	Golden Gate storage plasmid of *SynGGR*; assembled fragments: YTK001 and *SynGGR*	This study
JBV164	Golden Gate plasmid for the expression of *AtGGR* with *URA3* as selection marker; assembled fragments: SiHV005, JBV160, YTK014, YTK055	This study

JBV165	Golden Gate plasmid for the expression of *SaGGR* with *URA3* as selection marker; assembled fragments: SiHV005, JBV161, YTK014, YTK055	This study
JBV166	Golden Gate plasmid for the expression of *ScGGR* with *URA3* as selection marker; assembled fragments: SiHV005, JBV162, YTK014, YTK055	This study
JBV167	Golden Gate plasmid for the expression of *SynGGR* with *URA3* as selection marker; assembled fragments: SiHV005, JBV163, YTK014, YTK055	This study
JBV168	*CEN6.ARS4, KanR, ClonNAT ColE1, ConS, pPGK1-XdcrtE-tENO1, pTDH3-trHMG1-tHMG1, AP7-YlHPPD-tCYC1, AP6- AtVTE1$^{tr[142-1467]}$ -tTDH1, AP8-HPT-tPGK1*	This study
JBV169	pRCC-K, CRISPR/Cas9 plasmid targeting *DPP1*	This study
JBV173	Golden Gate integrational plasmid of *BTS1^{co}* and *LEU2*; assembled fragments: SiHV111, YTK009, *BTS1^{co}*, YTK052	This study
JBV178	Golden Gate cassette plasmid; assembled fragments: YTK095, YTK002, YTK011, *XdcrtI*, YT056, YTK067	This study
JBV179	Golden Gate cassette plasmid; assembled fragments: YTK095, YTK003, YTK013, *XdcrtYB*, YT055, YTK072	This study
JBV180	Golden Gate plasmid for the expression of *XdcrtI* and *XdcrtYB* with *URA3* as selection marker; assembled fragments: SiHV005, JBV178, JBV179	This study
JBV188	pRCC-K, CRISPR/Cas9 plasmid targeting *ClonNAT*	This study
JBV189	Golden Gate storage plasmid of *AtMPBQMT$^{tr[153-864]}$*; assembled fragments: YTK001 and *AtMPBQMT$^{tr[153-864]}$*	This study
JBV190	Golden Gate cassette plasmid; assembled fragments: YTK095, YTK002, YTK013, V189, YTK051, YTK067	This study
JBV192	Golden Gate cassette plasmid; assembled fragments: YTK095, YTK003, YTK012, *Atγ-TMT$^{tr[121-1047]}$* YTK055, YTK072	This study
JBV193	Golden Gate integrational plasmid of *AtMPBQMT$^{tr[153-864]}$*, *Atγ-TMT$^{tr[121-1047]}$* and *LEU2*; assembled fragments: SiHV111, JBV190, JBV192	This study

2.1.5 Cultivation and Storage of *E. coli*

For subcloning, the bacterium, *E. coli* was employed. The strain NEB 5-alpha was mainly used for cloning procedures of small plasmids (< 5000 bp) while NEB 10-beta and DH10B strains were used for plasmids larger than 5000 bp (Table 7). Cells were cultivated in lysogeny broth medium (LB medium) and grown on LB agar plates at 37 °C. Depending on the selection marker, appropriate antibiotics were added (Table 2). Commercially available chemical competent and electrocompetent cells were obtained from New England Biolabs (NEB) and transformed according to the manufacturer's protocols.

Table 7 *E. coli* strains

Strain	Characteristics	Reference
NEB 5-alpha	*fhuA2Δ(argF-lacZ)U169 phoA glnV44 Φ80Δ(lacZ)M15 gyrA96 recA1 relA1*	NEB
NEB 10-beta	*Δ(ara-leu) 7697 araD139 fhuA ΔlacX74 galK16 galE15 e14- ϕ80dlacZΔM15 recA1 relA1 endA1 nupG rpsL (StrR) rph spoT1 Δ(mrr-hsdRMS-mcrBC)*	NEB
DH10B	*F–mcrA Δ(mrr-hsdRMS-mcrBC) φ80lacZΔM15 ΔlacX74 recA1 endA1 araD139 Δ(ara-leu)7697 galU galK λ-rpsL(StrR) nupG*	Thermo Fisher Scientific

2.1.6 DNA Isolation

2.1.6.1 Isolation of DNA from *S. cerevisiae*

The method of Lõoke et al. (2011) for the isolation of genomic DNA from yeast for PCR based assays was adapted. First, a single colony was suspended in 50 µl of a 200 mM lithium acetate 1% (w/v) SDS solution and incubated for 5 min at 70 °C. Second, 150 µl 99 % (v/v) ethanol were added for DNA precipitation. The samples were centrifuged for 3 min at 15000 g and the supernatant was discarded. Then, the pellet was washed with 250 µl 70 % (v/v) ethanol, centrifuged for 3 min at 15000 g and dried for 5 min at 50 °C. Finally, the pellet was suspended in 50 µl DNA elution buffer (Macherey-Nagel), incubated for 15 minutes at 42 °C, and the supernatant was used for PCR based applications.

Isolation of plasmids from *S. cerevisiae* was performed with the commercially available kit from Zymo Research (Table 17) according to protocols of the manufacturer.

2.1.6.2 Isolation of DNA from *E. coli*

The isolation of plasmids from *E. coli* was performed with commercially available kits from Macherey-Nagel and Thermo Fisher Scientific (Table 17) according to the corresponding protocols of the manufacturer.

2.2 Molecular Biological Methods

2.2.1 Synthetic DNA

All synthetic oligomers and their applications are described in Table 21. They were synthesised by Eurofins Genomics GmbH, Biomers.net GmbH and Microsynth Seqlab GmbH. Recombinant genes were codon optimized for *S. cerevisiae* gene expression according to Wiedemann and Boles (2008). The codon adaptation index (CAI) was calculated with the online tool *GenScript Rare Codon Analysis Tool* (GenScript, Piscataway, NJ, USA). Synthetic genes were ordered as strings or clonal vectors from Twist Bioscience or Thermo Fisher Scientific. As these genes were subsequently used for Golden Gate assembly, BsaI and BsmBI cut sides were replaced by silent mutations. All heterologous sequences are listed in the appendix.

2.2.2 Polymerase Chain Reaction

Many molecular biological processes require the amplification of DNA. Therefore, polymerase chain reactions (PCR) were performed. Different applications call for diverse procedures. Polymerases owning a proofreading function were used if precise amplifications were required. Here, the Q5 High-Fidelity DNA polymerase (2.2.2.1) or the Phusion High-Fidelity DNA polymerase (2.2.2.2), were the products of choice. Applications which did not require high precision were performed with the DreamTaq DNA polymerase (2.2.2.3). Exemplary purposes were amplifications for visualization of genetic deletions and insertions in agarose gels. Generally, the standard PCR cycling protocol (Table 8) was applied. The lid of the thermocycler was pre-heated to 96 °C. The length of the DNA extension was variable, depending on the polymerase. In general, the manufacturer's protocols were utilised. The online application *NEB Tm calculator* (NEB) was employed to calculate primer annealing temperatures. The amplified products were verified in agarose gels (2.2.3).

Table 8 Standard PCR cycling protocol

Repeats	Temperature [°C]	Time [s]	Function
1x	98	30	Initial denaturation of the DNA
25-35x	98	10	Denaturation of the DNA
	45-70	20	Primer annealing
	72	variable	DNA extension
1x	72	300	Final extension
1x	4-10	∞	Hold

2.2.2.1 Q5 DNA Polymerase PCR Reactions

Table 9 displays the composition of PCR mixtures which were performed with the Q5 High Fidelity DNA polymerase (NEB). The conditions of the standard PCR cycling protocol were applied (Table 8). The DNA extension time was 20 s/kb. Usually, all PCRs for clonal or sequencing applications were performed with the Q5 DNA polymerase.

Table 9 Q5 PCR mixture

	Final concentration	**Volume [µl]**
5x Q5 reaction buffer	1x	10
10 mM dNTPs	200 µM	1
$Q5^{HF}$ DNA Polymerase	0.02 U/µl	0.5
Primer forward	0.5 µM	2.5
Primer reverse	0.5 µM	2.5
Template	1-50 ng	variable
		Fill up to 50 µl with ddH_2O

2.2.2.2 Phusion DNA Polymerase PCR Reactions

If DNA amplification with the Q5 protocol did not result in the desired product, the Phusion DNA polymerase was chosen. The conditions of the standard PCR cycling protocol were applied (Table 8). Here, the DNA extension time was 30 s/kb. The reaction mixture for PCRs with the Phusion DNA Polymerase is shown in Table 10.

Table 10 Phusion PCR mixture

	Final concentration	**Volume [µl]**
5x Phusion HF buffer	1x	10
10 mM dNTPs	200 µM	1
$Phusion^{HF}$ DNA polymerase	0.02 U/µl	0.5
DMSO	3 %	1.5
Primer forward	0.5 µM	2.5
Primer reverse	0.5 µM	2.5
Template	1-50 ng	variable
		Fill up to 50 µl with ddH_2O

2.2.2.3 DreamTaq Polymerase PCR Reactions

The standard PCR cycling protocol (Table 8) was used for PCRs performed with the DreamTaq polymerase with a DNA extension time of 1 min/kb and the initial temperature of DNA denaturation was changed to 95 °C. The composition of the reaction mixture is displayed in Table 11. The corresponding DreamTaq Green PCR master mix.

Table 11 DreamTaq RCR mixture

	Final concentration	**Volume [µl]**
10x DreamTaq green buffer	1x	1.25
10 mM dNTPs	200 µM of each	0.25
DreamTaq DNA Polymerase	1.75 U/µl	0.35
Primer forward	0.5 µM	0.625
Primer reverse	0.5 µM	0.625
Template	10 pg – 1µg	variable
		Fill up to 12.5 µl with ddH_2O

2.2.3 Agarose Gel Electrophoresis and DNA Extraction from Agarose Gels

The size of DNA fragments was monitored in 1 % (w/v) agarose gels. The agarose gel was prepared with 1 % (w/v) agarose in 1x TAE-buffer. If the ROTI GelStain Red was utilised for visualisation of the DNA fragments, the substance was added while preparing the gel according to the manufacturers' protocols. Depending on the laboratory, visualisation was also performed by incubation of the gel in an ethidium bromide bath after the gel electrophoresis. If the DreamTaq Green PCR master mix had been utilised before no DNA loading dye was required. Otherwise, DNA products were mixed with the 6X purple gel loading dye (NEB). Depending on the size of the DNA products, an appropriate DNA ladder was utilised (NEB). Typically, gels were run at 100 V for 45 minutes. Subsequently, DNA fragments were monitored under UV-light (254 nm) in a gel documentation. The NucleoSpin Extract II-Kit (Macherey-Nagel) was utilised for purification of the DNA according to the manufacturer's protocol.

2.2.4 Cloning Procedures

Different cloning procedures were applied dependent on the application. Usually, the Golden Gate system was utilised for the construction of expression plasmids and integration vectors, which were linearised prior to integration by the enzyme NotI. If Golden Gate was not applicable for the assembly, for instance due to too many BsaI or BsmBI restrictions sites in

the sequence, Gibson assembly was utilised. Furthermore, Gibson assembly was used to generate CRISPR/Cas9 plasmids and GFP-tagged plasmid for fluorescence microscopy. After both assembly methods, *E. coli* transformation were performed (2.1.5). Afterwards, plasmids were isolated from individual *E. coli* transformants according to section 2.1.6.2 and verified by enzymatic restriction digest and sequencing (2.2.5).

2.2.4.1 Golden Gate Assembly

Golden Gate Assembly is a modular, multipart cloning tool, based on type IIS restriction enzymes (Lee et al., 2015). The MoClo-YTK Yeast Toolkit (Addgene kit #1000000061) was utilised for subcloning in this work. Each plasmid in this toolkit consists of specific parts (for instance promoters, genes and terminators) which are connectable in a modular manner. Hereby, Golden Gate overhangs with the specific enzymatic recognition sites are used for each part. First, Golden Gate storage plasmids had to be constructed. Therefore, the genetic elements of interest (GEOI), mostly genes or promoters, were synthesised with specific overhangs. If the GEOI were amplified by PCR, these overhangs were part of the corresponding oligomers. The Golden Gate storage plasmids only consist of the GEOI, without any regulatory elements, and the backbone YTK001. Storage plasmids were built to introduce the GEOI into the modular system to quickly assemble new plasmids. Second, Golden Gate cassette plasmids were built. Cassette plasmids consist of the backbone YTK095, promoters, genes and terminators. If several gene expression cassettes were cloned into one vector, connector plasmids of the YTK Toolkit were used. Furthermore, Golden Gate expression and integrative plasmids were built from these cassette plasmids.

The Golden Gate assembly was performed according to the Golden Gate assembly protocol (Table 12) and the Golden Gate cycling protocol (Table 13). Assemblies of up to 5 parts were performed with 15 repeats of the assembly step, while this step was repeated 25 times if 6 or more parts were used. Instead of BsmBI, its isoschizomer Esp3I, with a temperature optimum at 37 °C, was employed for Golden Gate assemblies. If additional BsaI or BsmBI restriction sites could not be omitted in the sequence, the Golden Gate troubleshooting protocol was applied (Table 14).

Table 12 Golden Gate Assembly Protocol

Component	Concentration of the assembly mixture	Volume [µl]
T4 ligase buffer (10x)	1x	1
T7 ligase	1500 U	0.5
Type IIS restriction enzyme (BsaI/Esp3I)	5-10 U	0.5
DNA (each part plasmid)	variable	50 ng of each part
		Fill up to 10 µl with ddH_2O

Table 13 Golden Gate Cycling Protocol

Repeats	Temperature [°C]	Time [min]	Function
1x	37	10	Initial digest
15x/25x	37	1.5	Digest
	16	3	Annealing and ligation
1x	37	5	Final digest
1x	50	5	Ligase inactivation
1x	80	10	Restriction enzyme inactivation

Table 14 Golden Gate Troubleshooting Cycling Protocol

Repeats	Temperature [°C]	Time [min]	Function
1x	37	10	Initial digest
15x	34	1.5	Digest
	16	3	Annealing and ligation
1x	50	5	Ligase inactivation
1x	80	10	Restriction enzyme inactivation

2.2.4.2 Gibson Isothermal Assembly

For the assembly of plasmids with up to 6 fragments, either the Gibson Isothermal assembly (Gibson et al., 2009) or the NEBuilder HiFi DNA Assembly Cloning Kit (E5520S, NEB, Ipswich MA) were utilised. Hereby, overlapping DNA fragments (25 bp overhang) were assembled by a 5'-exonuclease, DNA amplification and ligation approach. If the reaction was performed with the NEBuilder HiFi DNA Assembly Cloning Kit, the procedure was performed according to the manufacturer's protocols. Otherwise, a 5x Isothermal reaction buffer (Table 15), and the Gibson Assembly master mix (Table 16), aliquoted in 5 µl single use mixtures, were prepared and stored at -20 °C. To perform the assembly, 50 ng of the plasmid backbone DNA were mixed with up to 5 DNA fragments in the molar ratio of 1:3, filled up with ddH_2O and added to a 2X Gibson master mix. The reaction was incubated at 50 °C in a thermocycler for 1 h.

Table 15 5x Isothermal reaction buffer

Component	Concentration
PEG-8000	25 %
Tris-HCl, pH 7.5	500 mM
$MgCl_2$	50 mM
DTT	50 mM
dNTPs	1 mM
NAD^+	5 mM

Table 16 2x Gibson Master Mix

	Concentration
Isothermal reaction buffer	1x
T5 exonuclease	10 U/µl
Taq DNA ligase	40 U/µl
Phusion DNA polymerase	2 U/µl

2.2.5 DNA Sequencing

PCR amplification-based cloning procedures, assembled plasmids and genome-based modifications were verified by DNA sequencing with appropriate primers. The DNA sequencing was either performed by Microsynth Seqlab GmbH or Eurofins Genomics GmbH. DNA samples were prepared according to the service provider.

2.3 Analysis

Several analytical methods were applied for the quantitative analysis of fermentation samples. Due to the change of laboratories, GGOH was either analysed by high performance liquid chromatography (HPLC) or gas chromatography (GC). The associated method of each experiment was noted in the respective experiment (result section). HGA and tocochromanol titers were evaluated by HPLC. Notably, GGOH was analysed to infer GGPP biosynthesis, due to its fast dephosphorylation, as it is common in current research (Callari et al., 2018).

2.3.1 Sample Preparation

Depending on the metabolite to be analysed, one of the following methods was applied. Metabolite extraction after cultivations was required when the cultivation was performed without an organic overlay. Otherwise, dodecane samples of *in-situ* cultivations were prepared according to section 2.3.1.4.

2.3.1.1 Sample Preparation for HGA Measurement

HGA was directly measurable from the aqueous phase of cultivation samples. First, 1 ml of the culture was centrifuged (15000 g, 5 min, RT) and 900 µl of the supernatant were transferred into fresh tubes. Then, 100 µl acetonitrile were added and mixed well. Samples were centrifuged (15000 g, 5 min, RT) and analysed in the HPLC as described in section 2.3.2.1.

2.3.1.2 Methanol Extraction

Samples of the intracellular metabolites were prepared by a methanol extraction method which was modified from Callari et al. (2018). First, 2 ml of the culture were harvested (15000 g, 5 min, RT) and the pellet was washed with 1 ml ddH2O. The cell pellet was either used directly or frozen until measurement. Subsequently, the pellet was dissolved in 500 µl methanol, disrupted in the thermo shaker (10 min, 60 °C, 1450 rpm) and centrifuged (15000 g, 5 min, RT). The organic phase was transferred into 1.5 ml tubes and the methanol was evaporate for 24 h (RT) in a fume hood. For GGOH detection in the GC, the samples were dissolved in 500 µl ethyl acetate and measured directly.

2.3.1.3 Homogenisation for GGOH and Tocochromanol Analysis

1 ml samples of cultivation samples were harvested (15000 g, 5 min, RT) and the pellet was washed with 1 ml ddH2O. Subsequently, pellets were resuspended well in 200 µl ddH20 and 500 µl acetone and transferred into 2 ml lysis tubes, bearing glass beads (Precellys glas-kit VK05). Following that, the yeast cells were homogenized in the Precellys homogenizer (6800 rpm 2x 30 s, 30 s break). 1 ml acetone was added and mixed well. Then the samples were incubated for 10 min RT and the acetone phase was harvested (30 min, max speed 4 °C). This extraction step was performed twice. Subsequently, tocochromanol and GGOH titers of the samples were determined by HPLC.

2.3.1.4 *In-situ* Extraction for GGOH and Tocochromanol Analysis

Following *in-situ* extraction of intracellular metabolites 2 ml of the dodecane phase were harvested (10000 rpm, 5 min, RT) and transferred into fresh 2 ml tubes. Samples were either measured directly or frozen at this point until measurement. If dodecane samples were analysed by HPLC, the dodecane phase was directly measured in the HPLC system. For GC analysis the samples were mixed well with ethyl acetate (1:1) and measured in the GC system.

2.3.2 HPLC Analysis

2.3.2.1 Analysis of HGA by HPLC

The supernatant samples were analysed with an Agilent Zorbax SB-C8 column (4.6 × 150 mm, 3.5 µm) or the Nucleodur 100-5 C18 ec (250 x 4.6 mm, 5 µm) from Macherey-Nagel at 40 °C in a BioLC HPLC system or the Ultimate3000 HPLC system, respectively (Table 18). Eluent A (0.1 % formic acid in ddH2O) and eluent B (0.1% formic acid in acetonitrile) were applied with a flow rate of 1 ml/min using the following gradient: 0-20 min 100 % eluent A, 20-25 min up to 10 % eluent B, 25-29 min from 10 % to 25 % eluent B, 29-35 min back to 100 % eluent A. The HGA was detected by UV absorption at 288 nm. The quantitative analysis was performed with a serial dilution of a commercially available standard of HGA (Sigma Aldrich).

2.3.2.2 Analysis of Tocochromanols and GGOH by HPLC

A quantitative analysis of intracellular tocochromanols and GGOH was performed with samples prepared after method 2.3.1.2 and 2.3.1.3. The Nucleodur 100-5 C18 ec (250 x 4.6 mm, 5 µm) column of Macherey-Nagel was used at 40 °C in the Ultimate3000 HPLC system (Table 18). Tocochromanols were detected by the fluorescence detector (FLD-3100) with an excitation 297 nm / emission 326 nm. UV absorption at 210 nm was used for the detection of GGOH. An isocratic method with the following solvents was run for 40 min with a flow rate of 1 ml/min: 75 % methanol, 15 % acetonitrile with 0.1 % (v/v) formic acid, 15 % ddH2O with 0.1 % (v/v) formic acid. Commercially available reference material of δ-tocotrienol and δ-tocopherol were obtained from Sigma Aldrich for the quantitative analysis. A mixture of tocotrienols was obtained from Davos Life Science Pte Ltd. (Singapore) for a qualitative analysis of tocotrienols. Reference material of GGOH was obtained from Sigma Aldrich for the quantitative analysis of GGOH.

2.3.2.3 Qualitative Analysis of β-Carotene

Analytical detection of β-carotene was performed using the Ultimate3000 HPLC system equipped with the Nucleosil 50-5 (250 x 4.6 mm, 5 µm) column of Macherey-Nagel at 22 °C. UV absorption at 445 nm was used for β-carotene detection. An isocratic method with the following solvents was run for 30 min: 80 % n-heptane and 20 % acetone with a flow rate of 1.5 ml/min. Commercially available reference material was obtained from LGC for the qualitative analysis of β-carotene.

2.3.3 Gas Chromatography

GGOH quantification was also carried out by gas chromatography (GC). Samples for GC analysis were prepared as described in 2.3.1.2. The Elite 200 column (30 m, 0.2 mm I.D., 0.25 µm) in a Clarus 680 GC system (Perkin Elmer) was employed (Table 18). 1 µl of the samples was injected in 1/10 split mode at 250 °C and detected by flame ionization detector (FID). The following GC program was run: 80 °C for 2 min, raised to 220 °C at 10 °C/min, raised to 240 °C at 3 °C/min, ramped at rate 25 °C/min to 300 °C and held for 5 min. Helium was used as carrier gas with a constant flow rate of 1 ml/min.

2.4 Chemicals, Kits and Devices

Chemicals and kits that were used during this work are listed in Table 17. Devices besides the standard laboratory equipment which were utilised within this study, are listed in Table 18.

Table 17 Chemicals and Kits

Chemicals	Manufacturer
Acetone	Roth
Acetonitrile	Roth
Adenine	Roth
Agar agar	Roth
Agarose	Roth
Agarose low melt	Roth
Ammonium-sulphate	Roth
Ampicillin	Roth
Bacillol	Roth
Calcium acetate	Roth
Calcium hydroxide	Roth
Carbenicillin	Sigma Aldrich
Chloramphenicol	Sigma Aldrich
D-glucose monohydrate	Roth
D-glucose	Roth
Dimethyl sulfoxide (DMSO)	Roth
DNA ligases	New England BioLabs
dNTPs	Thermo Fisher Scientific
Dodecane	Roth
DreamTaq polymerase, including master mix	Thermo Fisher Scientific
Ethanol	Roth
Ethidium bromide	Roth
Ethyl acetate	Roth
Ethylenediaminetetraacetic acid (EDTA)	Roth
Geneticin sulphate (G418)	Roth
Geranylgeraniol analytical standard	Sigma Aldrich
Glycerol	Roth
Hydrogen chloride (HCl)	Roth
Heptane	Roth
Homogentisic acid analytical standard	Sigma Aldrich
Kanamycin	Roth
Kohrsolin	Roth
L-alanine	Roth
L-arginine	Roth
L-asparagine	Roth
L-cysteine	Roth
L-histidine	Roth
L-glutamine	Roth
L-isoleucine	Roth

L-leucine	Roth
L-lysine	Roth
L-methionine	Roth
L-phenylalanine	Roth
L-proline	Roth
L-threonine	Roth
L-tryptophan	Roth
L-tyrosine	Roth
L-valine	Roth
Lithium acetate (LiAc)	Roth
Magnesium sulphate ($MgSO_4$)	Roth
Methanol	Roth
MitoTracker™ Red CMXRos	Thermo Fisher Scientific
Nourseothricin (ClonNAT)	Werner BioAgents
Polyethylene glycol (PEG) 4000	Roth
Peptone	BD Bacto, Roth
Phusion High Fidelity Polymerase, including buffer	New England BioLabs
Potassium chloride (KCl)	Roth
Potassium dihydrogen-phosphate (KH_2PO_4)	Roth
Potassium hydroxide (KOH)	Roth
Potassium sulphate (K_2SO_4)	Roth
Q5 high fidelity DNA polymerase, including buffer	New England BioLabs
Restriction enzymes and buffers	New England BioLabs
ROTI GelStain Red	Roth
Single stranded carrier DNA (salmon sperm DNA)	Roth
Sodium chloride (NaCl)	Roth
Sodium hydroxide (NaOH)	Roth
Sodium sulphate (Na_2SO_4)	Roth
TAE buffer (TRIS base, acetic acid and EDTA buffer)	Roth
Tocotrienols	Davos Life Science Pte Ltd. (Singapore).
TRIS (tris(hydroxymethyl)-aminomethane)	Roth
Tryptone	BD Bacto
Uracil	Sigma Aldrich
Yeast extract	BD Bacto, Roth
Yeast nitrogen base without amino acids and ammonium sulphate	Difco
Yeast nitrogen base without amino acids and ammonium sulphate, without folic acid and without riboflavin	MP Biomedicals, Santa Ana, CA
Yeast Synthetic Drop-out Media Supplements	Sigma Aldrich
β-carotene reference material	LGC
δ-tocopherol analytical standard	Sigma Aldrich
δ-tocotrienol analytical standard	Sigma Aldrich
Kits:	
GeneJET Plasmid-Miniprep-Kit	Thermo Fisher Scientific
NucleoSpin Gel and PCR Clean-up	Macherey-Nagel
NucleoSpin Extract II-Kit	Macherey-Nagel
Zymoprep Yeast Plasmid Miniprep II	Zymo Research

Table 18 Laboratory equipment

Device	Manufacturer
Analytical balance - Secura 225D-1S	Sartorius
Autoclave VX-150	Systec
BioSpectrometer	Eppendorf
Cell Density Meter	Thermo Fisher Scientific
Cell electroporator	Bio-Rad
Cell growth quantifier	Aquila Biolabs
Centrifuges (5424 R, 5810R, 5920R, 5415D, 5702)	Eppendorf
Dispensette - S organic 10-100 ml	Brand
Fermenter - MiniBio 250 ml microbial	Applikon
Fermenter – my-control	Applikon
Gel electrophoresis chamber and power pac	Bio-Rad
Gel electrophoresis chambers	Neolab
Gel documentation - Universal Hood 2	Bio Rad
Gel documentation - UV crosslinker	Vilber Lourmat
Homogenizer - Precellys 24 Touch	Bertin Instruments
Incubator - Innova 42	New Brunswick
Infors Shake Incubator - Multitron	Infors
Magnetic stirrer	IKA
Microscope - BA210 Digital	Motic
Microscope camera Axiocam 305 color	Carl Zeiss Microscopy
Multipette E3x	Eppendorf
Ozone generator - Aquarizon 4.0	Innotec
PCR Cycler, labcycler triple block	SensoQuest
PCR Mastercycler X50s, X50i	Eppendorf
pH meter - 765 Calimatic	Knick
pH meter - pH 3110	WTW
Pipette Research plus 0.1 - 2.5 µl	Eppendorf
Pipette Research plus 0.5 - 10 µl	Eppendorf
Pipette Research plus 2 – 20 µl	Eppendorf
Pipette Research plus 20 - 200 µl	Eppendorf
Pipette Research plus 100 – 1000 µl	Eppendorf
Pipette Research plus 1 - 10 ml	Eppendorf
Pipetting aid Easypet 3	Eppendorf
Platereader - CLARIOstar Plus	BMG LABTECH
Platereader - FLUOstar Omega	BMG LABTECH
Precision balance - Entris BCE6202I-1S	Sartorius
Spectrophotometer NanoDrop 1000	Thermo Fisher Scientific
Spectrophotometer Ultrospec 2100 pro	Amersham Bioscience
Thermoblock - ThermoMixer C	Eppendorf
Ultrasonic bath - Elmasonic S80H	Elma
Vibrax VXR basic	IKA
Vortex 3	IKA
Confocal Laser Scanning Microscope Zeiss LSM 780	Carl Zeiss Microscopy
Zeiss Inverted microscope AxioVert A1 FL LED	Carl Zeiss Microscopy
96 well plates (Greiner, flat bottom, black)	Sigma Aldrich

HPLC systems:	
BioLC:	
Autosampler - AS50	Thermo Fisher Scientific
Column Compartment - TCC-100	Thermo Fisher Scientific
Degaser Ultimate3000	Thermo Fisher Scientific
Detector -VWD-3100 Dionex	Thermo Fisher Scientific
Gradient pump - GS50	Thermo Fisher Scientific
Ultimate 3000:	
Autosampler WPS-3000 TSL	Thermo Fisher Scientific
Column Compartment TCC-3000 SD	Thermo Fisher Scientific
Detector Dionex DAD-3000 RS	Thermo Fisher Scientific
Fluorescence detector - FLD-3100	Thermo Fisher Scientific
Gradient pump - SD	Thermo Fisher Scientific
Solvent rack LPG-3400 SD	Thermo Fisher Scientific
HPLC columns:	
HPLC pre-column EC 4/3 Nucleodur 100-5 C18ec	Macherey-Nagel
Nucleodur 100-5 C18 ec (250 x 4.6 mm, 5 µm)	Macherey-Nagel
Nucleosil 50-5 (250 x 4.6 mm, 5 µm)	Macherey-Nagel
ZORBAX SB-C8 (4.6 x 150 mm, 3.5 µm)	Agilent Technologies
GC system:	
Clarus 680 GC system	Perkin Elmer
Elite 200 column	Perkin Elmer
Flame ionization detector	Perkin Elmer

2.5 Software

Excel 2021 (Microsoft) was utilised for data storage and Graphpad Prism 9.0.0 (GraphPad, USA) for the graphical illustration. Clone manager 9 (Scientific & Educational Software) and Geneious Prime 2020.2 were used for the design of genetic elements. EndNote X9.3.3 was utilised for reference organisation and citation.

3 Results

The aim of this work was to establish a pathway for the synthesis of tocochromanols on a laboratory scale in *S. cerevisiae*. First, the implementation of an enhanced isopentenyl diphosphate biosynthesis, more precisely GGPP, was desired. Second, a heterologous pathway for tocochromanol biosynthesis should be established. During the strain construction, limitations of the pathways were identified, and strategies needed to be applied to overcome emerging challenges. Reifenrath and Boles (2018) engineered a CEN.PK2-1C strain (MRY33) for the *de novo* biosynthesis of mandelic acid via the aromatic amino acid pathway. MRY33 exhibits a high precursor supply of the tyrosine branch. Therefore, MRY33 was employed for the implementation of HGA biosynthesis in *S. cerevisiae* during a preceding master thesis: The heterologous *YlHPPD* of *Y. lipolytica* was introduced into the *PYK2* locus under the control of *pPGK1* and *tFBA1* for the construction of the strain JBY2. This strain resulted in the production of 435 mg/L of the first precursor homogentisic acid during a 144 h shake flask fermentation (Bauer, 2019). Consequently, JBY2 was utilised for further strain engineering during this study.

3.1 Artificial Promoter Engineering

This study was started with the screening of artificial promoter sequences for gene expression in *S. cerevisiae*. The strain JBY2 is already highly engineered and therefore numerous strong promoters are already utilised within this strain. It is beneficial to vary sequences for a genomically stable strain since sequence homologies can lead to homologous recombination events. For further strain engineering and the overexpression of additional genes, novel promoters were favourable. Therefore, a set of 17 artificial promoter sequences (*AP1-AP17*) was investigated. These promoter sequences are also part of a patent (WO2023094429A1), which was filed during this study (Dietz et al., 2023).

The strength of the artificial promoters was compared with the strong, endogenous promoter *pPGK1* and the weak promoter *pRAD27* (Lee et al., 2015). Thus, all artificial promoter sequences were ordered as synthetic strings and introduced into the Golden Gate system. The *YFP-Venus* gene was cloned under the control of each promoter to measure the strength of expression (plasmids: JBV49-JBV61, JBV69 and JBV72-JBV76). Subsequently, CEN.PK2-1C was transformed with the corresponding plasmids, cultivations and fluorescence measurements were performed as described in 2.1.2.4. Figure 5 illustrates the relative fluorescence intensity of the artificial promoters in relation to the control *pPGK1*, which was set to 1. Thereby, five

strong promoters were identified (*AP6*, *AP7*, *AP8*, *AP11* and *AP17*). The novel promoter *AP8* resulted in the highest fluorescence intensity, which was 2.37 times stronger than the control *pPGK1* (Figure 5 A). These strong artificial promoter sequences were utilised for the overexpression of genes during this study. Moreover, five medium strong promoters and seven weak promoters were identified (Figure 5 B). Within complex metabolic networks, different strengths of gene expression are essential to fulfil different purposes. Thus, these sequences are applicable if a lower gene dosage is required.

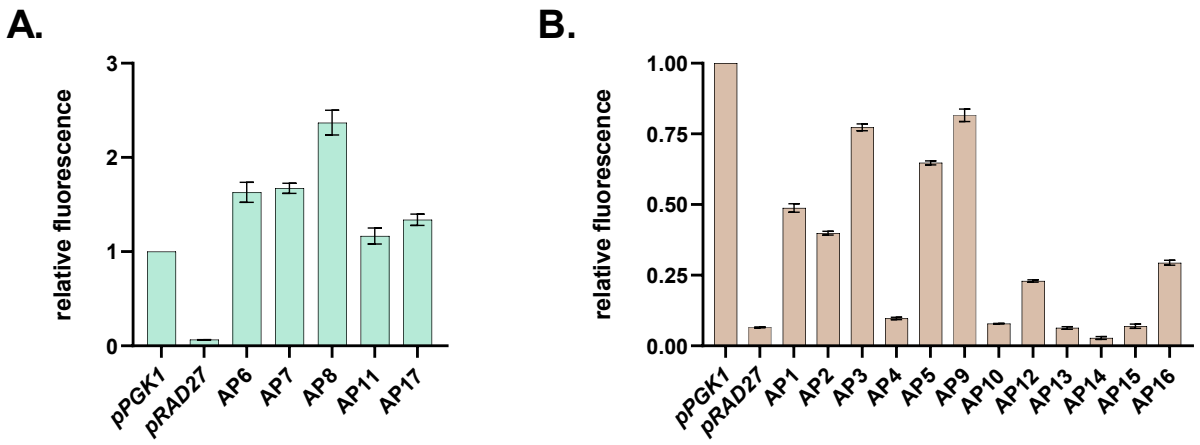

Figure 5 Relative fluorescence intensity of an artificial set of promoters

CEN.PK2-1C expressing YFP-Venus under the control of a set of 17 artificial promoters (AP1-AP17) and two control promoters, *pPGK1* and *pRAD27.* The fluorescence intensity was normalised to the reference promoter *pPGK1*, which was set to 1. The bars are equipped with error bars, representing the corresponding standard deviation of 6 replicates (sample size (n) = 6). **A.** Artificial promoters leading to a stronger fluorescence intensity than the reference promoter *pPGK1*. **B.** Artificial promoters leading to a medium and low fluorescence intensity compared to the strong reference *pPGK1*.

3.2 Metabolic Engineering of the Isopentenyl Diphosphate Biosynthesis

Due to the sufficient biosynthesis of HGA, the focus was driven on the isopentenyl synthesis. The second precursor, GGPP, is produced endogenously by *S. cerevisiae*. Due to its rapid dephosphorylation, GGOH was analysed to infer GGPP biosynthesis. However, GGOH was barely detectable (< 0.1 mg/L) in the *S. cerevisiae* strain JBY2 (Figure 6). Consequently, the mevalonate and the isopentenyl diphosphate pathway were successively engineered to ensure sufficient GGPP supply for tocochromanol biosynthesis.

3.2.1 Eliminating *HMG1* Downregulation and Identification of *BTS1* Limitation

The first limitation to address was the HMGCR, encoded by *HMG1*. Natively, *HMG1* is feedback regulated on several levels. Therefore, the first 1572 bp at the N-terminus were truncated to create the feedback-resistant construct containing only the catalytic domain and the linker as described by Donald et al. (1997). Furthermore, *HMG1* was overexpressed by exchanging the native promoter with the strong glycolytic promoter *pTDH3*. This promoter was amplified by PCR (primers: JBP021 and JBP022) with overhangs for the truncated *HMG1* including an artificial start codon. These genetic modifications were performed in JBY2 by CRISPR/Cas9 with the CRISPR/Cas9 plasmid JBV28, targeting *HMG1*. After successful transformation, the new strain JBY3 needed to be characterised. Besides *HMG1*, the native GGPP synthase, encoded by *BTS1,* is a constraining factor (Tokuhiro et al., 2009). Thus, a plasmid-based overexpression approach was chosen and the *BTS1* overexpression plasmid, JBV31, was constructed by Golden Gate assembly. The native *BTS1* coding sequence was amplified via PCR from genomic DNA of CEN.PK2-1C with corresponding overhangs for Golden Gate assembly by the primers JBP013 and JBP014. *BTS1* expression was put under the control of the promoter *pPGK1* and the terminator *tENO1*. Then, JBY2 and JBY3 were transformed with the plasmid JBV31 and the empty vector (EV) control (SiHV006). A shake flask cultivation was performed in biological triplicates in SCM-$D_{\text{-Leu}}$ medium. Sample preparation and analytics were performed as described in section 2.3.1.2 and 2.3.3.

Figure 6 displays the GGOH titers in mg/L and the OD_{600} after 168 h of cultivation. GGOH was measurable only in minor amounts in JBY2 (< 0.1 mg/L), while plasmid-based *BTS1* overexpression enhanced titers to 0.4 mg/L. Furthermore, JBY3 overexpressing the truncated *HMG1* resulted in higher GGOH titers than its parent strain JBY2. Additional *BTS1* overexpression through JBV31 resulted in the production of 4.79 mg/L GGOH. These results substantiate the necessity to overexpress the truncated, feedback-resistant *HMG1* and the GGPP synthase, *BTS1,* for an enhanced GGPP production.

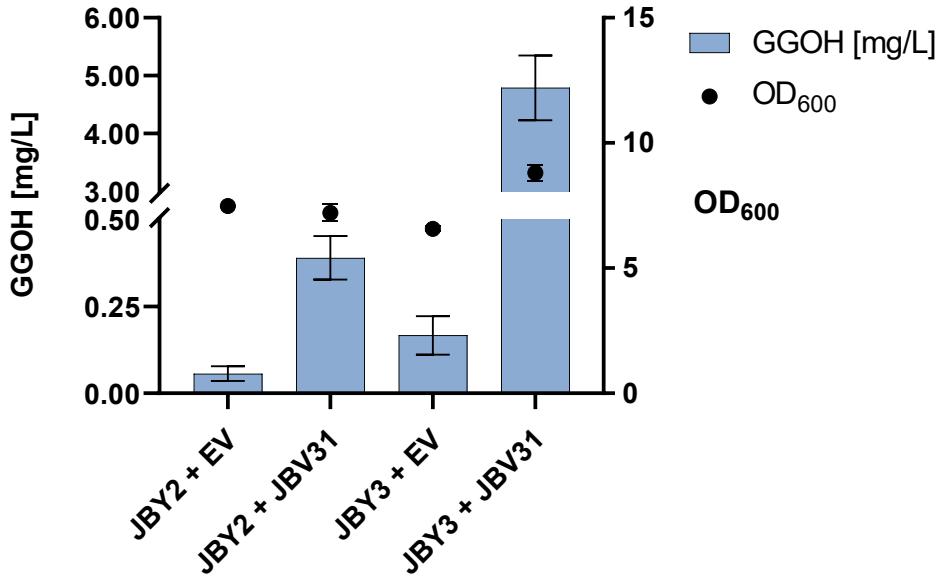

Figure 6 Overexpression of the truncated *HMG1* and *BTS1* affected GGOH titers

OD_{600} values and GGOH titers in mg/L of the strains JBY2 and JBY3 are displayed after 168 h of cultivation in SCM-D_{-LEU} medium. Both strains carried either the *BTS1* overexpression plasmid (JBV31), or the EV control (SiHV006). The mean GGOH titers of biological triplicates (n=3) are represented by blue bars. The standard deviation is shown by error bars. OD_{600} values are displayed by black dots equipped with error bars indicating the standard deviation. The error bars were not drawn if the corresponding standard deviation was smaller than the projected symbol.

For further characterisation, the cellular localisation of *BTS1* was analysed by fluorescence microscopy. At the time the experiment was conducted, the mitochondria were described as location of Bts1p on Uniprot[1]. Meanwhile, Uniprot has updated the subcellular localisation to cytoplasm by similarity. The plasmid JBV124 was built, bearing *BTS1* with a C-terminal GFP tag, which were connected by a linker (5'GCGGCCGCTGGTGCTGGT3'). After transformation of CEN.PK2-1C with JBV124 and shake flask cultivations (method 2.1.2.4), laser confocal microscopy was utilised for the visualisation of *BTS1* expression as described by Tamayo Rojas et al. (2021). Figure 7 illustrates the expression of the envyGFP-tagged *BTS1* in CEN.PK2-1C. Mitochondria were stained with a *MitoTracker* for differentiation of cellular components and to exclude *BTS1* expression within the mitochondria (Figure 7 B). By fluorescence microscopy an even distribution of the fluorescent Bts1p was observed and could be distinguished from the mitochondria in the merged picture C.

[1] https://www.uniprot.org/uniprotkb/Q12051/entry#subcellular_location

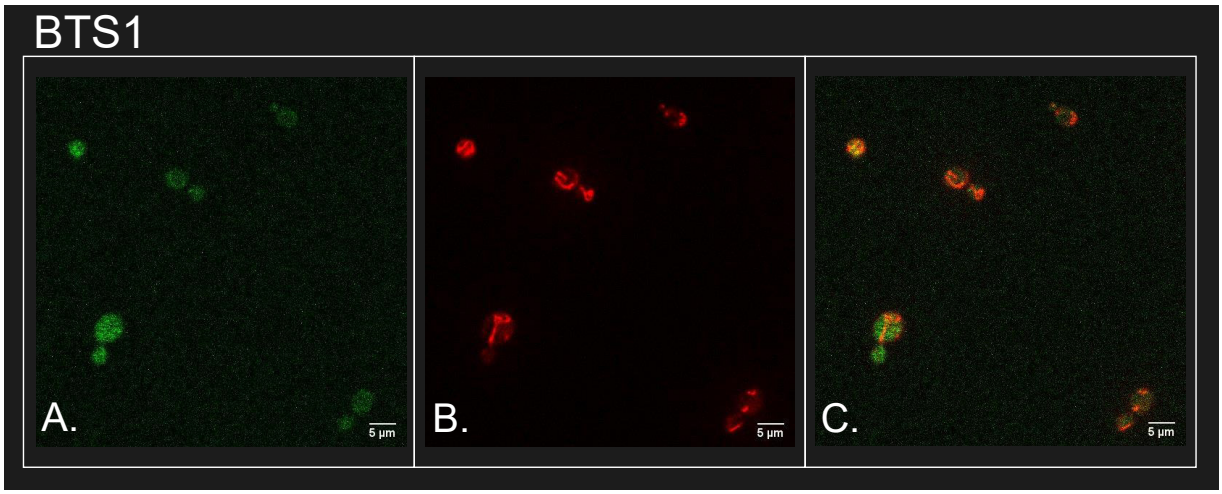

Figure 7 Laser confocal microscopy of envyGFP-tagged Bts1p

CEN.PK2-1C cells expressing *BTS1* with a C-terminal envyGFP tag (JBV124). After cultivation of the transformants in synthetic low fluorescent medium, cells were immobilised with 0.6 % (w/v) low melt agarose. Their localisation was monitored with a confocal laser scanning microscope (Zeiss LSM 780). The 5 µm scale indicates the size ratio. **A**. Bts1p expression in several CEN.PK2-1C cells visualised by GFP. **B**. Illustration of the cellular localisation of the mitochondria of the same image section as displayed in A. for subcellular differentiation. **C.** Merged picture of image A and B to differentiate subcellular components.

With respect to the fact that the expression of the heterologous HPPD delivered sufficient amounts of HGA in *S. cerevisiae,* further characterisation of its cellular localisation was desired. Thus, the *HPPD-envyGFP* plasmid (JBV123) was generated in the same manner as described for JBV124. Subsequently, fluorescence microscopy of CEN.PK2-1C bearing JBV123 was conducted, and the images are portrayed in Figure 8. Hereby, a strong *HPPD* expression within the cytoplasm was observed (A). The merged picture of the envyGFP and the *MitoTracker* is displayed in Figure 8 C to distinguish the cytoplasm and mitochondria. By the visualisation of the expression of Bts1p and HPPD, the conclusion can be drawn that both related enzymatic products may be most abundant in the cytoplasm.

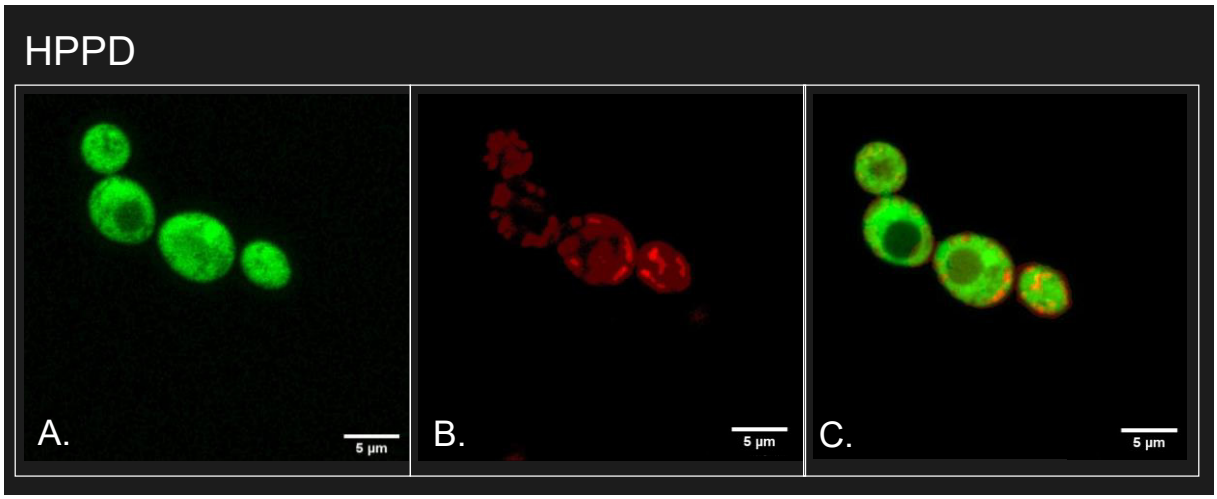

Figure 8 Laser confocal microscopy of envyGFP-tagged HPPD

CEN.PK2-1C cells expressing *HPPD* with a C-terminal envyGFP tag (JBV123). Subsequent to cultivation in synthetic low fluorescent medium cells were immobilised with 0.6% (w/v) low melt agarose. Their HPPD expression was analysed with a confocal laser scanning microscope (Zeiss LSM 780) and the 5 µm scale indicates the size ratio. **A**. HPPD expression in CEN.PK2-1C cells visualised by a C-terminal envyGFP tag. **B**. Illustration of the cellular localisation of the mitochondria of the same image section as displayed in A. for subcellular differentiation. **C.** Merged picture of image A and B to differentiate subcellular components.

3.2.2 Downregulation of the Competing Ergosterol Pathway

The results in section 3.2.1 demonstrated the limitation of the endogenous GGPP synthase Bts1p. One approach to overcome this limitation was the downregulation of the ergosterol pathway to direct the metabolic flux into the synthesis of GGPP, since the GGPP synthase has to compete for its substrate FPP with the enzyme Erg9p. Therefore, the native promoter of *ERG9*, was exchanged by the ergosterol sensitive promoter *pERG1*, as described by Callari et al. (2018). The gene *PTH1* is encoded 247 bp upstream of *ERG9*. Thus, only 150 bp upstream of *ERG9* were deleted to keep the terminator sequence of *PTH1* intact. The native promoter was replaced by the ergosterol sensitive promoter *pERG1.* This promoter was amplified by PCR from genomic DNA of CEN.PK2-1C with 40 bp overhangs homologous to the integration side *ERG9* (primers: JBP027 and JBP028). The integration locus was targeted by CRISPR/Cas9 with the plasmid JBV27, which was generated by PCR and Gibson assembly. The promoter exchange was conducted in JBY3 generating the strain JBY4. Subsequently, JBY4 was transformed with JBV31 and SiHV006 (EV) to evaluate if *BTS1* was still limiting GGPP biosynthesis. A shake flask cultivation was performed with biological triplicates in SCM-D$_{-Leu}$ medium. Once again, the indispensability of the upregulation of *BTS1* gene was demonstrated

(Figure 9). The graph shows a similar growth behaviour of both strains by their OD_{600} values. GGOH was barely detectable (< 0.1 mg/L) in JBY4 expressing the EV control, although more than 5 mg/L GGOH was measured in JBY4 transformed with JBV31. Consequently, the GGPP synthase Bts1p was clearly identified as keystone for enhanced GGPP synthesis. Therefore, the stable integration of a second *BTS1* expression cassette into the genome was desired for further improvement of the GGPP synthesis in *S. cerevisiae*.

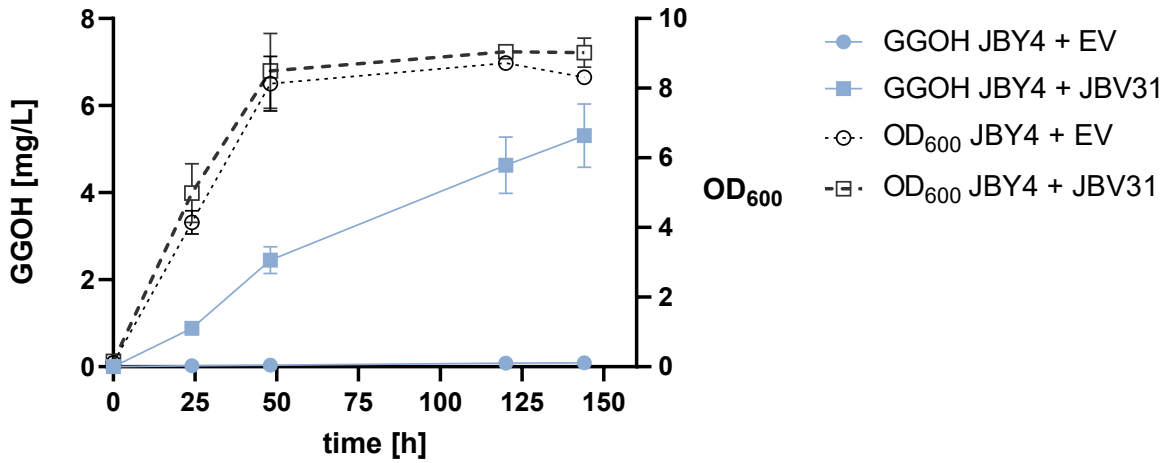

Figure 9 Plasmid-based *BTS1* overexpression led to detectable GGOH titers

GGOH titers in mg/L and OD_{600} values are displayed depending on the time. Error bars show the standard deviation of the biological triplicates (n=3). The error bars were not drawn if the corresponding standard deviation was smaller than the projected symbol. OD_{600} values are displayed by blank, black framed symbols. GGOH titers are illustrated by filled-out symbols in blue. Squares represent data points of JBY4 overexpressing *BTS1*, while circles symbolise the empty vector control.

3.2.3 Genome-based *BTS1* Overexpression

The construct for the genome-based approach was built as integrative plasmids by Golden Gate assembly (JBV66). The integration of the second copy of *BTS1* was performed by homologous recombination employing a ClonNAT cassette as selection marker. The strains JBY3 and JBY4 are leucine auxotroph due to 2 point mutations in the *LEU2* gene of their parent strain CEN.PK2-1C. Hence, the unfunctional *LEU2* was completely replaced to serve as second integration locus for *BTS1*. The ClonNAT resistance cassette is located downstream of the expression cassette *pPGK1-BTS1-tENO1* in JBV66. JBY3 and JBY4 were transformed with the linearised plasmid, generating in the strains JBY5 and JBY6, respectively. Shake flask fermentations revealed that the GGPP synthesis was only slightly increased in JBY6 (data not shown). Therefore, JBY6 was transformed with JBV31 and the EV control, JBY4 was

transformed with JBV31 as additional control. A shake flask fermentation was performed over 120 h in SCM-D$_{-LEU}$ medium. Samples were taken at 48 h, 72 h, 96 h and 120 h. Figure 10 A shows the OD_{600} values depended on the time and Figure 10 B displays the GGOH titers of the 120 h samples (method 2.3.1.2 and 2.3.3). While the growth behaviour was comparable in all three strains, the insufficiency of *BTS1* for GGPP synthesis was demonstrated by the additional plasmid-based overexpression of *BTS1* in JBY6. GGOH titers were improved from 5.25 mg/L (EV) to 13.71 mg/L (JBV31) when the plasmid was introduced. Moreover, the plasmid-based overexpression led to higher titers in JBY4 transformed with JBV31, than the stable integration in JBY6 (Figure 10 B). These results indicate the potential for further improvements of the GGPP supply in *S. cerevisiae*.

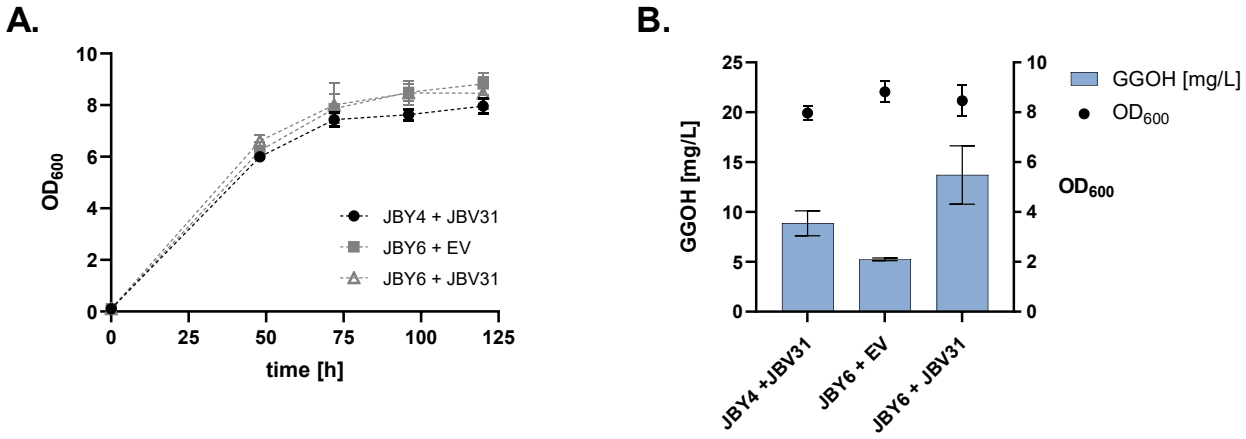

Figure 10 *BTS1* was still limiting GGPP production

JBY6 was transformed with JBV31 and the EV control (SiHV006); JBY4 was transformed with JBV31. The shake flask cultivations in biological triplicates (n=3) were performed in SCM-D$_{-LEU}$ medium over 120 h. The error bars display the standard deviation of the triplicates but were not drawn if the corresponding standard deviation was smaller than the projected symbol. **A.** The biomass formation of JBY4 transformed with JBV31 (black dot), and JBY6 either transformed with JBV31 (blank grey triangle) or EV control (grey square), is presented by OD_{600} values depending on the time. **B.** GGOH titers [mg/L] of the 120 h sample are illustrated by blue bars, OD_{600} values of these samples are displayed by black dots.

3.2.4 Increase of GGPP Synthesis by *ERG20* Overexpression

Another approach to enhance the GGPP synthesis was to target the preceding reaction in the pathway. Thus, the FPP synthetase (*ERG20*) was amplified by PCR from genomic DNA of CEN.PK2-1C (primers: JBP52 and JBP53) and introduced into the Golden Gate system (JBV90). Interestingly, sequencing of *ERG20* from the plasmid JBV90 revealed 22 point

mutations within the gene on DNA level between the *S. cerevisiae* strain S288C and CEN.PK2-1C. However, on protein level, the sequence is highly conserved within these two species, carrying only two amino acid changes. The negatively charged glutamic acid was exchanged by the negatively charged aspartic acid (E308D). The second exchange was also between amino acids with similar chemical properties (I318V). Due to the high protein similarity, JBV90 was utilised for the construction of the *ERG20* expression plasmid JBV91 under the control of *pTEF2* and *tENO2*. After transformation of JBY6 with JBV91 and the EV control, a cultivation was conducted in biological duplicates in 50 ml SCM-D_{-URA} medium. Analytics were performed according to method 2.3.1.2 and 2.3.3. Figure 11 illustrates the production of GGOH in mg/L and the OD_{600} after 144 h. The plasmid-based overexpression of *ERG20* enhanced GGOH titers from 12.54 mg/L to 26.82 mg/L compared to the EV control.

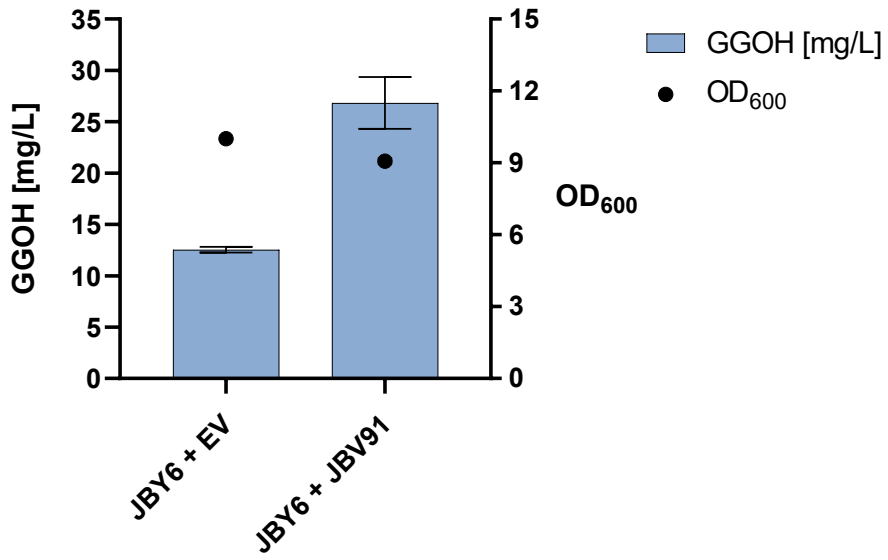

Figure 11 Increasement of GGOH titers by *ERG20* overexpression

GGOH titers [mg/L] and OD_{600} values of the strains JBY6 expressing *ERG20* (JBV91) and the EV control (SiHV005) are displayed after 144 h of cultivation in SCM-D_{-URA} medium. The mean GGOH values of biological duplicates are represented by blue bars. Error bars represent the range of both measured values (n=2). OD_{600} values are displayed by black dots. No error bars were drawn here since the corresponding range between samples was smaller than the projected symbol.

3.2.5 Plasmid-based Characterisation of Heterologous GGPP Synthases

As the preceding results conclusively demonstrated the indispensability of the overexpression of a GGPP synthase, two heterologous enzymes were investigated on a plasmid-based approach besides the endogenous GGPP synthase Bts1p. The expression of the bifunctional GGPP synthases of *Phomopsis amygdali* and *S. acidocaldarius* have been shown to be beneficial for an enhanced GGPP biosynthesis (Chen et al., 2016; Hu et al., 2020). Therefore, these were codon optimized, ordered as synthetic genes and expression plasmids (JBV33 and JBV94) were constructed as described for JBV31. However, the transformation of JBY3 with neither of the plasmids was successful. Consequently, the expression plasmids JBV64 (*PaGGPPS*) and JBV101 (*SaGGPPS*) were constructed with the GGPP synthases under the control of the inducible promoter *pGAL1* by Golden Gate assembly. These were characterised in two different cultivations during different stages of this work. However, both cultivations are presented in Figure 12 to draw a comprehensive picture of the challenges of plasmid-based overexpressions of heterologous genes. After successful transformation of JBY3 with JBV31 and JBV64 on solid SCM-D$_{-LEU}$ agar plates, pre cultures were grown in SCM-D$_{-LEU}$ medium. Subsequently, the cultivation was performed over 144 h in SCM-G$_{-LEU}$ medium to induce expression and samples were taken at 0, 19, 24, 48, 72, 120 and 144 h. Growth curves are illustrated in Figure 12 A, while Figure 12 C shows a snapshot of GGOH titers in mg/L (method 2.3.1.2 and 2.3.3) and the OD_{600} value at 144 h. JBY3 expressing the heterologous *PaGGPP*S led to 1.60 mg/L GGOH after 144 h, while 25.02 mg/L GGOH was measured with the endogenous *BTS1* overexpression variant. The increased GGOH titers in JBY3 transformed with JBV31 compared to the results represented in Figure 6 might derive from the galactose catabolism being beneficial for GGPP synthesis. More importantly, the *PaGGPPS* variant resulted in a decreased growth phenotype, which is undesirable for industrial applications.

Attention needs to be drawn to the fact that the following experiment was conducted with the strain JBY6, already bearing a second *BTS1* overexpression cassette. JBY6 was successfully transformed with JBV30, JBV101 and the EV. These vectors carried *URA3* as a selection marker, however, JBV30 bore the same *BTS1* expression cassette as JBV31. Cultures were first grown in SCM-D$_{-URA}$ medium. Subsequently, the cultivation was performed over 168 h in SCM-G$_{-URA}$ medium, and samples were taken at 0, 24, 48, 72 and 168 h. Biomass formation is illustrated by OD_{600} values in Figure 12 B while Figure 12 D displays a snapshot of the GGOH titers in mg/L and the OD_{600} at 168 h. It has to be taken into the account that the more efficient *in-situ* extraction (method 2.3.1.4), that will be described in section 3.3.2, was utilised for

GGOH extraction. The analysis was performed as described in 2.3.3. Therefore, titers should only be compared within interrelated cultivations. The highest GGOH titers were measurable in JBY6 additionally expressing *BTS1* on a plasmid (40.25 mg/L). The variant expressing the heterologous *SaGGPP*S produced 15.27 mg/L GGOH while 13.70 mg/L was detectable in the EV control. Furthermore, *PaGGPPS* and *SaGGPPS* were expressed under the control of *pGAL1*, while the *BTS1* expression was controlled by *pPGK1*. Reider Apel et al. (2016) demonstrated that there is no difference in the expression intensity of genes under the control of *pPGK1* if the medium was supplemented with glucose or galactose. However, the expression of genes under the control of *pGAL1* is 6 times higher compared to *pPGK1* in medium containing galactose (Reider Apel et al., 2016). Taking this into account, the GGOH titers might have been higher if *pGAL1* would have been utilised instead of *pPGK1* for *BTS1* expression.

Concisely, the plasmid-based overexpression of both heterologous variants is undesirable to enhance GGPP, due to decreased growth and production titers. Moreover, transformation of the plasmid was demanding and only successful with the inducible promoter *pGAL1*. Consequently, characterisation of additional heterologous GGPP synthases was essential to increase GGPP production titers.

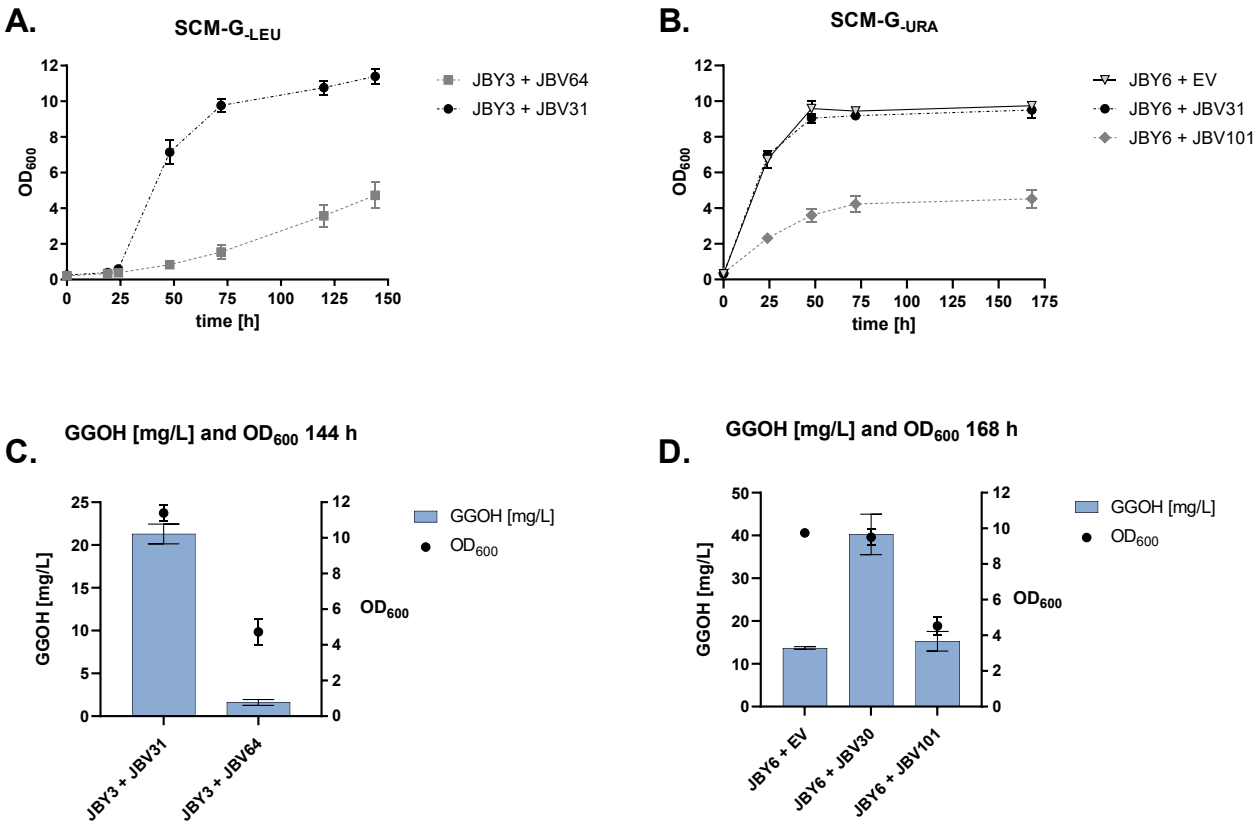

Figure 12 Plasmid-based overexpression of heterologous GGPP synthases

Cultivations of JBY3, bearing expression plasmids for *BTS1* and *PaGGPPS,* in SCM-G-$_{LEU}$ over 144 h and JBY6, carrying expression plasmids for *BTS1*, *SaGGPPS* and the EV control (SiHV006), in SCM-G-$_{URA}$ over 168 h were performed. OD_{600} values are displayed depending on the time by dots equipped with error bars, showing the standard deviation of biological triplicates (n=3). Error bars were not drawn if the corresponding standard deviation was smaller than the projected symbol. GGOH titers [mg/L] are illustrated by blue bars with error bars representing the standard deviation of biological triplicates. **A**. Biomass formation illustrated by OD_{600} values of JBY3 carrying either the *BTS1* expression plasmid (black dots) or the *PaGGPPS* variant (grey squares). **B**. Biomass formation illustrated by OD_{600} values of JBY6 carrying either the EV control (framed white triangles), *BTS1* expression plasmid (black dots) or the *SaGGPPS* variant (grey rhombus). **C**. GGOH titers in mg/L and OD_{600} values at 144 h of the cultivation of JBY3 overexpressing *BTS1* (JBV31) and *PaGGPPS* (JBV64). **D.** GGOH titers in mg/L and OD_{600} values at 168 h of the cultivation of JBY6 overexpressing *BTS1* (JBV30), *PaGGPPS* (JBV101) and the EV control (SiHV005).

3.3 Proof of Concept by δ-Tocotrienol Biosynthesis

Besides the metabolic engineering in the GGPP branch, priority was given to prove the concept of the tocotrienol biosynthesis pathway. Based on current research, the heterologous genes *HPT* of *Synechocystis* sp. PCC 6803 and *VTE1* of *A. thaliana* were chosen to be characterized in *S. cerevisiae* (Albermann et al., 2008; Shen et al., 2020; Jiao et al., 2022; Xiao et al., 2022). *AtVTE1* encodes the tocopherol cyclase which is naturally located inside the chloroplasts. During a preceding master thesis, the full-length *AtVTE1* and a truncated variant *AtVTE1*$^{tr[229\text{-}1467]}$, in which the predicted chloroplast localisation sequence was omitted, were characterised by a plasmid-based approach. However, the transformation efficiency and biomass formation during cultivations decreased when these plasmids were used. Moreover, no δ-tocotrienol was detectable during shake flask fermentations using these variants (Bauer, 2019). Based on these results, a new strategy was attempted, using galactose induction, as presented in 3.2.5. Thus, the plasmid JBV86 for the expression of *SynHPT* under the control of *pGAL1* and carrying *LEU2* as prototrophic marker was generated by Golden Gate assembly. Two plasmids for *AtVTE1* and *AtVTE1*$^{tr[229\text{-}1467]}$ expression under the control of *pGAL1* with *URA3* as prototrophic marker were generated, JBV88 and JBV89, respectively. Both combinations (JBV86 and JBV88 or JBV86 and JBV89) were co-transformed into JBY6 and incubated on solid SCM-D$_{\text{-LEU, -URA}}$ agar plates. Thereby, the poor transformation efficiency and the decreased growth were bypassed. Nevertheless, δ-tocotrienol was still not detectable in the fermentation samples of a galactose-induced shake flask fermentation (data not shown).

One drawback might have been the plasmid-based expression itself. The utilised strains were already highly engineered for GGPP and HGA synthesis. Both plasmids carried prototrophic marker genes which additionally burden the protein biosynthesis machinery. Therefore, one new strategy was the stable integration of genes for their characterisation. Moreover, *LEU2* was used as selection marker for the genomic integration and thereby recovered in the strain JBY12. The advantages of endogenous *LEU2* expression over the supplementation of leucine were also in focus of current research (Yan et al., 2023). Therefore, the recovery of the Leu$^+$ prototrophy enhances the flexibility for these strains. The cells can balance the *in-house* synthesis of leucine and the import of supplemented leucine from the medium. Additionally, the *BTS1* expression cassette was integrated for sufficient GGPP synthesis. First, the donor DNA for the integration of a the *SynHPT*, under the control of *AP8* and *tPGK1*, and the *AtVTE1,* under the control of *AP6* and *tTDH1* was constructed by Golden Gate assembly (JBV131), bearing a ClonNAT cassette as resistance marker. Analogously, the donor DNA for *BTS1*, using *AP7* and *tADH1* as

regulatory elements, and carrying *LEU2* as marker gene, was built (JBV134). Successively, both integrations were performed by transformation of their parent strain JBY4 to generate the strains JBY11 and JBY12.

The strain JBY12 was characterised by shake flask fermentations of SCM-D medium and YPD medium for 144 h in biological duplicates (method 2.1.2.1). HGA samples were prepared from the supernatant and analysed by HPLC (method 2.3.1.1 and 2.3.2.1). However, the detected HGA titers probably underestimate the total HGA formation since the brownish discoloration from pyomelanin was observed within all shake flasks of the YPD cultivation. This phenomenon is due to the autooxidation of HGA resulting in the formation of pyomelanin pigments (Coon et al., 1994; Carreira et al., 2001; Larroude et al., 2021). This corresponds to the lower titers of 62.30 mg/L HGA in the YPD cultivation, compared to 219.65 mg/L HGA in SCM-D medium (Figure 13). Moreover, lower pH values were determined at the end of the fermentation in SCM-D medium (pH 2.8) compared to YPD (pH 4.7) medium. 9.98 mg/L (YPD) and 4.06 mg/L (SCM-D) of GGOH were detected after 144 h of cultivation (method 2.3.1.2 and 2.3.3). Higher biomass formation was monitored by the OD_{600} measurements after 144 h within the YPD cultures. Furthermore, δ-tocotrienol was detectable for the first time during this study in JBY12. The extraction and analysis were performed with the pellet of the whole culture (method 2.3.1.2 and 2.3.2.2). 1.53 mg δ-tocotrienol was detected in total from a 50 ml SCM-D culture. No δ-tocotrienol was detectable in the samples of the cultivation performed in YPD.

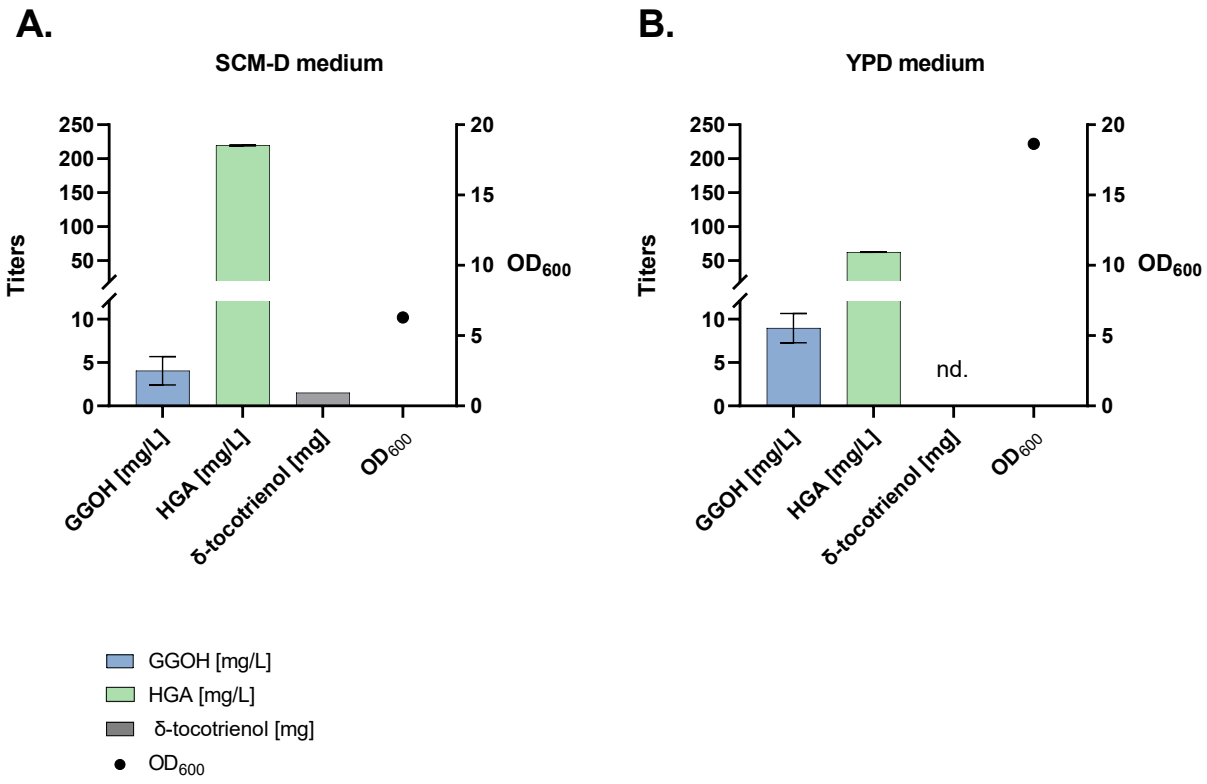

Figure 13 Shake flask cultivations of JBY12

Shake flask cultivations of JBY12 were performed in SCM-D and YPD medium, depicting metabolite titers and biomass formation at 144 h. Illustrated values correspond to the mean and the error bars to the range of biological duplicates (n=2). OD_{600} values are displayed by dots without error bars since the corresponding range was smaller than the projected symbol. GGOH titers [mg/L] are portrayed by blue bars, green bars illustrate HGA titers [mg/L] and the δ-tocotrienol titer in mg (whole culture was harvested) is shown by a grey bar; no bar was drawn if δ-tocotrienol was not detectable (nd.). **A**. Metabolite titers and biomass formation of the cultivation performed with SCM-D medium **B**. Metabolite titers and biomass formation of the cultivation conducted in YPD medium.

The absence of tocotrienol synthesis might correspond to the autooxidation of HGA in YPD medium. Thus, less precursor molecules would be available for the tocotrienol biosynthesis. Combined with the deficient performance of the full-length *VTE1*, the production rate of tocotrienol might be below the detection limit. Furthermore, δ-tocotrienol titers are much lower than the detected precursors. Since there was no commercially available standard of the product of the HPT, MGGBQ, it was difficult to determine whether HPT or VTE1 was the rate-limiting enzyme. To draw a clearer picture of the HPT and VTE1, their expression was monitored using a GFP tag. Expression plasmids (JBV125 and JBV126), bearing a C-terminal envyGFP tag, were construed and characterised in CEN.PK2-1C as performed for *BTS1* and *HPPD* (3.2.1). Figure 14 displays the expression of both enzymes in *S. cerevisiae*. Unfortunately, only 10 - 15 % of the cells were fluorescent under the microscope. Hereby, the plasmid-based expression

of the enzymes led also to a decreased growth phenotype, and therefore the conclusion was drawn that the enzymes might have a toxic effect in the cells. *URA3* was used as selection marker on the expression plasmid. Usually, cells carrying the plasmid are able to synthesise uracil and maintain the survival pressure of the medium. If the burdening heterologous proteins have a survival disadvantage, the cells would be more likely to survive if they had lost the plasmid. By re-integration of the *URA3* expression cassette into the genome, cells would have been able to overgrow the culture. Furthermore, dysfunctional heterologous genes are rapidly degraded.

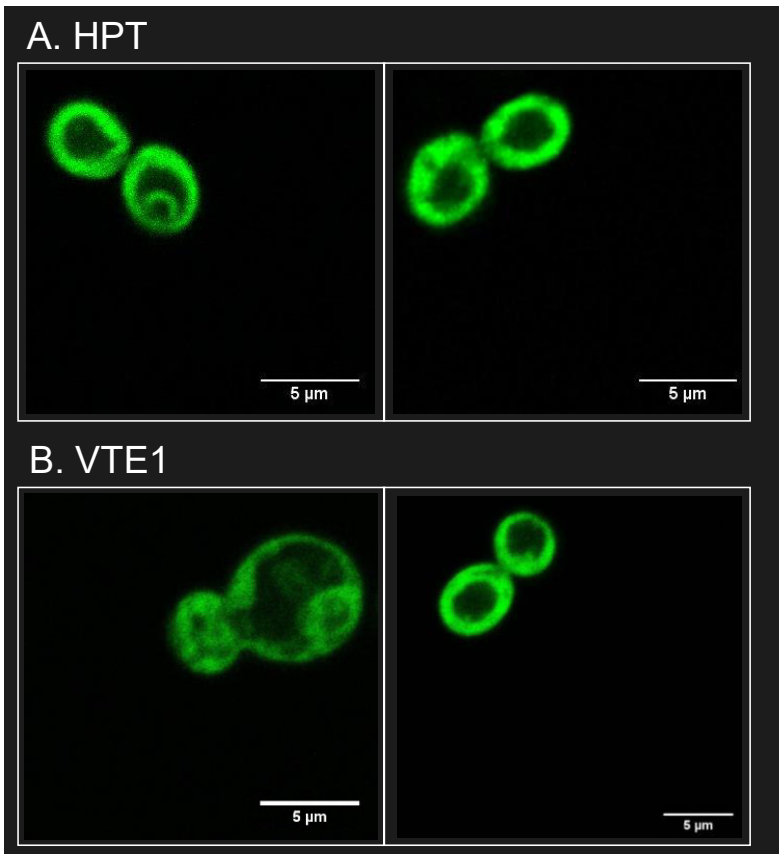

Figure 14 Laser confocal microscopy of envyGFP-tagged SynHPT and AtVTE1

Expression of the *SynHPT* and the full-length *AtVTE1*, carrying a C-terminal envyGFP tag in CEN.PK2-1C. After cultivation in synthetic low fluorescent medium, cells were immobilised with 0.6% (w/v) low melt agarose. Fluorescence of the GFP was observed with a confocal laser scanning microscope (Zeiss LSM 780). The 5 µm scale indicates the size ratio of each image. **A**. HPT protein distribution in CEN.PK2-1C cells visualised by envyGFP. **B.** VTE1 protein distribution in CEN.PK2-1C cells visualised by envyGFP.

3.3.1 Increasing δ-Tocotrienol Titers by *XdcrtE* Expression and the Truncation of the Chloroplast Targeting Signal of *AtVTE1*

Based on current research, various truncated versions of the *AtVTE1* were characterised and the highest cyclase activity was achieved by the truncation of 47 amino acids of the chloroplast transit peptide (CTP) (Shen et al., 2020). Therefore, the *AtVTE1*$^{tr[142\text{-}1467]}$ was generated by PCR (primers: JBP096 and JBP097) and the integrational plasmid JBV150 was built via Golden Gate assembly. JBY4 was transformed with the linearised plasmid to generate the strain JBY17.

In parallel, attention was drawn to the bottleneck of the GGPP synthesis. Another heterologous GGPP synthase, crtE of *X. dendrorhous,* that was obtained by directed evolution from Xie et al. (2015) was ordered as a synthetic gene, introduced to the Golden Gate system and the *XdcrtE* expression plasmid JBV146 was built. A comprehensive analysis for δ-tocotrienol production was performed by the transformation of JBY12 and JBY17 with a *BTS1* expression plasmid (JBV30), the *XdcrtE* expression plasmid (JBV146) and the empty vector control, followed by cultivation in SCM-D$_{-URA}$ medium. The analysis of GGOH and δ-tocotrienol was performed according to the foregoing cultivation in section 3.3. Figure 15 A illustrates GGOH titers in mg/L. The EV controls had the lowest GGOH titers (< 5 mg/L). In both strains, the additional expression of BTS1 increased GGOH titers to 18.55 mg/L (JBY12 + JBV30) and 14.08 mg/L (JBY17 + JBV30). Further improvement was achieved by the plasmid-based expression of the *XdcrtE*, leading to 24.82 mg/L in JBY12 and 17.47 mg/L in JBY17, respectively. Higher GGPP synthesis in JBY12 is due to the stable integration of a second *BTS1* cassette in JBY12. However, in both strains, the heterologous GGPP synthase *XdcrtE* performed better than the endogenous *BTS1*. Therefore, the attention was drawn to the differences in the δ-tocotrienol biosynthesis in JBY12 and JBY17 transformed with *XdcrtE.* Figure 15 B illustrates the δ-tocotrienol titers in mg of the whole 50 ml culture. The plasmid-based expression of *XdcrtE* led to 1.09 mg δ-tocotrienol in JBY17, bearing the truncated variant *AtVTE1*$^{tr[142\text{-}1467]}$, while only 0.22 mg were detectable in JBY12, carrying the full-length *AtVTE1*. Titers below 0.3 mg were detectable in all transformants of JBY12, while more than 1 mg was analysed in JBY17 transformants. By virtue of these results, higher δ-tocotrienol titers can be achieved with the CTP truncated variant (*AtVTE1*$^{tr[142\text{-}1467]}$) in *S. cerevisiae*. Nevertheless, the EV control of JBY17 demonstrates that additional GGPP synthase overexpression is required for a sufficient tocotrienol precursor supply. Consequently, the new strain JBY17 was employed for stable gene integration of *BTS1* and *XdcrtE*.

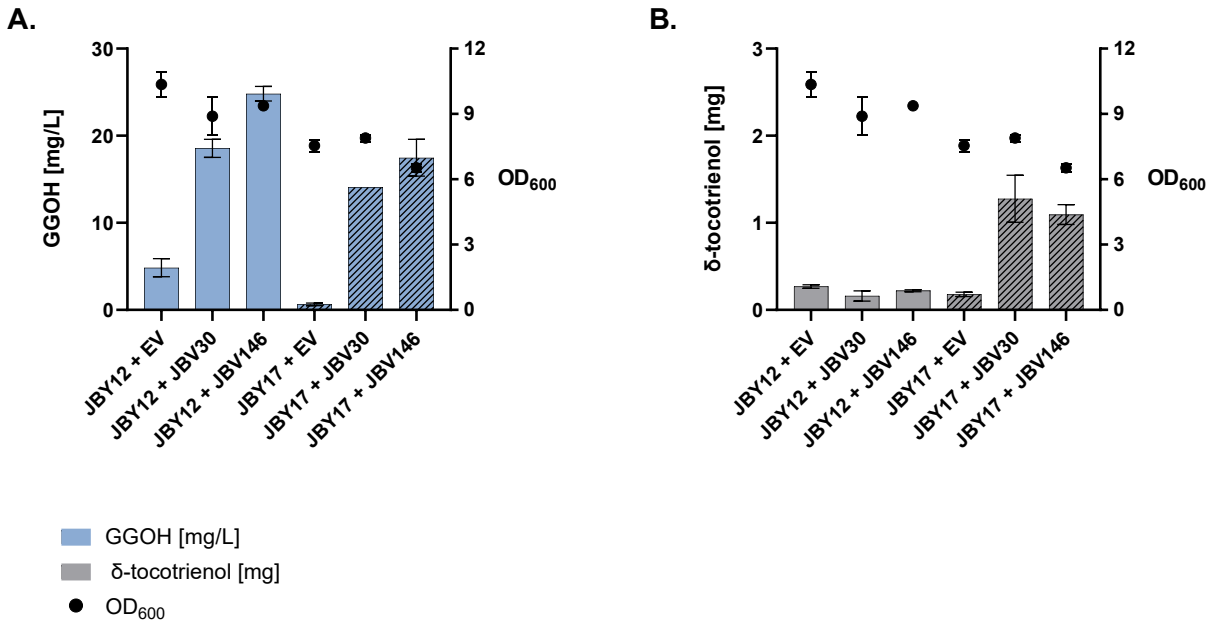

Figure 15 *XdcrtE* and *AtVTE1*$^{tr[142-1467]}$ improved tocotrienol synthesis

Shake flask fermentations of the strains JBY12 and JBY17 carrying JBV30 (*BTS1*), JBV146 (*XdcrtE*) or the EV control (SiHV005) were performed in SCM-D$_{-URA}$ medium. The graph shows the values of the 144 h samples of the fermentation. Blue bars represent GGOH titers in mg/L, grey bars show the δ-tocotrienol titers in mg and OD_{600} values are displayed by dots. For a better distinguishment between strains, JBY12 bars are illustrated without pattern while JBY17 bars are shaded. Symbols correspond to the mean and are equipped with error bars showing the range of the biological duplicates (n=2). If the corresponding range was smaller than the projected symbol, error bars were not drawn. **A**. GGOH titers in mg/L and the biomass formation of JBY12 and JBY17, carrying the GGPP synthase expression plasmids JBV30, JBV146 and the EV control. **B**. Biomass formation and δ-tocotrienol titers in mg, extracted from a 50 ml culture of JBY12 and JBY17, carrying JBV30, JBV146 and the EV control.

3.3.2 Comparison of Genome-based *BTS1* and *XdcrtE* Overexpression

The preceding analytics were performed using methanol extraction (method 2.3.1.2). For the improvement of the extraction, the methanol extraction was compared with an *in-situ* extraction fermentation (method 2.3.1.4). Therefore, a 30 % dodecane overlay was added to the fermentation medium. First, the validation of the *in-situ* extraction was performed for GGOH analysis with the strain JBY6. After transformation of JBY6 with the *BTS1* overexpression plasmid (JBV31) and the empty vector control (SiHV006), shake flask cultivations following the methods 2.1.2.1 and 2.1.2.2 were performed in biological triplicates in SCM-D$_{-LEU}$ medium. The results of two comparative shake flask fermentations are illustrated in Figure 16. The measured values have been multiplied by the culture volume and divided by the volume of the dodecane phase. Therefore, these values represent titers in mg per L culture volume and are not

overestimated due to concentration effects. More importantly, the *in-situ* extraction led to enhanced GGOH titers from 5.47 mg/L to 12.65 mg/L in JBY6, bearing the empty vector control. In the *BTS1* overexpression variant, the titers increased from 13.46 mg/L to 32.46 mg/L. The residual GGOH titers in the cell pellets of the dodecane cultivations were 1.04 mg/L (JBY6 + EV) and 1.41 mg/L (JBY6 + JBV31), respectively. These results conclusively show the limitation of the methanol extraction method due to its incomplete GGOH extraction. An additional advantage is the avoidance of the time-consuming GGOH extraction step from the cells since the main proportion of the GGOH is already extracted into the dodecane phase during the cultivation. It was concluded that the higher GGOH titers were due to this method being a better extraction method, contrary to the idea that the extraction during the cultivation might improve the GGOH synthesis. This theory was strengthened by the implementation of another extraction method (2.3.1.3) during a later stage of this study (3.5.3).

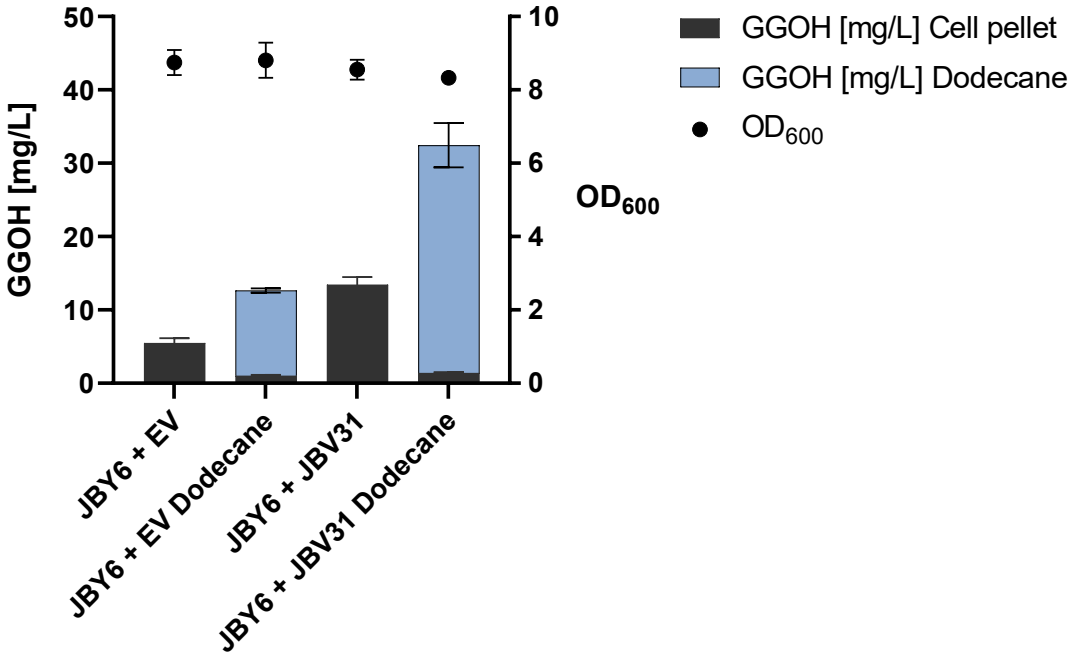

Figure 16 Dodecane overlay led to higher GGOH titers

OD_{600} values and GGOH titers in mg/L of the strain JBY6, bearing the plasmid JBV31 (*BTS1*) and SiHV006 (EV), are displayed after 144 h of cultivation. SCM-D_{-LEU} medium was used with and without a dodecane overlay, respectively (n=3). The GGOH titers of the dodecane phase are represented by blue bars, while residual GGOH in the pellets is illustrated by black bars. The standard deviation is shown by error bars. OD_{600} values are displayed by black dots with error bars indicating the standard deviation. The error bars were not drawn if the corresponding standard deviation was smaller than the projected symbol.

Second, the *in-situ* extraction was characterised regarding the tocotrienol analytics. In consequence of this, the strains JBY18 and JBY20 were constructed to avoid the requirement of plasmid-based expressions. Analogous to the construction of JBY12, the δ-tocotrienol producer strain JBY17 was employed for the integration of a second *BTS1* overexpression cassette with JBV134, generating JBY18. For the integration of *XdcrtE* under the control of *pTDH3* and *tSSA1,* the integrational plasmid JBV147 was built by Golden Gate assembly. A *LEU2* expression cassette was used as selection marker. JBY17 was transformed with the linearised JBV147 and the cassette was integrated upstream of the *HO* locus by homologous recombination for the construction of JBY20.

A comprehensive characterisation of JBY18 and JBY20 was achieved through cultivation in SCM-D medium and SCM-D medium with a 30 % dodecane overlay, respectively. Analysed δ-tocotrienol samples validated the *in-situ* extraction method by achieving higher titers in both strains (Figure 17). First, only the production titers of the cultivations without dodecane are discussed for comparison with the cultivation depicted in Figure 15. GGOH titers increased from 14.08 mg/L (JBY17 + JBV30) to 22.16 mg/L by the stable integration of *BTS1* (JBY18), and from 17.47 mg/L (JBY17 + JBV146) to 32.73 mg/L by the integration of *XdcrtE* (JBY20). The whole pellet was extracted according to method 2.3.1.2 for cultivations without the dodecane overlay. Measured values were recalculated to 50 ml culture volumes for a coherent presentation of δ-tocotrienol titers in mg/L (Figure 17 B). The δ-tocotrienol titers were enhanced from 0.03 mg/L (JBY17 + JBV30) to 0.22 mg/L (JBY18). Moreover, in JBY20 the stable integration of *XdcrtE* enhanced δ-tocotrienol titers from 0.02 mg/L to 0.22 mg/L. Apart from this, even higher titers were measured by the *in-situ* dodecane extraction, detecting 30.19 mg/L GGOH in JBY18 and 50.84 mg/L GGOH in JBY20, respectively (Figure 17). Due to the increased GGPP synthesis, higher δ-tocotrienol titers were achievable in both strains. JBY20 was the best performing strain, producing 1.66 mg/L δ-tocotrienol. By virtue of these results, subsequent cultivations were performed using the *in-situ* extraction method (2.3.1.4).

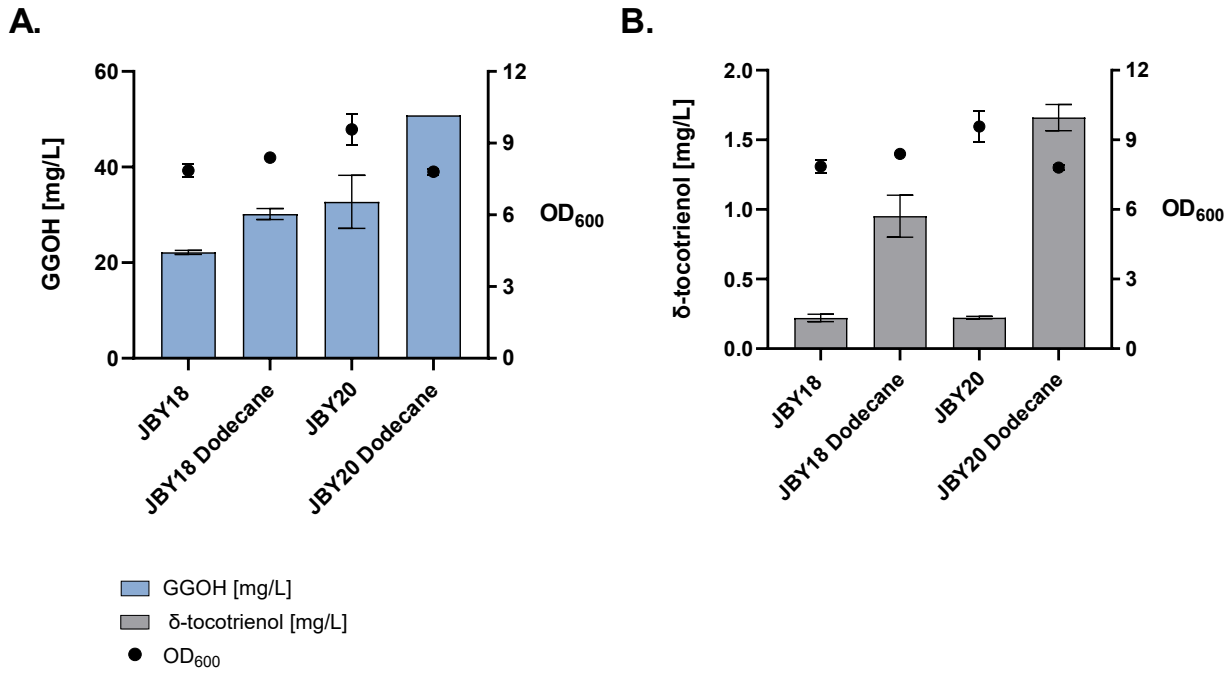

Figure 17 Comparison of genome-based overexpression of *BTS1* and *XdcrtE*

Shake flask fermentations of the strains JBY18 and JBY20 were performed in SCM-D$_{-URA}$ medium, with and without a dodecane overlay (n=2). Blue bars illustrate GGOH titers in mg/L, while grey bars represent δ-tocotrienol titers in mg/L. OD_{600} values are displayed by dots of the 144 h samples. All symbols correspond to the mean and are equipped with error bars, showing the range of biological duplicates. If the corresponding range was smaller than the projected symbol, error bars were not drawn. **A**. GGOH titers in mg/L and the OD_{600} values of JBY18 and JBY20 extracted by methanol extraction (2.3.1.2) or *in-situ* dodecane extraction (2.3.1.4). **B**. Biomass formation and δ-tocotrienol titers in mg/L of JBY18 and JBY20 extracted by methanol extraction (2.3.1.2) or *in-situ* dodecane extraction (2.3.1.4).

3.3.3 Limitations of Endogenous Gene Overexpression

To find other steps in addition to the limitation of the endogenous *BTS1*, several other strains were constructed and characterised, whether they improve δ-tocotrienol titers. Since *ERG20* overexpression led to an increased GGOH synthesis (section 3.2.4) the *BTS1-ERG20* overexpression strain JBY23 and the *XdcrtE-ERG20* overexpression strain JBY24 were built. Therefore, integrative plasmids were assembled by Golden Gate (JBV133 and JBV149) and strain construction for JBY23 and JBY24 was conducted analogously to JBY20. However, the additional *ERG20* expression cassette did not increase GGOH or δ-tocotrienol synthesis (data not shown). Therefore, additional *ERG20* overexpression was not included in further strain engineering.

Another approach was the codon optimisation of the endogenous *BTS1* gene, due to its inferior performance compared to *XdcrtE*. Thus, the strain JBY58 was built analogously to the foregoing strains with the integrative plasmid JBV173 (*BTS1*^{co}). The strains JBY18 (*BTS1*), JBY20 (*XdcrtE*) and JBY58 (*BTS1*^{co}) only differed regarding the overexpression of the GGPP synthase. A comprehensive shake flask fermentation of these strains was performed in biological triplicates over 144 h. The fermentation was performed with SC-D medium with a 30 % dodecane overlay for *in-situ* extraction. Samples of the following time points were analysed: 0 h, 24 h, 48 h, 72 h, and 144 h (method 2.3.1.4 and 2.3.2.2). Figure 18 illustrates the metabolite titers and biomass formation of the different strains depending on the time. The growth curves of all samples were similar reaching OD_{600} values of 18.2 (JBY18), 18.8 (JBY20) and 18.4 (JBY58) after 144 h of cultivation. The effect of the different GGPP synthases was visualised by GGOH and δ-tocotrienol analysis. JBY20 (*XdcrtE*) was the best performing strain synthesising 55.66 mg/L GGOH and 1.7 mg/L δ-tocotrienol after 144 h. Moreover, the codon optimisation of *BTS1* improved GGOH titers from 13.76 mg/L to 31.56 mg/L and δ-tocotrienol titers from 0.93 mg/L to 1.2 mg/L.

Consequently, the additional codon optimisation of endogenous genes is a powerful method to increase gene expression and metabolite titers. Moreover, it is more likely that an endogenous gene leads to a functional protein. Therefore, it may be an alternative to codon optimise endogenous genes before screening various heterologous genes. The calculation of the codon adaptation index (CAI) demonstrates whether it is useful to optimise the sequence of the endogenous gene. With respect of the *BTS1* the CAI was increased from 0.74 to 0.85 in the *BTS1*^{co} (method 2.2.1). The enhanced GGOH titers in JBY58 compared to JBY18 might be due to the higher CAI, that positively correlates with the level of gene expression. However, JBY20 (*XdcrtE*) was the best performing strain and therefore was utilised for further strain engineering.

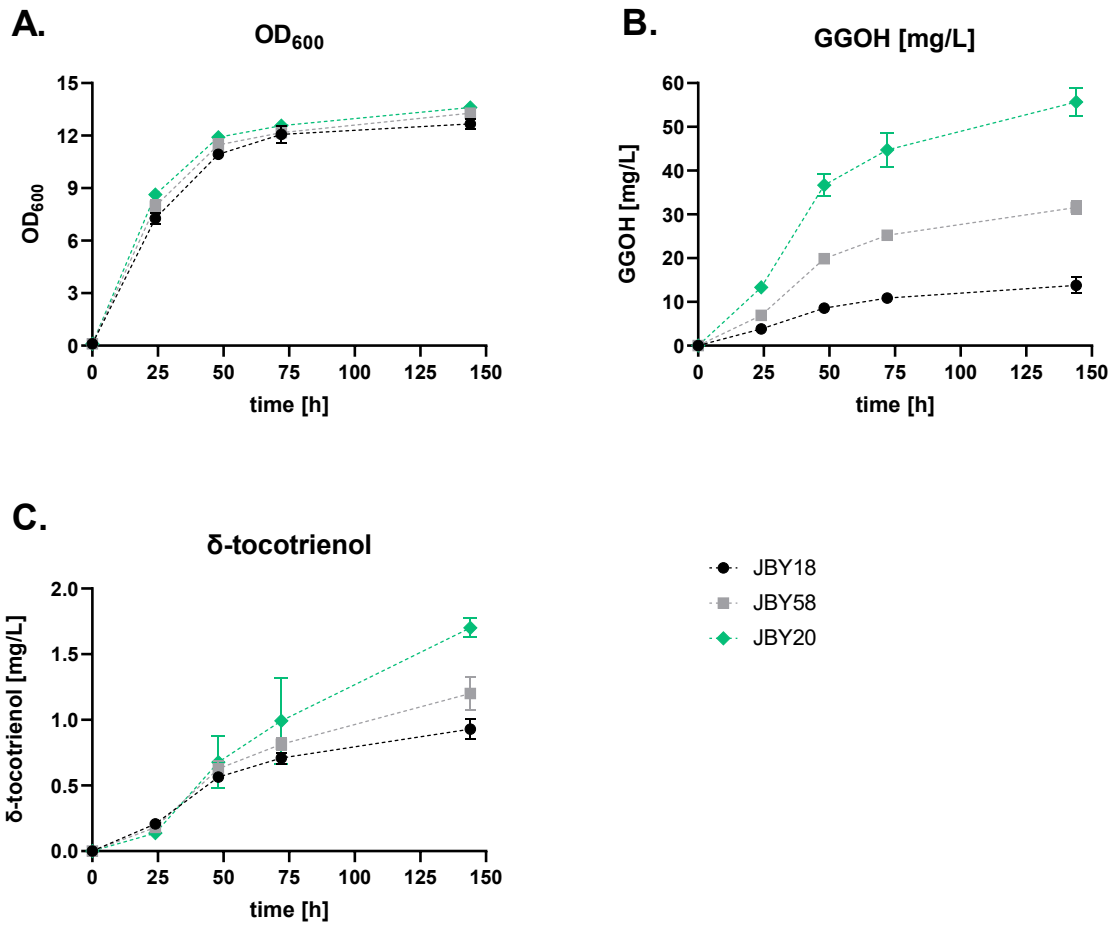

Figure 18 Comprehensive analysis of *BTS1*, *BTS1^{co}* and *XdcrtE*

Cultivations of JBY18 (*BTS1*), JBY58 (*BTS1^{co}*) and JBY20 (*XdcrtE*) were performed in SC-D medium with a 30 % dodecane overlay over 144 h. Metabolite titers and OD_{600} values are displayed depending on the time by a black dot (JBY18), a grey square (JBY58) and a green diamond (JBY20). GGOH and δ-tocotrienol were extracted by dodecane overlay and analysed by HPLC. Symbols are equipped with error bars showing the standard deviation of biological triplicates (n=3). Error bars were not drawn if the corresponding standard deviation was smaller than the projected symbol. **A**. Biomass formation illustrated by OD_{600} values over 144 h. **B.** GGOH titers in mg/L over 144 h. **C.** Formation of δ-tocotrienol in mg/L over 144 h.

3.3.4 Heterologous Tocotrienol Pathway Affecting Precursor Titers

The two foregoing experiments demonstrated that the heterologous *XdcrtE* was the best performing GGPP synthase. Nevertheless, the parent strain of JBY20 (JBY17) was already bearing the two enzymes of the tocotrienol pathway and therefore consumes GGPP. For a comprehensive analysis of the improvement of the isopentenyl diphosphate biosynthesis, a strain for improved GGPP biosynthesis that lacks the tocotrienol biosynthesis pathway was constructed (JBY61). Analogous to JBY20, JBY61 was generated with the linearised

integration plasmid JBV147, but JBY4 was utilised as the parent strain instead of JBY17. Therefore, JBY61 has the same genotype as JBY20, except for the absence of the tocochromanol biosynthesis enzymes *SynHPT* and *AtVTE1*$^{tr[142-1467]}$. Subsequently, biological triplicates of JBY20 and JBY61 were cultivated in SC-D medium in shake flasks for 144 h and GGOH was extracted by *in-situ* extraction (method 2.1.2.2). Method 2.3.1.1 and 2.3.3 were used for the analysis of HGA and GGOH, respectively. Figure 19 illustrates the titers of the precursors GGPP and HGA in both strains after 144 h of cultivation. 54.03 mg/L GGOH was detected in JBY20 and 64.23 mg/L GGOH in JBY61. The influence on the precursor consumption was notably stronger for HGA, detecting 194.22 mg/L HGA in JBY20 cultures and 429.48 mg/L for JBY61. In concordance with these data, the assumption can be made that both precursors are consumed by the enzymes of the tocotrienol biosynthesis pathway.

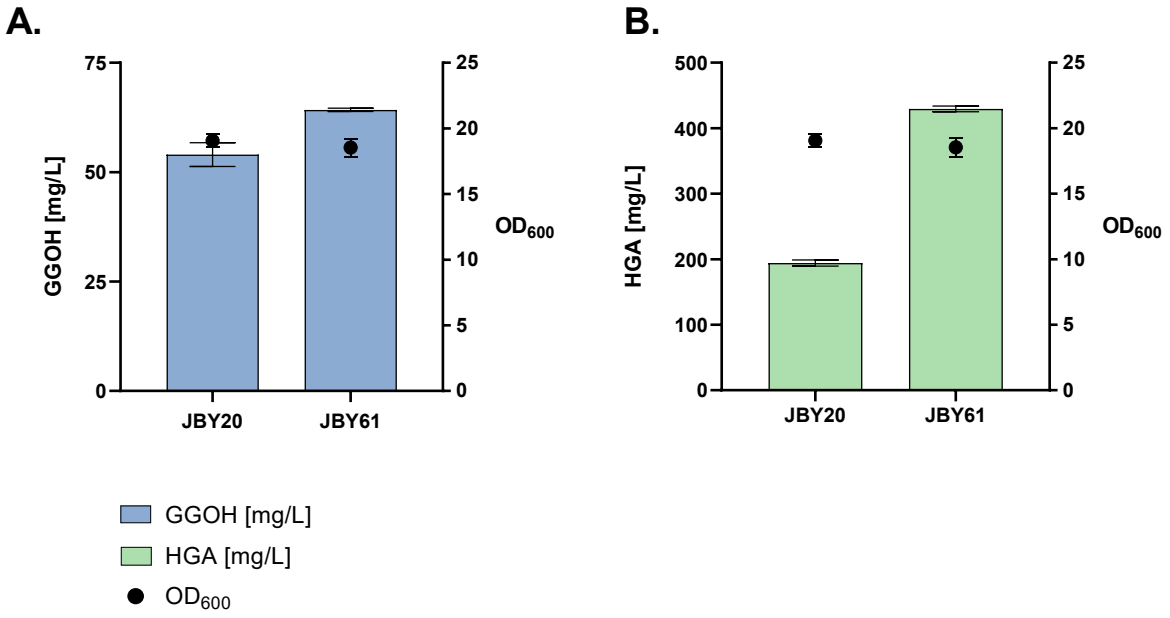

Figure 19 The impact of the expression of tocotrienol pathway enzymes on precursor titers

Shake flask cultivations of biological triplicates of JBY20 and JBY61 were performed in SC-D medium with in-situ dodecane extraction. Metabolite titers are illustrated by bars and correspond to the mean of biological triplicates (n=3). OD_{600} values are displayed by dots. The standard deviation is presented by error bars. **A**. GGOH titers [mg/L] are portrayed by blue bars, and biomass formation of JBY20 and JBY61. **B**. Green bars illustrate HGA titers in mg/L and the corresponding growth of the cultures is shown by OD_{600} values.

3.4 Beta Carotene Synthesis Illustrating a Sufficient GGPP Supply

In view of the engineered isopentenyl diphosphate biosynthesis, the strains qualified for further engineering of the β-carotene biosynthesis pathway. Therefore, two heterologous enzymes needed to be introduced into *S. cerevisiae*, crtYB and crtI of *X. dendrorhous* (Verwaal et al., 2007). Due to the orange coloration of β-carotene, the proof of concept of β-carotene synthesis was visible by the naked eye. Another advantage was the indirect demonstration of enhanced GGPP biosynthesis. In foregoing experiments, GGPP titers were inferred by measurement of the dephosphorylated GGOH. Here, the synthesis of β-carotene serves as a second indirect detection method for GGPP biosynthesis.

3.4.1 Proof of Concept for β-Carotene Synthesis Using a Plasmid-Based Approach

A plasmid-based gene expression approach was chosen to prove the concept of β-carotene synthesis in the strains JBY18 and JBY20. The δ-tocotrienol producer strain JBY18 overexpresses a second cassette of *BTS1* while JBY20 bears an overexpression cassette of the heterologous GGPP synthase *XdcrtE*. First, the synthetic genes *XdcrtI* and *XdcrtYB* of *X. dendrorhous* were ordered as codon optimized genes for *S. cerevisiae* with overhangs for Golden Gate cloning. Two cassette plasmids were generated by Golden Gate assembly. The phytoene desaturase *XdcrtI* was cloned under the control of *pPGK1* and *tTDH1* (JBV178), while the bifunctional phytoene synthase and lycopene cyclase *XdcrtYB* was under the control of *pTEF1* and *tENO2* (JBV179). Subsequently, both plasmids were assembled by Golden Gate cloning with SiHV005 to generate one *XdcrtI* and *XdcrtYB* expression plasmid, carrying *URA3* as selection marker (JBV180). JBY18 and JBY20 were transformed with JBV180 and the EV (SiHV005) control. The transformation efficiency of both strains with JBV180 was insufficient, yielding only two colonies each, while the efficiency with the empty vector control was plentiful. Therefore, a genome-based approach was chosen for further investigation of β-carotene biosynthesis. Nevertheless, the successfully transformed colonies and the empty vector control of JBY20 were streaked out one selective SC-D_{-URA} plates for comparison. The yellowish staining, signalling the production of β-carotene, was directly visible by the naked eye (Figure 20). Moreover, JBY20 appeared to produce more β-carotene due to its stronger orangish colour compared to JBY18.

Figure 20 Plasmid-based β-carotene synthesis in *S. cerevisiae*

JBY18 and JBY20 were transformed with the *XdcrtYB* and *XdcrtI* overexpression plasmid (JBV180) using *URA3* as selection marker. JBY20 transformed with the EV control (SiHV005) was portrayed as a control. Transformants were streaked on a SC-D_{-URA} agar plate for comparison of the transformants on the same plate. From top to bottom, JBY20, bearing the EV control (SiHV005), JBY18 and JBY20, carrying the *XdcrtYB-XdcrtI* overexpression plasmid (JBV180).

3.4.2 Construction of a Stable β-Carotene Producer Strain

For further investigation of the influence on β-carotene biosynthesis, *XdcrtYB* and *XdcrtI* were introduced into the genome of *S. cerevisiae*. The strain JBY4 was employed as the parent strain for the stable biosynthesis of β-carotene. For this reason, the integrational plasmid (JBV187) was assembled of JBV178, JBV179 and SiHV110 by Golden Gate cloning. The linearized plasmid enabled the integration of the *XdcrtYB* and *XdcrtI* expression cassettes into the *LEU2* locus of JBY4 using ClonNAT as selection marker, generating JBY62. The yellowish colouration of JBY62 was directly visible (Figure 21 B). Moreover, the GGPP synthase *XdcrtE* was integrated for improved β-carotene production. Therefore, the linearized integration plasmid JBV147 was utilised for the integration by homologous recombination upstream of the *HO* locus of JBY62, generating JBY63. JBV147 carried a *LEU2* cassette as selective marker, and thereby recovered the leucine prototrophy of this strain. Figure 21 B visually displays the improved β-carotene synthesis in JBY62 and JBY63 after 24 h of shake flask cultivation in SC-D medium. This substantiates the importance of the introduction of the heterologous GGPP synthase *XdcrtE* besides the endogenous expression of *BTS1*, in both strains.

Furthermore, the deletion of a membrane-associated lipid phosphatase was a candidate to target an increase of the GGPP pool in *S. cerevisiae*. *DPP1* encodes for the diacylglycerol pyrophosphate phosphatase, which not only dephosphorylates diacylglycerol pyrophosphate but is also involved in the dephosphorylation of GGPP (Toke et al., 1998). Consequently, a CRISPR/Cas9 plasmid targeting *DPP1* was constructed (JBV169). The strain JBY63 was transformed with JBV169 and the corresponding donor DNA, JBP117. After successful strain construction, the strain JBY66 was obtained, lacking the ORF of *DPP1*.

To determine the influence of *XdcrtYB* and *XdcrtI* expression on GGPP titer, a shake flask fermentation of JBY20, JBY63 and JBY66 was performed (method 2.3.1.4 and 2.3.3). Figure 21 A portrays the GGOH titers in mg/L and the corresponding OD_{600} of the 144 h sample. JBY20 produced 52.13 mg/L of GGOH, while the β-carotene producer strains produced 20.99 mg/L (JBY63) and 17.12 mg/L (JBY66), respectively. The biomass formation was comparable in all strains. The significantly lower GGOH titers in the β-carotene producer strains might refer to the more efficient consumption of GGPP by the enzymes *XdcrtI* and *XdcrtYB*. Due to the *DPP1* deletion (JBY66), less GGPP may be converted into GGOH. Consequently, more GGPP will be available for downstream metabolic pathways. In JBY20, GGPP is consumed by the *SynHPT* and further converted by the *AtVTE1*. Due to higher GGOH titers in JBY20, the consumption of the substrate GGPP appeared to be more efficient by the enzymes of the β-carotene branch, compared to the enzymes of the tocotrienol pathway.

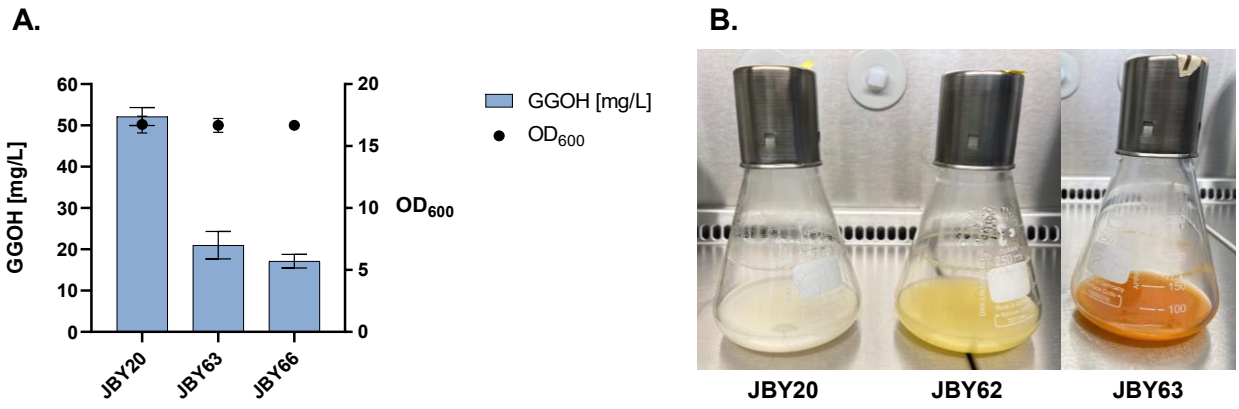

Figure 21 *XdcrtE* integration improves β-carotene synthesis

A shake flask fermentation of JBY20, JBY63 and JBY66 was performed in biological triplicates for 144 h in SC-D medium. **A**. GGOH titers [mg/L] and OD_{600} values of the strains JBY20, JBY63 and JBY66 are displayed after 144 h of cultivation. The mean GGOH values are represented by blue bars and OD_{600} values are illustrated by black dots. Symbols are equipped with error bars representing the standard deviation. No error bars were drawn when the standard deviation was smaller than the projected symbol. **B**. Photos of a representative shake flask culture of JBY20, JBY62 and JBY63 after 144 h of cultivation.

3.5 Metabolic Engineering of the Tocochromanol Biosynthesis Pathway

By virtue of the foregoing results, the metabolic engineering for an improved GGPP precursor supply was successful. Moreover, by the sufficient production of both precursors and the successful implementation of the δ-tocotrienol biosynthesis pathway 1.66 mg/L δ-tocotrienol was produced by JBY20. The next challenges were to increase the titer and to achieve the biosynthesis of other forms of tocotrienol besides δ-tocotrienol.

3.5.1 Identification of a Second Functional HPT

The consumption of GGPP by the enzymes of the β-carotene biosynthesis demonstrated limitations within the tocotrienol pathway of JBY20. Consequently, the characterisation of alternative heterologous enzymes was desired in *S. cerevisiae*. Thus, a literature research and a sequence analysis were conducted to select further heterologous genes encoding for the HPT and the TC in addition to *SynHPT* and the *AtVTE1*, respectively. The TC sequences of the following organisms were codon optimised for *S. cerevisiae* and cloned into expression plasmids by Golden Gate assembly: *Hordeum vulgare* TC (KAE8812750.1), *Oryza sativa* TC (BAD21816.1), *Anabaena* sp. UHCC 0204 TC (WP_168492005.1) and *Synechocystis* sp. PCC 6803 (BAA17775.1). The plasmid-based expression of these TCs (JBV119-JBV122), in combination with the *SynHPT*, did not result in any δ-tocotrienol production (data not shown). Thus, the following section will focus on the characterisation of the heterologous HPTs.

The enzymes varied in their substrate specificity, using either PDP or GGPP to produce MPBQ or MGGBQ, respectively. Naturally, PDP is the preferred substrate of the *SynHPT* (Collakova and DellaPenna, 2001). Hence, variants which prefer GGPP as a substrate were intentionally included in the search. Two heterologous sequences from plants and two sequences from cyanobacteria were chosen based on sequence distinctions and enzyme properties. Within the plant category the gene *EgHPT* of *Elaeis guineensis* (NP_001291355.1) was selected, having only 32 % sequence identity and 46 % similarity on a protein level with the *SynHPT* (EMBOSS Needle Alignment EMBL-EBI; EBLOSUM62, Gap penalty 10, extend penalty 0.5)[2]. Furthermore, the genes *HvHGGT* of *H. vulgare* (AAP43911.1) and *NosHGGT* (BAY79411.1) of *Nostoc linckia* NIES-25, which have a higher substrate specificity for GGPP, were chosen. (Cahoon et al., 2003; Yang et al., 2011). The *NosHPT* (WP_174711478.1) from *Nostoc* sp. TCL240-02 was also selected. All heterologous sequences were codon optimised, ordered as

[2] https://www.ebi.ac.uk/Tools/psa/emboss_needle/

synthetic genes, and cloned into expression and integrative vectors by Golden Gate assembly. First, a screening of the new variants was performed by plasmid-based overexpression (JBV115, JBV116, JBV117 and JBV118). Out of the four variants, only the *NosHPT (Nostoc* sp. TCL240-02) led to detectable δ-tocotrienol formation (data not shown). Thus, the strain JBY20 was reconstructed with the *NosHPT* instead of the *SynHPT*. Therefore, the integrational plasmid JBV159 and successively the strains JBY21 and JBY22 were generated. The same procedure was conducted as for the generation of JBY20 (section 3.3.2) and therefore the only distinction between JBY20 and JBY22 is the *HPT* gene variant.

A shake flask fermentation over 144 h was performed with both strains to evaluate their δ-tocotrienol synthesis. The cultures were grown in biological triplicates in SCM-D, metabolites were *in-situ* extracted by a dodecane overlay and analysed according to 2.3.3 and 2.3.2.2. Figure 22 illustrates the detection of 30.3 mg/L GGOH in JBY20 and 35.72 mg/L GGOH in JBY22. JBY20 produced 0.95 mg/L δ-tocotrienol while 0.41 mg/L was detected in JBY22. Higher accumulation of the precursor GGOH and a lower production titer of δ-tocotrienol lead to the conclusion that the *SynHPT* is the better performing prenyltransferase in *S. cerevisiae*. Thus, this study was continued with the *SynHPT*.

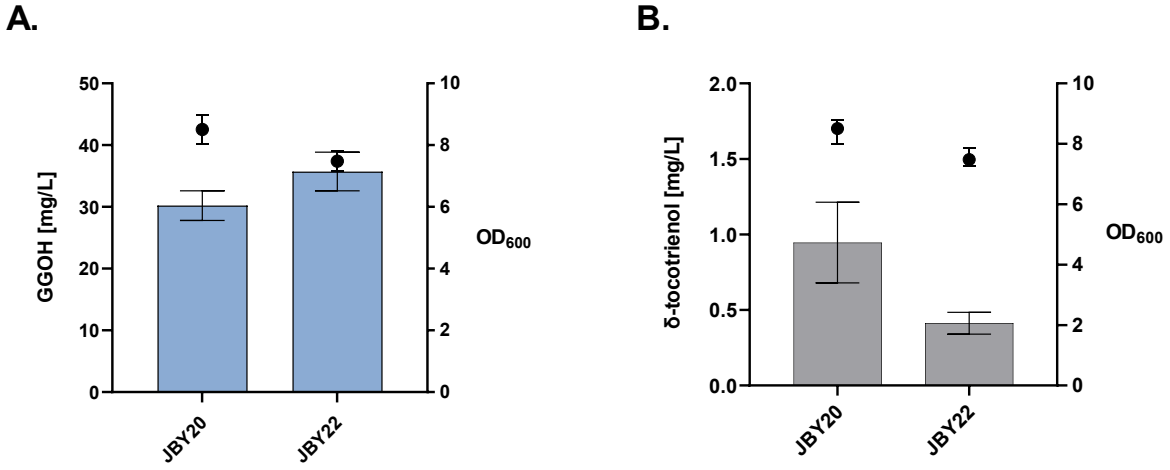

Figure 22 Suitability of two different heterologous prenyltransferases for δ-tocotrienol synthesis

Shake flask cultivations of JBY20 (*SynHPT*), JBY22 (*NosHPT*) were performed in SCM-D medium with a dodecane overlay. The final metabolite titers of the 144 h samples are illustrated by bars and error bars correspond to the mean of biological triplicates (n=3). OD_{600} values are displayed by dots. **A**. Blue bars illustrate GGOH titers in mg/L and the final OD_{600} values of the 144 h samples are displayed. **B**. Grey bars illustrate δ tocotrienol titers in mg/L and the corresponding growth of the cultures is shown by their OD_{600} values.

3.5.2 *DPP1*Δ and Integration of a Second *HPT-trVTE1* Expression Cassette

Within the complex metabolism of *S. cerevisiae*, products and intermediates of the tocotrienol pathway also correlate with competing or degrading pathways. In theory, the deletion of *DPP1* in JBY20 will decrease dephosphorylation of GGPP into GGOH and thereby increase the GGPP pool for further tocotrienol biosynthesis. Moreover, the *DPP1* locus was utilised as locus for the integration of a second *SynHPT-AtVTE1*$^{tr[142-1467]}$ expression cassette to further improve δ-tocotrienol biosynthesis. The expression cassette of both genes (JBV150) was amplified by PCR with overhangs for the *DPP1* locus (primers: JBP142 and JBP143). Subsequently, the strain JBY67 was constructed by the transformation of JBY20 with the CRISPR/Cas9 plasmid JBV169 and the corresponding donor DNA. Two control strains were generated. First, the *DPP1* deletion strain JBY57, without any combined integration, was constructed from JBY20, as described for JBY66 (3.4.2). Then, the strain JBY68 with an intact *DPP1* locus, but bearing a second *SynHPT-AtVTE1*$^{tr[142-1467]}$ expression cassette was built. Here, the second cassette was amplified from JBV150 (primers: JBP144 and JBP145), bearing overhangs for the integration into *ChrIV 53688-53756Δ* of JBY20. This locus lies between *GCS1* and the re-integrated *LEU2* gene and was targeted with the CRISPR/Cas9 plasmid JBV70.

A comprehensive shake flask fermentation was performed with biological triplicates of JBY20, JBY57, JBY67 and JBY68 in SC-D medium with a dodecane overlay over 144 h (method 2.3.1.4 and 2.3.2.2). The final GGOH titers were comparable in the *DPP1* deletion strain and its parent strain, detecting 52.05 mg/L (JBY20) and 49.42 mg/L (JBY57) of GGOH. In addition, 1.03 mg/L δ-tocotrienol was detected in JBY20 and 1.26 mg/L in JBY57. Consequently, the *DPP1* deletion did not have a major impact on the GGOH or δ-tocotrienol titers. However, the integration of a second *SynHPT-AtVTE1*$^{tr[142-1467]}$ expression cassette led to increased GGOH titers of 60.69 mg/L in JBY67 and 61.52 mg/L in JBY68. Moreover, the limitation of the enzymes of the tocotrienol pathway was verified by the integration of the second expression cassette. The δ-tocotrienol synthesis was increased to 2.94 mg/L in JBY68 and 3.55 mg/L in JBY67. Consequently, the effect of the *SynHPT-AtVTE1*$^{tr[142-1467]}$ integration into *DPP1* was higher than the *DPP1* deletion alone. Furthermore, the integration into the *DPP1* locus led to higher titers than the integration into *ChrIV 53688-53756Δ* without a *DPP1* deletion. On the one hand, the effect might derive from the lower conversion rate of GGPP in the *DPP1* deletion strains. Whereas on the other hand, the higher availability of GGPP combined with a higher enzyme concentration of HPT and VTE1, improved tocotrienol biosynthesis. Consequently, the subsequent experiments were conducted with the best performing strain JBY67.

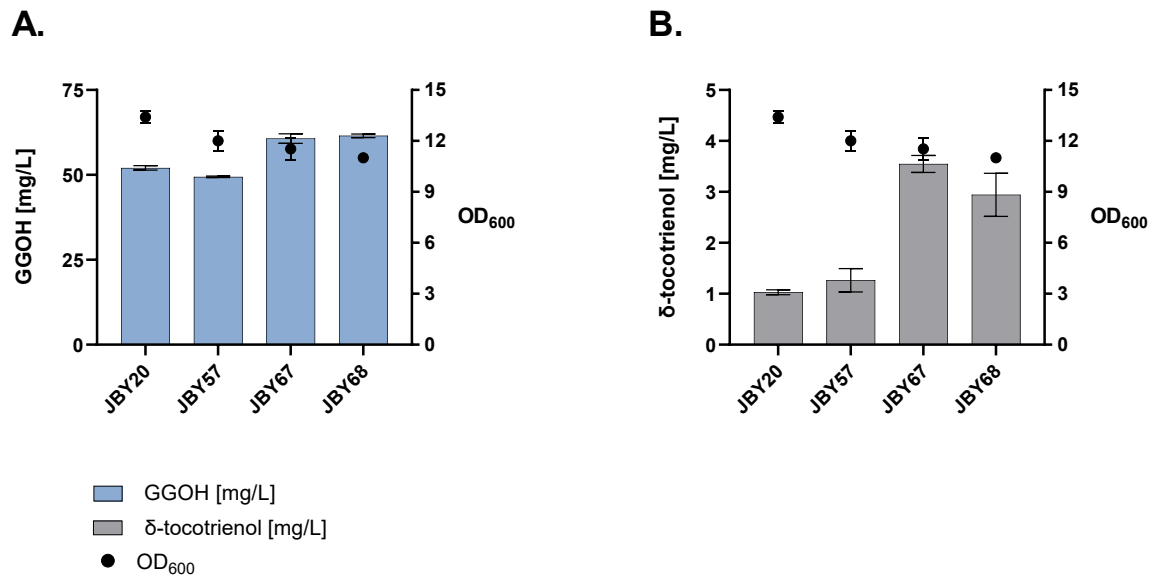

Figure 23 Illustration of the limitation of the tocotrienol pathway

Shake flask cultivations of JBY20, JBY57 (*dpp1Δ*), JBY67 (*dpp1Δ::SynHPT-AtVTE1$^{tr[142-1467]}$*), and JBY68 (*ChrIV53688-53756Δ::SynHPT- AtVTE1$^{tr[142-1467]}$*) were performed in SC-D medium with a dodecane overlay. The final metabolite titers of the 144 h samples are illustrated by bars and correspond to the mean of biological triplicates (n=3). OD_{600} values are displayed by dots. Error bars represent the standard deviation of the samples but were not drawn if the corresponding range was smaller than the projected symbol. **A**. GGOH titers [mg/L] at 144 h are represented by blue bars and the final OD_{600} values were drawn. **B**. Grey bars illustrate δ-tocotrienol titers in mg/L and the corresponding growth of the cultures is shown by their OD_{600} values.

Besides strain engineering by metabolic engineering, attention was drawn to the fermentation medium. In section 3.3, no tocotrienol production was observed when JBY12 was cultivated in YPD medium. Thus, comprehensive shake flask fermentations with different media were performed with the best performing strain, JBY67. One hypothesis was that the high concentration of aromatic amino acids (76 mg/L each) in SC-D medium improves HGA synthesises and thereby leads to higher δ-tocotrienol titers. Thus, a shake flask fermentation was performed in SC-D medium, YPD medium and YPD medium supplemented with 76 mg/L of each aromatic amino acid (YPD + AAA), which is the standard supplementation, generally used for SC-D medium (2.1.1). The fermentation was performed in biological triplicates over 168 h. Samples were taken at 72 h, 96 h, 120 h, 144 h and 168 h since production titers are higher during a later stage of the fermentation. Figure 24 illustrates the precursor, δ-tocotrienol and biomass formation of JBY67. The cultivations reached OD_{600} values of 15.2 (YPD) and 14.93 (YPD + AAA), while a lower OD_{600} value of 11.07 was measured for JBY67 in SC-D medium. Furthermore, the GGOH titers of the YPD based cultivations were higher than in SC-D

medium (Figure 24 C). However, in relation to their growth, GGOH titers were comparable in both YPD media, while they were higher in SC-D medium. Moreover, HGA and δ-tocotrienol titers were enhanced in SC-D medium, despite the lower growth. Thereby, 30 % higher HGA titers were reached in SC-D medium compared to YPD-based media after 168 h (Figure 24 B). Notably, pyomelanin formation was observed by the brownish discoloration of the cultures in YPD-based media. As observed in section 3.3, the final pH remained higher in YPD medium and thus, a lower pH might prevent excessive autooxidation of the HGA in SC-D medium. Consequently, the increased autooxidation of HGA could have led to an underestimation of the real production titers in YPD media. Due to this, less precursor would have been available for the synthesis of δ-tocotrienol in the YPD cultures. Hypothesising that the tocotrienol pathway enzymes are the limiting factor, a high concentration of HGA would be indispensable for an efficient tocotrienol biosynthesis and the reduced precursor supply would have led to decreased δ-tocotrienol formation. Consequently, SC-D medium was the medium of choice for further cultivations.

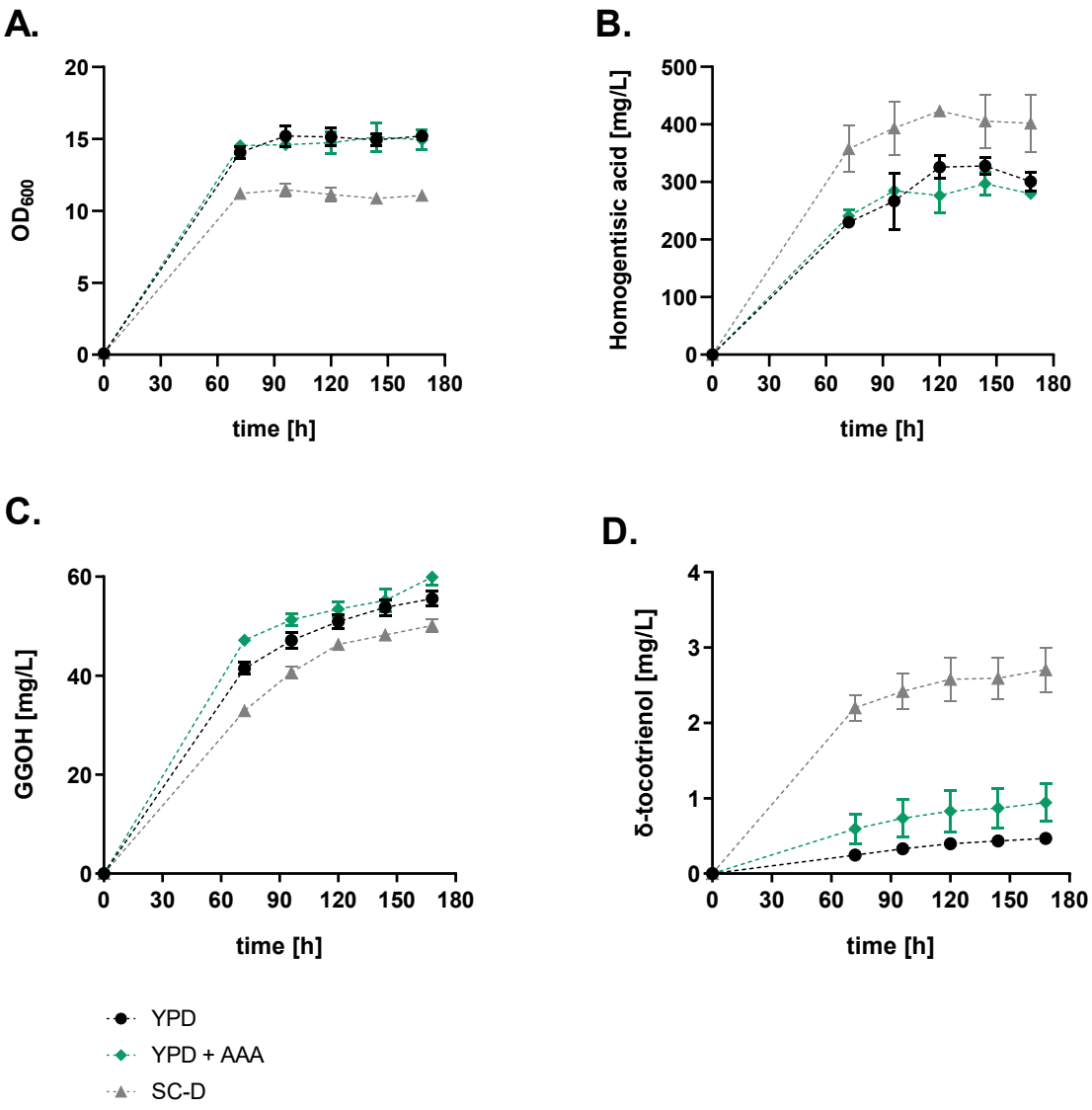

Figure 24 Fermentation of different media by JBY67

Shake flask cultivations of JBY67 fermenting YPD, YPD supplemented with aromatic amino acids (YPD + AAA) and SC-D medium, each with a 30 % dodecane overlay, over 168 h. Metabolite titers and OD_{600} values are displayed depending on the time by a black dot (YPD), a green diamond (YPD + AAA) and a grey triangle (SC-D). Symbols are equipped with error bars showing the standard deviation of biological triplicates. Error bars were not drawn if the corresponding standard deviation was smaller than the projected symbol. **A**. Biomass formation illustrated by OD_{600} values. **B.** Analysed HGA titers [mg/L] over time **C.** GGOH titers in mg/L analysed by HPLC **D**. Detected δ-tocotrienol formation in mg/L over 168 h.

3.5.3 Evaluation of Fermentative Conditions

Besides the evaluation of the media, a fed-batch fermentation of the strain JBY67 was conducted under monitored conditions utilising the *MiniBioreactors* (method 2.1.2.5). Due to the increased autooxidation of HGA in YPD medium, whereby a higher pH was measured, two distinct fed-batch fermentations were performed. The first one in a pH controlled environment (pH 5.5, with KOH) and the second where the pH was controlled with KOH below the level of 3.5. Batch shake flask controls were performed with the same precultures and medium. The dodecane overlay was not applicable for the *in situ* extraction within the bioreactors. Therefore, an alternative extraction protocol based on homogenisation was established (2.3.1.3). The method was validated by the detection of the same δ-tocotrienol titers after the homogenisation method and fermentations with a dodecane overlay (data not shown). Thus, the conclusion can be drawn that the dodecane overlay itself did not enhance δ-tocotrienol titers by its extraction from the cells during the cultivation process.

The δ-tocotrienol titers and the biomass formation after 96 h of cultivation are illustrated in Figure 25 D. The δ-tocotrienol titers decreased by 85 % on average when fermentations were performed in the bioreactor compared to the shake flask controls. The growth of the cells in the bioreactor with pH control below 3.5 (final pH was 3.5) was comparable to the shake flask controls. With pH control at 5.5, the biomass formation was higher, although less δ-tocotrienol was detected. The shake flask controls were started in the same medium, however they were not fed. Consequently, another shake flask fermentation was performed with biological triplicates of JBY67 with and without feeding to evaluate the influence of the feeding procedure on the δ-tocotrienol biosynthesis (Figure 25 A-C). After 24 h of cultivation the cells were fed with 2 ml of the feeding medium, every 24 h. Except for the feeding, the standard shake flask fermentation protocol was applied for this 144 h fermentation (method 2.1.2.1) and extraction was performed by homogenisation after 2.3.1.3. Figure 25 illustrates that the GGOH titers were higher in the fed cultures compared to the standard conditions. However, δ-tocotrienol and HGA titers decreased when the cultures were fed. It was suggested that the feeding procedure had a negative influence on the δ-tocotrienol biosynthesis. Consequently, the fed-batch procedure would be accountable for the decreased titers in the bioreactor fermentations. Therefore, the most favourable fermentation condition for δ-tocotrienol biosynthesis was the shake flask fermentation in SC-D medium without additional feeding or pH control, which achieved an average titer of 2.81 mg/L of δ-tocotrienol.

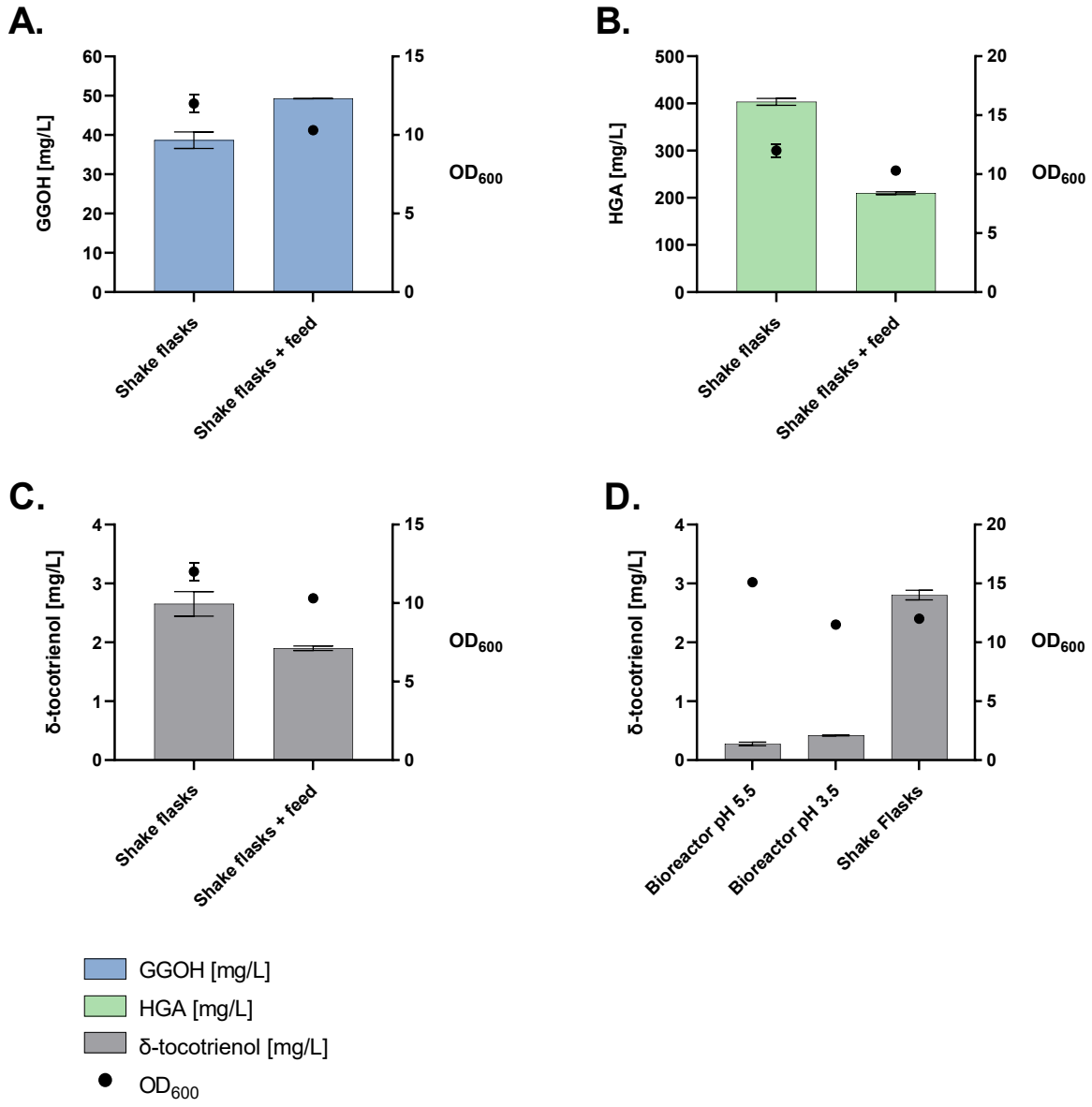

Figure 25 Fed-batch fermentations of JBY67

JBY67 was cultivated in shake flasks and the *MiniBioreactor* to assess a fed-batch procedure in a controlled environment. **A.-C.** Shake flask fermentation in biological triplicates of JBY67 in SC-D medium with and without feeding (feeding medium, after 24 h: 2 ml every 24 h) over 144 h. The final metabolite titers of the 144 h samples are illustrated by bars and correspond to the mean of biological triplicates (n=3). OD_{600} values are displayed by dots. Error bars represent the standard deviation of the samples but were not drawn if the corresponding range was smaller than the projected symbol **A.** Final GGOH titers are illustrated by blue bars in mg/L. **B.** The final HGA production titers are represented by green bars **C.** Grey bars illustrate δ tocotrienol titers in mg/L. **D.** Fermentations were performed in the 250 ml *MiniBioreactor* with pH control (KOH) below a pH of 5.5 and 3.5, respectively. A shake flask control fermentation was conducted in biological triplicates from the same preculture. The δ-tocotrienol titers after 96 h of cultivation are represented by grey bars. OD_{600} values are displayed by dots. Error bars correspond to the mean of technical triplicates (bioreactor samples) or biological triplicates (shake flask fermentation).

3.6 Synthesis of Further Tocochromanol Forms in *S. cerevisiae*

Apart from δ-tocotrienol, the other forms of tocotrienol are synthesised by methylation of the aromatic ring. Therefore, two heterologous methyltransferases needed to be introduced in *S. cerevisiae*. Based on current research, the *γ-TMT* and *MPBQMT* genes were obtained from *A. thaliana*. Since plasmid-based expression of the full-length *Atγ-TMT* and *AtMPBQMT* only resulted in δ-tocotrienol production (data not shown), a different approach was pursued. The sequence of the CTP of both genes was truncated as described by Shen et al. (2020) and an integrational vector for both methyltransferases was built (JBV193). The ClonNAT resistance cassette was chosen as integration locus since the antibiotic resistance marker was undesirable in the laboratory producer strain. Thus, the CRISPR/Cas9 vector JBV188 was constructed. Subsequently, JBY67 was transformed with the donor DNA of the linearised JBV193 and JBV188 to generate the strain JBY69.

The synthesis of α-, β- γ- and δ-tocotrienol was demonstrated by shake flask cultivations of the strain JBY69. JBY67 and JBY69 were cultivated for 144 h in biological triplicates in SC-D medium with a 30 % dodecane overlay for tocotrienol extraction. Figure 26 B illustrates the δ-tocotrienol titers of both strains and their biomass after 144 h. Moreover, the relative α-, β- γ-tocotrienol titers were normalised to δ-tocotrienol, which was set to 1 (Figure 26 B). Thereby, the unmethylated δ-tocotrienol was the most abundant form, detecting 2.77 mg/L in JBY67 and 3.27 mg/L in JBY69. Relative to their biomass, the δ-tocotrienol biosynthesis was comparable in both strains, as the δ-tocotrienol titer per OD_{600} was 0.28 [mg L^{-1}/OD_{600}] for both strains. Furthermore, the strain JBY69 was able to synthesise all other tocotrienol forms. However, their synthesis was considerably less compared to the biosynthesis of δ-tocotrienol. The second most common form was γ-tocotrienol, which only achieved 50 % of the δ-tocotrienol production titer, whereas α- and β-tocotrienol, were only detected in minor amounts (> 0.03 %). Their biosynthesis requires the second methyltransferase, the *Atγ-TMT*. Since the concentrations of both precursors, γ- and δ-tocotrienol, are significantly higher, a limitation of the *Atγ-TMT* is likely. However, by virtue of these results the conclusion can be drawn that both heterologous methyltransferases generally operate in JBY69. To enhance production titers of other tocotrienol isoforms, the overexpression of the endogenous SAM synthetase *SAM2* should be considered. Shen et al. (2020) increased titer of the 2-fold methylated β/γ-tocotrienol by 10 % and the 3-fold methylated α-tocotrienol by 20 %, respectively, by *SAM2* overexpression.

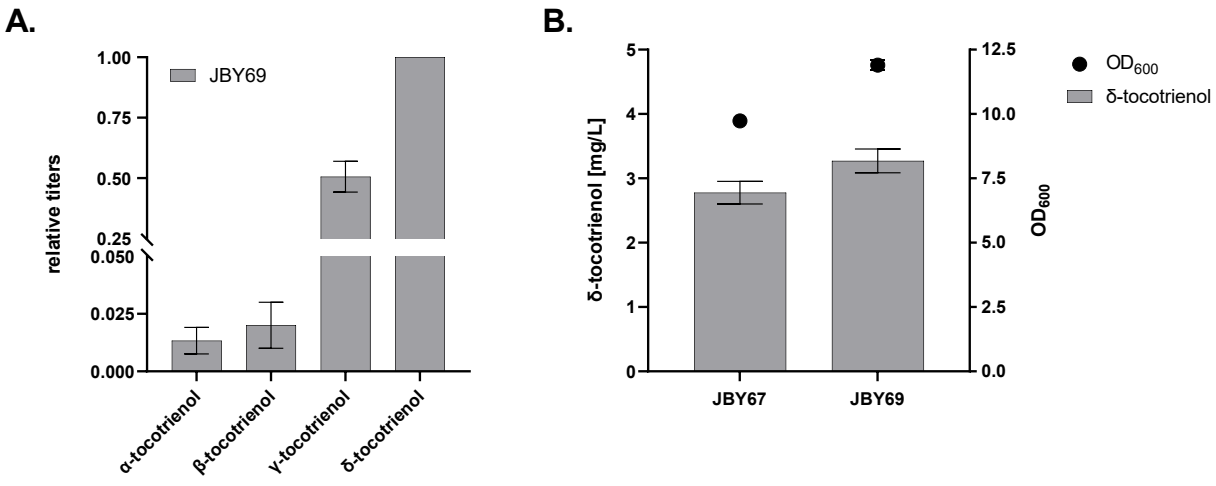

Figure 26 Expression of heterologous methyltransferases

JBY67 and JBY69 were cultivated in shake flasks for 144 h in SC-D medium with a 30 % dodecane overlay. The grey bars illustrate tocotrienol titers while OD_{600} values are displayed by dots (n=3). The error bars represent the standard deviation of the samples but were not drawn if the corresponding range was smaller than the projected symbol**. A.** Normalised titers of all tocotrienol forms detected in JBY69 after 144 h, whereby δ-tocotrienol was set to 1. **B.** Final δ-tocotrienol titers of JBY67 and JBY69 in mg/L and corresponding OD_{600} values.

After the successful proof of concept of the synthesis of all tocotrienol forms, the implementation of the tocopherol biosynthesis was desired. In *S. cerevisiae* only the tocotrienol precursor GGPP is synthesised. Counter to that, the precursor of tocopherols is PDP. In order to obtain PDP, four heterologous geranylgeranyl reductases were investigated. The following reductases were ordered as synthetic genes and introduced into the Golden Gate system: *AtGGR* (*A. thaliana*), *SaGGR* (*S. acidolarius*), *ScGGR* (*S. coelior*) and the *SynGGR* (*Synechocystis* sp.). Subsequently, overexpression plasmids for each reductase were constructed (JBV164-JBV167) and characterized in JBY67. However, no form of tocopherol was detectable and the δ-tocotrienol titers in all strains were comparable to the empty vector control (data not shown). As none of the reductases yielded detectable tocopherol titers the focus was shifted to the δ-tocotrienol producer JBY67.

3.7 Laboratory Tocotrienol Producer Strains

The foregoing results led to the successful implementation of the δ-tocotrienol biosynthesis pathway and its enhanced precursor supply in *S. cerevisiae*. Straightaway, adverse elements of the metabolic engineering process should be omitted in the strain JBY67. Hence, the deletion of the ClonNAT cassette was performed using the CRISPR/Cas9 vector JBV188 as described in section 3.6. After successful verification of the new strain JBY70, a comprehensive shake flask fermentation was performed. Notably, production titers can vary from fermentation to fermentation due to various factors such as extraction efficiency. Therefore, a comprehensive shake flask fermentation of all δ-tocotrienol strains will reflect the modifications in the strain which increased δ-tocotrienol titers. JBY20 (*SynHPT-AtVTE1$^{tr[142-1467]}$*), JBY67 (JBY20*, dpp1Δ::SynHPT-AtVTE1$^{tr[142-1467]}$*) and JBY70 (JBY67, *ClonNATΔ)* were cultivated in SC-D medium, carrying a 30 % dodecane overlay. Metabolite titers were extracted and analysed according to section 2.3.1.4 and 2.3.2. Figure 27 portrays the biomass formation and the biosynthesis of δ-tocotrienol in JBY20, JBY67 and JBY70 after 144 h of cultivation. The integration of the second *SynHPT-AtVTE1$^{tr[142-1467]}$* expression cassette into the *DPP1* locus enhanced δ-tocotrienol titers by a factor of 6.83 to 2.79 mg/L. Furthermore, the deletion of the antibiotic resistance cassette increased biomass formation and further improved the biosynthesis by a factor of 1.47, reaching a δ-tocotrienol titer of 4.09 mg/L in JBY70.

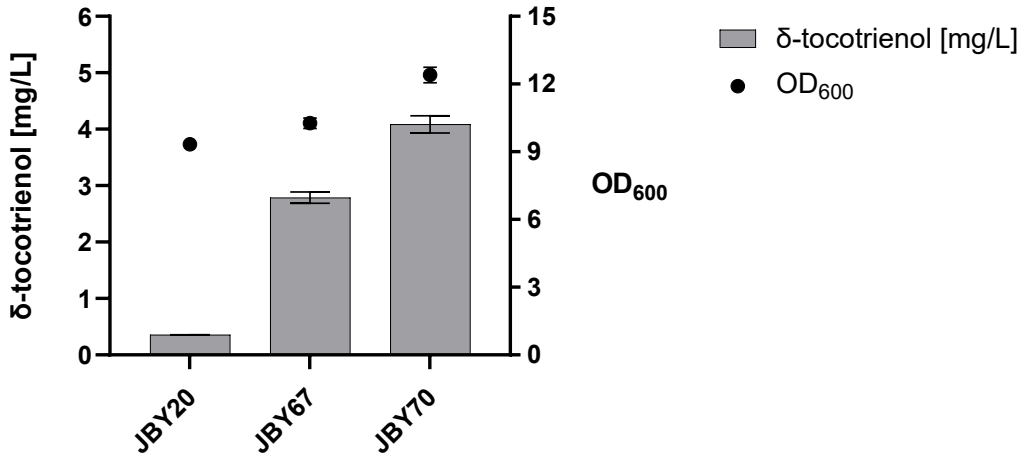

Figure 27 Improvement of δ-tocotrienol biosynthesis by metabolic engineering

Shake flask cultivations of JBY20, JBY67 (JBY20, *dpp1Δ::SynHPT-AtVTE1$^{tr[142-1467]}$*), and JBY70 (JBY67, *ClonNATΔ*) were cultivated in SC-D medium with *in-situ* dodecane extraction. OD_{600} values are displayed by dots. The final δ-tocotrienol titers of the 144 h samples are illustrated by grey bars and correspond to the mean of biological triplicates. Their error bars represent the standard deviation but were not drawn if the corresponding range was smaller than the projected symbol.

3.8 Evolutionary Engineering by Ozone Treatment

A concept for the evolutionary engineering of *S. cerevisiae* for enhanced δ-tocotrienol biosynthesis was established with the δ-tocotrienol producer strains JBY20 and JBY67. The approach is based on the antioxidant properties of the lipid soluble compound δ-tocotrienol. Ozone is a powerful oxidant and thus, a procedure was developed for the fumigation of yeast cells with ozone. Inside yeast cells, ozone leads to the formation of free radicals and hydroperoxides, particularly from the unsaturated lipids of their membranes. Ozone has been shown to be toxic to *S. cerevisiae* and is an approved method for the sterilization of microorganisms (Dubeau and Chung, 1979; Zargaran et al., 2017). The concept behind this approach was that yeast cells might have a survival benefit if they produced higher levels of δ-tocotrienol. The antioxidant δ-tocotrienol would protect the yeast cells from lipid peroxidation. Ozone itself is mutagenic and therefore mutations are more likely to occur, as demonstrated by Hamelin and Chung (1974) for mutagenesis in *E. coli*. Cells may have a survival advantage in an ozone-rich environment if they acquire beneficial mutations that directly or indirectly enhance the tocotrienol biosynthetic pathway. Thereby, the yeast strain would evolve for an increased δ-tocotrienol biosynthesis through several successive ozone treatments. The exact procedure of the ozone treatment that was applied to JBY20 and JBY67 is described in section 2.1.3.4.

The first ozone treatment was performed to the strain JBY20 for 0, 0.5, 1, 2, 3 and 5 minutes at the highest intensity. Subsequently, the ozone-treated cells were inoculated in 25 ml fresh YPD medium and grown to the exponential phase. Hereby, the following cultures survived: 0, 0.5, 1, 2 and 3 min. The culture that survived 3 minutes of ozone fumigation was kept and used for the next ozone treatment. In particular, the whole cultures of each generation, which most likely contain a mixture of strains, were retained. During the first series of ozone fumigation, six generations of JBY20 (JBY20_1-6) were created. Table 19 shows the generated strains and the corresponding ozone exposure time of the first series of evolutionary engineering. In each case, the cultures that survived the longest time of ozone exposure were retained and used for the next round of ozone treatment. After each round of ozone treatment, the culture surviving the longest time of exposure was stored in 25 % (v/v) glycerol at -80 °C.

Table 19 First series of ozone treatment of JBY20

Utilised strain/culture	Generated culture	Time of ozone exposure [min]	Longest time of exposure that was survived [min]
JBY20	JBY20_1	0, 0.5, 1, 2, 3, 5	3
JBY20_1	JBY20_2	2, 3, 5, 10	5
JBY20_2	JBY20_3	3, 5, 8, 10	5
JBY20_3	JBY20_4	5, 8, 10	10
JBY20_4	JBY20_5	5, 10, 12, 15	12
JBY20_5	JBY20_6	5, 10, 12, 15	15
JBY20_6	-	15, 20	-

After six ozone treatments, a shake flask cultivation in SC-D medium with a 30 % dodecane overlay was performed over 144 h with the generated cultures (JBY20_1-6) and the parent strain JBY20. The analysed δ-tocotrienol titers are illustrated in Figure 28. In the JBY20 control, 1.09 mg/L of δ-tocotrienol was measured, while 1.90 mg/L was detected in the culture JBY20_6 (Figure 28 A).

As cultivations were performed with the whole culture obtained from the ozone treatment, the evaluation of individual strains was desired. Therefore, the culture of JBY20_6 was streaked onto solid YPD agar plates for the isolation of individual strains. Single clones were streaked twice and subsequently 16 individual clones of JBY20_6 were further characterised. The tocotrienol pathway genes were integrated into the *LEU2* locus of JBY20 using *ClonNAT* as selection marker (*leu2Δ::AP8-SynHPT-tPGK1-pPGK1-AtVTE1*$^{tr[142-1467]}$*-tTDH1_ClonNAT)*. It was observed, that 14 out of 16 single clones lost their ability to grow on YPD-ClonNAT agar plates. Clone 2 and 10 maintained the resistance. Furthermore, the *leu2Δ* integration loci of six individual clones were sequenced (c1-c5, c10). The *SynHPT* and the *AtVTE1* expression cassettes remained intact in all strains, whereas a deletion of 3 bp (337-379) within the ClonNAT resistance gene was observed in the four clones that lost the ability to grow on YPD-ClonNAT agar plates. In addition to that, a shake flask fermentation of single clones was conducted to analyse whether the increase in δ-tocotrienol biosynthesis was reproducible by an individual strain. Thus, JBY20, ten individual clones of JBY20_6 (c1-c10), and a mixture of the 10 clones (c1-c10) were cultivated in SC-D medium with a 30 % dodecane overlay and δ-tocotrienol titers were analysed by HPLC (Figure 28 B). The fermentation was performed with biological duplicates of each strain. All characterised clones exhibited enhanced δ-tocotrienol titers compared to the control strain JBY20. The cultures c1 (1.91 mg/L), c3 (1.96 mg/L) and c4 (1.90 mg/L) produced comparable amounts as the mixture of all clones

(1.84 mg/L). Within the cultures of the clones that carried the ClonNAT resistance (c2, c10), the lowest δ-tocotrienol titers were measured. Consequently, the first evolutionary engineering approach increased δ-tocotrienol biosynthesis from 0.86 mg/L (JBY20) to 1.96 mg/L (JBY20_6 c3), which corresponds to an increase by a factor of 2.28 (Figure 28 B).

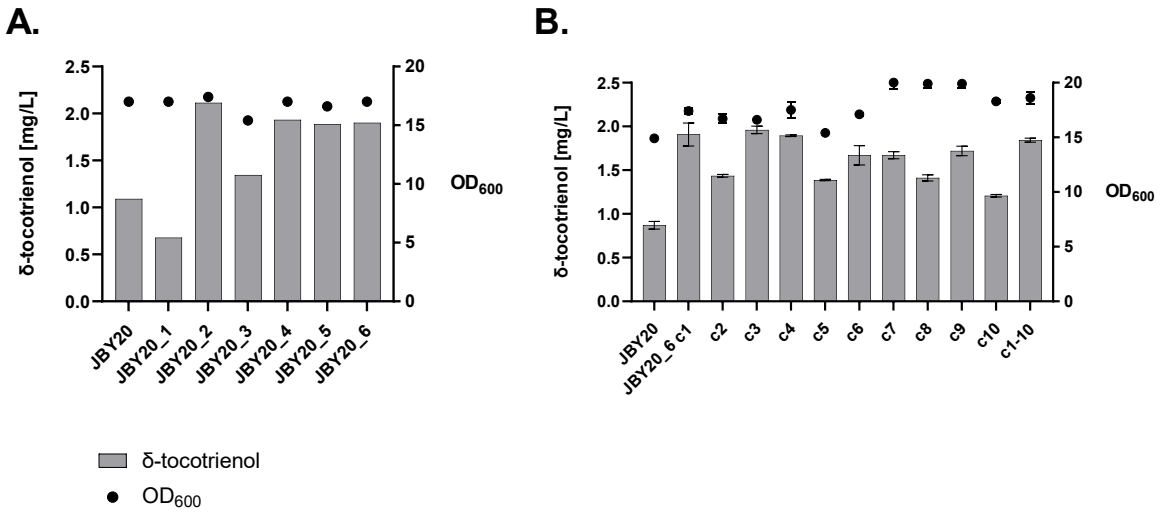

Figure 28 Biosynthesis of δ-tocotrienol of ozone treated cultures

Shake flask cultivations after evolutionary engineering by ozone treatments of JBY20. Fermentations were cultivated in SC-D medium with *in-situ* dodecane extraction. The final δ-tocotrienol titers of the 144 h samples are illustrated by grey bars. OD_{600} values are displayed by dots. **A.** The δ-tocotrienol titers of JBY20 and six cultures (n=1), generated by sequential ozone treatments (JBY20_1-6) are illustrated **B.** Cultures of JBY20, ten individual clones of JBY20_6 (c1-c10) and a mixture of all ten clones were analysed for their δ-tocotrienol production. Grey bars represent the mean of biological duplicates (n=2), equipped with error bars representing the range of the samples. These were not drawn if the corresponding range was smaller than the projected symbol.

As the concept of evolutionary engineering by ozone treatment successfully increased the δ-tocotrienol biosynthesis, a second series of ozone treatments was conducted. Therefore, the treatment was continued with the strain JBY20_6. Moreover, a new series of treatments was started with the strains JBY20 and JBY67 to further evaluate the applicability of the ozone assay for the evolutionary engineering of *S. cerevisiae*. Notably, the medium of the cultivations between the ozone treatments was changed from YPD to SC-D medium, since in previous experiments higher δ-tocotrienol titers were detected by the fermentation of SC-D medium.

Table 20 provides an overview of the second series of evolutionary engineering. After the first ozone treatments of 8, 10 and 12 min, the unevolved strains JBY20 and JBY67 did not survive the ozone fumigation, while JBY20_6 survived 8 min of ozone treatment. Since JBY67

produced higher amounts of δ-tocotrienol than JBY20_6 (data not shown), additional beneficial adaptations must have occurred within JBY20_6 during the first series of ozone treatments. However, the time of ozone exposure could be increased progressively during the second series, indicating that these adaptations may be reproducible. Within this series, the cultures JBY20_7-14, JBY20_II_1-9 and JBY67_1-6 were generated.

Table 20 Second series of ozone treatment of JBY20_6, JBY20 and JBY67

Utilised strain/culture	**Generated culture**	**Time of ozone exposure [min]**	**Longest time of exposure that was survived [min]**
JBY20_6	JBY20_7	8, 10, 12	8
JBY20_7	JBY20_8	7, 8, 9, 10	8
JBY20_8	JBY20_9	7, 8, 8.5	8.5
JBY20_9	JBY20_10	8, 8.5, 9	9
JBY20_10	JBY20_11	8, 9	8
JBY20_11	JBY20_12	8, 9	9
JBY20_12	JBY20_13	9, 9.5, 10	9
JBY20_13	JBY20_14	9, 9.5, 10	9.5
JBY20_14	-	9.5, 10	-
Utilised strain/culture	Generated culture	Time of ozone exposure [min]	Highest exposure that was survived [min]
JBY20	-	8, 10, 12	-
JBY20	JBY20_II_1	2, 3, 4, 5	5
JBY20_II_1	JBY20_II_2	4, 5, 6	6
JBY20_II_2	JBY20_II_3	6, 7	6
JBY20_II_3	JBY20_II_4	5, 6, 7	5
JBY20_II_4	JBY20_II_5	5, 6	6
JBY20_II_5	JBY20_II_6	6, 7, 8	7
JBY20_II_6	JBY20_II_7	7, 8, 9	9
JBY20_II_7	JBY20_II_8	9, 9.5, 10	9.5
JBY20_II_8	JBY20_II_9	9.5, 10, 11	10
JBY20_II_9	-	10, 11	-
Utilised strain/culture	Generated culture	Time of ozone exposure [min]	Highest exposure that was survived [min]
JBY67	-	8, 10, 12	-
JBY67	JBY67_1	2, 3, 4, 5	5
JBY67_1	JBY67_2	4, 5, 6	6
JBY67_2	-	6, 7	-
JBY67_2	JBY67_3	5, 6	6
JBY67_3	JBY67_4	6, 7, 8	8
JBY67_4	JBY67_5	7, 8, 9	9
JBY67_5	JBY67_6	9, 9.5, 10	9

As described for the preceding series of ozone treatments, a shake flask fermentation in SC-D medium with a 30 % dodecane overlay was performed over 144 h. First, the δ-tocotrienol production titers of the generated cultures (JBY20_6-14, JBY20_II_1-9 and JBY67_1-6) were compared to their parent strains, JBY20 and JBY67, respectively (Figure 29 A). The cultures JBY20_6-10 did not show any major changes in δ-tocotrienol production, whereas the cultures past JBY20_10 produced significantly less δ-tocotrienol. Moreover, the biomass formation of these generations decreased. In all generated strains (JBY20_7-14) no difference in HGA production was detected compared to the parent strain JBY20, while GGOH titers were halved after the generation JBY20_10 (data not shown). Consequently, one or more adverse events must have occurred due to the ozone treatment of JBY20_10.

The second series of evolutionary engineering, starting from JBY20 led to different results than the first series. From culture JBY20_II_3 onwards, the δ-tocotrienol titers and biomass formation decreased. Here, detected HGA and GGOH titers were unchanged compared to the parent strain JBY20 (data not shown). Due to the mutagenicity of ozone, unwanted mutation events must be expected. Unfortunately, the screening process of enhanced δ-tocotrienol biosynthesis requires time consuming fermentations and HPLC analysis. However, a more frequent screening process, such as a high-throughput screening method, may be advantageous in order not to carry over deleterious mutations. As opposed to the first two strains, the evolutionary engineering approach increased δ-tocotrienol titers in JBY67 (Figure 29 A). The shake flask fermentation of JBY67_1-6 was repeated with biological triplicates and confirmed JBY67_3 as highest δ-tocotrienol producer (data not shown). This shake flask fermentation reproduced the titers and ratios of the presented fermentation. Consequently, JBY67_3 was chosen for an evaluation of single clones as described for JBY20_6. Hereby, eight individual clones were isolated and investigated (JBY67_3 c1-c8). The δ-tocotrienol titers and biomass formation after 144 h of cultivation in SC-D medium with a 30 % dodecane overlay is illustrated in Figure 29 B. The fermentation was performed with biological duplicates of each strain. JBY67 and a mixture of all clones (c1-c8) were utilised as controls. The mean δ-tocotrienol production of the mixed culture of JBY67_3 c1-c8 was 3.97 mg/L, while the JBY67 only produced 2.84 mg/L. Notably, δ-tocotrienol titers can vary between fermentations, most likely due to the extraction procedure. Therefore, it is important to compare titers only within a shake flask fermentation experiment. Figure 29 B portrays that the individual cultures c4 (4.25 mg/L), c7 (3.99 mg/L) and c8 (4.12 mg/L) produced higher titers than the mixed culture (3.97 mg/L). Consequently, the increased δ-tocotrienol titer in JBY67_3 was reproducible by individual strains of this culture. The δ-tocotrienol biosynthesis increased by 50 % in the engineered strain

JBY67_3 c4 compared to the control strain JBY67. Due to the enhanced δ-tocotrienol biosynthesis after ozone treatments in JBY20_6 c3 and JBY67_3 c4, the ozone assay is a promising tool for evolutionary engineering of tocochromanols and potentially other antioxidants in *S. cerevisiae*.

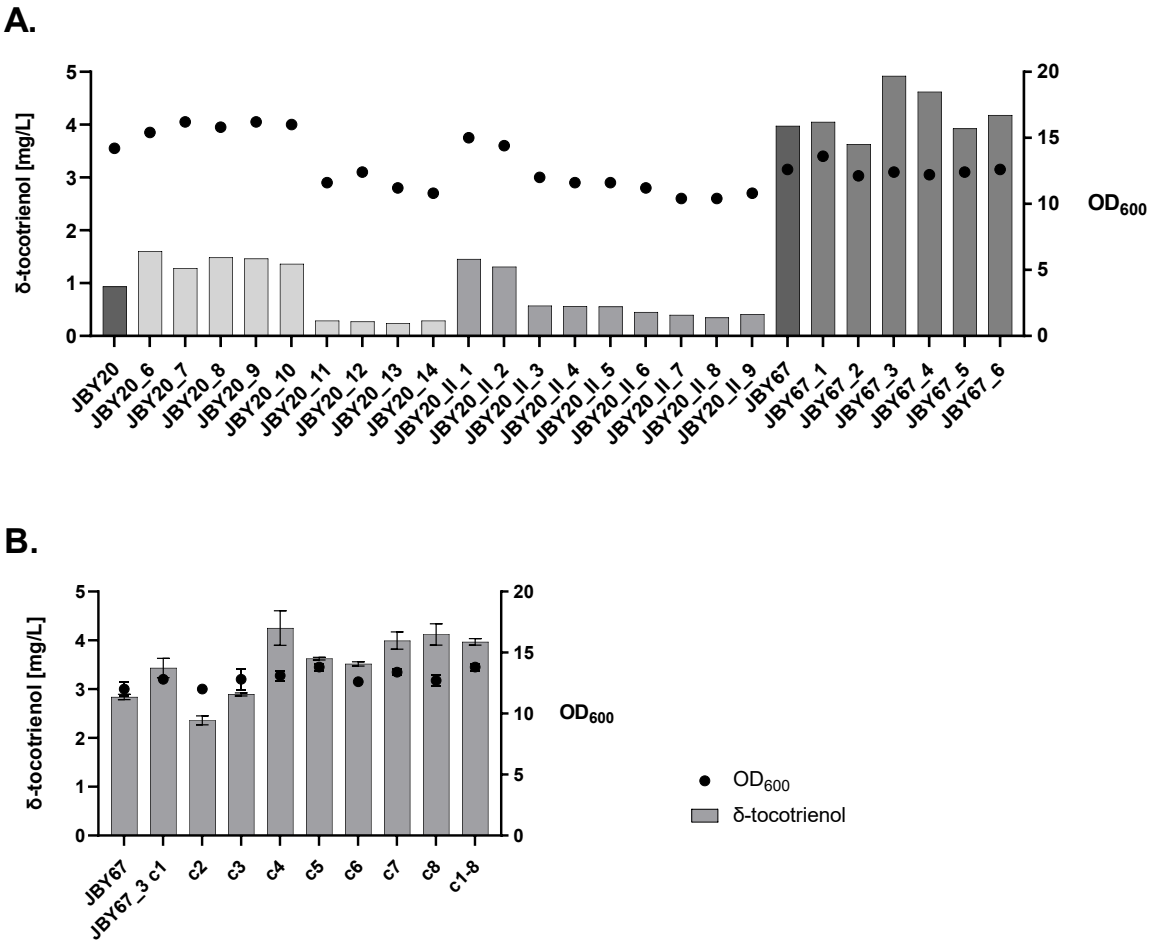

Figure 29 Biosynthesis of δ-tocotrienol after second series of ozone treatments

Shake flask cultivations after the second series of evolutionary engineering by ozone treatments. Fermentations were performed in SC-D medium with in-situ extraction by dodecane overlay. The final δ-tocotrienol titers of the 144 h samples are illustrated by grey bars. OD_{600} values are displayed by dots. **A.** The generated cultures JBY20_6-14, JBY20_II_1-9 and JBY67_1-6 are illustrated. The controls JBY20 and JBY67 are portrayed with darker grey bars. **B.** Cultures of JBY67, eight single clones of JBY67_3 (c1-c8), and a mixture of all 8 clones were analysed for δ-tocotrienol production. Grey bars represent the mean of biological duplicates, equipped with error bars representing the range of the samples (n=2). These were not drawn if the corresponding range was smaller than the projected symbol.

4 Discussion

The aim of this work was to establish a tocochromanol pathway in a laboratory *S. cerevisiae* strain. For the proof of concept, the biosynthesis of δ-tocotrienol was chosen. Therefore, a metabolic engineering strategy was developed to enable the recombinant biosynthesis of tocochromanols in *S. cerevisiae*. First, the strain was engineered for an improved precursor supply, through the upregulation of required pathways and the downregulation of competing branches. Thereby, limitations of the preceding pathway were identified, and strategies were developed to face these boundaries. Then, the heterologous tocochromanol pathway needed to be introduced into *S. cerevisiae.* Hereby, one challenge was the functionality and efficiency of the recombinant enzymes. After the successful generation of a tocotrienol producer strain, the fermentation conditions were characterised, and further limitations of these were evaluated. Due to the various constraints, both within the heterologous pathway and the fermentation environment, a comprehensive solution-focused approach was desired. Thus, a concept for evolutionary engineering of a tocochromanol producer strain was developed.

4.1 Tried and Trusted Engineering Strategies Improving Production Titers

Metabolic engineering often comes with several adverse traits of the engineered organism, especially if highly engineered strains are employed. Several genes, or even entire pathways, are introduced into the genome, which will influence and manipulate existing catabolic and anabolic networks. The overexpression of many genes can burden the protein biosynthesis machinery at the expense of the basal metabolism. This often comes with reduced biomass formation, longer lag-phases or reduced stress tolerance. This phenomenon is known as metabolic burden and is rooted in the finite resources encompassing cofactors and energy building blocks (Wu et al., 2016). Therefore, prevention of these negative traits is one of the key interests for industrial applications of engineered strains. This requires a comprehensive understanding about the molecular and biochemical processes within the engineered strains and is often challenging. Common successful metabolic engineering concepts consider the following strategies which have been described by Pickens et al. (2011): a sufficient supply of precursors, the elimination and downregulation of competing pathways, a sufficient cofactor supply, the transcriptional regulation and an improvement of enzyme specificity.

The provision of a sufficient precursor supply and the elimination of competing pathways were decisive strategies to enable the tocochromanol biosynthesis in the *S. cerevisiae* strains JBY20,

JBY67 and JBY70. The rational approach for the improvement of the metabolic engineering strategy of this study is discussed throughout selected examples of this work within the following subchapters. Particularly challenging was the metabolic engineering process concerning heterologous proteins. Due to the importance of recombinant protein expression during this work, this aspect will be discussed in the following chapter 4.2.

4.1.1 Sufficient Precursor Supply

First, a sufficient precursor supply is essential for an efficient tocochromanol biosynthesis. Consequently, the optimisation of upstream metabolic routes is crucial. Reifenrath and Boles (2018) efficiently engineered the aromatic amino acid biosynthetic pathway for an improved HPP biosynthesis and by adopting this engineered pathway, the production of 435 mg/L of HGA in JBY2 was enabled (Bauer, 2019). Metabolic engineering of the aromatic amino acid pathway is well studied since aromatic compounds such as flavonoids and alkaloids are highly desired (Liu et al., 2019). Therefore, it should be taken into consideration that further engineering of the aromatic amino acid pathway or its supply would improve tocochromanol biosynthesis. The limiting substrate of the first enzyme of the pathway is E4P, due to its lower bioavailability and the increased affinity of the DAHP towards PEP (Paravicini et al., 1989; Schnappauf et al., 1998a). Consequently, an improvement of the E4P synthesis would be a target for further engineering for an enhanced precursor provision. One frequently applied strategy to increase E4P production is the deletion of G6P dehydrogenase (*ZWF1*) paired with the overexpression of the transketolase, *TKL1* (Curran et al., 2013). However, *zwf1* deletion blocks the oxidative branch of the PPP which is undesirable since this cuts off the main production route for NADPH synthesis (Zhang et al., 2015). Another successful strategy for enhanced E4P biosynthesis was presented by Liu et al. (2019) and included rewiring of the carbon metabolism with a heterologous phosphoketolase pathway. With their engineering strategy the production of the aromatic compound p-hydroxycinnamic acid was drastically increased and therefore rewiring of the carbon metabolism should be taken into consideration for further enhancement of HGA biosynthesis.

Besides E4P, the efficiency of the HGA biosynthesis pathway itself should be evaluated. Improvements of the aromatic amino acid pathway through feedback-resistant enzymes were shown for Aro7p and Tyr1p. The expression of the feedback-resistant variant of the native chorismate mutase (Aro7p) was demonstrated to increase intracellular tyrosine levels in *S. cerevisiae* (Schnappauf et al., 1998b; Gold et al., 2015). During this work, *ARO7*^{fbr} was

expressed on a plasmid in JBY2, but did not increase HGA titers (data not shown). Furthermore, the heterologous cyclohexadienyl dehydrogenase (TyrC) from *Zymomonas mobilis* or the feedback-resistant chorismate mutase/prephenate dehydrogenase ($TyrA^{fbr}$), which enhanced tyrosine biosynthesis in *E. coli*, did not enhance HGA biosynthesis in *S. cerevisiae* (Lütke-Eversloh and Stephanopoulos, 2005; Chávez-Béjar et al., 2008; Bauer, 2019). Consequently, neither Aro7p nor Tyr1p might be the limiting enzymes of the already highly engineered aromatic amino acid biosynthesis pathway of JBY2, which directs the metabolic flux to the tyrosine branch for further HGA biosynthesis. Moreover, the measured titers of HGA are considerably higher compared to detected tocotrienol titers (Figure 25). Therefore, the HGA supply from the aromatic amino acid biosynthesis pathway is most likely sufficient for further tocochromanol biosynthesis in *S. cerevisiae*.

This study was started with several strategies for improvement of the mevalonate and isopentenyl diphosphate pathway for a sufficient precursor supply of GGPP. The most efficient modifications were the truncation and overexpression of the rate-limiting *HMG1* (section 3.2.1), the utilisation of the heterologous GGPP synthase, *XdcrtE,* (section 3.3.1) and the deletion of the gene for the diacylglycerol pyrophosphate phosphatase, *DPP1* (3.5.2). Another possibility to further strengthen the GGPP biosynthesis, could be an increase of the starting molecule of this pathway, acetyl-CoA. The oleaginous yeast, *Y. lipolytica,* naturally produces high amounts of acetyl-CoA, through its predominant lipid metabolism, enabling higher GGPP titers (Larroude et al., 2018). Therefore, an enhancement of the acetyl-CoA pool in *S. cerevisiae* should be taken into consideration. One approach is the redirection of the metabolism towards an enhanced acetyl-CoA formation by the deletion of the major genes encoding for the alcohol dehydrogenases (Li et al., 2014). The scientific community provides several more successful strategies to increase the acetyl-CoA pool in *S. cerevisiae*, such as the restriction of acetyl-CoA degrading pathways or an engineered PDH-bypass, if further optimisation is desired (Lian and Zhao, 2015; Zhang et al., 2021).

4.1.2 Restriction and Elimination of Competing Pathways

The second strategy is the downregulation or deletion of competing pathways. This approach has been repeatedly applied within this work. First, a prominent example is the highly regulated ergosterol pathway. Ergosterol is a metabolite of high importance in *S. cerevisiae*. Besides its essential role in membrane fluidity, ergosterol is a crucial molecule in yeast stress adaptation. Thereby, higher ergosterol levels are associated with enhanced tolerances to lower temperatures, higher alcohol concentrations or oxidative stress (Jordá and Puig, 2020). The metabolic flux of FPP is majorly directed into the ergosterol biosynthesis since the native GGPP synthase (Bts1p*)* does not compete with squalene synthase (Erg9p*)* (Jiang et al., 1995; Callari et al., 2018). To direct the metabolic flux of FPP into the GGPP synthesis branch, the downregulation of the first enzyme of the ergosterol pathway and the upregulation of the GGPP biosynthesis were intended. Asadollahi et al. (2008) demonstrated, that a promoter exchange of *pERG9* to the regulatable *pMET3* promoter reduced the ergosterol concentration and increased the content of FPP related products. However, an external gene regulation with methionine is neither cost nor time efficient for an industrial process and the utilisation of auxotrophic strains is rather unlikely for industrial applications (Mao et al., 2002; Steensels et al., 2014). Furthermore, a decreased stress resistance of potential production strains due to an insufficient ergosterol content is undesired. Moreover, a sufficient ergosterol biosynthesis is desired to maintain membrane integrity (Abe and Hiraki, 2009). This is especially important when operating with lipophilic metabolites such as tocochromanols, since these compounds tend to accumulate within membranes (Jiao et al., 2022). Therefore, regulating *ERG9* with the ergosterol sensitive promoter *pERG1* was attempted as described by Callari et al. (2018). The downregulation of the ergosterol branch by the promoter exchange of *ERG9* was performed in the strain JBY3, generating JBY4. Hereby, the strain JBY4 remained prototrophic for ergosterol biosynthesis, and the fitness of the strain was not decreased in shake flask cultivations, compared to its parent strain JBY3 (section 3.2.1 and 3.2.2). Other strategies for an increased metabolic flux into GGPP could be the spatial proximity of the related enzymes and substrates. The fused gene of *BTS1-ERG20* or Erg20p mutants which also synthesise GGPP are successful examples for increased titers through spatial proximity of the converting enzymes (Tokuhiro et al., 2009; Callari et al., 2018). Özaydın et al. (2013) fused Erg20p with the heterologous bisabolene synthase of *Abies grandis* and successfully increased bisabolene biosynthesis. Therefore, a fusion protein of *ERG20* and the heterologous *XdcrtE* might be advantageous to further increase GGPP production.

Second, another degrading pathway involves the diacylglycerol pyrophosphate phosphatase, encoded by *DPP1*. GGPP is a target molecule of endogenous phosphatases, catalysing the reaction from GGPP to GGOH. Indeed, this conversion is highly abundant in the metabolism of *S. cerevisiae,* and therefore GGOH analytics are often performed to infer GGPP titers, as it was also performed during this study (Callari et al., 2018; Sun et al., 2020; Wang et al., 2021). However, if this conversion is prevalent in yeasts' metabolism, GGPP uptake by downstream enzymes would have to be highly efficient to improve tocochromanol titers. The results of this work indicated the constraints of the downstream tocochromanol enzymes (section 3.5.2). On the other side, the GGPP pool could be increased by a decreased dephosphorylation of GGPP, by restricting or eliminating endogenous phosphatases. *S. cerevisiae* contains various phosphatases which are essential for numerous metabolic routes and therefore, a targeted elimination of unspecific phosphatases might be disadvantageous (Offley and Schmidt, 2019). However, it has been shown that specific phosphatases, such as Dpp1p and Lpp1p, are predominantly involved in GGPP dephosphorylation (Faulkner et al., 1999). The gene product of *DPP1* was first isolated and predicted as an integral membrane protein by Toke et al. (1998). Dpp1p is predominantly involved in diacylglycerol phosphorylation and lipid signalling pathways, where the transmembrane protein Dpp1p was localised within membranes of the vacuoles. Nevertheless, *dpp1*-Δ mutants were shown to be viable without a growth phenotype (Toke et al., 1998; Oshiro et al., 2003). Moreover, a high phosphatase activity towards the highly abundant GGPP in membranes was demonstrated in a reverse scenario, where *DPP1* overexpression, together with $HMG1^{tr}$ and *BTS1* upregulation, increased GGOH production (Tokuhiro et al., 2009). Indeed, GGOH titers decreased when *DPP1* was deleted in JBY66, compared to JBY63 with the wild-type *DPP1* locus (Figure 21). Moreover, JBY67, where the *DPP1* locus was replaced by a second $SynHPT\text{-}AtVTE1^{tr[142\text{-}1467]}$ expression cassette, produced higher amounts of δ-tocotrienol than JBY68, where only a second $SynHPT\text{-}AtVTE1^{tr[142\text{-}1467]}$ expression cassette was present, but *DPP1* remained intact (section 3.5.2). For further strain engineering, additional deletion of the gene encoding the second phosphatase mentioned, *LPP1,* should be considered since Lpp1p exhibits homologies to Dpp1p (Oshiro et al., 2003).

However, the sufficiency of GGPP supply in the generated strains was illustrated through production of the metabolite β-carotene. In section 3.4 it was demonstrated that the precursor supply of the isopentenyl diphosphate pathway delivered sufficient amounts of GGPP to produce β-carotene in JBY63. Verwaal et al. (2007) employed a CEN.PK113-7D strain for the metabolic engineering for β-carotene biosynthesis, reaching titers of 5.9 mg/g DCW. Precisely, the heterologous genes *XdcrtE*, *XdcrtYB* and *XdcrtI* were integrated and the native *HMG1* was

truncated (Verwaal et al., 2007). The same strategy was utilised for the generation of the β-carotene producer JBY63 and was further improved by the deletion of *DPP1* in JBY66. The decreased GGOH titers and efficient β-carotene synthesis in the β-carotene producer strains (JBY63 and JBY66) compared to the δ-tocotrienol producer strain (JBY20) indicate that the precursor supply of GGPP was sufficient. Consequently, the biosynthesis of β-carotene in JBY63 and JBY66 demonstrated that the precursor supply for GGPP might not be the limiting factor for tocochromanol biosynthesis in the engineered *S. cerevisiae* strain.

Third, degradation of the second precursor, HGA, needs to be controlled. Advantageously, HGA degradation pathways by a homogentisate dioxygenase are absent in *S. cerevisiae*, since naturally no HGA is formed. The absence of degrading pathways strengthens the utilisation of *S. cerevisiae* as production host. Another route, where the precursor HGA is irreversibly degraded is its autoxidation. Extracellular accumulation of HGA leads to its autoxidation and self-polymerisation, forming a brownish pigment, often referred as pyomelanin (Plonka and Grabacka, 2006; Larroude et al., 2021). In section 3.3 and 3.5.2 the formation of a brownish pigment was observed when JBY12 and JBY67 were cultivated in YPD medium. This brownish pigment formation is often recognised in *Y. lipolytica* through the autooxidation of intermediates of its tyrosine catabolism, namely HGA (Carreira et al., 2001; Larroude et al., 2021). The observed metabolite accumulation pattern was comparable to the results of Larroude et al. (2021): first the precursor HGA accumulated in the extracellular environment during the exponential growth phase of the cultures and subsequently, pyomelanin formation was observed, visually. The brownish discoloration was not observed in the control cultures, cultivated in SC-D medium. At the end of the fermentations, a final pH of 2.8 was measured in the SCM-D and SC-D cultures, while a pH of 4.7 was measured in YPD cultures (results 3.3 and 3.5.2). Hence, the dependence of HGA autoxidation and pyomelanin formation on the pH was taken into consideration. Naturally, yeasts acidify the medium over the duration of cultivation through the release of organic acids to the medium (Murakami et al., 2011). This acidification remains lower when *S. cerevisiae* is cultivated in YPD medium compared to synthetic medium (Weinberger et al., 2010). The more acidic environment of SCM-D and SC-D medium might decrease autooxidation of HGA and therefore no pyomelanin formation was observed and HGA titers were higher compared to YPD cultivations. More importantly, this affected the δ-tocotrienol biosynthesis. The δ-tocotrienol titers of the same strain increased by a factor of 4.78 when cultivated in SC-D medium, compared to YPD medium (Figure 24).

This substantiates the importance of a sufficient provision of the precursor HGA. The brownish pigment formation can be observed in shake flask fermentations of the tocotrienol producer

strain of Jiao et al. (2022), who conducted their cultivation in YPD medium, and thus might have wasted high amounts of the precursor HGA. However, a rapid consumption of HGA by the HPT before the precursor accumulates in the extracellular environment would be an efficient approach to increase tocotrienol biosynthesis. Consequently, the most powerful strategy would be a highly efficient enzymatic step chain, with low K_m values and a high turnover number of the heterologous enzymes. Furthermore, spatial proximity towards their substrates is crucial, especially for the first enzyme of the pathway, HPT.

4.1.3 Transcriptional Regulation in Metabolic Engineering

The previously presented approaches in metabolic engineering focused on the sufficiency of the precursor supply and the restriction of degrading pathways. However, metabolic engineering encompasses more strategies such as gene regulation including promoters and transcriptional regulators. Promoters are key regulatory elements, determining the intensity and initiation of gene expression. In *S. cerevisiae*, promoters generally consist of a regulatory element and a core promoter. The latter includes, but is not limited to, the TATA-box, the initiator element (INR), the downstream promoter element (DPE) and the TFIIB recognition element (BRE). Here, the transcription preinitiation complex is formed by the RNA polymerase II and general transcription factors. The regulatory element predominantly contains upstream activation sequences (UAS) and upstream repression sequences (URS) (Struhl, 1995; Hahn and Young, 2011). The structure and regulation of *S. cerevisiae* promoters and their regulatory elements are well studied and accessible, enabling the engineering of promoters. Due to the key role of promoters in gene expression, their application and modification became indispensable in metabolic engineering. From this, the field of promoter engineering was developed, enabling various applications in synthetic biology (He et al., 2023). Hereby methods range from primary rational approaches, such as promoter hybridisation and bioinformatic modelling, to sequence randomisation (Jin et al., 2019).

For the extensive metabolic engineering during this study, a variety of promoters were required. Since numerous genes needed to be strongly expressed, various promoters with a diverse DNA sequence were essential for stable gene expression on a high level. The utilisation of the artificial promoter sequences, which were characterised with YFP as reporter gene (Figure 5), facilitated the creation of the tocochromanol producer strains. Moreover, the variety of promoter strengths could be applied for future fine-tuning of the pathway to improve or direct the metabolic flux. Deliberately selected promoters could enable a targeted expression of the

enzymes of the tocochromanol pathway and bear potential to generate different tocochromanol producer strains. This could be applied for the creation of strains producing different α-, β-, γ- and δ-tocotrienol patterns.

The promoters used for the overexpression of the pathway, such as *pHXT7*, *pTDH3*, *pPGK1* and *pTPI1*, predominantly consist of regulatory elements which are activated during glucose metabolism (Reider Apel et al., 2016; He et al., 2023). Therefore, the expression of the related genes of the tocochromanol pathway are highly expressed during fermentations utilising glucose as carbon source. With regard to the knowledge of factors for gene regulation in *S. cerevisiae*, there are endogenous transcriptional regulators affecting the products and precursors of the tocochromanol pathway. By manipulating transcriptional regulators, Hu et al. (2020) increased GGOH accumulation in several ways. First, the deletion of the UAS of *pERG9* decreased the metabolic flux of FPP into the ergosterol branch, while GGOH production was improved. Moreover, the deletion of a transcription factor encoded by *ROX1*, a known repressor during hypoxia affecting the sterol pathway, increased GGOH titers (Montañés et al., 2011; Hu et al., 2020; Wang et al., 2021). These are successful applications of manipulating transcriptional regulators to increase production titers. However, the effects when transcriptional regulators are exploited are not easily predictable since they often regulate several genes and can affect entire pathways. Contrary effects for two transcriptional regulators were observed in different studies: on the one hand, the deletion of the transcriptional regulators *YJL064W* and *YPL062W* improved GGOH and bisabolene production titers and were also beneficial for growth and plasmid maintenance (Özaydın et al., 2013; Hu et al., 2020). On the other hand, *YJL064W* and *YPL062W* deletion caused a decreased growth phenotype and the GGOH titers drastically dropped (Wang et al., 2021). A decreased growth phenotype was also observed during this study when the *BTS1* overexpression cassette was integrated into *YJL064W* (JBY4, *yjl064w*Δ*::AP8-BTS1-tSSA1_ClonNAT*), illustrating that the manipulation of transcriptional regulators can be challenging in different environments (data not shown).

4.2 Challenges of Recombinant Protein Expression

An important aspect in metabolic engineering is the expression of recombinant proteins. A recurring limitation of this pathway was the endogenous GGPP synthase *BTS1*. Successful genomic integration of the heterologous *XdcrtE* increased both GGOH and δ-tocotrienol titers (section 3.3.2). There are several other examples where the expression of the *XdcrtE* increased GGPP, and its downstream metabolites titers (Verwaal et al., 2007; Xie et al., 2015). However, there are several challenges when considering heterologous protein expression. First, often theoretical knowledge of potential heterologous enzymes cannot substitute the experimental work of characterising the heterologous genes about their functionality in the desired strain. During this work, the bifunctional heterologous GGPP synthases of *P. amygdali* and *S. acidocaldarius* were overexpressed since they had been shown to improve GGPP titers in *S. cerevisiae* (Chen et al., 2016; Hu et al., 2020). However, the plasmid-based overexpression in JBY3 and JBY6, respectively, did not increase GGOH formation. On the contrary, the expression of these genes was even paired with a decreased growth phenotype (section 3.2.5). Heterologous proteins which increased the desired metabolite titers in one yeast strain, do not necessary work within another strain due to strain polymorphisms (De Paiva et al., 2018). Different yeast strains inhabit individual traits and, therefore heterologous protein expression that has proved beneficial in one strain may lead to issues in another strain. Furthermore, differently engineered pathways can inherit diverse constraints and therefore the limitation of an enzyme can also only become evident if another strain is used. Consequently, it has to be considered that heterologous protein expression always requires time consuming screening processes and characterisation of the recombinant proteins in the desired host. However, the heterologous protein expression of the *crtE* of *X. dendrorhous* illustrates that the characterisation of recombinant enzymes can be beneficial when endogenous enzymes are limiting the pathway. Another case, where the expression of heterologous enzymes was necessary, was the tocochromanol pathway itself. Thereby, several enzymes of the tocochromanol pathway originated from plants and cyanobacteria.

4.2.1 The Heterologous Prenyltransferase HPT is Limiting Production Titers

By the successful engineering of the aromatic amino acid biosynthesis pathway and the isoprenoid pathway, 429.48 mg/L HGA and 64.23 mg/L GGOH were produced with the strain JBY61 (section 3.3.4). In comparison to these production titers, the detected amounts of tocochromanols were only minor. Sun et al. (2020) also demonstrated that HGA and GGPP are not efficiently utilised by the downstream δ-tocotrienol pathway enzymes since the titers of the precursors were significantly higher.

During this work, several strategies were investigated to overcome the constraints of the tocochromanol pathway. First, the recombinant enzymes of the tocochromanol pathway were expressed in the strain with an optimised precursor supply (section 3.3). Thereby, the heterologous enzymes themselves appeared to be a limiting factor. It has to be evaluated if the recombinant prenyltransferase HPT efficiently utilises the synthesised GGPP before it is dephosphorylated by phosphatases such as Dpp1p and Lpp1p (Faulkner et al., 1999). Another constraint is the utilisation of FPP and GGPP as important molecules for post-translational modifications (PTM) in *S. cerevisiae*, as proteins are prenylated with isoprenoid moieties, enabling them to anchor to membranes (Stein et al., 2015). Consequently, the heterologous HPT will have to compete with endogenous prenyltransferases, especially with the GGPP-consuming prenyltransferase, encoded by *BET2*. Bet2p is involved in the geranylgeranylation of small GTP-binding proteins, required for vesicular transport (Jiang et al., 1995). In current research, always the *SynHPT* is utilised for the prenylation of HGA and GGPP, because no other functional HPT has been identified yet (Albermann et al., 2008; Shen et al., 2020; Sun et al., 2020; Jiao et al., 2022). The lengthiness of this screening process is made clear by Shen et al. (2020), screening twelve plant HPTs with and without codon optimisation, but without success. However, shortly before their paper was published the endeavour to find another functional HPT was also present during this study. Through excessive literature research and sequence analysis, four heterologous prenyltransferases were chosen for characterisation. Independent of each other, the same plant genes, *EgHPT* of *E. guineensis* (NP_001291355) and *HvHGGT* of *H. vulgare* (AY222860.1), were expressed in *S. cerevisiae* by Shen et al. (2020) and this work (section 3.5.1), both confirming their dysfunctionality. However, during this study, another functional HPT in *S. cerevisiae* was identified for the first time (Figure 22). The *NosHPT* of *Nostoc* sp. TCL240-02 (WP_174711478.1) was the only HPT other than the *SynHPT* that resulted in detectable δ-tocotrienol titers. On the protein level, both prenyltransferases share 51.1 % identical amino acids and have a similarity score of 66.9 %

(EMBOSS Needle Alignment EMBL-EBI; EBLOSUM62, Gap penalty 10, extend penalty 0.5)[3]. This enables sequence variability on a DNA level for further *HPT* overexpression. Thus, the conclusion can be drawn that the selection and screening process of potential recombinant enzymes is often a time-consuming process that is necessary to pave new paths for the implementation of heterologous pathways.

Another approach for a preferred utilisation of GGPP by the HPT over other prenyltransferases could be the channelling between the GGPP synthase and HPT. Channelling ensures spatial proximity of the consecutively operating enzymes (Srere, 1987). In 4.1.2, the concept was presented to fuse proteins to ensure spatial proximity and thereby directing the metabolic flux to increased titers of desired metabolites. Fusion of the heterologous tocochromanol pathway enzymes with prior operating enzymes could be advantageous to increase the flux into the tocochromanol pathway.

4.2.2 Protein Localisation and Truncation of the Chloroplast Transit Peptide

It has been demonstrated that the catalytic activity of TC, encoded by the full-length *AtVTE1* was insufficient since the intermediate MGGBQ accumulated in *E. coli* and *S. cerevisiae* (Albermann et al., 2008; Shen et al., 2020). As mentioned in chapter 3.3, the expression of the full-length *VTE1* did only lead to minor δ-tocotrienol production in JBY12. Hereby another challenge of recombinant protein expression must be addressed: the correct localisation of the recombinant enzymes. In *A. thaliana*, tocopherol accumulation was detected in lipoprotein particles within the chloroplasts, namely plastoglobuli. Moreover, the localisation of the tocopherol cyclase VTE1 was associated with the plastoglobuli, indicating tocopherol biosynthesis taking place within these particles (Vidi et al., 2006). However, these cellular environments are absent in yeast. For an estimation of the subcellular protein localisation of the SynHPT and the AtVTE1, C-terminal envyGFP tagged proteins were expressed in *S. cerevisiae* (Figure 14). Hereby, only a few cells in the low double-digit percentage range of the samples were fluorescent. Opposed to this, the consistent expression of the heterologous envyGFP tagged HPPD (Figure 8) was more successful. Therefore, a degradation of the unfunctional HPT and VTE1 proteins by the ubiquitin-proteasome system is very likely (Finley et al., 2012). Furthermore, a toxic effect of the tocochromanol pathway enzymes in *S. cerevisiae* was hypothesised, leading to the loss of the plasmids. The δ-tocotrienol biosynthesis was only

[3] https://www.ebi.ac.uk/Tools/psa/emboss_needle/

detectable when a stable integration of the tocochromanol pathway genes into the genome was performed and remained absent when expressed plasmid-based (section 3.3). However, the GFP-tagged proteins were also expressed from a plasmid and thus the subcellular localisation of the tocochromanol enzymes in yeast remained unclear.

It was theorised that the tocotrienols and their associated enzymes are most likely abundant in the membranes of *S. cerevisiae* since synthesised lipophilic compounds tend to accumulate within biological membranes (Jiao et al., 2022). Moreover, it has been demonstrated that α-tocopherol is most abundant within membrane systems (Oram et al., 2001). Therefore, it is most likely that the other tocochromanol compounds, such as δ-tocotrienol, are also stored within membranes. Thus, the membrane capacity itself was taken into consideration as a constraining factor for tocochromanol biosynthesis since an equilibrated system is important for membrane integrity (Abe and Hiraki, 2009). However, β-carotin production in JBY63 and JBY66 indicated that the membrane capacity itself was not the limiting factor within this work. The lipophilic carotenoids, such as β-carotene, have been demonstrated to accumulate within membranes and their organisation is mainly driven by Van der Waals interactions with chemical residues of other lipid membrane molecules. Amphiphilic carotenoids, such as zeaxanthin, tend to form lipid bilayers with their polar head group anchored in the polar environments (Gruszecki and Strzałka, 2005). Considerably higher amounts of β-carotene have been synthesised in an engineered *S. cerevisiae* strain compared to the tocochromanol titers (section 3.4). Moreover, the biosynthesis of 5.9 mg/g per DCW of β-carotene has been reported (Verwaal et al., 2007). Consequently, the membrane capacity was most likely not a limiting factor for the tocochromanol biosynthesis in *S. cerevisiae* during this study.

Proteins often undergo different PTMs before they are able to perform their associated functions. Notably, PTMs vary in different expression hosts with a great effect on protein function itself and the regulation of metabolic fluxes. PTMs encompass the addition of chemical residues, such as phosphorylation, methylation, acetylation, glycosylation and lipidation, but also ubiquitination processes and proteolysis (Oliveira and Sauer, 2012). Consequently, the consideration of PTMs is inevitable, especially for heterologous protein expression. Regarding the heterologous expression of plant proteins, one important factor which has to be taken into account is the CTP and its cleavage, comparable to the mitochondrial targeting sequence of endogenous mitochondrial proteins (Turk et al., 2013). The results presented in chapter 3.3.1 substantiate the importance of the correct truncation of the CTP for an increased δ-tocotrienol biosynthesis. The CTP is located at the N-terminus of a protein and responsible for the correct localisation of chloroplast-associated proteins. Usually, the CTP is cleaved inside the

chloroplasts and does not contribute to the proteins' natural function (Bruce, 2000). Nonetheless, to conduct these functions, the correct subcellular localisation is crucial. When the full-length *AtVTE1* was first heterologously expressed in *E. coli*, the tocopherol cyclization step was identified as the keystone for the limitation of δ-tocotrienol synthesis (Albermann et al., 2008). By the stable integration of the full-length genes within the strain JBY12, δ-tocotrienol biosynthesis was achieved in *S. cerevisiae*, but only in minor amounts. Therefore, an N-terminal truncation of the CTP was desired and the bioinformatic webtool (ChloroP 1.1) was utilised to predict the sequence (Emanuelsson et al., 1999). The first 76 amino acids were predicted with a high probability score to be the CTP. However, the expression of the 76 amino acid truncated $AtVTE1^{tr[229\text{-}1467]}$ did not lead to detectable tocotrienol production (3.3). Shortly after these experiments were performed Shen et al. (2020) published their work and proposed that that the catalytic activity of the tocopherol cyclase VTE1 is reduced in *S. cerevisiae.* Moreover, they demonstrated that the deletion of 98 amino acids led to the inactivation of the enzyme. In view of that, the dysfunctionality of the $AtVTE1^{tr[229\text{-}1467]}$ might derive from the deletion of amino acids that contribute to the enzymes function. Shen et al. (2020) further characterised the cleavage of 4 more predicted CTPs, identifying that the truncation of the first 47 amino acids ($AtVTE1^{tr[142\text{-}1467]}$) was the best performing variant. The stable integration of the $AtVTE1^{tr[142\text{-}1467]}$ in JBY17 increased δ-tocotrienol biosynthesis by a factor of 3.95 compared to the full-length variant inherent in JBY12 (Figure 15). The precise truncation of the CTP was also essential for the expression of the methyltransferases MPBQMT and γ-TMT in *S. cerevisiae*. Attempts to create methylated tocotrienol forms beside δ-tocotrienols failed when the full-length methyltransferases were utilised (data not shown). The correct truncation of the CTP of both methyltransferases, as presented by Shen et al. (2020), led to the detection of all other tocotrienol forms (chapter 3.6). By virtue of these results, the bioinformatic CTP prediction is a powerful tool in today's research. However, experimental studies are still of high relevance to identify the correct CTP truncation for heterologous protein expression.

Truncation of the CTP increased the efficiency of the VTE1, although the enzyme was still limiting δ-tocotrienol biosynthesis (Shen et al., 2020). Consequently, protein engineering of the VTE1 or the identification of another functional active cyclase would be beneficial to enhance the efficiency of tocochromanol production. Shen et al. (2020) characterised several other recombinant TCs in yeast, although all of them exhibited a none or lower enzymatic activity than AtVTE1. During this study, four additional heterologous TCs were investigated in *S. cerevisiae*. However, their expression did not lead to any δ-tocotrienol production. Therefore, another strategy was the upregulation of the heterologous pathway. In a plasmid-based

approach, the overexpression of the *SynHPT* and the *AtVTE1* already increased δ-tocotrienol titers (data not shown). Thus, a second overexpression cassette of these genes was integrated into the *DPP1* locus. The increased δ-tocotrienol titers (section 3.5.2) demonstrated that the downstream usage of GGPP and HGA was not efficient, and the increased enzyme dosage from the additional copies of the heterologous genes increased the conversion of the precursors into δ-tocotrienol.

4.3 Evaluation of the Evolutionary Engineering

Metabolic engineering is applied if specific genotypic modifications are desired to direct the metabolic flux or increase protein activity. Hereby, the methodology is rational and based on molecular biological knowledge (Bailey et al., 1996). During this study, rational metabolic engineering enabled the optimisation of the precursor supply and the novel biosynthesis of tocochromanols in *S. cerevisiae*. However, these procedures can be very time consuming, especially if numerous or complex pathways have to be engineered. Moreover, a complete metabolic understanding would be required for the prediction of secondary processes, to omit unexpected events and drawbacks and guarantee a successful rational approach (Nevoigt, 2008). Furthermore, the cloning procedures in industrial strains can be lengthy and restricted due to their robustness and traits such as polyploidy (Cakar et al., 2012).

During the metabolic engineering process of this work, various limitations of the heterologous tocochromanol pathway and its precursor supply were identified. Therefore, an evolutionary engineering strategy was developed to optimise the tocochromanol producer strain in general. Evolutionary engineering is inspired by natural evolution, creating variation from which preferred phenotypes can be selected (Sauer, 2001). Furthermore, it enables strain optimisation when molecular biological knowledge is limiting. However, a suitable screening method for a desired phenotype is required and often constraints the success of the evolutionary engineering approach. Unfortunately, tocochromanol biosynthesis is not directly applicable by classical screening procedures, such as identification of desired phenotypes with fluorescence-activated cell sorting (FACS). Thus, the conscious decision was made not to use a classical random mutagen, but to implement a mutagenic application that targets the desired traits. Therefore, a concept for an engineering approach was developed, based on the antioxidant properties of tocochromanols in *S. cerevisiae*. Ozone was chosen as powerful oxidant to maintain evolutionary pressure towards a higher antioxidant synthesis in tocochromanol producing strains. It was demonstrated that ozone had toxic effects on *S. cerevisiae* and was mutagenic to

microbes (Hamelin and Chung, 1974; Dubeau and Chung, 1979). Thus, a procedure of sequential ozone treatments of yeast cultures was developed, where cells producing higher amounts of the antioxidant δ-tocotrienol might have a survival benefit in an ozone-rich environment (section 3.8). First, single ozone treatments were performed with CEN.PK2-1C to establish a method for the evolutionary engineering and to evaluate critical ozone concentrations on yeast cultures (data not shown). Thereby, a procedure with a stable ozone intake was developed and the variable factor was the time of ozone exposure. Progressively, the time of ozone exposure could be increased, indicating an adaptation of the cells towards longer ozone exposure periods. Moreover, unevolved cultures (JBY20 and JBY67) did not survive the same treatment which was performed with the already evolved strain (JBY20_6) but were able to adapt the ozone pressure after a few treatments (Table 19 and Table 20). Of higher importance, the δ-tocotrienol titers increased in several evolutionary engineered strains. After the successful isolation of single clones following the first series of ozone treatments, an increase in the δ-tocotrienol titer by a factor of 2.28 was achieved in JBY20_6 c3 compared to the parent strain JBY20 (Figure 28 B). During the second series of ozone treatments, the δ-tocotrienol titers of the isolated strain JBY67_3 c4 increased by 50 % compared to the control strain JBY67 (Figure 29 B). The isolation of single strains from the population is essential since effects like polymorphic coevolution can complicate the identification of the desired phenotype. Hereby, the population shows a phenotype which is not reproducible by an isolated clone of the culture (Sauer, 2001). However, the enhancement of the δ-tocotrienol production was reproducible and even stronger in several isolates, compared to the whole culture.

To evaluate the reasons for the improvement, the encoding loci of the tocochromanol pathway genes were sequenced. However, no mutations were observed within these genes or their adjacent regulatory elements. In JBY20_6 c3, a deletion of 3 base pairs was observed within the adjoining *ClonNAT* gene, leading to the loss of the ClonNAT resistance of this strain. The fermentation results of the strain JBY70 (*ClonNATΔ*), presented in section 3.7, indicate that the increased δ-tocotrienol production might be related to the loss of ClonNAT resistance in JBY20_6 c3. Further mutations were not revealed through the sequencing of specific regions. A more suitable method for the evaluation of the evolutionary engineering approach would be a whole genome sequencing to investigate which mutations elsewhere in the genome were beneficial for the tocochromanol biosynthesis. However, Stojiljković et al. (2022) demonstrated that it can be difficult to link specific changes in the DNA sequence to the desired traits. Therefore, the evolutionary engineering of JBY67_3 c4 should be continued and a new series

should be started with the best performing metabolic engineered strain JBY70 to further increase δ-tocotrienol titers.

Consequently, the developed method of sequential ozone treatments is a promising tool for further improvement of tocochromanol production in *S. cerevisiae*. Thereby, the combination of specific rational metabolic engineering strategies for the introduction of heterologous genes and an evolutionary engineering approach paves the way for further engineering of tocochromanol producer strains.

4.4 Establishment of a Fermentation Process and Potential of a Microbial Platform Organism for Tocotrienol Biosynthesis

An important decision to make and a commonly used variable for optimisation is the fermentation medium. Sun et al. (2020) successfully improved δ-tocotrienol titers through the optimisation of the fermentation medium. Thereby, computer-based modelling and simulations were utilised to develop an optimised ratio of yeast extract, peptone and glucose that increased the δ-tocotrienol titer by 2.6-fold (Sun et al., 2020). Consequently, media optimisation bears an enormous potential to further enhance tocotrienol titers.

After the successful proof of concept, the δ-tocotrienol producer JBY70 would be a candidate to establish a fermentation process, using the knowledge of foregoing fermentations. In chapter 3.3, it was observed that JBY12 only produced δ-tocotrienol when cultivated in synthetic medium, but not in YPD medium. First, the supplementation of the aromatic amino acids within synthetic medium was assumed to be beneficial for an aromatic amino acid auxotrophic strain. Thus, δ-tocotrienol production titers of JBY67 were compared using different media (SC-D medium, YPD medium and YPD + AAA) in shake flask cultivations (Figure 24). These experiments showed that, δ-tocotrienol production titers remained highest in SC-D medium, but increased in YPD supplemented with aromatic amino acids, compared to YPD. However, it is not likely that the increased concentration of aromatic amino acids enhanced production titers from the reverse biosynthesis route. Usually, the enzymes of the Ehrlich pathway, Aro8p and Aro9p, convert the supplemented tyrosine and would thereby feed the HGA pathway from another branch (Braus, 1991). However, both encoding genes (*ARO8* and *ARO9*) were deleted in the parent strain of all tocotrienol producer strains generated during this work (Reifenrath and Boles, 2018). Consequently, HGA biosynthesis is limited to one biosynthesis direction since the absence of Aro8p and Aro9p blocks the branch which converts supplemented tyrosine.

Further variable conditions that may affect the production titers are the pH, the composition of the medium, especially regarding the carbon source, the feed, the O_2 and CO_2 concentration, and general process variables (Mazzoleni et al., 2015). The different pH levels in YPD and SC-D media and their influence on production titers was already mentioned in section 4.1.2. Although pH values as low as 2.5 are tolerated by *S. cerevisiae*, a pH below 3.5 is undesirable for an industrial process due to reduced growth. Hereby, the metabolic capacities of yeast are depleted to maintain the endogenous pH through the proton-translocating ATPase, inherent within the membrane (Carmelo et al., 1996). During the fed-batch fermentation (results 3.5.3), further constraints were revealed. Noticeable differences were the decreased HGA and δ-tocotrienol titers of cultures which had been fed, compared to the batch cultures. Moreover, δ-tocotrienol production titers were low during the exponential growth phase and increased during the stationary phase (Figure 18 and Figure 24). Therefore, a separation of the growth phase and the production phase might be beneficial in a production process. Usually, a fed-batch process using glucose is preferable for metabolite production in *S. cerevisiae* due to a repressed Crabtree-effect in conjunction with a suppressed ethanol production (De Deken, 1966). Moreover, without feeding, resources are depleted during the fermentation process and can become a constraining factor. Insufficient nitrogen is often accountable for reduced biomass formation in fed-batch cultures (Shang et al., 2006). Further components which can become a limiting factor are vitamins and trace elements. However, all these components were elements of the feeding medium utilised for the fed-batch fermentation (van Hoek et al., 2000). It is not the first time that a feeding process decreased production titers in *S. cerevisiae*, as observed for muconic acid biosynthesis (unpublished data, Boles Group). Consequently, another feeding strategy is required for future fermentations. The separation of the growth phase and production phase can be coupled with the utilisation of another carbon source. Ethanol would be an alternative since it increases the acetyl-CoA pool (Deng et al., 2023). Acetyl-CoA is the key building block of the mevalonate pathway and therefore its enhanced supply is beneficial for tocochromanol biosynthesis. Glucose could be used as initial carbon source of the batch phase to obtain high cell densities and ethanol would be the carbon source of the feeding medium. When biomass formation and product accumulation are temporally displaced, a reduced O_2 concentration for the latter should be considered. During the fed-batch fermentation, dissolved O_2 was set at a level of 40 % to ensure a high metabolic turnover rate (3.5.3). However, a reduced O_2 concentration may be desirable for antioxidant production, to avoid depletion of the antioxidant product, δ-tocotrienol, due to an oxidative environment.

It should be discussed whether the biosynthesis of tocochromanols from microbial hosts would be a reasonable alternative for a sustainable production process. Reasons for a heterologous production include slow growth rates of the native production host and undesirable traits during fermentative processes (Pickens et al., 2011). Hereby, microorganisms with a high proliferation rate are superior to slow-growing plants for a sustainable production process. Moreover, independency over crop and climate would be gained by biobased fermentative processes. Another advantage from the industrial perspectives is a decreased dependence on fluctuating markets by the better predictability of a fermentative approach. Furthermore, microorganism can be precisely engineered. Thereby, only desired products are synthesised and less resources are wasted through unwanted by-products. Hereby, specific forms with higher antioxidant properties can be synthesised which occur rather rarely in natural resources, such as tocotrienols. Moreover, the generation of a platform cell factory creates the freedom to quickly adapt to new requirements. Antioxidants are in high demanded in the pharmaceutical, food, and cosmetic industries, which offer a wide spectrum of lipophilic substances and therefore versatile applications for different forms of tocochromanol. Especially natural antioxidants such as tocochromanols are highly demanded (Pereira et al., 2022).

In this study, the δ-tocotrienol biosynthesis in *S. cerevisiae* was implemented through extensive metabolic engineering. The precursor biosynthesis was enhanced for a sufficient supply, and competing pathways were downregulated or restricted. Hereby, the GGOH precursor biosynthesis was improved by a factor of 642 to 64.23 mg/L in JBY61 compared to the parent strain JBY2. Subsequently, the recombinant tocochromanol pathway was implemented in JBY12 and JBY20. Thereby, valuable insights about heterologous tocochromanol biosynthesis in *S. cerevisiae* were achieved. Limitations of the pathways, the production host and the fermentation process itself were discussed and evaluated. Various improvements to enhance production titers were addressed and increased δ-tocotrienol titers from 2.79 mg/L in JBY67 to 4.09 mg/L in JBY70, paving the way for further strain engineering of a platform production strain for tocochromanols. Moreover, a valuable method for further evolutionary engineering of an antioxidant producer was developed. Thus, this study lays a foundation for further research of tocochromanol biosynthesis in *S. cerevisiae*.

5 Deutsche Zusammenfassung

Seit Jahrtausenden wird die Bäckerhefe *Saccharomyces cerevisiae* vom Menschen zur mikrobiellen Herstellung von Bier, Wein und Backwaren verwendet. Heutzutage ist *S. cerevisiae* aber weit mehr: ein gut erforschter Modellorganismus und etablierter Produktionswirt in der Biotechnologie. *S. cerevisiae* wird als Produktionsorganismus für verschiedenste Anwendungen wie zum Beispiel i) Bioethanolproduktion ii) Biosynthese von Hormonen wie Insulin oder iii) Biosynthese von Cannabinoiden, genutzt. Dabei hat sich *S. cerevisiae* durch eine ausgeprägte Toleranz gegenüber niedrigen pH-Werten und hohen Salzkonzentrationen, sowie Robustheit gegenüber industriellen Prozessen für ein breites Spektrum industrieller Anwendungen qualifiziert. Darüber hinaus hat die FDA (*Food and Drug Administration*) Produkte aus *S. cerevisiae* als GRAS (*generally regarded as safe*) eingestuft, wodurch eine Vielzahl an biotechnologischen Anwendungen durchführbar wurden. Es gibt verschiedenste Mechanismen zur gezielten gentechnischen Veränderung von *S. cerevisiae*, deren Methoden leicht zugänglich und etabliert sind. Des Weiteren sind Veränderungen mittels CRISPR/Cas9 durch native DNA- Reparaturmechanismen hoch effizient. Aufgrund des breiten industriellen Anwendungsspektrums von *S. cerevisiae* ist dieser Organismus ein idealer Kandidat für die angewandte Erforschung der rekombinanten Biosynthese von Tocochromanolen im Rahmen dieser Arbeit.

Tocopherole und Tocotrienole sind den Tocochromanolen zugehörige, lipophile Verbindungen, welche allgemein mit der Vitamin E Aktivität assoziiert werden. Deren prominentestes Beispiel, α-Tocopherol, ist ein essenzieller Bestandteil der menschlichen und tierischen Ernährung. Natürlicherweise werden Tocochromanole fast ausschließlich von photoautotrophen Organismen wie Pflanzen oder Cyanobakterien synthetisiert. Tocochromanole bestehen aus einem Chromanring und einer isoprenoiden Seitenkette, welche in Tocopherolen gesättigt und in Tocotrienolen dreifach ungesättigt ist. Der Methylierungsgrad des Chromanrings unterscheidet hierbei zwischen α-, β-, γ- und δ-Tocochromanol. In lipophilen Umgebungen, wie Membranen, wirken Tocochromanolverbindungen stark antioxidativ, indem sie reaktive Sauerstoffspezies (ROS) eliminieren und die Ausbreitung von Lipidoxidationen an freien Fettsäuren verhindern. In der aktuellen Forschung ist das Interesse an Tocotrienolen gestiegen, da ihnen neuroprotektive, cholesterinsenkende und krebshemmende Eigenschaften zugeschrieben werden. Folglich sind Tocochromanole wertvolle Verbindungen, welche in der Lebensmittel-, Kosmetik- und Pharmaindustrie eingesetzt werden.

Die *Metabolic Engineering* Strategie zur Biosynthese von Tocochromanolen in *S. cerevisiae* umfasst die gezielte genetische Modifizierung von drei Hauptsynthesewegen: dem aromatischen Aminosäurebiosyntheseweg, dem Mevalonatweg und nachgeschaltetem Isopentenyldiphosphatstoffwechselweg, sowie dem heterologen Tocochromanol-biosyntheseweg. Der native Biosyntheseweg der aromatischen Aminosäuren wird hierbei zur Gewinnung der ersten Vorstufe, der Homogentisinsäure (HGA), genutzt. Wesentlich ist hierbei die Hochregulierung bestimmter Schlüsselenzyme und die gezielte Direktion des metabolischen Flusses in den Tyrosinbiosyntheseweg. Durch einen optimierten aromatischen Aminosäurebiosyntheseweg wurde von Reifenrath und Boles (2018) ein Hefestamm (MRY33) mit einer gesteigerten 4-Hydroxyphenylpyruvat (HPP) Produktion entwickelt. Die heterologe HPP Dioxygenase (HPPD) konvertiert HPP in HGA. In meiner vorangegangenen Masterarbeit wurde MRY33 als Ausgangsstamm zur Charakterisierung verschiedener heterologer für die HPPD kodierende Gene genutzt. Fünf verschiedene *HPPD* Genvarianten wurden in *S. cerevisiae* exprimiert und hinsichtlich ihrer HGA-Produktion evaluiert. Die vielversprechendste Variante stammte aus *Yarrowia lipolytica* (*YlHPPD*) und wurde daraufhin in das Genom von MRY33 integriert. Der resultierende Stamm, JBY2, produzierte 435 mg/L HGA in einer Schüttelkolbenfermentation.

Diese Arbeit wurde somit mit einem genetisch hoch modifizierten Hefestamm gestartet, der bereits eine Vielzahl an Genen besitzt, welche durch starke Promotoren reguliert werden. Für die weitere Stammentwicklung war es somit vorteilhaft eine hohe Sequenzvariabilität zu erhalten, um genomische Instabilitäten durch Sequenzhomologien zu verhindern. Daher wurden 17 artifizielle Promotoren (*AP1-AP17*) charakterisiert. Die Evaluierung der Expressionsstärke der artifiziellen Promotoren erfolgte durch die Expression von *YFP* (*yellow fluorescent protein*) unter der Kontrolle der verschiedenen Promotoren. Im Rahmen dieser Arbeit wurde ein Patent bezüglich der artifiziellen Promotorsequenzen ausgearbeitet (WO2023094429A1).

Die Konzeptionierung der *Metabolic Engineering* Strategie zur Tocochromanolsynthese in dem Hefestamm JBY2 bildete den nächsten Kernpunkt dieser Arbeit. Durch die erfolgreich etablierte Synthese der ersten Vorstufe (HGA) konnte der Fokus auf die zweite Vorstufe Geranylgeranyldiphosphat (GGPP), die Polyprenyl-Seitenkette der Tocochromanole, gelegt werden. Natürlicherweise produziert *S. cerevisiae* GGPP bereits über den Isopentenyldiphosphatbiosyntheseweg. Im Stamm JBY2 konnte Geranylgeraniol (GGOH), welches als indirekter Nachweis für die GGPP-Biosynthese gemessen wurde, jedoch nur in geringen Mengen (< 0,1 mg/L) detektiert werden. Die gezielte Optimierung des

Isopentenyldiphosphatstoffwechselweges durch *Metabolic Engineering*, für eine gesteigerte GGPP-Produktion war somit essenziell. Die 3-Hydroxy-3-methylglutaryl-CoA-Reduktase, welche unter anderem von *HMG1* kodiert wird, ist das limitierende Enzym des Mevalonatstoffwechselweges. Eine Verkürzung des kodierenden Genes führt zur Expression einer *feedback-resistenten* Variante, welche durch einen Promotoraustausch überexprimiert wurde. Weiterhin wurde der Promotor des Gens der Squalensynthase (*pERG9*) durch den ergosterolsensitiven Promotor *pERG1* ersetzt, um den metabolischen Fluss aus dem Mevalonatstoffwechsel in den Ergosterolbiosyntheseweg zu minimieren. Des Weiteren wurde im Laufe dieser Arbeit eine Limitierung der GGPP-Synthese durch die endogene GGPP-Synthase (*BTS1*) beobachtet. Daher wurden die native *BTS1* und eine für *S. cerevisiae* codonoptimierte Variante in *S. cerevisiae* überexprimiert. Weitere Strategien zur Steigerung der GGPP-Synthese, waren die Deletion des Gens der Diacylglycerolpyrophosphat-Phosphatase (*DPP1*), welche eine übermäßige Dephosphorylierung von GGPP zu GGOH verhindern sollte, sowie die Überexpression der Farnesylpyrophosphat-Synthetase (*ERG20*). Die höchste Steigerung der GGPP-Biosynthese wurden jedoch durch ein Screening mehrerer heterologer GGPP-Synthasen in *S. cerevisiae* erzielt. Die genomische Integration der heterologen GGPP-Synthase aus *X. dendrorhous* (*XdcrtE*) ermöglichte die Produktion von 64,23 mg/L GGOH mit dem Stamm JBY61 (JBY2, *hmg1Δ::pTDH3-HMG1*$^{tr[1573-3165]}$*, pERG9Δ::pERG1, ChrIV-49293-49345Δ::pTDH3-XdcrtE-tSSA1_LEU2*). Folglich verbesserte diese *Metabolic Engineering* Strategie die GGOH-Produktion im Vergleich zum Ausgangsstamm (JBY2) um den Faktor 642.

Die erfolgreiche Biosynthese der beiden Vorstufen, HGA und GGPP, legte den Grundstein für die Etablierung des dritten Stoffwechselweges, dem Tocochromanolbiosyntheseweg. Die entsprechenden Enzyme kommen *in vivo* nur in Pflanzen und Cyanobakterien vor und müssen heterolog in Hefe exprimiert werden. Zuerst muss eine Kondensationsreaktion von HGA und GGPP durch eine Homogentisatphytyltransferase (HPT) durchgeführt werden, wobei 2-Methyl-6-Geranylgeranyl-1,4-Benzochinol (MGGBQ) entsteht. Anschließend folgt der Ringschluss innerhalb von MGGBQ durch die Tocopherolzyklase, welche zur Synthese der ersten Tocochromanolform, δ-Tocotrienol, führt. Diese zwei Syntheseschritte wurden in *S. cerevisiae* durch die Integration der heterologen *SynHPT* von *Synechocystis* sp. PCC 6803 und einer verkürzten Variante der Tocopherolzyclase, *AtVTE1*$^{tr[142-1467]}$, aus *A. thaliana* erreicht (JBY20).

Im Vergleich zu den Produktionstitern der Vorstufen waren die in JBY20 detektierten δ-Tocotrienol Titer deutlich geringer, was auf eine Limitierung der Enzyme des Tocochromanolweges hindeutete. Um diese Hypothese zu überprüfen, wurde ein Stamm zur Biosynthese von β-Carotin konstruiert. Die genetischen Modifikationen der Vorläuferstoffwechselwege des δ-Tocotrienol produzierenden Stamms (JBY20) und des β-Carotin produzierenden Stamms (JBY63) waren identisch. Anstelle der Enzyme des Tocochromanolstoffwechselweges, HPT und VTE1, inhäriert JBY63 die Enzyme crtI und crtYB aus *X. dendrorhous* zur Biosynthese von β-Carotin. Eine deutliche Produktion des β-Carotins wurde durch eine ausgeprägte orangene Färbung der Zellen unmittelbar nach der Transformation sichtbar. Wesentlich für die Beantwortung der Hypothese ist jedoch, dass die GGOH-Titer von JBY63 im Vergleich zu JBY20, 60 % niedriger waren. Folglich wurden höhere Mengen der Vorstufe GGPP für die β-Carotinsynthese als für die δ-Tocotrienolbiosynthese, verwendet. Diese Ergebnisse implizieren eine gesteigerte Umsetzungsrate des Substrates GGPP durch die Enzyme des β-Carotinstoffwechselweges gegenüber den Enzymen der Tocochromanolsynthese und verifizieren die prognostizierte Limitierung des letztgenannten Biosyntheseweges. Folglich sollte die Bereitstellung von GGPP im Produktionsstamm JBY20 kein limitierender Faktor für die Tocochromanolsynthese sein.

Daher wurde der Fokus der *Metabolic Engineering* Strategie auf die Optimierung der Tocochromanolbiosynthese gelegt. Zunächst wurde eine zweite Genkassette zur Steigerung der Expression von *SynHPT* und $AtVTE1^{tr[142\text{-}1467]}$ genomisch in JBY20 integriert. Die Steigerung der Enzymkonzentration führte dazu, dass höhere δ-Tocotrienol Titer detektiert wurden, was die Hypothese der Limitierung von HPT und VTE1 bestärkte. Die zweite Expressionskassette wurde hierbei in den *DPP1*-Lokus von JBY20 integriert, woraus der Stamm JBY67 resultierte. Die zweite Integration erhöhte die δ-Tocotrienol Titer im Stamm JBY67 um den Faktor 6,83 auf 2,79 mg/L im Vergleich zum Ausgangsstamm JBY20. Aufgrund einer klassischen Klonierung verblieb eine ClonNAT-Resistenzkassette im Genom von JBY67. Die folgende Deletion der Resistenzkassette führte zu einer weiteren Steigerung des δ-Tocotrienol Titers um den Faktor 1,47 auf 4,09 mg/L in dem neu generierten Stamm JBY70. Darüber hinaus wurde eine zweite, in *S. cerevisiae* funktionelle, HPT aus *Nostoc* sp. TCL240-02 identifiziert. Dies ermöglicht eine erhöhte Sequenzvariabilität für eine zusätzliche HPT-Überexpression in Tocochromanol produzierenden Hefestämmen.

Neben der Biosynthese von δ-Tocotrienol wurde ebenfalls die Synthese weiterer Tocotrienolformen durch *S. cerevisiae* angestrebt. Hierzu wurden die um die Chloroplastenlokalisationsequenz verkürzten Varianten zweier Methyltransferasen (*AtMPBQMT*$^{tr\text{-}[153\text{-}864]}$ und *Atγ-TMT*$^{tr[121\text{-}1047}$) aus *A. thaliana* in das Genom von *S. cerevisiae* integriert (JBY69). Dies ermöglichte die Biosynthese aller Tocotrienolformen (α-, β-, γ- und δ-Tocotrienol) in einer Schüttelkolbenfermentation mit dem Produktionsstamm JBY69. Die vorherrschende Verbindung war weiterhin δ-Tocotrienol, gefolgt von γ-Tocotrienol, welches 50 % des δ-Tocotrienol-Produktionstiters ausmachte. Im Gegensatz zu δ-Tocotrienol, wurden die Metabolite α- und β-Tocotrienol, für deren Synthese die zweite Methyltransferase verantwortlich ist (*Atγ-TMT*), nur in geringen Konzentrationen (> 0,03 %) nachgewiesen. Die signifikant niedrigeren Titer implizieren eine Limitierung der zweiten Methyltransferase, da es zur Akkumulation der Intermediate γ- und δ-Tocotrienol kam. Trotzdem konnte gezeigt werden, dass beide Methyltransferasen in *S. cerevisiae* grundsätzlich funktionell aktiv sind.

Aufgrund der vielseitigen Limitationen der heterologen Enzyme des Tocochromanolweges aus Pflanzen und Cyanobakterien wurde ein Konzept zum *Evolutionary Engineering* ausgearbeitet. Hierzu wurden die antioxidativen Eigenschaften von δ-Tocotrienol genutzt, indem Hefezellen einer oxidativen Umgebung ausgesetzt wurden, um einen natürlichen Selektionsvorteil zu generieren. Somit hätten Hefezellen, welche höhere Konzentrationen an δ-Tocotrienol produzieren, einen Überlebensvorteil gegenüber Zellen, die kein oder weniger δ-Tocotrienol synthetisieren. Ozon wurde als starkes Oxidationsmittel angewandt, um einen Selektionsdruck hinsichtlich einer gesteigerten Antioxidantienproduktion in *S. cerevisiae* zu generieren. Hierzu wurde ein Verfahren von mehreren aufeinanderfolgenden Ozonbegasungen der Hefekulturen entwickelt, bei denen solche Zellen einen Überlebensvorteil haben, die hohe Mengen von δ-Tocotrienol akkumuliert haben. Es wurden mehrere Zyklen der Ozonbehandlungen mit verschiedenen δ-Tocotrienol produzierenden Stämmen durchgeführt, wobei die Methode kontinuierlich verbessert wurde. Dies führte dazu, dass die δ-Tocotrienol Titer in mehreren Stämmen, welche aus dem *Evolutionary Engineering* mit Ozon hervorgingen, erhöht wurden. Die δ-Tocotrienol Titer der dritten Generation des Stammes JBY67 stiegen beispielsweise um 50 % im Vergleich zum Kontrollstamm JBY67. Daraus resultierend ist das innerhalb dieser Arbeit entwickelte Konzept des *Evolutionary Engineering* mittels Ozonbegasung ein vielversprechendes Werkzeug für die weitere Stammentwicklung zur Steigerung der Tocochromanolbiosynthese und potentiell weiterer Antioxidantien in *S. cerevisiae*.

6 References

Abe, F., and T. Hiraki. 2009. Mechanistic role of ergosterol in membrane rigidity and cycloheximide resistance in *Saccharomyces cerevisiae*. *Biochimica et Biophysica Acta (BBA) - Biomembranes*. 1788:743-752. DOI: 10.1016/j.bbamem.2008.12.002.

Albermann, C., S. Ghanegaonkar, K. Lemuth, T. Vallon, M. Reuss, W. Armbruster, and G.A. Sprenger. 2008. Biosynthesis of the vitamin E compound delta-tocotrienol in recombinant *Escherichia coli* cells. *ChemBioChem*. 9:2524-2533. DOI: 10.1002/cbic.200800242.

Anderson, M.S., M. Muehlbacher, I.P. Street, J. Proffitt, and C.D. Poulter. 1989. Isopentenyl diphosphate:dimethylallyl diphosphate isomerase. An improved purification of the enzyme and isolation of the gene from *Saccharomyces cerevisiae*. *Journal of Biological Chemistry*. 264:19169-19175. DOI: 10.1016/S0021-9258(19)47283-9.

Asadollahi, M.A., J. Maury, K. Møller, K.F. Nielsen, M. Schalk, A. Clark, and J. Nielsen. 2008. Production of plant sesquiterpenes in *Saccharomyces cerevisiae*: Effect of *ERG9* repression on sesquiterpene biosynthesis. *Biotechnology and Bioengineering*. 99:666-677. DOI: 10.1002/bit.21581.

Baeshen, N.A., M.N. Baeshen, A. Sheikh, R.S. Bora, M.M.M. Ahmed, H.A.I. Ramadan, K.S. Saini, and E.M. Redwan. 2014. Cell factories for insulin production. *Microbial Cell Factories*. 13. DOI: 10.1186/s12934-014-0141-0.

Bailey, J.E., A. Sburlati, V. Hatzimanikatis, K. Lee, W.A. Renner, and P.S. Tsai. 1996. Inverse metabolic engineering: A strategy for directed genetic engineering of useful phenotypes. *Biotechnology and Bioengineering*. 52:109-121. DOI: 10.1002/(sici)1097-0290(19961005)52:1<109::Aid-bit11>3.0.Co;2-j.

Bauer, J. 2019. Metabolic engineering of *Saccharomyces cerevisiae* for an enhanced tocopherol precursor supply. Master Thesis Johann Wolfgang-Goethe Universität.

Benner, S.A., and A.M. Sismour. 2005. Synthetic biology. *Nature Reviews Genetics*. 6:533-543. 10.1038/nrg1637.

Blaner, W.S., I.O. Shmarakov, and M.G. Traber. 2021. Vitamin A and Vitamin E: Will the Real Antioxidant Please Stand Up? *Annual Review of Nutrition*. 41:105-131. DOI: 10.1146/annurev-nutr-082018-124228.

Bonrath, W., and T. Netscher. 2005. Catalytic processes in vitamins synthesis and production. *Applied Catalysis A: General*. 280:55-73. DOI: 10.1016/j.apcata.2004.08.028.

Braus, G.H. 1991. Aromatic Amino Acid Biosynthesis in Yeast *Saccharomyces cerevisiae*: a Model System for the Regulation of a Eukaryotic Biosynthetic Pathway. *Microbiological reviews*. 1991:349–370. DOI: 10.1128/mr.55.3.349-370.1991.

Bruce, B.D. 2000. Chloroplast transit peptides: Structure, function and evolution. *Trends in Cell Biology*. 10:440–447. DOI: 10.1016/s0962-8924(00)01833-x.

Bruder, S., M. Reifenrath, T. Thomik, E. Boles, and K. Herzog. 2016. Parallelised online biomass monitoring in shake flasks enables efficient strain and carbon source dependent

growth characterisation of *Saccharomyces cerevisiae*. *Microbial Cell Factories*. 15:127. DOI: 10.1186/s12934-016-0526-3.

Buettner, G.R. 1992. The Pecking Order of Free Radicals and Antioxidants: Lipid Peroxidation, α-Tocopherol, and Ascorbate. *Archives of Biochemistry and Biophysics*. 300:535-543. DOI:10.1006/abbi.1993.1074.

Cahoon, E.B., S.E. Hall, K.G. Ripp, T.S. Ganzke, W.D. Hitz, and S.J. Coughlan. 2003. Metabolic redesign of vitamin E biosynthesis in plants for tocotrienol production and increased antioxidant content. *Nature Biotechnology*. 21:1082-1087. DOI: 10.1038/nbt853.

Cakar, Z.P., B. Turanli-Yildiz, C. Alkim, and U. Yilmaz. 2012. Evolutionary engineering of *Saccharomyces cerevisiae* for improved industrially important properties. *FEMS Yeast Research*. 12:171-182. DOI: 10.1111/j.1567-1364.2011.00775.x.

Callari, R., Y. Meier, D. Ravasio, and H. Heider. 2018. Dynamic Control of *ERG20* and *ERG9* Expression for Improved Casbene Production in *Saccharomyces cerevisiae*. *Frontiers in Bioengineering and Biotechnology*. 6:160. DOI: 10.3389/fbioe.2018.00160.

Cameron, D.E., C.J. Bashor, and J.J. Collins. 2014. A brief history of synthetic biology. *Nature Reviews Microbiology*. 12:381-390. DOI: 10.1038/nrmicro3239.

Carmelo, V., P. Bogaerts, and I. Sá-Correia. 1996. Activity of plasma membrane H^+-ATPase and expression of *PMA1* and *PMA2* genes in *Saccharomyces cerevisiae* cells grown at optimal and low pH. *Archives of Microbiology*. 166:315-320. DOI: 10.1007/s002030050389.

Carreira, A., L.M. Ferreira, and V. Loureiro. 2001. Production of brown tyrosine pigments by the yeast *Yarrowia lipolytica*. *Journal of Applied Microbiology*. 90:372-379. DOI: 10.1046/j.1365-2672.2001.01256.x.

Chang, C.-K., K.-H. Teng, S.-W. Lin, T.-H. Chang, and P.-H. Liang. 2013. Control Activity of Yeast Geranylgeranyl Diphosphate Synthase from Dimer Interface through H-Bonds and Hydrophobic Interaction. *Biochemistry*. 52:2783-2792. DOI: 10.1021/bi4001276.

Chávez-Béjar, M.I., A.R. Lara, H. López, G. Hernández-Chávez, A. Martinez, O.T. Ramírez, F. Bolívar, and G. Gosset. 2008. Metabolic engineering of *Escherichia coli* for L-tyrosine production by expression of genes coding for the chorismate mutase domain of the native chorismate mutase-prephenate dehydratase and a cyclohexadienyl dehydrogenase from *Zymomonas mobilis*. *Applied and environmental microbiology*. 74:3284–3290. DOI: 10.1128/aem.02456-07.

Chen, M., W.K.W. Chou, T. Toyomasu, D.E. Cane, and D.W. Christianson. 2016. Structure and Function of Fusicoccadiene Synthase, a Hexameric Bifunctional Diterpene Synthase. *ACS Chemical Biology*. 11:889-899. DOI: 10.1021/acschembio.5b00960.

Chen, S., H. Li, and G. Liu. 2006. Progress of vitamin E metabolic engineering in plants. *Transgenic Research*. 15:655-665. DOI: 10.1007/s11248-006-9012-8.

Cheng, Z., S. Sattler, H. Maeda, Y. Sakuragi, D.A. Bryant, and D. DellaPenna. 2003. Highly divergent methyltransferases catalyze a conserved reaction in tocopherol and

plastoquinone synthesis in cyanobacteria and photosynthetic eukaryotes. *The Plant Cell*. 15:2343–2356. DOI: 10.1105/tpc.013656.

Collakova, E., and D. DellaPenna. 2001. Isolation and functional analysis of homogentisate phytyltransferase from *Synechocystis* sp. PCC 6803 and Arabidopsis. *Plant Physiology*. 127:1113-1124. DOI: 10.1104/pp.010421.

Coon, S.L., S. Kotob, B.B. Jarvis, S. Wang, W.C. Fuqua, and R.M. Weiner. 1994. Homogentisic acid is the product of MelA, which mediates melanogenesis in the marine bacterium *Shewanella colwelliana* D. *Applied and Environmental Microbiology*. 60:3006–3010. DOI: 10.1128/aem.60.8.3006-3010.1994.

Cooney, R.V., A.A. Franke, P.J. Harwood, V. Hatch-Pigott, L.J. Custer, and L.J. Mordan. 1993. Gamma-tocopherol detoxification of nitrogen dioxide: superiority to alpha-tocopherol. *Proceedings of the National Academy of Sciences*. 90:1771-1775. DOI: 10.1073/pnas.90.5.1771.

Cordier, H., C. Lacombe, F. Karst, and T. Bergès. 1999. The *Saccharomyces cerevisiae* Mevalonate Diphosphate Decarboxylase (Erg19p) Forms Homodimers In Vivo, and a Single Substitution in a Structurally Conserved Region Impairs Dimerization. *Current Microbiology*. 38:290-294. DOI: 10.1007/pl00006804.

Curran, K.A., J.M. Leavitt, A.S. Karim, and H.S. Alper. 2013. Metabolic engineering of muconic acid production in *Saccharomyces cerevisiae*. *Metab Eng*. 15:55-66. DOI: 10.1016/j.ymben.2012.10.003.

Dai, Z., Y. Liu, L. Huang, and X. Zhang. 2012. Production of miltiradiene by metabolically engineered *Saccharomyces cerevisiae*. *Biotechnology and Bioengineering*. 109:2845-2853. DOI: 10.1002/bit.24547.

Dashko, S., N. Zhou, C. Compagno, and J. Piškur. 2014. Why, when, and how did yeast evolve alcoholic fermentation? *FEMS Yeast Research*. 14:826-832. DOI: 10.1111/1567-1364.12161.

De Deken, R.H. 1966. The Crabtree Effect: A Regulatory System in Yeast. *Journal of General Microbiology*. 44:149-156. DOI: 10.1099/00221287-44-2-149.

De Paiva, D.P., T.B. Rocha, M.R. Rubini, A.M. Nicola, V.C.B. Reis, F.A.G. Torres, and L.M.P. De Moraes. 2018. A study on the use of strain-specific and homologous promoters for heterologous expression in industrial *Saccharomyces cerevisiae* strains. *AMB Express*. 8. DOI: 10.1186/s13568-018-0613-4.

DellaPenna, D., and B.J. Pogson. 2006. Vitamin synthesis in plants: tocopherols and carotenoids. *Annual Review of Plant Biology*. 57:711-738. DOI: 10.1146/annurev.arplant.56.032604.144301.

Deng, H., M. Wang, and E. Li. 2023. Continuous fed-batch strategy decreases acetic acid production and increases volatile ester formation in wines under high-gravity fermentation. *OENO One*. 57:363-374. DOI: 10.20870/oeno-one.2023.57.1.7238.

Dietz, H., J. Bauer, and M. Kracht. 2023. Artificial yeast promoter regions. WO2023094429A1.

Dimster-Denk, D., M.K. Thorsness, and J. Rine. 1994. Feedback regulation of 3-hydroxy-3-methylglutaryl coenzyme A reductase in *Saccharomyces cerevisiae*. *Molecular Biology of the Cell*. 5:655-665. DOI: 10.1091/mbc.5.6.655.

Donald, K.A., R.Y. Hampton, and I.B. Fritz. 1997. Effects of overproduction of the catalytic domain of 3-hydroxy-3-methylglutaryl coenzyme A reductase on squalene synthesis in *Saccharomyces cerevisiae*. *Applied and Environmental Microbiology*. 63:3341-3344. DOI: 10.1128/aem.63.9.3341-3344.1997.

Dubeau, H., and Y.S. Chung. 1979. Ozone response in wild type and radiation-sensitive mutants of *Saccharomyces cerevisiae*. *Molecular Genetics and Genomics*. 176:393-398. DOI: 10.1007/bf00333103.

Emanuelsson, O., H. Nielsen, and G.v. Heijne. 1999. ChloroP, a neural network-based method for predicting chloroplast transit peptides and their cleavage sites. *Protein Science*. 8:978–984. DOI: 10.1110/ps.8.5.978.

Evans, H.M., and K.S. Bishop. 1922. On the Existence of a Hitherto Unrecognized Dietary Factor Essential for Reproduction. *Science*. 56:650-651. DOI: 10.1126/science.56.1458.650.

Ewald, J.C. 2018. How yeast coordinates metabolism, growth and division. *Current Opinion in Microbiology*. 45:1-7. DOI: 10.1016/j.mib.2017.12.012.

Falk, J., and S. Munné-Bosch. 2010. Tocochromanol functions in plants: antioxidation and beyond. *Journal of Experimental Botany*. 61:1549-1566. DOI: 10.1093/jxb/erq030.

Farwick, A., S. Bruder, V. Schadeweg, M. Oreb, and E. Boles. 2014. Engineering of yeast hexose transporters to transport D-xylose without inhibition by D-glucose. *Proceedings of the National Academy of Sciences*. 111:5159-5164. DOI: 10.1073/pnas.1323464111.

Faulkner, A., X. Chen, J. Rush, B. Horazdovsky, C.J. Waechter, G.M. Carman, and P.C. Sternweis. 1999. The *LPP1* and *DPP1* Gene Products Account for Most of the Isoprenoid Phosphate Phosphatase Activities in *Saccharomyces cerevisiae*. *Journal of Biological Chemistry*. 274:14831-14837. DOI: 10.1074/jbc.274.21.14831.

Feldmann, H. 2012. Yeast: Molecular and Cell Biology. John Wiley & Sons.

Ferreira, R., A. Limeta, and J. Nielsen. 2019. Tackling Cancer with Yeast-Based Technologies. *Trends Biotechnology*. 37:592-603. DOI: 10.1016/j.tibtech.2018.11.013.

Finley, D., H.D. Ulrich, T. Sommer, and P. Kaiser. 2012. The ubiquitin-proteasome system of *Saccharomyces cerevisiae*. *Genetics*. 192:319-360. DOI: 10.1534/genetics.112.140467.

Fuller, G.G., and J.K. Kim. 2021. Compartmentalization and metabolic regulation of glycolysis. *Journal of Cell Science*. 134. DOI: 10.1242/jcs.258469.

Gambacorta, F.V., J.J. Dietrich, Q. Yan, and B.F. Pfleger. 2020. Rewiring yeast metabolism to synthesize products beyond ethanol. *Current Opinion in Chemical Biology*. 59:182-192. DOI: 10.1016/j.cbpa.2020.08.005.

Garcia, I., M. Rodgers, C. Lenne, A. Rolland, A. Sailland, and M. Matringe. 1997. Subcellular localization and purification of a p-hydroxyphenylpyruvate dioxygenase from cultured

carrot cells and characterization of the corresponding cDNA. *Biochemical Journal*. 325:761–769. DOI: 10.1042/bj3250761.

Generoso, W.C., M. Gottardi, M. Oreb, and E. Boles. 2016. Simplified CRISPR-Cas genome editing for *Saccharomyces cerevisiae*. *Journal of Microbiological Methods*. 127:203-205. DOI: 10.1016/j.mimet.2016.06.020.

Ghanegaonkar, S., J. Conrad, U. Beifuss, G.A. Sprenger, and C. Albermann. 2012. Towards the in vivo production of tocotrienol compounds: engineering of a plasmid-free *Escherichia coli* strain for the heterologous synthesis of 2-methyl-6-geranylgeranyl-benzoquinol. *Journal of Biotechnology*. 164:238-247. DOI: 10.1016/j.jbiotec.2012.08.010.

Gibson, B.R., S.J. Lawrence, J.P.R. Leclaire, C.D. Powell, and K.A. Smart. 2007. Yeast responses to stresses associated with industrial brewery handling. *FEMS Microbiology Reviews*. 31:535-569. DOI: 10.1111/j.1574-6976.2007.00076.x.

Gibson, D.G., L. Young, R.-Y. Chuang, J.C. Venter, C.A. Hutchison, and H.O. Smith. 2009. Enzymatic assembly of DNA molecules up to several hundred kilobases. *Nature Methods*. 6:343–345. DOI: 10.1038/nmeth.1318.

Gietz, R.D., and R.H. Schiestl. 2007. Frozen competent yeast cells that can be transformed with high efficiency using the LiAc/SS carrier DNA/PEG method. *Nature Protocols*. 2:1-4. DOI: 10.1038/nprot.2007.17.

Gold, N.D., C.M. Gowen, F.-X. Lussier, S.C. Cautha, R. Mahadevan, and V.J.J. Martin. 2015. Metabolic engineering of a tyrosine-overproducing yeast platform using targeted metabolomics. *Microbial cell factories*. 14:73. DOI: 10.1186/s12934-015-0252-2.

Górnaś, P., G. Baškirovs, and A. Siger. 2022. Free and Esterified Tocopherols, Tocotrienols and Other Extractable and Non-Extractable Tocochromanol-Related Molecules: Compendium of Knowledge, Future Perspectives and Recommendations for Chromatographic Techniques, Tools, and Approaches Used for Tocochromanol Determination. *Molecules*. 27:6560. DOI: 10.3390/molecules27196560.

Gottardi, M., M. Reifenrath, E. Boles, and J. Tripp. 2017. Pathway engineering for the production of heterologous aromatic chemicals and their derivatives in *Saccharomyces cerevisiae*: Bioconversion from glucose. *FEMS Yeast Research*. 17. DOI: 10.1093/femsyr/fox035.

Grabińska, K., and G. Palamarczyk. 2002. Dolichol biosynthesis in the yeast *Saccharomyces cerevisiae*: an insight into the regulatory role of farnesyl diphosphate synthase. *FEMS Yeast Research*. 2:259-265. DOI: 10.1016/s1567-1356(02)00110-1.

Gruszecki, W.I., and K. Strzałka. 2005. Carotenoids as modulators of lipid membrane physical properties. *Biochimica et Biophysica Acta (BBA) - Molecular Basis of Disease*. 1740:108-115. DOI: 10.1016/j.bbadis.2004.11.015.

Gutbrod, K., J. Romer, and P. Dörmann. 2019. Phytol metabolism in plants. *Progress in Lipid Research*. 74:1-17. DOI: 10.1016/j.plipres.2019.01.002.

Hahn, S., and E.T. Young. 2011. Transcriptional Regulation in *Saccharomyces cerevisiae*: Transcription Factor Regulation and Function, Mechanisms of Initiation, and Roles of

Activators and Coactivators. *Genetics*. 189:705-736. DOI: 10.1534/genetics.111.127019.

Hamacher, T., J. Becker, M. Gárdonyi, B. Hahn-Hägerdal, and E. Boles. 2002. Characterization of the xylose-transporting properties of yeast hexose transporters and their influence on xylose utilization. *Microbiology*. 148:2783–2788. DOI: 10.1099/00221287-148-9-2783.

Hamelin, C., and Y.S. Chung. 1974. Optimal conditions for mutagenesis by ozone in *Escherichia coli* K12. *Mutation Research/Fundamental and Molecular Mechanisms of Mutagenesis*. 24:271-279. DOI: 10.1016/0027-5107(74)90175-4.

Hampton, R.Y., and J. Rine. 1994. Regulated degradation of HMG-CoA reductase, an integral membrane protein of the endoplasmic reticulum, in yeast. *Journal of Cell Biology*. 125:299-312. DOI: 10.1083/jcb.125.2.299.

Hartmann, M., T.R. Schneider, A. Pfeil, G. Heinrich, W.N. Lipscomb, and G.H. Braus. 2003. Evolution of feedback-inhibited β/α barrel isoenzymes by gene duplication and a single mutation. *Proceedings of the National Academy of Sciences*. 100:862-867. DOI: 10.1073/pnas.0337566100.

Hazelwood, L.A., J.-M. Daran, A.J.A. van Maris, J.T. Pronk, and J.R. Dickinson. 2008. The Ehrlich pathway for fusel alcohol production: a century of research on *Saccharomyces cerevisiae* metabolism. *Applied and Environmental Microbiology*. 74:2259-2266. DOI: 10.1128/AEM.02625-07.

He, S., Z. Zhang, and W. Lu. 2023. Natural promoters and promoter engineering strategies for metabolic regulation in *Saccharomyces cerevisiae*. *Journal of Industrial Microbiology and Biotechnology*. 50. DOI: 10.1093/jimb/kuac029.

Henritzi, S., M. Fischer, M. Grininger, M. Oreb, and E. Boles. 2018. An engineered fatty acid synthase combined with a carboxylic acid reductase enables de novo production of 1-octanol in *Saccharomyces cerevisiae*. *Biotechnology for biofuels*. 11:150. 10.1186/s13068-018-1149-1.

Hiser, L., M.E. Basson, and J. Rine. 1994. *ERG10* from *Saccharomyces cerevisiae* encodes acetoacetyl-CoA thiolase. *Journal of Biological Chemistry*. 269:31383-31389. DOI: 10.1016/S0021-9258(18)31705-8.

Hitschler, J., and E. Boles. 2020. Improving 3-methylphenol (m-cresol) production in yeast via in vivo glycosylation or methylation. *FEMS Yeast Research*. 20. DOI: 10.1093/femsyr/foaa063.

Hong, K.-K., and J. Nielsen. 2012. Metabolic engineering of *Saccharomyces cerevisiae*: a key cell factory platform for future biorefineries. *Cellular and Molecular Life Sciences*. 69:2671-2690. DOI: 10.1007/s00018-012-0945-1.

Hsu, C.-Y., P.-W. Wang, A. Alalaiwe, Z.-C. Lin, and J.-Y. Fang. 2019. Use of Lipid Nanocarriers to Improve Oral Delivery of Vitamins. *Nutrients*. 11:68. DOI: 10.3390/nu11010068.

Hu, T., J. Zhou, Y. Tong, P. Su, X. Li, Y. Liu, N. Liu, X. Wu, Y. Zhang, J. Wang, L. Gao, L. Tu, Y. Lu, Z. Jiang, Y.J. Zhou, W. Gao, and L. Huang. 2020. Engineering chimeric

diterpene synthases and isoprenoid biosynthetic pathways enables high-level production of miltiradiene in yeast. *Metabolic Engineering*. 60:87-96. DOI: 10.1016/j.ymben.2020.03.011.

Jiang, Y., P. Proteau, D. Poulter, and S. Ferro-Novick. 1995. *BTS1* Encodes a Geranylgeranyl Diphosphate Synthase in *Saccharomyces cerevisiae*. *Journal of Biological Chemistry*. 270:21793-21799. DOI: 10.1074/jbc.270.37.21793.

Jiao, X., B. Shen, M. Li, L. Ye, and H. Yu. 2022. Secretory Production of Tocotrienols in *Saccharomyces cerevisiae*. *ACS Synthetic Biology*. DOI: 10.1021/acssynbio.1c00484.

Jin, L.-Q., W.-R. Jin, Z.-C. Ma, Q. Shen, X. Cai, Z.-Q. Liu, and Y.-G. Zheng. 2019. Promoter engineering strategies for the overproduction of valuable metabolites in microbes. *Applied Microbiology and Biotechnology*. 103:8725-8736. DOI: 10.1007/s00253-019-10172-y.

Jordá, T., and S. Puig. 2020. Regulation of Ergosterol Biosynthesis in *Saccharomyces cerevisiae*. *Genes (Basel)*. 11:795. DOI: 10.3390/genes11070795.

Kamal-Eldin, and Appelqvist. 1996. The chemistry and antioxidant properties of tocopherols and tocotrienols. *Lipids*. DOI: 10.1007/BF02522884.

Kayikci, Ö., and J. Nielsen. 2015. Glucose repression in *Saccharomyces cerevisiae*. *FEMS Yeast Research*. 15. DOI: 10.1093/femsyr/fov068.

Keller, Y., F. Bouvier, A. d'Harlingue, and C. B. 1998. Metabolic compartmentation of plastid prenyllipid biosynthesis evidence for the involvement of a multifunctional geranylgeranyl reductase. *European Journal of Biochemistry*. DOI: 10.1046/j.1432-1327.1998.2510413.x.

Kellis, M., B.W. Birren, and E.S. Lander. 2004. Proof and evolutionary analysis of ancient genome duplication in the yeast *Saccharomyces cerevisiae*. *Nature*. 428:617-624. DOI: 10.1038/nature02424.

Khalil, A.M. 2020. The genome editing revolution: review. *Journal of Genetic Engineering and Biotechnology*. 18. DOI: 10.1186/s43141-020-00078-y.

Khanna, S., V. Patel, C. Rink, S. Roy, and C. Sen. 2005. Delivery of orally supplemented α-tocotrienol to vital organs of rats and tocopherol-transport protein deficient mice. *Free Radical Biology and Medicine*. 39:1310-1319. DOI: 10.1016/j.freeradbiomed.2005.06.013.

Krivoruchko, A., C. Serrano-Amatriain, Y. Chen, V. Siewers, and J. Nielsen. 2013. Improving biobutanol production in engineered *Saccharomyces cerevisiae* by manipulation of acetyl-CoA metabolism. *Journal of Industrial Microbiology and Biotechnology*. 40:1051-1056. DOI: 10.1007/s10295-013-1296-0.

Kruk, J., R. Szymańska, J. Cela, and S. Munne-Bosch. 2014. Plastochromanol-8: Fifty years of research. *Phytochemistry*. 108:9-16. DOI: 10.1016/j.phytochem.2014.09.011.

Larroude, M., E. Celinska, A. Back, S. Thomas, J.M. Nicaud, and R. Ledesma-Amaro. 2018. A synthetic biology approach to transform *Yarrowia lipolytica* into a competitive

biotechnological producer of β-carotene. *Biotechnology and Bioengineering*. 115:464-472. DOI: 10.1002/bit.26473.

Larroude, M., D. Onésime, O. Rué, J.M. Nicaud, and T. Rossignol. 2021. A *Yarrowia lipolytica* Strain Engineered for Pyomelanin Production. *Microorganisms*. 9. DOI: 10.3390/microorganisms9040838.

Lee, M.E., W.C. DeLoache, B. Cervantes, and J.E. Dueber. 2015. A Highly Characterized Yeast Toolkit for Modular, Multipart Assembly. *ACS Synthetic Biology*. 4:975-986. DOI: 10.1021/sb500366v.

Li, X., D. Guo, Y. Cheng, F. Zhu, Z. Deng, and T. Liu. 2014. Overproduction of fatty acids in engineered *Saccharomyces cerevisiae*. *Biotechnology and Bioengineering*. 111:1841-1852. DOI: 10.1002/bit.25239.

Lian, J., and H. Zhao. 2015. Recent advances in biosynthesis of fatty acids derived products in *Saccharomyces cerevisiae* via enhanced supply of precursor metabolites. *Journal of Industrial Microbiology and Biotechnology*. 42:437-451. DOI: 10.1007/s10295-014-1518-0.

Liu, Q., T. Yu, X. Li, Y. Chen, K. Campbell, J. Nielsen, and Y. Chen. 2019. Rewiring carbon metabolism in yeast for high level production of aromatic chemicals. *Nature communications*. 10:4976-4976. DOI: 10.1038/s41467-019-12961-5.

Liu, W., B. Zhang, and R. Jiang. 2017. Improving acetyl-CoA biosynthesis in *Saccharomyces cerevisiae* via the overexpression of pantothenate kinase and PDH bypass. *Biotechnology for Biofuels*. 10. DOI: 10.1186/s13068-017-0726-z.

Liu, Z., K.E.J. Tyo, J.L. Martínez, D. Petranovic, and J. Nielsen. 2012. Different expression systems for production of recombinant proteins in *Saccharomyces cerevisiae*. *Biotechnology and Bioengineering*. 109:1259-1268. DOI: 10.1002/bit.24409.

Liu, Z., J. Wang, and J. Nielsen. 2022. Yeast synthetic biology advances biofuel production. *Current Opinion in Microbiology*. 65:33-39. DOI: 10.1016/j.mib.2021.10.010.

Lõoke, M., K. Kristjuhan, and A. Kristjuhan. 2011. Extraction of genomic DNA from yeasts for PCR-based applications. *BioTechniques*. 50:325-328. DOI: 10.2144/000113672.

Luo, X., M.A. Reiter, L. D'Espaux, J. Wong, C.M. Denby, A. Lechner, Y. Zhang, A.T. Grzybowski, S. Harth, W. Lin, H. Lee, C. Yu, J. Shin, K. Deng, V.T. Benites, G. Wang, E.E.K. Baidoo, Y. Chen, I. Dev, C.J. Petzold, and J.D. Keasling. 2019. Complete biosynthesis of cannabinoids and their unnatural analogues in yeast. *Nature*. 567:123-126. DOI: 10.1038/s41586-019-0978-9.

Lütke-Eversloh, T., and G. Stephanopoulos. 2005. Feedback inhibition of chorismate mutase/prephenate dehydrogenase (TyrA) of *Escherichia coli*: Generation and characterization of tyrosine-insensitive mutants. *Applied and environmental microbiology*. 71:7224–7228. DOI: 10.1128/aem.71.11.7224-7228.2005.

Ma, Y., Y. Zu, S. Huang, and G. Stephanopoulos. 2023. Engineering a universal and efficient platform for terpenoid synthesis in yeast. *Proceedings of the National Academy of Sciences*. 120:e2207680120. DOI: 10.1073/pnas.2207680120.

Mannhaupt, G., R. Stucka, U. Pilz, C. Schwarzlose, and H. Feldmann. 1989. Characterization of the prephenate dehydrogenase-encoding gene, *TYR1*, from *Saccharomyces cerevisiae*. *Gene*. 85:303-311. DOI: 10.1016/0378-1119(89)90422-8.

Mao, X., Y. Hu, C. Liang, and C. Lu. 2002. *MET3* Promoter: A Tightly Regulated Promoter and Its Application in Construction of Conditional Lethal Strain. *Current Microbiology*. 45:37-40. DOI: 10.1007/s00284-001-0046-0.

Mathiasen, D.P., and M. Lisby. 2014. Cell cycle regulation of homologous recombination in *Saccharomyces cerevisiae*. *FEMS Microbiol Rev*. 38:172-184. DOI: 10.1111/1574-6976.12066.

Mazzoleni, S., C. Landi, F. Cartenì, E. De Alteriis, F. Giannino, L. Paciello, and P. Parascandola. 2015. A novel process-based model of microbial growth: self-inhibition in *Saccharomyces cerevisiae* aerobic fed-batch cultures. *Microbial Cell Factories*. 14. DOI: 10.1186/s12934-015-0295-4.

McGovern, P., M. Jalabadze, S. Batiuk, M.P. Callahan, K.E. Smith, G.R. Hall, E. Kvavadze, D. Maghradze, N. Rusishvili, L. Bouby, O. Failla, G. Cola, L. Mariani, E. Boaretto, R. Bacilieri, P. This, N. Wales, and D. Lordkipanidze. 2017. Early Neolithic wine of Georgia in the South Caucasus. *Proceedings of the National Academy of Sciences*. 114:E10309-E10318. DOI: 10.1073/pnas.1714728114.

Meadows, C.W., F. Mingardon, B.M. Garabedian, E.E.K. Baidoo, V.T. Benites, A.V. Rodrigues, R. Abourjeily, A. Chanal, and T.S. Lee. 2018. Discovery of novel geranylgeranyl reductases and characterization of their substrate promiscuity. *Biotechnology for Biofuels and Bioproducts*. 11:340. DOI: 10.1186/s13068-018-1342-2.

Mesa, T., and S. Munné-Bosch. 2023. α-Tocopherol in chloroplasts: Nothing more than an antioxidant? *Current Opinion in Plant Biology*. 74:102400. DOI: 10.1016/j.pbi.2023.102400.

Miozzari, G., P. Niederberger, and R. Hütter. 1978. Tryptophan biosynthesis in *Saccharomyces cerevisiae*: control of the flux through the pathway. *Journal of Bacteriology*. 134:48-59. DOI: 10.1128/jb.134.1.48-59.1978.

Miyazawa, T., G.C. Burdeos, M. Itaya, K. Nakagawa, and T. Miyazawa. 2019. Vitamin E: Regulatory Redox Interactions. *IUBMB Life*. 71:430-441. DOI: 10.1002/iub.2008.

Montañés, F.M., A. Pascual-Ahuir, and M. Proft. 2011. Repression of ergosterol biosynthesis is essential for stress resistance and is mediated by the Hog1 MAP kinase and the Mot3 and Rox1 transcription factors. *Molecular Microbiology*. 79:1008-1023. DOI: 10.1111/j.1365-2958.2010.07502.x.

Moran, G.R. 2005. 4-Hydroxyphenylpyruvate dioxygenase. *Archives of Biochemistry and Biophysics*. 433:117-128. DOI: 10.1016/j.abb.2004.08.015.

Moran, G.R. 2014. 4-Hydroxyphenylpyruvate dioxygenase and hydroxymandelate synthase: exemplars of the α-keto acid dependent oxygenases. *Archives of Biochemistry and Biophysics*. 544:58-68. DOI: 10.1016/j.abb.2013.10.022.

Mumberg, D., R. Muller, and M. Funk. 1994. Regulatable promoters of *Saccharomyces cerevisiae*: comparison of transcriptional activity and their use for heterologous expression. *Nucleic Acids Research*. 22:5767-5768. DOI: 10.1093/nar/22.25.5767.

Murakami, C.J., V. Wall, N. Basisty, and M. Kaeberlein. 2011. Composition and Acidification of the Culture Medium Influences Chronological Aging Similarly in Vineyard and Laboratory Yeast. *PLoS ONE*. 6:e24530. DOI: 10.1371/journal.pone.0024530.

Nandy, S.K., and R.K. Srivastava. 2018. A review on sustainable yeast biotechnological processes and applications. *Microbiological research*. 207:83–90. DOI: 10.1016/j.micres.2017.11.013.

Nevoigt, E. 2008. Progress in Metabolic Engineering of *Saccharomyces cerevisiae*. *Microbiology and Molecular Biology Reviews*. 72:379-412. DOI: 10.1128/mmbr.00025-07.

Newcomb, L.L., J.A. Diderich, M.G. Slattery, and W. Heideman. 2003. Glucose regulation of *Saccharomyces cerevisiae* cell cycle genes. *Eukaryotic Cell*. 2:143-149. DOI: 10.1128/ec.2.1.143-149.2003.

Nielsen, J. 2015. Yeast cell factories on the horizon. *Science*. 349:1050-1051. DOI: 10.1126/science.aad2081.

Nielsen, J. 2019. Yeast Systems Biology: Model Organism and Cell Factory. *Biotechnology Journal*. 14:1800421. DOI: 10.1002/biot.201800421.

Nielsen, J., and J.D. Keasling. 2016. Engineering Cellular Metabolism. *Cell*. 164:1185-1197. DOI: 10.1016/j.cell.2016.02.004.

Norris, S.R., X. Shen, and D. DellaPenna. 1998. Complementation of the Arabidopsis *pds1* mutation with the gene encoding p-hydroxyphenylpyruvate dioxygenase. *Plant Physiology*. 117:1317-1323. DOI: 10.1104/pp.117.4.1317.

Offley, S.R., and M.C. Schmidt. 2019. Protein phosphatases of *Saccharomyces cerevisiae*. *Current Genetics*. 65:41-55. DOI: 10.1007/s00294-018-0884-y.

Ohnuma, S., M. Suzuki, and T. Nishino. 1994. Archaebacterial ether-linked lipid biosynthetic gene. Expression cloning, sequencing, and characterization of geranylgeranyl-diphosphate synthase. *Journal of Biological Chemistry*. 269:14792-14797. DOI: 10.1016/S0021-9258(17)36694-2.

Oliveira, A.P., and U. Sauer. 2012. The importance of post-translational modifications in regulating *Saccharomyces cerevisiae* metabolism. *FEMS Yeast Research*. 12:104-117. DOI: 10.1111/j.1567-1364.2011.00765.x.

Oram, J.F., A.M. Vaughan, and R. Stocker. 2001. ATP-binding Cassette Transporter A1 Mediates Cellular Secretion of α-Tocopherol. *Journal of Biological Chemistry*. 276:39898-39902. DOI: 10.1074/jbc.m106984200.

Oshiro, J., G.-S. Han, and G.M. Carman. 2003. Diacylglycerol pyrophosphate phosphatase in *Saccharomyces cerevisiae*. *Biochimica et Biophysica Acta (BBA) - Molecular and Cell Biology of Lipids*. 1635:1-9. DOI: 10.1016/j.bbalip.2003.10.002.

Oswell, N.J., H. Thippareddi, and R.B. Pegg. 2018. Practical use of natural antioxidants in meat products in the U.S.: A review. *Meat Science*. 145:469-479. DOI: 10.1016/j.meatsci.2018.07.020.

Oulmouden, A., and F. Karst. 1991. Nucleotide sequence of the *ERG12* gene of *Saccharomyces cerevisiae* encoding mevalonate kinase. *Current Genetics*. 19:9-14. DOI: 10.1007/bf00362081.

Özaydın, B., H. Burd, T.S. Lee, and J.D. Keasling. 2013. Carotenoid-based phenotypic screen of the yeast deletion collection reveals new genes with roles in isoprenoid production. *Metabolic Engineering*. 15:174-183. DOI: 10.1016/j.ymben.2012.07.010.

Paravicini, G., H.U. Mösch, T. Schmidheini, and G. Braus. 1989. The general control activator protein GCN4 is essential for a basal level of *ARO3* gene expression in *Saccharomyces cerevisiae*. *Molecular and Cellular Biology*. 9:144-151. DOI: 10.1128/mcb.9.1.144-151.1989.

Pellaud, S., and L. Mène-Saffrané. 2017. Metabolic Origins and Transport of Vitamin E Biosynthetic Precursors. *Frontiers in Plant Science*. 8:1959. DOI: 10.3389/fpls.2017.01959.

Pereira, R., M. Costa, C. Velasco, L.M. Cunha, R.C. Lima, L.F. Baião, S. Batista, A. Marques, T. Sá, D.A. Campos, M. Pereira, D. Jesus, S. Fernández-Boo, B. Costas, M. Pintado, and L.M.P. Valente. 2022. Comparative Analysis between Synthetic Vitamin E and Natural Antioxidant Sources from Tomato, Carrot and Coriander in Diets for Market-Sized *Dicentrarchus labrax*. *Antioxidants*. 11:636. DOI: 10.3390/antiox11040636.

Pickens, L.B., Y. Tang, and Y.-H. Chooi. 2011. Metabolic Engineering for the Production of Natural Products. *Annual Review of Chemical and Biomolecular Engineering*. 2:211-236. DOI: 10.1146/annurev-chembioeng-061010-114209.

Piskur, J., E. Rozpedowska, S. Polakova, A. Merico, and C. Compagno. 2006. How did *Saccharomyces* evolve to become a good brewer? *Trends in Genetics*. 22:183-186. DOI: 10.1016/j.tig.2006.02.002.

Plonka, P.M., and M. Grabacka. 2006. Melanin synthesis in microorganisms--biotechnological and medical aspects. *Acta Biochimica Polonica*. 53:429-443. DOI: 10.18388/abp.2006_3314.

Porfirova, S., E. Bergmüller, S. Tropf, R. Lemke, and P. Dörmann. 2002. Isolation of an *Arabidopsis* mutant lacking vitamin E and identification of a cyclase essential for all tocopherol biosynthesis. *Proceedings of the National Academy of Sciences (PNAS)*. 99:12495-12500. DOI: 10.1073/pnas.182330899.

Pronk, J.T., H. Yde Steensma, and J.P. Van Dijken. 1996. Pyruvate metabolism in *Saccharomyces cerevisiae*. *Yeast*. 12:1607-1633. DOI: 10.1002/(sici)1097-0061(199612)12:16<1607::aid-yea70>3.0.co;2-4.

Qureshi, A.A. 2022. Tocotrienols: Exciting Biological and Pharmacological Properties of Tocotrienols and Naturally Occurring Compounds, Part II. *Annals of Clinical Case Reports*. 7. PMID: 36540866.

Reider Apel, A., L. d'Espaux, M. Wehrs, D. Sachs, R.A. Li, G.J. Tong, M. Garber, O. Nnadi, W. Zhuang, N.J. Hillson, J.D. Keasling, and A. Mukhopadhyay. 2016. A Cas9-based toolkit to program gene expression in *Saccharomyces cerevisiae*. *Nucleic Acids Research*. 45:496-508. DOI: 10.1093/nar/gkw1023.

Reifenrath, M., M. Bauer, M. Oreb, and E. Boles. 2018. Bacterial bifunctional chorismate mutase-prephenate dehydratase PheA increases flux into the yeast phenylalanine pathway and improves mandelic acid production. *Metabolic Engineering Communications*. 7:e00079. DOI: 10.1016/j.mec.2018.e00079.

Reifenrath, M., and E. Boles. 2018. Engineering of hydroxymandelate synthases and the aromatic amino acid pathway enables de novo biosynthesis of mandelic and 4-hydroxymandelic acid with *Saccharomyces cerevisiae*. *Metabolic Engineering*. 45:246-254. DOI: 10.1016/j.ymben.2018.01.001.

Sauer, U. 2001. Evolutionary engineering of industrially important microbial phenotypes. *Advances in Biochemical Engineering/Biotechnology*. 73:129-169. DOI: 10.1007/3-540-45300-8_7.

Schadeweg, V., and E. Boles. 2016. Increasing n-butanol production with *Saccharomyces cerevisiae* by optimizing acetyl-CoA synthesis, NADH levels and trans-2-enoyl-CoA reductase expression. *Biotechnology for Biofuels*. 9. DOI: 10.1186/s13068-016-0673-0.

Schledz, M., A. Seidler, P. Beyer, and G. Neuhaus. 2001. A novel phytyltransferase from *Synechocystis* sp. PCC 6803 involved in tocopherol biosynthesis. *FEBS Letters*. 499:15-20. DOI: 10.1016/S0014-5793(01)02508-X.

Schnappauf, G., M. Hartmann, M. Künzler, and G.H. Braus. 1998a. The two 3-deoxy-d-arabino-heptulosonate-7-phosphate synthase isoenzymes from *Saccharomyces cerevisiae* show different kinetic modes of inhibition. *Archives of Microbiology*. 169:517-524. DOI: 10.1007/s002030050605.

Schnappauf, G., S. Krappmann, and G.H. Braus. 1998b. Tyrosine and Tryptophan Act through the Same Binding Site at the Dimer Interface of Yeast Chorismate Mutase. *Journal of Biological Chemistry*. 273:17012-17017. DOI: 10.1074/jbc.273.27.17012.

Schneider, C. 2005. Chemistry and biology of vitamin E. *Molecular Nutrition & Food Research*. 49:7-30. DOI: 10.1002/mnfr.200400049.

Shang, F., S. Wen, X. Wang, and T. Tan. 2006. Effect of nitrogen limitation on the ergosterol production by fed-batch culture of *Saccharomyces cerevisiae*. *Journal of Biotechnology*. 122:285-292. DOI: 10.1016/j.jbiotec.2005.11.020.

Shen, B., P. Zhou, X. Jiao, Z. Yao, L. Ye, and H. Yu. 2020. Fermentative production of Vitamin E tocotrienols in *Saccharomyces cerevisiae* under cold-shock-triggered temperature control. *Nature Communications*. 11:5155. DOI: 10.1038/s41467-020-18958-9.

Skrzypek, M.S., R.S. Nash, E.D. Wong, K.A. MacPherson, S.T. Hellerstedt, S.R. Engel, K. Karra, S. Weng, T.K. Sheppard, G. Binkley, M. Simison, S.R. Miyasato, and J.M. Cherry. 2018. *Saccharomyces* genome database informs human biology. *Nucleic acids research*. 46:D736-D742. DOI: 10.1093/nar/gkx1112.

Srere, P.A. 1987. Complexes of sequential metabolic enzymes. *Annual Review of Biochemistry*. 56:89-124. DOI: 10.1146/annurev.bi.56.070187.000513.

Steensels, J., T. Snoek, E. Meersman, M.P. Nicolino, K. Voordeckers, and K.J. Verstrepen. 2014. Improving industrial yeast strains: exploiting natural and artificial diversity. *FEMS Microbiology Reviews*. 38:947-995. DOI: 10.1111/1574-6976.12073.

Stein, V., M.H. Kubala, J. Steen, S.M. Grimmond, and K. Alexandrov. 2015. Towards the Systematic Mapping and Engineering of the Protein Prenylation Machinery in *Saccharomyces cerevisiae*. *PLOS ONE*. 10:e0120716. DOI: 10.1371/journal.pone.0120716.

Stojiljković, M., A. Claes, Q. Deparis, M.M. Demeke, A. Subotić, M.R. Foulquié-Moreno, and J.M. Thevelein. 2022. Whole-Genome Transformation of Yeast Promotes Rare Host Mutations with a Single Causative SNP Enhancing Acetic Acid Tolerance. *Molecular and Cellular Biology*. 42:1-25. DOI: 10.1128/mcb.00560-21.

Struhl, K. 1995. Yeast Transcriptional regulatory mechanisms. *Annual Review of Genetics*. 29:651-674. DOI: 10.1146/annurev.ge.29.120195.003251.

Sun, H., J. Yang, X. Lin, C. Li, Y. He, Z. Cai, G. Zhang, and H. Song. 2020. De Novo High-Titer Production of Delta-Tocotrienol in Recombinant *Saccharomyces cerevisiae*. *Journal of Agricultural and Food Chemistry*. DOI: 10.1021/acs.jafc.0c00294.

Sussmann, R.A.C., C.B. Angeli, V.J. Peres, E.A. Kimura, and A.M. Katzin. 2011. Intraerythrocytic stages of Plasmodium falciparum biosynthesize vitamin E. *FEBS Letters*. 585:3985-3991. DOI: 10.1016/j.febslet.2011.11.005.

Szymańska, R., and J. Kruk. 2010. Plastoquinol is the main prenyllipid synthesized during acclimation to high light conditions in *Arabidopsis* and is converted to plastochromanol by tocopherol cyclase. *Plant and Cell Physiology*. 51:537-545. DOI: 10.1093/pcp/pcq017.

Tamayo Rojas, S.A., S. Schmidl, E. Boles, and M. Oreb. 2021. Glucose-induced internalization of the *S. cerevisiae* galactose permease Gal2 is dependent on phosphorylation and ubiquitination of its aminoterminal cytoplasmic tail. *FEMS Yeast Res*. 21. DOI: 10.1093/femsyr/foab019.

Thorsness, M., W. Schafer, L. D'Ari, and J. Rine. 1989. Positive and negative transcriptional control by heme of genes encoding 3-hydroxy-3-methylglutaryl coenzyme A reductase in *Saccharomyces cerevisiae*. *Molecular and Cellular Biology*. 9:5702-5712. DOI: 10.1128/mcb.9.12.5702-5712.1989.

Toke, D.A., W.L. Bennett, D.A. Dillon, W.-I. Wu, X. Chen, D.B. Ostrander, J. Oshiro, A. Cremesti, D.R. Voelker, A.S. Fischl, and G.M. Carman. 1998. Isolation and Characterization of the *Saccharomyces cerevisiae DPP1* Gene Encoding Diacylglycerol Pyrophosphate Phosphatase. *Journal of Biological Chemistry*. 273:3278-3284. DOI: 10.1074/jbc.273.6.3278.

Tokuhiro, K., M. Muramatsu, C. Ohto, T. Kawaguchi, S. Obata, N. Muramoto, M. Hirai, H. Takahashi, A. Kondo, E. Sakuradani, and S. Shimizu. 2009. Overproduction of geranylgeraniol by metabolically engineered *Saccharomyces cerevisiae*. *Applied and Environmental Microbiology*. 75:5536-5543. DOI: 10.1128/aem.00277-09.

Toyomasu, T., M. Tsukahara, A. Kaneko, R. Niida, W. Mitsuhashi, T. Dairi, N. Kato, and T. Sassa. 2007. Fusicoccins are biosynthesized by an unusual chimera diterpene synthase in fungi. *Proceedings of the National Academy of Sciences (PNAS)*. 104:3084-3088. DOI: 10.1073/pnas.0608426104.

Traber, M.G., and H. Sies. 1996. Vitamin E in Humans: Demand and Delivery. *Annual Review of Nutrition*. 16:321-347. DOI: 10.1146/annurev.nu.16.070196.001541.

Traber, M.G., and J.F. Stevens. 2011. Vitamins C and E: Beneficial effects from a mechanistic perspective. *Free radical biology & medicine*. 51:1000–1013. DOI: 10.1016/j.freeradbiomed.2011.05.017.

Tsay, Y.H., and G.W. Robinson. 1991. Cloning and characterization of *ERG8*, an essential gene of *Saccharomyces cerevisiae* that encodes phosphomevalonate kinase. *Molecular and Cellular Biology*. 11:620-631. DOI: 10.1128/mcb.11.2.620-631.1991.

Turk, E.M., V. Das, R.D. Seibert, and E.D. Andrulis. 2013. The Mitochondrial RNA Landscape of *Saccharomyces cerevisiae*. *PLoS ONE*. 8:e78105. DOI: 10.1371/journal.pone.0078105.

Valentin, H.E., K. Lincoln, F. Moshiri, P.K. Jensen, Q. Qi, T.V. Venkatesh, B. Karunanandaa, S.R. Baszis, S.R. Norris, B. Savidge, K.J. Gruys, and R.L. Last. 2006. The *Arabidopsis* vitamin E pathway *gene5-1* mutant reveals a critical role for phytol kinase in seed tocopherol biosynthesis. *Plant Cell*. 18:212-224. DOI: 10.1105/tpc.105.037077.

Valentin, H.E., and Q. Qi. 2005. Biotechnological production and application of vitamin E: current state and prospects. *Applied Microbiology and Biotechnology*. 68:436-444. DOI: 10.1007/s00253-005-0017-7.

van Hoek, P., E. de Hulster, J.P. van Dijken, and J.T. Pronk. 2000. Fermentative capacity in high-cell-density fed-batch cultures of baker's yeast. *Biotechnology and Bioengineering*. 68:517-523. DOI: 10.1002/(SICI)1097-0290(20000605)68:5<517::AID-BIT5>3.0.CO;2-O.

Vereinigung für Allgemeine und Angewandte Mikrobiologie. 2022. MICROBE OF THE YEAR 2022: Baker´s yeast *Saccharomyes cerevisiae*.

Verwaal, R., J. Wang, J.P. Meijnen, H. Visser, G. Sandmann, J.A. van den Berg, and A.J. van Ooyen. 2007. High-level production of beta-carotene in *Saccharomyces cerevisiae* by successive transformation with carotenogenic genes from *Xanthophyllomyces dendrorhous*. *Applied and Environmental Microbiology*. 73:4342-4350. DOI: 10.1128/AEM.02759-06.

Vidi, P.-A., M. Kanwischer, S. Baginsky, J.R. Austin, G. Csucs, P. Dörmann, F. Kessler, and C. Bréhélin. 2006. Tocopherol cyclase (VTE1) localization and vitamin E accumulation in chloroplast plastoglobule lipoprotein particles. *The Journal of biological chemistry*. 281:11225–11234. DOI: 10.1074/jbc.M511939200.

Voigt, C.A. 2020. Synthetic biology 2020-2030: six commercially-available products that are changing our world. *Nature Communications*. 11:6379. DOI: 10.1038/s41467-020-20122-2.

vom Dorp, K., G. Hölzl, C. Plohmann, M. Eisenhut, M. Abraham, A.P.M. Weber, A.D. Hanson, and P. Dörmann. 2015. Remobilization of Phytol from Chlorophyll Degradation Is Essential for Tocopherol Synthesis and Growth of *Arabidopsis*. *The Plant Cell*. 27:2846-2859. DOI: 10.1105/tpc.15.00395.

Walsh, G. 2005. Therapeutic insulins and their large-scale manufacture. *Applied Microbiology and Biotechnology*. 67:151-159. DOI: 10.1007/s00253-004-1809-x.

Wang, J., L. Zhu, Y. Li, S. Xu, W. Jiang, C. Liang, Y. Fang, A. Chu, L. Zhang, Z. Ding, and G. Shi. 2021. Enhancing Geranylgeraniol Production by Metabolic Engineering and Utilization of Isoprenol as a Substrate in *Saccharomyces cerevisiae*. *Journal of Agricultural and Food Chemistry*. 69:4480-4489. DOI: 10.1021/acs.jafc.1c00508.

Weber, C., A. Farwick, F. Benisch, D. Brat, H. Dietz, T. Subtil, and E. Boles. 2010. Trends and challenges in the microbial production of lignocellulosic bioalcohol fuels. *Applied Microbiology and Biotechnology*. 87:1303-1315. DOI: 10.1007/s00253-010-2707-z.

Wei, W., S.T. Yount, Z.D. Allen, K.F. Bechdol, W. Xia, H. Mo, and A.M. Mabb. 2022. The mevalonate suppressor δ-tocotrienol increases AMPA receptor-mediated neurotransmission. *Biochemical and Biophysical Research Communications*. 638:112-119. DOI: 10.1016/j.bbrc.2022.11.052.

Weinberger, M., A. Mesquita, T. Carroll, L. Marks, H. Yang, Z. Zhang, P. Ludovico, and W.C. Burhans. 2010. Growth signaling promotes chronological aging in budding yeast by inducing superoxide anions that inhibit quiescence. *Aging*. 2:709-726. DOI: 10.18632/aging.100215.

Wiedemann, B., and E. Boles. 2008. Codon-optimized bacterial genes improve L-Arabinose fermentation in recombinant *Saccharomyces cerevisiae*. *Applied and Environmental Microbiology* 74:2043-2050. DOI: 10.1128/aem.02395-07.

Wu, G., Q. Yan, J.A. Jones, Y.J. Tang, S.S. Fong, and M.A.G. Koffas. 2016. Metabolic Burden: Cornerstones in Synthetic Biology and Metabolic Engineering Applications. *Trends in Biotechnology*. 34:652-664. DOI: 10.1016/j.tibtech.2016.02.010.

Xiao, T., A. Khan, Y. Shen, L. Chen, and J.D. Rabinowitz. 2022. Glucose feeds the tricarboxylic acid cycle via excreted ethanol in fermenting yeast. *Nature Chemical Biology*. 18:1380-1387. DOI: 10.1038/s41589-022-01091-7.

Xie, W., M. Liu, X. Lv, W. Lu, J. Gu, and H. Yu. 2014. Construction of a controllable beta-carotene biosynthetic pathway by decentralized assembly strategy in *Saccharomyces cerevisiae*. *Biotechnology and Bioengineering*. 111:125-133. DOI: 10.1002/bit.25002.

Xie, W., X. Lv, L. Ye, P. Zhou, and H. Yu. 2015. Construction of lycopene-overproducing *Saccharomyces cerevisiae* by combining directed evolution and metabolic engineering. *Metabolic Engineering*. 30:69-78. DOI: 10.1016/j.ymben.2015.04.009.

Yan, C., N. Gao, X. Cao, L. Yao, Y.J. Zhou, and J. Gao. 2023. Auxotrophs compromise cell growth and fatty acid production in *Saccharomyces cerevisiae*. *Biotechnology Journal*:2200510. DOI: 10.1002/biot.202200510.

Yang, W., R.E. Cahoon, S.C. Hunter, C. Zhang, J. Han, T. Borgschulte, and E.B. Cahoon. 2011. Vitamin E biosynthesis: functional characterization of the monocot homogentisate

geranylgeranyl transferase. *The Plant Journal*. 65:206-217. DOI: 10.1111/j.1365-313X.2010.04417.x.

Zargaran, M., M. Fatahinia, and A. Zarei Mahmoudabadi. 2017. The efficacy of gaseous ozone against different forms of *Candida albicans*. *Current Medical Mycology*. 3:26-32. DOI: 10.18869/acadpub.cmm.3.2.26.

Zhang, J., A.T. Pierick, H.M. Van Rossum, R. Maleki Seifar, C. Ras, J.-M. Daran, J.J. Heijnen, and S. Aljoscha Wahl. 2015. Determination of the Cytosolic NADPH/NADP Ratio in *Saccharomyces cerevisiae* using Shikimate Dehydrogenase as Sensor Reaction. *Scientific Reports*. 5:12846. DOI: 10.1038/srep12846.

Zhang, Q., W. Zeng, S. Xu, and J. Zhou. 2021. Metabolism and strategies for enhanced supply of acetyl-CoA in *Saccharomyces cerevisiae*. *Bioresource Technology*. 342:125978. DOI: 10.1016/j.biortech.2021.125978.

Zhou, P., Z. Zhu, M. Hidayatullah Khan, P. Zheng, M. Teng, and L. Niu. 2018. Crystal structure of cytoplasmic acetoacetyl-CoA thiolase from *Saccharomyces cerevisiae*. *Acta Crystallographica Section F*. 74:6-13. DOI: 10.1107/s2053230x17016971.

7 Appendix

7.1 Abbreviations

° C	Degree Celsius
µg	Microgram
µl	Microliter
µM	Micromolar
CoA	Coenzyme A
A	Adenine
AAA	Aromatic Amino Acids
Acetyl-CoA	Acetyl coenzyme A
ADP	Adenosine diphosphate
ATP	Adenosine triphosphate
bp	Base pairs
C	Cytosine
CGQ	Cell Growth Quantifier
ClonNAT	Nourseothricin
co	Codon optimised
CO_2	Carbon dioxide
CoA	Coenzyme A
CTP	Chloroplast Transit Peptide
D	Glucose
DAHP	3-Deoxy-D-arabino-heptulosonate-7-phosphate
ddH_2O	Double-distilled water
DHQ	3-Dehydroquinate
DHS	3-Dehydroshikimate
DMAPP	Dimethylallyl diphosphate
DMGGBQ	2,3-Dimethyl-5-geranylgeranyl-1,4-benzoquinone
DMPBQ	2,3-Dimethyl-5-phytyl-1,4-benzoquinone
DMSO	Dimethyl sulfoxide
DNA	Deoxyribonucleic acid
dNTP	Deoxynucleotide triphosphate
DPE	downstream promoter element
DTT	1,4-Dithiothreitol
E4P	Erythrose-4-phosphate
EDTA	Ethylenediaminetetraacetic acid
EFSA	European Food Safety Authority
et al.	*et alii*
EPSP	5-Enolpyruvylshikimate-3-phosphate
FACS	Fluorescence-Activated Cell Sorting
fbr	Feedback-resistant
FDA	Food and Drug Administration
FPP	Farnesyl diphosphate
g	Gram
G	Guanine
G418	Geneticin sulphate
G6P	Glucose-6-phosphate
GC	Gas Chromatography
gDNA	Guide DNA
***Gene*Δ**	Deletion of indicated gene
Gene1* Δ*::Gene2	Replacement of indicated Gene1 by Gene2
GEOI	Genetic Element of Interest
GFP	Green Fluorescent Protein
GGOH	Geranylgeraniol
GGPP	Geranylgeranyl diphosphate
GMO	genetically modified organism
GPP	Geranyl diphosphate
gRNA	Guide RNA
h	Hours
HIS	histidine
HPPD	Hydroxyphenylpyruvate dioxygenase
HCl	Hydrogen chloride
HGA	Homogentisic acid
HGGT	Homogentisate geranylgeranyl transferase
HMG-CoA	3-hydroxy-3-methylglutaryl-Coenzyme A
HMGCR	3-hydroxy-3-methylglutaryl-Coenzyme A reductase
HPLC	High Performance Liquid Chromatography
HPP	4-Hydroxyphenylpyruvate
HPT	Homogentisate phytyltransferase
IPP	Isopentenyl diphosphate
K_2SO_4	Potassium sulphate
kb	Kilobases

KCl	Potassium chloride
KH_2PO_4	Potassium dihydrogen-phosphate
KOH	Potassium hydroxide
L	Litre
LB	Lysogeny broth
Leu	Leucine
LiAc	Lithium acetate
M	Molar concentration
Mevalonate-P	Mevalonate-5-phosohat
Mevalonate-PP	Mevalonate diphosphate
mg	Milligram
MGGBQ	2-Methyl-6-geranylgeranyl-1,4-benzoquinol
$MgSO_4$	Magnesium sulphate
min	Minutes
ml	Millilitre
mM	Millimolar concentration
n	Sample size
MPBQ	2-Methyl-6-phytyl-1,4-benzoquinol
NAD^+	Nicotinamide adenine dinucleotide (oxidized)
NADH	Nicotinamide adenine dinucleotide (reduced)
$NADP^+$	Nicotinamide adenine dinucleotide phosphate (oxidized)
NADPH	Nicotinamide adenine dinucleotide phosphate (reduced)
Na_2SO_4	Sodium sulphate
NaCl	Sodium chloride
NAD	Nicotinamide adenine dinucleotide
NADP	Nicotinamide adenine dinucleotide phosphate
NaOH	Sodium hydroxide
nd	Not detectable
ng	Nanogram
nm	Nanometre
O_2	Dioxygen
OD_{600}	Optical density at 600 nm
PC-8	plastochromanol-8
PCR	Polymerase Chain Reaction
PDH	Pyruvate dehydrogenase
PDP	Phytyl diphosphate
PEG	Polyethylene glycol
PEP	Phosphoenolpyruvate
PMP	Phytyl monophosphate
PTM	Post-translational modification
QPS	Qualified Presumption of Safety
RNA	Ribonucleic acid
rpm	Revolutions per minute
ROS	Reactive oxygen species
RT	Room temperature
S.O.C.	Super optimal broth with catabolite repression
SAM	S-adenosylmethionine
SC	Synthetic complete
SCM	Synthetic complete medium after Bruder et al. (2016)
SHP	Shikimate-5-phosphate
sp.	species
T	Thymine
TAE	Tris-acetate-EDTA
TC	Tocopherol cyclase
tr	Truncated (gene or protein)
TRIS	Tris(hydroxymethyl)-aminomethane
U	Enzyme unit
UAS	Upstream activation sequences
URA	Uracil
URS	Upstream repression sequences
V	Volt
v/v	Volume per volume
w/v	Weight per volume
wt	Wild-type
YFP	Yellow Fluorescent Protein
YP	Yeast extract Peptone

7.2 Synthetic Oligomers

Table 21 Synthetic oligomers

Name	Sequence	Description - Source
CHAP029	GGTGCTGGTTCTAAAGGCGAG	Assembly of the backbone of the GFP vector FGD97 forward - Laboratory Stock, Prof. Dr. Boles
GDP153	GAGTATGGATGGGGGTAATAGAATTG	Assembly of the backbone of the GFP vector FGD97 reverse - Laboratory Stock, Prof. Dr. Boles
MOP289	CAAGAACAAACAAGCTCAAC	Sequencing of genes under the control of *pHXT7* - Laboratory Stock, Prof. Dr. Boles
MOP290	ACCTAGACTTCAGGTTGTC	Sequencing of genes under the control of *tCYC1* - Laboratory Stock, Prof. Dr. Boles
RPP141	GAGCTTCCAGGGGGAAACG	Sequencing of the guide DNA in CRISPR/Cas9 plasmids - Laboratory Stock, Prof. Dr. Boles
SiH001	TCCTGGCCTTTTGCTGG	Sequencing of the Golden Gate storage and expression plasmids - Laboratory Stock, Prof. Dr. Boles
SiH002	GGACTCCTGTTGATAGATC	Sequencing of the Golden Gate storage and expression plasmids - Laboratory Stock, Prof. Dr. Boles
SiHP175	GAAAGAATTTAAGGGCATAAATACCTTTCA	Verification of integrations into the *LEU2*, upstream forward - Laboratory Stock, Prof. Dr. Boles
SiHP176	TACAATCCTTGCCCGTGATG	Verification of integrations into the *LEU2* upstream reverse - Laboratory Stock, Prof. Dr. Boles
SiHP177	ACTCGTATCGCATGTCGGTG	Verification of integrations into the *LEU2* downstream forward - Laboratory Stock, Prof. Dr. Boles
SiHP178	CTTCCCTAGAACCTTCTTATGTTTTACATG	Verification of integrations into the *LEU2* downstream reverse - Laboratory Stock, Prof. Dr. Boles
SiHP179	ATTCACATCATTTTCGTGGATCC	Verification of integrations upstream of the *HO* locus, upstream forward - Laboratory Stock, Prof. Dr. Boles
SiHP180	ACAGCGATGGAACTTACGGC	Verification of integrations upstream of the *HO* locus, upstream reverse - Laboratory Stock, Prof. Dr. Boles
SiHP181	TATCGTGTTGCATCTGCGGC	Verification of integrations upstream of the *HO* locus, downstream forward - Laboratory Stock, Prof. Dr. Boles
SiHP182	TGCCTTTGGACTTAAAATGGCGT	Verification of integrations upstream of the *HO* locus, downstream reverse - Laboratory Stock, Prof. Dr. Boles
WGP234	CTCCATTGTCTGCTTCTATGATTAAGAGATACGACGAACACCACCAAG	Amplification with overhangs for gDNA of CRISPR/Cas9 plasmids primer 1 forward - Laboratory Stock, Prof. Dr. Boles
WGP235	GAGCCTTGGTAATTTCGGTGTTAACTCTCAAAATGTCAGACAACA	Amplification with overhangs for gDNA of CRISPR/Cas9 plasmids primer 1 reverse - Laboratory Stock, Prof. Dr. Boles
WGP243	TCTTCTTGAAGTAGTCTTCC	Amplification with overhangs for gDNA of CRISPR/Cas9 plasmids primer 2 forward - Laboratory Stock, Prof. Dr. Boles
WGP245	GGCTATTGTTGACTTGTTG	Amplification with overhangs for gDNA of CRISPR/Cas9 plasmids primer 2 reverse - Laboratory Stock, Prof. Dr. Boles
JBP011	GGCTATTGTTGACTTGTTGTTC	Amplification of CRISPR/Cas9 plasmids PCR 1 reverse

JBP012	GTAGTCTTCCTTCAATTGCTTAAC	Amplification of CRISPR/Cas9 plasmids PCR 2 reverse
JBP013	CGTCTCGTCGGTCTCATATGGAGGC CAAGATAGATG	Amplification of genomic *BTS1* forward Golden Gate Cloning forward
JBP014	CGTCTCAGGTCGGTCTCAGGATTCA CAATTCGGATAAGTGG	Amplification of genomic *BTS1* forward Golden Gate Cloning reverse
JBP015	CGTCTCGTCGGTCTCATATGGACCA ATTGGTGAAAACTGAAG	Amplification of the truncated *HMG1* for Golden Gate Cloning forward
JBP016	CGTCTCAGGTCGGTCTCAGGATTTA GGATTTAATGCAGGTGACG	Amplification of the truncated *HMG1* for Golden Gate Cloning reverse
JBP017	TATAAATGGAAAGTTAGGACGTTTT AGAGCTAGAAATAGCAAGTTAAAA TAAGG	JBV27 gDNA CRISPR/Cas9 for the *pERG9* promoter exchange PCR 1 forward
JBP018	GTCCTAACTTTCCATTTATAGATCAT TTATCTTTCACTGCGGAG	JBV27 gDNA CRISPR/Cas9 for the *pERG9* promoter exchange PCR 2 forward
JBP019	GGACGTCAAACGGGTCTGCTGTTTT AGAGCTAGAAATAGCAAGTTAAAA TAAGG	JBV28 gDNA forward CRISPR/Cas9 for the truncated *HMG1* PCR 1 forward
JBP020	CAGCAGACCCGTTTGACGTCCGATC ATTTATCTTTCACTGCGGAG	JBV28 gDNA forward CRISPR/Cas9 for the truncated *HMG1* PCR 2 forward
JBP021	ACATGCTTTAAGTCCGAGAAACTAA GCTACAAAACGGAATCAGTTCGAGT TTATCATTATCAATAC	Amplification of the *pTDH3* with overhangs for the native *pHMG1* as donor DNA forward
JBP022	TAAAAGACTTCTTGGTGACTTCAGT TTTCACCAATTGGTCCATTTTGTTTG TTTATGTGTGTTTATTC	Amplification of the *pTDH3* with overhangs for the native *pHMG1* as Donor DNA reverse
JBP023	ATGGACCAATTGGTGAAAACTGAAG	Amplification of the truncated *HMG1* with artificial ATG and overhangs for the *pTDH3* as donor DNA forward
JBP024	TTAGGATTTAATGCAGGTGACG	Amplification of the truncated *HMG1* with artificial ATG and overhangs for the *pTDH3* as donor DNA reverse
JBP025	AGGCTAGACACAGCTCTTCAG	Sequencing of JBY3 truncated *HMG1* and promoter exchange
JBP026	CACATGGTGCTGTTGTGCTTC	Sequencing of JBY3 truncated *HMG1* and promoter exchange
JBP027	TTTCCACTGCACTTTGCATCGGAAG GCGTTATCGGTTTTGTGTCGAATACT ACTATGACCG	Amplification of the genomic *ERG1* promoter with overhangs for integration into the *ERG9* gene forward
JBP028	TCTCGACCGGATGCAATGCCAATTG TAATAGCTTTCCCATAGCTTATGAC CCTTTTCTC	Amplification of the genomic *ERG1* promoter with overhangs for integration into the *ERG9* gene reverse
JBP029	AACTCCGCAGGAACTACAAACC	Sequencing of JBY4 promoter exchange of *pERG9* to *pERG1*
JBP030	CAGCTTCAAAGCTGCCTTCATC	Sequencing of JBY4 promoter exchange of *pERG9* to *pERG1*
JBP031	AGTACAGTGCCCTGAGCGTAGTTTT AGAGCTAGAAATAGCAAGTTAAAA TAAGG	JBV70 gDNA for CRISPR Ca9 upstream of the *HO* locus PCR 1 forward
JBP032	TACGCTCAGGGCACTGTACTGATCA TTTATCTTTCACTGCGGAG	JBV70 gDNA for CRISPR Ca9 upstream of the *HO* locus PCR 2 forward
JBP037	AAGGGACTGCGTTGTTAGCC	Sequencing of the *Aro7* locus forward
JBP038	AAGAGCTGCTCCCGCCAATG	Sequencing of the *Aro7* locus reverse
JBP039	GGCCCAAATCAGTTTCTCAC	Sequencing upstream of *HO* locus for verification of the deletion of the *HO* region
JBP040	AAGCAAGTTGCGGAGCTAAG	Sequencing upstream of *HO* locus for verification of the deletion of the *HO* region
JBP041	CGTCTCGTCGGTCTCATATGGTTGCT GAATTGACCGC	Amplification of the *TyrAfbr* gene with GG overhangs forward

JBP042	CGTCTCAGGTCGGTCTCAGGATTTATTGTCTGTTGTCGTTAGCTTG	Amplification of the *TyrAfbr* gene with GG overhangs reverse
JBP043	CGACAACGTGGCAATTCGTCG	Sequencing of Golden Gate expression plasmids, binds in *ConS*
JBP044	CGTCTCGTCGGTCTCATATGTCTCCATCTGTTGAAGTTAC	Amplification of *YlHPPD* with Golden Gate overhangs forward
JBP045	CGTCTCAGGTCGGTCTCAGGATTTACAAGTTACCTCTCTTAGCTTGTTC	Amplification of *YlHPPD* with Golden Gate overhangs reverse
JBP046	TTTTTTTTTTAAATTGATGTATCTCATCGCAGGCACGGGCAAAACGAAGATTAAGATAAAGTTG	Amplification of the donor DNA for *AP8-BTS1-tENO1* Integration in front of the *HO* locus forward
JBP047	CAGGATCATTATTGATCAGCTCATCTATCTTGGCCTCCATCATTTTTTGATTAAAATTAAAAAAAC	Amplification of the donor DNA for *AP8-BTS1-tENO1* Integration in front of the *HO* locus reverse
JBP048	CACAAAAACAAAAAGTTTTTTTAATTTTAATCAAAAAATGATGGAGGCCAAGATAGATGAG	Amplification of the donor DNA for *AP8-BTS1-tENO1* part 2 Integration in front of the *HO* locus forward
JBP049	CTGGAATTATGTTAAAAGTTACATCCTTTTTTTCATTTTTATACATGGGTGACCAAAAG	Amplification of the donor DNA for *AP8-BTS1-tENO1* part 2 Integration in front of the *HO* locus reverse
JBP050	ATACTTCTTCACACAAAAGAACGCAGTTAGACAATCAACATTGATAGGTCAAGATCAATGTAAAC	Amplification of the donor DNA *ROX1-pTef2-Erg20-tENO2* forward
JBP051	ATAATATAATATAACGGAAAGAAGAAATGGAAAAAAAAAAAATTTTTCAAACTGCAAATTCAAG	Amplification of the donor DNA *ROX1-pTef2-Erg20-tENO2* reverse
JBP052	CGTCTCGTCGGTCTCATATGGCTTCAGAAAAAGAAATTAG	Amplification of genomic *ERG20* with overhangs for Golden Gate forward
JBP053	CGTCTCAGGTCGGTCTCAGGATCTATTTGCTTCTCTTGTAAAC	Amplification of genomic *ERG20* with overhangs for Golden Gate reverse
JBP054	GATCTGAGGGGTCGAGTTAGCCCT	Oligo was annealed with JBP055 as donor DNA for *ROX1* (Golden Gate Cloning CRISPR/Cas9 Plasmid Construction)
JBP055	AAACAGGGCTAACTCGACCCCTCA	Oligo was annealed with JBP054 as donor DNA for *ROX1* (Golden Gate Cloning CRISPR/Cas9 Plasmid Construction)
JBP056	GATCGGGACTCATGTGTCAGCACC	Oligo was annealed with JBP057 and as donor DNA for *YJL064W* (Golden Gate Cloning CRISPR/Cas9 Plasmid Construction)
JBP057	AAACGGTGCTGACACATGAGTCCC	Oligo was annealed with JBP056 and as donor DNA for *YJL064W* (Golden Gate Cloning CRISPR/Cas9 Plasmid Construction)
JBP058	TGATCGGGACTCATGTGTCAGCACCGTT	Oligo was annealed with JBP059 as donor DNA for *ROX1* (Golden Gate Cloning Double Cutter CRISPR/Cas9 Plasmid Construction)
JBP059	CTAAAACGGTGCTGACACATGAGTCCCG	Oligo was annealed with JBP058 as donor DNA for *ROX1* (Golden Gate Cloning Double Cutter CRISPR/Cas9 Plasmid Construction)
JBP071	AACAAGAGAGAATAGCGTCAGGATAGCTCGCTCGATGTGAATACATGGGTGACCAAAAG	Amplification of the donor DNA *AP8-BTS1-tENO1* forward the *YJL064W* locus reverse
JBP077	ACATAGGCGGAGTAAACTTCATTAGGGGGCAAAACGAAGATTAAGATAAAGTTG	Amplification of the donor DNA *AP8-BTS1-tENO1* forward the *YJL064W* locus forward
JBP078	GTCGTCGTCTTCGTCATTATC	Verification of integrations into the *YJL064W* locus forward
JBP079	GAAAGAACAGCGCTAACAATG	Verification of integrations into the *YJL064W* locus reverse
JBP080	TGTCTTAACTCTCCCTCTTC	Verification of integrations into the *ROX1* locus forward

JBP081	CCATCCTCGTCGCTTTATTATC	Verification of integrations into the *ROX1* locus reverse
JBP084	CAGATACATAGATACAATTCTATTACCCCCATCCATACTCATGTCTCCATCTGTTGAAG	Amplification of the *HPPD* with overhangs for the GFP vector forward
JBP085	GTAAACAATTCCTCGCCTTTAGAACCAGCACCAGCGGCCGCCAAGTTACCTCTCTTAGC	Amplification of the *HPPD* with overhangs for the GFP vector reverse
JBP086	CAGATACATAGATACAATTCTATTACCCCCATCCATACTCATGGAGGCCAAGATAGATG	Amplification of the *BTS1* with overhangs for the GFP vector forward
JBP087	TAAACAATTCCTCGCCTTTAGAACCAGCACCAGCGGCCGCCAATTCGGATAAGTGG	Amplification of the *BTS1* with overhangs for the GFP vector reverse
JBP088	CAGATACATAGATACAATTCTATTACCCCCATCCATACTCATGGCTACCATTCAAGCTTTC	Amplification of the *HPT* with overhangs for the GFP vector forward
JBP089	TAAACAATTCCTCGCCTTTAGAACCAGCACCAGCGGCCGCGAAAATGGTGTTAGAGAAGTTTG	Amplification of the *HPT* with overhangs for the GFP vector reverse
JBP090	CAGATACATAGATACAATTCTATTACCCCCATCCATACTCATGGAAATTAGATCTTTGATTGTTTC	Amplification of the *VTE1* with overhangs for the GFP vector forward
JBP091	TAAACAATTCCTCGCCTTTAGAACCAGCACCAGCGGCCGCCAAACCTGGTGGCTTG	Amplification of the *VTE1* with overhangs for the GFP vector reverse
JBP093	CATTATCCTCATCAAGATTGC	Sequencing of *VTE1* expression plasmids
JBP094	GATCTATCGATTTCAATTCAATTC	Sequencing of *HPT* reverse
JBP095	ATTGTTACTCCAATCCCCAAGTAG	Sequencing of the *HPT* forward
JBP096	CGTCTCGTCGGTCTCATATGGCTTCTATTTCTACCCCAAACTCTG	Amplification of the 47AA truncated *VTE1* forward
JBP097	CGTCTCAGGTCGGTCTCAG	Amplification of the 47AA truncated *VTE1* reverse
JBP098	CGTCTCGTCGGTCTCATATGGATTACGCGAACATCCT	Amplification of the *crtE* with GG overhangs forward
JBP099	CTAGCCGATATCCCTCTGTGAATCCTGAGACCGACCTGAGACG	Amplification of the *crtE* with GG overhangs reverse
JBP100	ATGGATTACGCGAACATCCTC	Sequencing of *crtE*
JBP101	TTTACCCAACTTTATCTTAATCTTCGTTTTGGCGCCATCACGTGCTATAAAAATAATTATAATT	Amplification of the backbone of V168 forward
JBP102	TAGTTCCTCACTCTTTCCTTACTCACCGTTGTATTGCGACGAATTGC	Amplification of the backbone of V168 reverse
JBP103	CAATTCGTCGCAATACAAC	Amplification of *crtE* for V168 assembly forward
JBP104	GCCATCCGATAAATGTAGGAGCAATGAAGCATACATGGGTGACCAAAAG	Amplification of *crtE* for V168 assembly reverse
JBP105	ATCCGCCCGCTCTTTTGGTCACCCATGTATGCTTCATTGCTCCTACATTTATCGGATGGC	Amplification of the truncated *HMG1* for V168 assembly forward
JBP106	GCCATCCCGGAGGGACAAAAAATAAAAAAACCGCGGCAGTTCGAGTTTATCATTATCAATAC	Amplification of the truncated *HMG1* for V168 assembly reverse
JBP107	GGCAGTATTGATAATGATAAACTCGAACTGCCGCGGTTTTTTTATTTTTTGTCCCTCC	Amplification of the promoter sequence for V168 assembly forward
JBP108	AGCTGGGGTAACTTCAACAGATGGAGACATCATTTTTTGATTAAAATTAAAAAAACT	Amplification of the promoter sequence for V168 assembly forward

JBP109	AAAAGTTTTTTTAATTTTAATCAAA AAATGATGTCTCCATCTGTTGAAGT TAC	Amplification of the *HPPD* for V168 assembly forward
JBP110	AATCGTATGTGAATGCTGGTCGCTA TACTGGGATCCGGGCGAATTGGGTA CC	Amplification of the *HPPD* for V168 assembly reverse
JBP111	TTTAATTTGCGGCCGGTACCCAATT CGCCCGGATCCCAGTATAGCGACCA GC	Amplification of the *KanR* for V168 assembly forward
JBP112	TAAATTATAATTATTTTTATAGCACG TGATGGCGCCAAAACGAAGATTAA GATAAAGTTGG	Amplification of the *KanR* for V168 assembly reverse
JBP113	ACATCTGAATCGTCCATCAAGTTTT AGAGCTAGAAATAGCAAGTTAAAA TAAGG	Amplification of CRISPR/Cas9 plasmids with overhangs for *DPP1* gDNA PCR 1 forward
JBP115	CTTGATGGACGATTCAGATGTGATC ATTTATCTTTCACTGCGGAG	Amplification of CRISPR/Cas9 plasmids with overhangs for *DPP1* gDNA PCR 2 forward
JBP117	AAGGCAAAGAATCAGAATTAAATC ATAGCAAACGACCAAAGAATAAAA AAGAATATATACTCCACATGACATA CGAAATA	Donor DNA for the *DPP1* locus
JBP118	ATGTTATCGGCGTTGATTC	Sequencing of the *DPP1* locus forward
JBP119	CTCAACTGCTTCCTAAGAAAC	Sequencing of the *DPP1* locus reverse
JBP120	ACTCTAACACCCTTCTTAACAG	Sequencing of *HPPD*
JBP121	CTCCTTCTAGTGCTATTTCTG	Sequencing of genes under the control of the *pTEF2*
JBP122	TTGACCTTCCCAACCAGACATGAC	Sequencing of the *crtYB* gene
JBP123	AAGGCAAAGAATCAGAATTAAATC ATAGCAAACGACCAAACCTTGCCAA CAGGGAGTTC	Donor DNA for the integration of *γ-TMT* and *MPBQMT* into the *DPP1* locus forward
JBP124	ATATTTCGTATGTCATGTGGAGTAT ATATTCTTTTTTATTCATTTTTCAAA CTGCAAATTCAAG	Donor DNA forward the integration of *γ-TMT* and *MPBQMT* into the *DPP1* locus reverse
JBP125	TAGGATGAGGCGGTGAAAGAG	Sequencing of genes under the control of *pHHF2*
JBP128	TCCCAAAGGGTTTGGGTTCTC	Sequencing of *MPBQMT*
JBP129	CCGACACCGTCTTTAGAGTAGATCA TTTATCTTTCACTGCGGAG	Amplification of CRISPR/Cas9 plasmids with overhangs for *ClonNAT* gDNA PCR 1 forward
JBP130	TACTCTAAAGACGGTGTCGGGTTTT AGAGCTAGAAATAGCAAGTTAAAA TAAGG	Amplification of CRISPR/Cas9 plasmids with overhangs for *ClonNAT* gDNA PCR 2 forward
JBP131	AGTTACAGAGATGTTACGAACCACT AGTGCACTGCAGTACAGTTTCCTTG CCAACAGGGAG	Amplification of the *MPBQMT* donor DNA for integration in the *ClonNAT* locus forward
JBP132	CCATTTTGTAATTTCGTGTCGCACCG ACATGCGATACGAGTACTCATTTTT CAAACTGCAAATTCAAG	Sequencing primer for V186
JBP133	CACCACTGACGAGCAGATTTC	Sequencing primer, annealing in *ConE* region
JBP134	CCATTTTGTAATTTCGTGTCGCACCG ACATGCGATACGAGTACTCATACAT GGGTGACCAAAAGAG	Amplification of the *MPBQMT* donor DNA for integration in the *ClonNAT* locus reverse
JBP135	TGTGGTGACGCGTGTATCCGCCCGC TCTTTTGGTCACCCATGTATCTTTCA TAGAATATACTATGATCCG	Amplification of *AP6* template forward
JBP136	TTTTGTTAATTTGTTGTTTTGATG	Amplification of *AP6* template reverse
JBP137	ATTTAATCAATCACACACAAACATC AAAACAACAAATTAACAAAAATGA AGGCTACTTTGGCTGC	Amplification of the *γ-TMT* forward

JBP138	TGAAAAAATAAGCAGAAAAGACTA ATAATTCTTAGTTAAAAGCACTTTA CAATGGCTTTTGACAAGTAATG	Amplification of the *γ-TMT* reverse
JBP139	ACCGACATGCGATACGAG	Sequencing of the *MPBQMT* Integration 1
JBP140	CGGTCATCAATTTCTCAAGTTTCAG	Sequencing of the *MPBQMT* Integration 2
JBP142	TGTTAAAGGCAAAGAATCAGAATTA AATCATAGCAAACGACCAAAAAAA CGAAGATTAAGATAAAGTTGG	Amplification of the donor DNA of *HPT* and *trVTE1* into the *DPP1* locus forward
JBP143	ACGTATATTTCGTATGTCATGTGGA GTATATATTCTTTTTTATTCCGTTCA GGGTAATATATTTTAACC	Amplification of the donor DNA of *HPT* and *trVTE1* into the *DPP1* locus reverse
JBP144	GTTATCGTGTTGCATCTGCGGCTTTA AATTGATGTATCTCATCGCAAAACG AAGATTAAGATAAAGTTGG	Amplification of the donor DNA of *HPT* and *trVTE1* into *ChrIV* (*ChrIV53688-53756Δ*) upstream of *HO* locus forward
JBP145	TACCCAATCGCTGCGTGCTGGAATT ATGTTAAAAGTTACATCCTTCGTTC AGGGTAATATATTTTAACC	Amplification of the donor DNA of *HPT* and *trVTE1* into *ChrIV* (*ChrIV53688-53756Δ*) upstream of *HO* locus reverse
JBP146	CGTCTCGTCGGTCTCATATGTCCTCT TCCGTTTCTTCCTC	Amplification of the truncated *MPBQMT* gene with overhangs for Golden Gate forward
JBP147	CGTCTCAGGTCGGTCTCAG	Amplification of the truncated *MPBQMT* gene with overhangs for Golden Gate reverse
JBP148	CTGTAACTTATTGGCAACTG	Sequencing primer annealing in *AP8*
JBP149	ATATTATCATCACGGGCAAGG	Sequencing of the *trMPBQMT*
JBP150	CGCTCCTCTTTTAATGCCTTTATG	Sequencing primer 1 for JBY20 and JBY67
JBP151	GATCTATCGATTTCAATTC	Sequencing primer 2 for JBY20 and JBY67
JBP152	CAGAGATGTTACGAACCACTAGTGC ACTGCAGTACAGTTTGAGTACTCGT ATCGCATGTCGGTGCGACACGAAAT TACAA	Donor DNA for the *ClonNAT* Deletion in JBY67

7.3 Codon Optimized Sequences of Heterologous Genes

Arabidopsis thaliana γ-TMT^{tr}

atgaccaccaccagaggtaacgttgctgttgctgctgctacctctaccgaagctttgagaaagggtattgctgaattctacaacgaaacctctggtt
tgtgggaagaaatttggggtgaccacatgcaccacggtttctacgacccagactcttctgttcaattgtctgactctggtcacaaggaagctcaaatta
gaatgattgaagaatctttgagattcgctggtgttaccgacgaagaagaagaaaagaagattaagaaggttgttgacgttggttgtggtattggtggttc
ttctagatacttggcttctaagttcggtgctgaatgtattggtattaccttgtctccagttcaagctaagagagctaacgacttggctgctgctcaatctttg
gctcacaaggcttctttccaagttgctgacgctttggaccaaccattcgaagacggtaagttcgacttggtttggtctatggaatctggtgaacacatgc
cagacaaggctaagttcgttaaggaattggttagagttgctgctccaggtggtagaattattattgttacctggtgtcacagaaacttgtctgctggtgaa
gaagctttgcaaccatgggaacaaaacattttggacaagatttgtaagaccttctacttgccagcttggtgttctaccgacgactacgttaacttgttgca
atctcactctttgcaagacattaagtgtgctgactggtctgaaaacgttgctccattctggccagctgttattagaaccgctttgacctggaagggtttggt
ttctttgttgagatctggtatgaagtctattaagggtgctttgaccatgccattgatgattgaaggttacaagaagggtgttattaagttcggtattattacct
gtcaaaagccattgtaa

Arabidopsis thaliana MPBQMT^{tr}

atgtcctcttccgtttcttcctctagaccatctgctcaaccaagattcattcaacacaagaaagaagcttactggttctacagattcttgtctattgtttacga
ccacgttattaacccaggtcactggactgaagacatgagagatgacgctttggaaccagctgacttgtctcacccagacatgagagttgtcgacgttg
gtggtggtactggtttcactaccttgggtattgttaagactgttaaggctaagaacgttactattttggaccaatctccacaccaattggctaaggctaag
caaaaggaaccattgaaggaatgtaagattgttgaaggtgacgctgaagatttgccattcccaactgactacgctgatagatacgtttctgctggttcta
ttgaatactggccagacccacaaagaggtattagagaagcttacagagttttgaagattggtggtaaggcttgtttgattggtccagtttacccaactttc
tggttgtctagattcttttctgacgtttggatgttgttcccaaaggaagaagaatacattgaatggttcaagaacgctggtttcaaggacgttcaattgaag
agaattggtccaaagtggtacagaggtgttagacgtcacggtttgattatgggttgttctgttactggtgttaagccagcttctggtgactctccattgca
attgggtccaaaggaagaagacgttgaaaagccagttaacaacccattctctttcttgggtagattcttgttaggtactttggctgccgcttggttcgtttt
gattccaatctacatgtggattaaggaccaaatcgttccaaaggaccaaccaatttaa

Arabidopsis thaliana VTE1

atggcttctatttctaccccaaactctgaaaccgataagatttctgttaagccagtttacgttccaacctctccaaacagagaattgagaaccccacactc
tggttaccacttcgatggtaccccaagaaagttcttcgaaggttggtacttcagagtttctattccagaaaagagagaatctttctgtttcatgtactctgtt
gaaaaccccagctttcagacaatctttgtctccattggaagttgctttgtacggtccaagattcaccggtgttggtgctcaaattttgggtgctaacgataa
gtacttgtgtcaatacgaacaagattctcacaacttctggggtgatagacacgaattggttttgggtaacaccttctctgctgttccaggtgctaaggctc
caaacaaggaagttccaccagaagaattcaacagaagagtttctgaaggtttccaagctaccccattctggcaccaaggtcacatttgtgatgatggt
agaaccgattacgctgaaaccgttaagtctgctagatgggaatactctaccagaccagtttacggttggggtgatgttggtgctaagcaaaagtctac
cgctggttggccagctgctttcccagttttcgaaccacactggcaaatttgtatggctggtggtttgtctaccggttggattgaatggggtggtgaaaga
ttcgaattcagagatgctccatcttactctgaaaagaactggggtggtggtttcccaagaaagtggttctgggttcaatgtaacgttttcgaaggtgctac
cggtgaagttgctttgaccgctggtggtggtttgagacaattgccaggtttgaccgaaacctacgaaaacgctgctttggtttgtgttcactacgatggt
aagatgtacgaattcgttccatggaacggtgttgttagatgggaaatgtctccatggggttactggtacattaccgctgaaaacgaaaaccacgttgtt
gaattggaagctagaaccaacgaagctggtacccccattgagagctccaaccaccgaagttggtttggctaccgcttgtagagattcttgttacggtga
attgaagttgcaaatttgggaaagattgtacgatggttctaagggtaaggttattttggaaaccaagtcttctatggctgctgttgaaattggtggtggtcc
atggttcggtacctggaagggtgatacctctaacaccccagaattgttgaagcaagctttgcaagttccattggatttggaatctgctttgggtttggttc
cattcttcaagccaccaggtttgtaa

Nostoc sp. TCL240-02 HPT

atgtctcaatcttctcaaaactctccattgccaagaaagccagttcaatcttacttccactggttgtacgctttctggaagttctctagaccacacaccatta
ttggtacctctttgtctgttttgtctttgtacttgattgctattgctacctctaacaacaccgcttctttgttcaccaccccaggttctttgtctccagctttcggt
gcttggattgcttgtttgtgtggtaacgtttacattgttggtttgaaccaattggaagacgttgacattgacaagattaacaagccacacttgccattggctt
ctggtgaattctctcaacaaaccggtcaattgattgttgcttctaccggtattttggctttggttgttgcttggttgaccggtccattcttgttcggtatggttg
ctatttctttggctattggtaccgcttactctttgccaccaattagattgaagcaattcccattctgggctgctttgtgtattttctctgttagaggtaccattgtt
aacttgggtttgtacttgcactactcttgggctttgaagcaatctcaaaccattccaccagttgtttgggttttgaccttgttcattttggttttcaccttggcta
ttgctattttcaaggacattccagacattgaaggtgacagattgtacaacattaccaccttcaccattaagttgggtccacaagctgttttcaacttggcttt
gtgggttattaccgtttgttacttgggtattattttggttggtgttttgcacgttgcttctattaacccaattttcttggttattgctcacttgggtttgttggcttgg
atgtggtggagatctttggctgttgacttgcaagacaagtctgctattgctcaattctaccaattcatttggaagttgttcttcattgaatacttgattttccca
attgcttgtttcttggcttaa

Phomopsis amygdali GGPPS

atgttgtctactggtttgtctttgtctccagttcattctaatgaaggtaaggacttgcaaagagttgataccgatcatatcttcttcgaaaaggctgttttgga
agctccatacgattacattgcttctatgccatctaagggtgtcagagatcaattcattgatgctttgaacgattggttgagagttccagatgttaaggttgg
taagattaaggatgctgttagagtcttgcacaactccagtttgttgttggatgatttccaagacaactccccattgagaagaggtaaaccatctacccata
acattttcggttctgctcaaactgttaacactgctacctactccattattaaggccattggtcaaatcatggaattctctgctggtgaatctgttcaagaagt
catgaactccatcatgatcttgtttcaaggtcaagccatggatttgttctggacttataatggtcatgttccatccgaagaagaatattacagaatgatcga
ccaaaagaccggtcaattattctctattgctacctccttgttgttgaacgctgctgataacgaaattccaagaactaagatccaatcctgcttgcatagatt
gaccagattattaggtagatgcttccaaatcagagatgactaccaaaacttggtttctgctgattacactaagcaaaagggtttctgcgaagatttggac
gaaggtaaatggtctttggctttgattcatatgatccacaagcaaagatcccatatggccttgttgaatgttttgtccactggtagaaaacatggtggtatg
actttggaacaaaagcaattcgttttggacatcattgaagaagaaaagtccttggactacaccagatctgttatgatggacttgcatgttcaattgagag
ccgaaattggtagaatcgaaatcttgttggattctccaaatccagccatgagattgttgttagaattattgagagttcatcatcaccatcaccactaa

Sulfolobus acidocaldarius GGPPS

atgtcttacttcgacaactacttcaacgaaattgttaactctgttaacgacattattaagtcttacatttctggtgacgttccaaagttgtacgaagcttcttac
cacttgttcacctctggtggtaagagattgaggccattgattttgaccatttcttctgacttgttcggtggtcaaagagaaagagcttactacgctggtgct
gctattgaagttttgcacaccttcaccttggttcacgacgacattatggaccaagacaacattagaagaggtttgccaaccgttcacgttaagtacggttt
gccattggctattttggctggtgacttgttgcacgctaaggctttccaattgttgacccaagctttgagaggtttgccatctgaaaccattattaaggctttc
gacattttcaccagatctattattattatttctgaaggtcaagctgttgacatggaattcgaagacagaattgacattaaggaacaagaatacttggacat
gatttctagaaagaccgctgctttgttctctgcttcttcttctattggtgctttgattgctggtgctaacgacaacgacgttagattgatgtctgacttcggta
ccaacttgggtattgctttccaaattgttgacgacattttgggtttgaccgctgacgaaaaggaattgggtaagccagttttctctgacattagagaaggt
aagaagaccattttggttattaagaccttggaattgtgtaaggaagacgaaaagaagattgttttgaaggctttgggtaacaagtctgcttctaaggaag
aattgatgtcttctgctgacattattaagaagtactctttggactacgcttacaacttggctgaaaagtactacaagaacgctattgactctttgaaccaag
tttcttctaagtctgacattccaggtaaggctttgaagtacttggctgaattcaccattagaagaagaaagtaa

Synechocystis spec 6803 HPT

atggctaccattcaagctttctggagattctctagaccacacaccattattggtaccaccttgtctgtttgggctgtttacttgttgaccattttgggtgatgg
taactctgttaactctccagcttctttggatttggttttcggtgcttggttggcttgtttgttgggtaacgtttacattgttggtttgaaccaattgtgggatgttg
atattgatagaattaacaagccaaacttgccattggctaacggtgatttctctattgctcaaggtagatggattgttggtttgtgtggtgttgcttctttggct
attgcttggggtttgggtttgtggttgggtttgaccgttggtatttctttgattattggtaccgcttactctgttccaccagttagattgaagagattctctttgtt
ggctgctttgtgtattttgaccgttagaggtattgttgttaacttgggtttgttcttgttcttcagaattggtttgggttacccaccaaccttgattaccccaattt
gggttttgaccttgttcattttggttttcaccgttgctattgctattttcaaggatgttccagatatggaaggtgatagacaattcaagattcaaaccttgacct
tgcaaattggtaagcaaaacgttttcagaggtaccttgattttgttgaccggttgttacttggctatggctatttggggtttgtgggctgctatgccattgaa
caccgctttcttgattgtttctcacttgtgtttgttggctttgttgtggtggagatctagagatgttcacttggaatctaagaccgaaattgcttctttctaccaa
ttcatttggaagttgttcttcttggaatacttgttgtacccattggctttgtggttgccaaacttctctaacaccatttttctaa

Xanthophyllomyces dendrorhous crtE

atggattacgcgaacatcctcacagcaattccactcgagtttactcctcaggatgatatcgtgctccttgaaccgtatcattacctaggaaagaaccctg
gaaaagaaattcgatcacaactcatcgaggctttcaactattggttggatgtcaagaaggaggatctcgaggtcatccagaacgttgttggcatgctac
ataccgctagcttattaatggacgatgtggaggattcatcggtcctcaggcgtgggtcgcctgtggcccatctaatttacgggattccgcagacaataa
acactgcaaactacgtctactttctggcttatcaagagatcttcaagcttcgcccaacaccgatacccatgcctgtaattcctccttcatctgcttcgcttc
aatcatccgtctcctctgcatcctcctcctcctcggcctcgtctgaaaacgggggcacgtcaactcctaattcgcagattccgttctcgaaagatacgta
tcttgataaagtgatcacagacgagatgctttccctccatagagggcaaggcctggagctattctggagagatagtctgacgtgtcctagcgaagag
gaatatgtgaaaatggttcttggaaagacgggaggtttgttccgtatagcggtcagattgatgatggcaaagtcagaatgtgacatagactttgtccag
cttgtcaacttgatctcaatatacttccagatcagggatgactatatgaaccttcagtcttctgagtatgcccataataagaattttgcagaggacctcaca
gaaggaaaattcagttttcccactatccactcgattcatgccaacccctcatcgagactcgtcatcaatacgttgcagaagaaatcgacctctcctgag
atccttcaccgctgtgtaaactacatgcgcacagaaacccactcattcgaatatactcaggaagtcctcaacaccttgtcaggtgcactcgagagaga
actaggaaggcttcaaggagagttcgcagaagctaactcaaagattgatcttggagacgtagagtcggaaggaagaacggggaagaacgtcaaat
tggaagcgatcctgaaaaagctagccgatatccctctgtga

Xanthophyllomyces dendrorhous crtI

atgggtaaggaacaagaccaagataagccaactgctattatcgttggttgtggtattggtggtatcgctactgctgccagattggctaaggaaggtttc
caagttactgtcttcgaaaagaacgactactctggtggtagatgttctttgattgaaagggacggttacagattcgaccaaggtccatctttgttattgttg
ccagacttgttcaagcaaactttcgaagacttgggtgaaaagatggaagactgggttgatttgattaagtgtgaaccaaactacgtttgtcacttccacg
acgaagaaactttcaccttctctactgacatggctttgttaaagagagaagttgaaagattcgaaggtaaggacggtttcgatagattcttgtctttcattc
aagaagctcacagacactacgaattggctgttgtccacgttttgcaaaagaacttcccaggtttcgctgccttcttgagattgcaattcattggtcaaatc
ttggctttgcacccattcgaatctatttggactagagtttgtagatacttcaagactgacagattgaggcgtgttttctctttcgctgttatgtacatgggtca
atctccatactctgctccaggtacttactctttgttacaatacactgaattgactgaaggtatttggtacccaagaggtggtttctggcaagttccaaacac
tttgttacaaattgttaagagaaacaacccatctgctaagttcaacttcaacgctccagtttctcaagttttgttatctccagctaaggacagagctactggt
gttagattggaatctggtgaagaacaccatgctgacgttgtcattgttaacgctgacttggtttacgcttctgaacacttgattccagacgatgctagaaa
caagattggtcaattgggtgaagttaagagatcttggtgggctgacttggttggtggtaagaaattgaagggttcttgttcctctttgtctttctactggtct
atggacagaattgttgacggtttgggtggtcacaacattttcttggctgaagacttcaagggttctttcgacactattttcgaagaattgggtttgccagct
gacccatctttctacgttaacgtcccatctagaattgacccatctgctgccccagaaggtaaggacgctattgttatcttggttccatgtggtcacattga
cgcttctaacccacaagactacaacaagttggttgctagagctagaaagttcgttattcaaactttgtctgctaagttgggtttgccagacttcgaaaaga
tgattgttgctgaaaaggttcacgacgctccatcttgggaaaaggaattcaacttgaaggacggttctattttgggtttggctcacaacttcatgcaagttt
tgggtttcagaccatctactagacacccaaagtacgacaagttgttctttgttggtgcttctactcacccaggtactggtgttccaattgttttggctggtg
ctaagttgactgctaaccaagttttggaatctttcgacagatctccagctccagacccaaacatgtctttgtccgttccatacggtaagccattgaagtct
aacggtactggtattgactctcaagttcaattgaagttcatggacttggaaagatgggtttacttgttagttttgttaattggtgctgttatcgctagatctgtt
ggtgtcttggctttctaa

Xanthophyllomyces dendrorhous crtYB

atgactgctttggcttactatcaaattcacttgatctacactttgccaattttgggtttgttaggtttgttaacttctccaattttgactaagttcgacatttacaa
gatctctattttggttttcatcgctttctctgctactaccccatgggactcttggattatcagaaacggtgcttggacttacccatctgctgaatctggtcaag
gtgttttcggtactttcttggacgttccatacgaagaatacgctttctttgttattcaaactgttatcactggtttggtttacgtcttggctactagacacttgtta
ccatctttggctttgccaaagactagatcttccgctttgtctttggctttgaaggctttgattccattgccaatcatttacttgttcactgctcacccatctccat
ccccagacccattggttactgaccactacttctacatgagagctttgtctttgttaattactccaccaactatgttgttagctgccttgtctggtgaatacgct
ttcgactggaagtctggtagagctaagtctactattgctgccatcatgattccaactgtttacttgatttgggttgactacgttgctgtcggtcaagactctt
ggtccattaacgacgaaaagattgttggttggagattgggtggtgttttgccaattgaagaagctatgttctttttgttaactaacttgatgattgttttgggt
ttgtctgcttgtgaccacactcaagctttgtacttgttacacggtagaactatttacggtaacaagaaaatgccatcttccttcccattgattactccaccag
ttttgtctttgttctttttcttccagaccatactcttcccaaccaaagagagacttggaattggctgttaagttgttagaaaagaaatctagatccttctttgttg
cttctgctggtttcccatctgaagttagagaaagattggttggtttgtacgctttctgtagagttactgacgatttgattgactctccagaagtttcttccaac
ccacacgctactattgacatggtttctgacttcttgactttgttattcggtccaccattgcacccatctcaaccagacaagattttgtcttccccattgttacc
accatctcacccatctagaccaactggtatgtacccattgccacctccaccatctttgtccccagctgaattggttcaattcttgactgaaagagttccag
tccaataccacttcgctttcagattgttagctaagttgcaaggtttgattccaagatacccattggacgaattgttaagaggttacactaccgacttgatttt
cccattgtctactgaagctgttcaagctagaaagactccaattgaaactaccgctgacttgttagattacggtttgtgtgttgctggttctgttgctgaattg
ttagtttacgtttcttgggcttctgctccatctcaagttccagctactattgaagaaagagaagctgttttggtcgcttctagagaaatgggtactgctttgc
aattggttaacattgctagagacatcaagggtgacgctactgaaggtagattctacttgccattgtctttctttggtttgagggacgaatctaagttggcta
ttccaactgactggactgaaccaagaccacaagacttcgataagttgttatctttgtccccatcttccactttgccatcttccaacgcttctgaatccttcag
attcgaatggaagacttactctttgccattggttgcttacgctgaagacttggctaagcactcttacaagggtattgacagattgccaactgaagttcaag
ctggtatgagagctgcctgtgcttcttacttgttaattggtagagaaatcaaggttgtctggaagggtgacgttggtgaaagacgtactgttgctggttg
gaggcgtgttagaaaggttttgtctgttgtcatgtctggttgggaaggtcaacaataa

Yarrowia lipolytica HPPD

atgtctccatctgttgaagttaccccagctcacaccccaacctcttacgaagttaccaactctttggactcttacagaggttacgaccacgttcactggta
cgttggtaacgctaagcaagctgcttctttctacattaccagaatgggtttctctccaattgcttacaagggtttggaaaccggttctagagacgttacca
cccacgttgttggtaacggtcaagttagattcgctttctcttctgctttgagaaccggtgaaccacaagctgacgaaattcacgctcacttggttaagca
cggtgacgctgttaaggacgttgctttcgaagttgacaacgttgaacaattgttctctgctgctgttaagaagggtgttagagttatttctgaaccaaagg
ttttgaaggacgctcaaggttctgttacctacgctgttatttctacctacggtgacaccacccacaccttgattgaaagaggttcttacgaaggtgctttct
tgccaggtttcgttgacacctctgctaacaaggacccaattgctgctttcttgccaaacattgaattgatgcacattgaccactgtgttggtaaccaagac
tggaacgaaatggacaacgcttgtaagtactacgaagaaaccttgggtttccacagattctggtctgttgacgacaaggacatttgtaccgaattctct
gctttgaagtctgttgttatggcttctccaaacgaaaagattaagatgccagttaacgaaccagctgttggtaagaagaagtctcaaattgaagaataca
ttgacttctacgacggtccaggtattcaacacattgctttgagaaccgactgtattttggacaccgttagagacttgagagctagaggtgttgaattcattt
ctgttccaggttcttactacgaaaacatgaaggaaagattggctaagtcttctttgaagttggaagaaaagttcgaagacattcaagctttgaacattttg
attgacttcgacgaaggtggttacttgttgcaattgttcaccaagccattgatggacagaccaaccgttttcattgaaattattcaaagaagaaacttcga
aggtttcggtgctggtaacttcaagtctttgttcgaagctattgaaagagaacaagctaagagaggtaacttgtaa